

2015

Mechanistic Studies of Silver-Catalyzed Single Electron Oxidations

Niki Patel
Lehigh University

Follow this and additional works at: <http://preserve.lehigh.edu/etd>

 Part of the [Chemistry Commons](#)

Recommended Citation

Patel, Niki, "Mechanistic Studies of Silver-Catalyzed Single Electron Oxidations" (2015). *Theses and Dissertations*. 2754.
<http://preserve.lehigh.edu/etd/2754>

This Dissertation is brought to you for free and open access by Lehigh Preserve. It has been accepted for inclusion in Theses and Dissertations by an authorized administrator of Lehigh Preserve. For more information, please contact preserve@lehigh.edu.

Mechanistic Studies of Silver-Catalyzed Single Electron Oxidations

by

Niki R. Patel

A Dissertation

Presented to the Graduate and Research Committee

of Lehigh University

in Candidacy for the Degree of

Doctor of Philosophy

in

Department of Chemistry

Lehigh University

May 18, 2015

© 2015 Copyright
Niki Rameshbhai Patel

Approved and recommended for acceptance as a dissertation in partial fulfillment of the requirements for the degree of Doctor of Philosophy

Niki R. Patel

Mechanistic Studies of Silver-Catalyzed Single Electron Oxidations

March 17, 2015

Defense Date

Dissertation Director

Approved Date

Committee Members:

Dr. Robert A. Flowers, II

Dr. David A. Vicic

Dr. Marcos Pires

Dr. Michael Kuchka

ACKNOWLEDGMENTS

First and foremost, I would like to offer my sincerest gratitude to my advisor and boss, Professor Robert Flowers. You have taught me so much in these past several years about not only chemistry, but about politics, music, and life. In addition to teaching, you have offered me so much support and guidance, without which I would not be where I am today. The opportunities you have provided me have allowed me to get to where I am in my career, and for that I am truly grateful.

I would also like to thank my research group for all of the help you have given me over the past several years. I would like to thank former group members including Dr. Brian Casey, Dr. Kimberly Choquette, Dr. Dhandapani Sadasivam, and especially Dr. James Devery for introducing me to life as a researcher, as well as teaching me everything that has allowed me to progress in graduate school. To my current group members including Gabrielle Haddad-Weiser, Tesia Chciuk, Godfred Fianu, and Dr. Lawrence Courtney, thank you for all of the support, advice, and especially the fun. Gaby, you have been with me from the beginning of this journey – thank you for being such a great friend. Tesia, we started out sitting one foot away from each other in silence and have somehow turned into best friends - these last two years have been great because of you.

I would like to offer my sincerest thanks and love to my family. To my parents, to whom I am deeply indebted – you have given me so much support, guidance, and love my whole life. You are the two most caring, supportive, and compassionate people that I know. I most definitely would not have been able to succeed without you. To my sisters,

you have taken care of me my whole life and I have learned so much from the two most successful women I know. Thank you for your care and kindness.

To my other family, my best friends – you really are the best. Teena, you are my third sister. You have been there for me since we became friends in seventh grade and I am so grateful for that. Eric, you are the most encouraging and hopeful person in my life, and without that these last few years would have been daunting. Lauren and Sneha, thank you for always being there for me no matter how busy or how far away from each other we are, providing an ear to talk to, a shoulder to lean on, and so much more. Benjamin and Eddie, thank you for always being so compassionate and caring and for making me laugh, a lot. To Roma, my cousin, niece, and especially my friend, thank you for bringing so much cheer and happiness into my life.

Again, I would like to thank Dr. Flowers, my group members, my friends, my family, and especially my Mom and Dad for everything that they have done for me.

Table of Contents

Acknowledgements.....	iv
Table of Contents.....	vi
List of Figures.....	xvi
List of Tables.....	xxiv
List of Schemes.....	xxvii
Solvent Abbreviations.....	xxxv
Abstract.....	1
Chapters	
1. Introduction to catalytic single electron oxidations in organic synthesis	
1.1 Origins of single electron oxidation.....	3
1.2 Mechanism of single electron transfer.....	4
1.3 Terminal oxidants.....	6
1.3.1 Persulfate.....	6
1.3.2 Peroxides.....	7
1.3.3 Molecular oxygen.....	8
1.3.4 Electrochemical oxidation.....	8
1.4 Metal-catalyzed single electron oxidation.....	9
1.4.1 Fe(III) catalysis.....	9
1.4.3 Cu(II) catalysis.....	12
1.4.4 Mn(III) catalysis.....	15
1.4.4 Ag(II) catalysis.....	18
1.4.5 Photoredox catalysis.....	21

1.4.6 Ce(IV) catalysis.....	30
1.5 Project goals.....	34
1.6 References.....	35
2. Mechanistic Studies of Ag(I)/Persulfate-Catalyzed Cross-Coupling of Arylboronic Acids to Electron-Deficient Pyridines	
2.1 Background and Significance.....	39
2.1.1 Catalytic Single Electron Oxidation	39
2.1.2 Silver(I)-Persulfate Catalysis.....	39
2.1.3 Minisci Reaction.....	43
2.1.4 Silver(I)/Persulfate-Catalyzed Cross-Coupling of Arylboronic Acids and Heteroarenes.....	47
2.2 Experimental.....	50
2.2.1 Materials	50
2.2.2 Instrumentation.....	50
2.2.3 Methods.....	50
2.2.3.1 Procedure for degassing solvents	50
2.2.3.2 Procedure for synthesis of 3	51
2.2.3.3 Procedure for Reaction Progress Kinetic Analysis Studies.....	51
2.2.3.4 Procedure for Pyridine ¹ H NMR studies.....	52
2.2.3.5 Procedure for ¹¹ B NMR studies.....	52
2.3 Results.....	53

2.3.1 Solvent and Solubility Studies.....	53
2.3.2 Kinetic Analysis.....	54
2.3.2.1 Catalyst Stability Experiments	55
2.3.2.2 Kinetic Order Experiments	56
2.3.3 Pyridine ¹ H NMR Studies.....	62
2.3.4 AgNO ₃ -Boronic Acid Studies.....	64
2.3.5 ¹¹ B NMR Studies.....	65
2.3.6 Allyl Acetate Studies.....	66
2.3.7 Proposed Mechanism for the Ag(I)/Persulfate- Catalyzed Cross- Coupling of Arylboronic acids and Electron-deficient Pyridines.....	68
2.3.7.1 Proposed Mechanism.....	68
2.3.7.2 Derivation of Rate Equation	68
2.3.7.3 Proposed Catalytic Cycle.....	70
2.3.8 Optimization of Reaction Conditions.....	70
2.4 Conclusions.....	71
2.5 References.....	72
 3. Mechanistic Studies of Ag(I)/Persulfate-Catalyzed Cross-Coupling of Arylboronic Acids to Quinones	
3.1 Background and Significance.....	75
3.1.1 Silver(I)/Persulfate-Catalyzed Cross-Coupling of Arylboronic Acids and Quinones.....	76
3.2 Experimental.....	77

3.2.1 Materials.....	77
3.2.2 Instrumentation.....	77
3.2.3 Methods.....	78
3.2.3.1 Procedure for degassing solvents.....	78
3.2.3.2 Procedure for synthesis of 4- methyl-[1,1'-biphenyl]- 2,5-dione (6).....	78
3.2.3.3 Procedure for Reaction Progress Kinetic Analysis studies.....	78
3.3 Results.....	79
3.3.1 Kinetic Analysis.....	79
3.3.1.1 Kinetic Order Experiments.....	79
3.3.2 Proposed Mechanism for the Ag(I)/Persulfate- Catalyzed Cross- Coupling of Arylboronic acids and Quinones.....	83
3.3.2.1 Proposed Mechanism.....	83
3.3.2.2 Proposed Catalytic Cycle.....	83
3.4 Conclusion.....	84
3.5 References.....	85
4. Mechanistic Studies of Ag(I)-Catalyzed Decarboxylative Fluorination	
4.1 Background and Significance.....	86
4.1.1 Importance of Carbon-Fluorine Bonds.....	86
4.1.2 Fluorinating Reagents	87
4.1.2.1 Nucleophilic fluorinating reagents.....	87
4.1.2.2 Electrophilic fluorinating reagents.....	88

4.1.3	Transition Metal-Mediated Electrophilic Fluorination.....	92
4.1.4	Aliphatic Carbon-Fluorine Bond Forming Reactions.....	97
4.1.5	Silver-Mediated Fluorination.....	99
4.2	Experimental.....	105
4.2.1	Materials.....	105
4.2.2	Instrumentation.....	105
4.2.3	Methods.....	106
4.2.3.1	Procedure for synthesis fluorinated products.....	106
4.2.3.2	Procedure for synthesis of 2,2-dimethylphenyl propanoic acid.....	106
4.2.3.3	Procedure for kinetic studies.....	107
4.2.3.4	Procedure for IR studies.....	108
4.2.3.5	Procedure for Ag- Selectfluor NMR studies.....	108
4.2.3.6	Procedure for BEt ₃ reaction of 2,2-dimethylglutaric Acid.....	108
4.2.3.7	Procedure for reaction using sodium persulfate.....	108
4.2.3.8	Procedure for reaction using NFSI and sodium persulfate.....	109
4.2.3.9	Procedure for pH Studies.....	109
4.2.3.10	Procedure for synthesis of 1-(chloromethyl)-1,4- diazobicyclo[2.2.2]octane tetrafluoroborate (TEDA-BF ₄)...	109
4.2.3.11	Procedure for crystallization of AgNO ₃ -TEDA- BF ₄	110

4.3 Results.....	110
4.3.1 Determination of Reaction Conditions.....	110
4.3.2 Kinetic Analysis.....	111
4.3.2.1 Catalyst Stability Experiments.....	111
4.3.2.2 Kinetic Order Experiments for 2,2-dimethylglutaric Acid.....	115
4.3.2.3 Kinetic Order Experiments for 2,2-dimethylbutyric Acid.....	119
4.3.2.4 Kinetic Order Experiments for 2,2-dimethylphenyl propanoic acid.....	123
4.3.2.5 Kinetic Order Experiments for Isobutyric Acid.....	127
4.3.2.6 Activation Parameters.....	130
4.3.3 Interaction of carboxylic acid with AgNO ₃ via IR Studies.....	131
4.3.4 Interaction of Selectfluor with AgNO ₃ via NMR Studies.....	132
4.3.5 Role of Water.....	135
4.3.6 pH studies.....	137
4.3.7 Identification of intermediates and mechanistic proposals after rate-limiting step.....	137
4.3.8 Ag(III) catalysis.....	139
4.3.9 Ag(II) is initiator.....	140
4.3.10 Ag(II) as Catalytic Oxidant studies.....	141
4.3.10.1 Persulfate studies.....	141

4.3.10.2 Kinetic studies of 2,2-dimethylglutaric acid using persulfate.....	143
4.3.10.3 Kinetic studies of 2,2-dimethylbutyric acid using persulfate.....	148
4.3.10.4 Proposed Mechanism of Persulfate Reaction.....	154
4.3.10.5 NFSI Studies.....	155
4.3.10.6 Proposed Mechanism of NFSI Reaction.....	156
4.3.11 Ag-ligand NMR studies with Selectfluor.....	157
4.3.11.1 ¹ H NMR Studies of 2,9-dimethyl-1,10-phenanthroline.....	157
4.3.11.2 ¹ H NMR Studies of terpyridine.....	159
4.3.12 Ag-TEDA-BF ₄ Studies.....	160
4.3.12.1 NMR studies of Ag-TEDA-BF ₄	160
4.3.12.2 Crystallization of Ag-TEDA-BF ₄	161
4.3.13 Proposed Mechanism for Ag(I)-Catalyzed Decarboxylative Fluorination.....	162
4.4 Conclusions.....	163
4.5 References.....	165
5. Development and Mechanistic Study of Silver-Catalyzed Decarboxylative Fluorination Using a Sterically Hindered N-Containing Ligand in Non-Aqueous Media	
5.1 Background and Significance.....	170
5.1.1 Silver-ligand complexes.....	170

5.1.2 Silver-ligand-catalyzed reactions.....	172
5.2 Experimental.....	175
5.2.1 Materials.....	175
5.2.2 Instrumentation.....	175
5.2.3 Methods.....	176
5.2.3.1 Procedure for synthesis of alkyl fluorides in acetonitrile.....	176
5.2.3.2 Procedure for kinetic studies.....	176
5.2.3.3 Procedure for crystallization of silver-ligand complexes.....	177
5.2.3.4 Procedure for silver-ligand NMR studies.....	177
5.3 Results.....	177
5.3.1 Decarboxylative fluorination using ligand in acetone/ water.....	177
5.3.2 Optimization of Reaction Conditions in Non-Aqueous Media.....	178
5.3.3 Mechanistic study of AgOTf-dmp catalyzed reaction	181
5.3.3.1 NMR Studies of AgOTf-dmp.....	183
5.3.3.2 Crystallization of AgOTf-dmp complex.....	183
5.3.3.3 Catalyst stability studies of AgOTf-dmp catalyzed reaction	184
5.3.3.4 Kinetic order studies of AgOTf-dmp catalyzed Reaction.....	186

5.3.3.5 Proposed Mechanism of AgOTf-dmp catalyzed Reaction.....	192
5.3.4 Mechanistic study of AgNO ₃ -dmp catalyzed reaction.....	193
5.3.4.1 Crystallization of AgNO ₃ -ligand complex.....	194
5.3.4.2 NMR Studies of AgNO ₃ -dmp complex.....	195
5.3.4.3 Kinetic order studies of AgNO ₃ -dmp catalyzed Reaction.....	196
5.3.5 Mechanistic study of AgOTf-dmp catalyzed reaction with persulfate.....	197
5.3.5.1 Kinetic order studies of AgOTf-dmp catalyzed reaction with persulfate.....	198
5.3.5.2 Proposed mechanism of AgOTf-dmp catalyzed reaction with persulfate.....	204
5.6 Conclusion.....	205
5.7 References.....	206
6. Conclusion	208
7. Appendix	
7.1 Mechanism of Ag/Persulfate-catalyzed cross-coupling of arylboronic acids to heteroarenes.....	211
7.2 Mechanism of Ag/Persulfate-catalyzed cross-coupling of arylboronic acids to quinones.....	225
7.3 Mechanistic study of decarboxylative fluorination in acetone/ water.....	230

7.4 Mechanistic study of decarboxylative fluorination with N-containing ligand in non-aqueous media.....	274
Curriculum Vitae.....	282

LIST OF FIGURES

1.1. Examples of commonly used photoredox catalysts in organic synthesis.....	22
1.2. Reductive and oxidative quenching cycle of Ru(bpy) ₃ ^{2+*}	23
2.1. Example of important compounds containing the 2-pyridyl subunit.....	49
2.2. Rate vs. [1] for same excess experiments.....	56
2.3. Rate vs. [3] for different excess experiments for 1.....	57
2.4. Rate vs. [1] for different excess experiments for AgNO ₃	58
2.5. Normalized Rate vs. [1] for different excess experiments for AgNO ₃	58
2.6. Rate vs. [1] for different excess experiments for K ₂ S ₂ O ₈	59
2.7. Rate vs. [1] for different excess experiments for Na ₂ S ₂ O ₈	60
2.8. Rate vs. [1] for different excess experiments for 2.....	61
2.9. Normalized Rate vs. [1] for different excess experiments for 2.....	63
2.10. ¹ H NMR spectra of 1 with additives.....	63
2.11. Rate vs. [1] plot comparing reaction with and without allyl acetate.....	67
3.1. Decay plot of Run 10.....	80
3.2. Linear fit of Run 10.....	81
3.3. Decay plot of Run 11	82
3.4. Linear fit of Run 11	82
3.5. Plot of rate vs. [4] for rate order for 2	83
4.1. Examples of important fluorinated compounds	87
4.2. Examples of commonly used nucleophilic fluorinating reagents.....	88

4.3. Examples of commonly used N-F electrophilic fluorinating reagents.....	90
4.4. Silver-catalyzed fluorination of complex small molecules by Ritter.....	100
4.5. Growth of fluorinated product 8 over time monitored by ^{19}F NMR in decarboxylative fluorination reaction of 7	112
4.6. Plot of [7] vs. time for Runs 1 and 2 for catalyst stability studies in decarboxylative fluorination reaction of 7	114
4.7. Time-adjusted profiles showing overlay of Runs 1 and 2 in decarboxylative fluorination reaction of 7	114
4.8. $-\text{d}[\mathbf{2}]/\text{dt}$ vs. [2] plot for order of AgNO_3 in decarboxylative fluorination reaction of 7	116
4.9. Turnover frequency of AgNO_3 in decarboxylative fluorination reaction of 7	117
4.10. $-\text{d}[\mathbf{2}]/\text{dt}$ vs. [2] plot for order of Selectfluor in decarboxylative fluorination reaction of 7	117
4.11. Normalized rate vs. [8] plot showing first order rate dependence on Selectfluor in decarboxylative fluorination reaction of 7	117
4.12. $-\text{d}[\mathbf{8}]/\text{dt}$ vs. [8] plot for order of 7 in decarboxylative fluorination reaction of 7	118
4.13. $-\text{d}[\mathbf{9b}]/\text{dt}$ vs. [9b] plot for order of AgNO_3 in decarboxylative fluorination reaction of 9a	120
4.14. Normalized rate plot showing rate order of AgNO_3 in decarboxylative fluorination reaction of 9a	121

4.15. $-d[9b]/dt$ vs. $[9b]$ plot for order of Selectfluor in decarboxylative fluorination reaction of 9a	121
4.16. Normalized rate plot showing rate order of Selectfluor in decarboxylative fluorination reaction of 9a	122
4.17. $-d[9b]/dt$ vs. $[9b]$ plot for order of 9a in decarboxylative fluorination reaction of 9a	122
4.18. $-d[10b]/dt$ vs. $[10b]$ plot for order of $AgNO_3$ in decarboxylative fluorination reaction of 10a	124
4.19. Normalized rate plot showing rate order of $AgNO_3$ in decarboxylative fluorination reaction of 10a	125
4.20. $-d[10b]/dt$ vs. $[10b]$ plot for order of Selectfluor in decarboxylative fluorination reaction of 10a	125
4.21. Normalized rate plot showing rate order of Selectfluor in decarboxylative fluorination reaction of 10a	126
4.22. $-d[10b]/dt$ vs. $[10b]$ plot for order of 10a in decarboxylative fluorination reaction of 10a	126
4.23. $-d[11b]/dt$ vs. $[11b]$ plot for order of $AgNO_3$ in decarboxylative fluorination reaction of 11a	128
4.24. Normalized rate plot showing rate order of $AgNO_3$ in decarboxylative fluorination reaction of 11a	128
4.25. $-d[11b]/dt$ vs. $[11b]$ plot for order of Selectfluor in decarboxylative fluorination reaction of 11a	129

4.26. Normalized rate plot showing rate order of Selectfluor in decarboxylative fluorination reaction of 11a	129
4.27. $-d[11b]/dt$ vs. $[11b]$ plot for order of 11a in decarboxylative fluorination reaction of 11a	130
4.28. Activation parameters of fluorination reaction of 7	131
4.29. FTIR spectra comparing 7 to product of 7 and $AgNO_3$	132
4.30. 1H NMR spectra showing shifts of Selectfluor upon addition of $AgNO_3$	133
4.31. ^{13}C NMR spectra showing shifts of Selectfluor upon addition of $AgNO_3$	134
4.32. ^{19}F NMR spectra showing loss of N-F signal of Selectfluor upon addition of $AgNO_3$	135
4.33. Proton NMR spectra suggesting coordination of water to $AgNO_3$	136
4.34. pH vs. time plot of decarboxylative fluorination reaction of 7	137
4.35. Equivalent of $Na_2S_2O_8$ vs. k_{obs} for the fluorination of 7	142
4.36. Plot of $[7]$ vs. time for Runs 18 and 19 for catalyst stability studies in decarboxylative fluorination reaction of 7 with sodium persulfate.....	143
4.37. Time-adjusted profiles showing overlay of Runs 18 and 19 in decarboxylative fluorination reaction of 7 with sodium persulfate.....	144
4.38. $-d[8]/dt$ vs. $[8]$ for rate order of $AgNO_3$ in decarboxylative fluorination reaction of 7 with sodium persulfate.....	145
4.39. Normalized rate plot showing rate order of $AgNO_3$ in decarboxylative fluorination reaction of 7 with sodium persulfate.....	146

4.40. -d[8]/dt vs. [8] for rate order of Selectfluor in decarboxylative fluorination reaction of 7 with sodium persulfate.....	146
4.41. -d[8]/dt vs. [8] for rate order of 7 in decarboxylative fluorination reaction of 7 with sodium persulfate.....	147
4.42. -d[8]/dt vs. [8] for rate order of sodium persulfate in decarboxylative fluorination reaction of 7 with sodium persulfate.....	147
4.43. Normalized rate plot showing rate order of sodium persulfate in decarboxylative fluorination reaction of 7 with sodium persulfate.....	148
4.44. Plot of [9a] vs. time for Runs 24 and 25 for catalyst stability studies in decarboxylative fluorination reaction of 9a with sodium persulfate.....	149
4.45. Time-adjusted profiles showing overlay of Runs 24 and 25 in decarboxylative fluorination reaction of 9a with sodium persulfate.....	149
4.46. -d[9b]/dt vs. [9b] for rate order of AgNO ₃ in decarboxylative fluorination reaction of 9a with sodium persulfate.....	151
4.47. Normalized rate plot showing rate order of AgNO ₃ in decarboxylative fluorination reaction of 9a with sodium persulfate.....	151
4.48. -d[9b]/dt vs. [9b] for rate order of Selectfluor in decarboxylative fluorination reaction of 9a with sodium persulfate.....	152
4.49. Normalized rate plot showing rate order of 9a in decarboxylative fluorination reaction of 9a with sodium persulfate.....	152
4.50. -d[9b]/dt vs. [9b] for rate order of sodium persulfate in decarboxylative fluorination reaction of 9a with sodium persulfate.....	152

4.51. Normalized rate plot showing rate order of sodium persulfate in decarboxylative fluorination reaction of 9a with sodium persulfate.....	152
4.52. ¹ H NMR spectrum of dmp with 1 equiv AgNO ₃ in MeCN-d ₃	157
4.53. ¹ H NMR spectrum of dmp with 1 equiv AgNO ₃ and Selectfluor in MeCN-d ₃	158
4.54. ¹ H NMR spectrum of terpy with 1 equiv AgNO ₃ in MeCN-d ₃	159
4.55. ¹ H NMR spectrum of terpy with 1 equiv AgNO ₃ and Selectfluor in MeCN-d ₃	159
4.56. Proton NMR spectra suggesting coordination of TEDA-BF ₄ to AgNO ₃	161
4.57. X-ray crystal structure showing coordination of TEDA-BF ₄ to AgNO ₃	162
5.1. Examples of sterically hindered diimine ligands.....	172
5.2. ¹ H NMR spectra showing downfield shifts in dmp upon addition of AgOTf.....	182
5.3. ¹ H NMR spectra showing paramagnetism upon addition of Selectfluor to AgOTf-dmp.....	183
5.4. Crystal structure of AgOTf-dmp complex.....	184
5.5. Plot of [9b] vs. time for Runs 1 and 2 for catalyst stability studies in AgOTf-dmp catalyzed decarboxylative fluorination.....	185
5.6. Time-adjusted profiles showing catalyst deactivation of Run 1 and 2 in AgOTf-dmp catalyzed decarboxylative fluorination.....	186
5.7. -d[9b]/dt vs. [9b] for order of Ag-dmp in AgOTf-dmp catalyzed decarboxylative fluorination.....	188

5.8. Normalized rate vs. [9b] for order of Ag-dmp in AgOTf-dmp catalyzed decarboxylative fluorination.....	188
5.9. $-d[9b]/dt$ vs. [9b] for order of Selectfluor in AgOTf-dmp catalyzed decarboxylative fluorination.....	189
5.10. Normalized rate vs. [9b] for order of Selectfluor in AgOTf-dmp catalyzed decarboxylative fluorination.....	190
5.11. $-d[9b]/dt$ vs. [9b] for order of 9b in AgOTf-dmp catalyzed decarboxylative fluorination.....	191
5.12. Line fits for order of 9b in AgOTf-dmp catalyzed decarboxylative fluorination.....	191
5.13. Crystal structure of AgNO ₃ -dmp complex.....	195
5.14. ¹ H NMR spectra showing shifts in dmp upon addition of AgNO ₃	195
5.15. $-d[9b]/dt$ vs. [9b] for order of Ag-dmp in AgNO ₃ -dmp catalyzed decarboxylative fluorination	197
5.16. $-d[9b]/dt$ vs. [9b] for order of Ag-dmp in AgOTf-dmp catalyzed decarboxylative fluorination with persulfate.....	199
5.17. Normalized rate vs. [9b] for order of Ag-dmp in AgOTf-dmp catalyzed decarboxylative fluorination with persulfate.....	199
5.18. $-d[9b]/dt$ vs. [9b] for order of Selectfluor in AgOTf-dmp catalyzed decarboxylative fluorination with persulfate.....	200
5.19. $-d[9b]/dt$ vs. [9b] for order of 9b in AgOTf-dmp catalyzed decarboxylative fluorination with persulfate.....	201

5.20. Line fits for order of 9b in AgOTf-dmp catalyzed decarboxylative fluorination with persulfate.....	201
5.21. $-d[9b]/dt$ vs. $[9b]$ for order of $Na_2S_2O_8$ in AgOTf-dmp catalyzed decarboxylative fluorination.....	202
5.22. $-d[9b]/dt$ vs. $[9b]$ for order of $(TBA)_2S_2O_8$ in AgOTf-dmp catalyzed decarboxylative fluorination.....	203

LIST OF TABLES

2.1. Catalyst stability experiment reaction conditions.....	55
2.2. Rate order experiment reaction conditions.....	57
2.3. Observed Rate Orders of Substrates in Cross-Coupling Reaction of 1 and 2	62
2.4. ¹ H NMR shifts of 1 with additives.....	64
3.1. Conditions for different excess experiments for rate order of 2	80
4.1. Reaction conditions for catalyst stability studies in decarboxylative fluorination reaction of 7	113
4.2. Reaction conditions for kinetic order studies for fluorination of 7	115
4.3. Rate Orders for each component in Ag(I)-catalyzed fluorination of 7	119
4.4. Reaction conditions for kinetic order studies for fluorination of 9a	120
4.5. Rate Orders for each component in Ag(I)-catalyzed fluorination of 9a	123
4.6. Reaction conditions for kinetic order studies for fluorination of 10a	124
4.7. Rate Orders for each component in Ag(I)-catalyzed fluorination of 10a	127
4.8. Reaction conditions for kinetic order studies for fluorination of 11a	127
4.9. Rate Orders for each component in Ag(I)-catalyzed fluorination of 11a	130
4.10. ¹ H NMR shifts of Selectfluor with AgNO ₃	133
4.11. ¹³ C NMR shifts of Selectfluor with AgNO ₃	134
4.12. Fluorination of 7 using increasing amounts of water.....	136

4.13. Reaction conditions for catalyst stability studies for fluorination of 7 using sodium persulfate.....	143
4.14. Reaction conditions for kinetic order studies for fluorination of 7 using sodium persulfate.....	145
4.15. Rate orders for each component in Ag(I)-Selectfluor-persulfate-mediated fluorination reaction.....	148
4.16. Reaction conditions for catalyst stability studies for fluorination of 9a using sodium persulfate.....	150
4.17. Reaction conditions for kinetic order studies for fluorination of 9a using sodium persulfate.....	150
4.18. Rate orders for each component in Ag(I)-Selectfluor-persulfate-mediated fluorination reaction.....	154
4.19. ¹ H NMR shifts of TEDA-BF ₄ with AgNO ₃	161
5.1. Yield of fluorinated product 8 with different silver salts	180
5.2. Decarboxylative fluorination of other carboxylic acids using AgOTf and dmp in MeCN.....	180
5.3. ¹ H NMR shifts of dmp with AgOTf.....	182
5.4. Reaction conditions for catalyst stability studies in fluorination reaction of 9a with AgOTf and dmp.....	185
5.5. Reaction conditions for kinetic order studies for fluorination of 9a with AgOTf and dmp.....	187
5.6. Rate order for each component in fluorination of 9a with AgOTf and dmp.....	192

5.7. ^1H NMR shifts of dmp with AgNO_3	196
5.8. Reaction conditions for kinetic order studies for fluorination of 9a with AgNO_3 - dmp.....	196
5.9. Reaction conditions for kinetic order studies for fluorination of 9a with AgOTf and dmp in the presence of sodium persulfate.....	198
5.10. Reaction conditions for kinetic order studies for fluorination of 9a with AgOTf and dmp in the presence of tetra-n-butyl ammonium persulfate.....	203
5.11. Rate order for each component in fluorination of 9a using AgNO_3 and dmp in the presence of sodium persulfate.....	203

LIST OF SCHEMES

1.1. Mechanism of the Kolbe reaction.....	3
1.2. Chain reaction metal-catalyzed reaction by single electron oxidation.....	5
1.3. Non-chain metal-catalyzed single electron oxidation mediated by terminal oxidant.....	5
1.4. Ag-catalyzed radical addition to heteroarene.....	7
1.5. Fe-catalyzed radical addition to heteroarene.....	7
1.6. Cu-catalyzed oxidation of alcohols.....	8
1.7. Addition of dimethyl bromomalonate radical to olefins via electrochemical Mn(III) catalysis.....	9
1.8. Fe(III)-catalyzed nitrosation of olefins to form dimers.....	10
1.9. Fe(III)-catalyzed [2+2]-cycloaddition of styrene derivatives.....	10
1.10. Fe(III)-catalyzed cycloaddition of styrene derivatives with quinone.....	11
1.11. Fe(III)-catalyzed intramolecular oxidative coupling	12
1.12. Fe(III)-catalyzed oxidative addition of alkoxy carbonyl radicals to alkenes.....	12
1.13. Cu(II)-catalyzed oxygenolysis of cyclopropylamines to epoxy ketones.....	13
1.14. Cu(II)-catalyzed enantioselective intramolecular carboamination of alkenes.....	14
1.15. Total synthesis of (S)-(+)-tylophorine via enantioselective intramolecular alkene carboamination.....	15
1.16. Cu(II)-catalyzed synthesis of oxindoles via C-H activation.....	15

1.17. Electrochemical Mn(III)-catalyzed carbon-carbon bond formation.....	16
1.18. Proposed mechanism of electrochemical Mn(III)-catalyzed carbon-carbon bond formation.....	16
1.19. Mn(III)-catalyzed radical addition of polybromomethane to olefin.....	17
1.20. Mn-catalyzed hydroperoxyalkylations of barbituric acid derivatives.....	17
1.21. Mn(III)-catalyzed radical addition of dimethyl malonate to olefins.....	17
1.22. Mn-catalyzed synthesis of α,β -epoxy ketones from cyclopropanols.....	18
1.23. Ag-catalyzed oxidation of glycine.....	19
1.24. Ag-catalyzed decarboxylative alkynylation.....	19
1.25. Tandem radical addition/cyclization via silver catalysis	20
1.26. Trifluoromethylation of arenes with TFA via silver catalysis.....	20
1.27. Reaction conditions for oxidative addition of arylboronic acid to heteroarene	21
1.28. Proposed mechanism involving oxidative addition of arylboronic acid to heteroarene	21
1.29. Excitation of $\text{Ru}(\text{bpy})_3^{2+}$ to $\text{Ru}^*(\text{bpy})_3^{2+}$ using visible light.....	23
1.30. Proposed reaction mechanism for the transformation of aryldiazonium salts to phenantrenes using $\text{Ru}(\text{bpy})_3^{2+}$	24
1.31. Proposed reaction mechanism for the oxidation of benzylic alcohols to aldehydes using RuL_3^{2+}	25
1.32. Photoredox-catalyzed [2+2] cycloaddition.....	26
1.33. Photoredox-catalyzed synthesis of 2-substituted benzothiazoles.....	26
1.34. Photoredox induced deboronative alkynylation.....	27

1.35. Photoredox-catalyzed addition of α -amino radicals to Michael acceptors.....	27
1.36. Photoredox-catalyzed [3+2] cycloaddition of cyclopropylamines with olefins	28
1.37. Photoredox-catalyzed radical cation Diels-Alder cycloadditions.....	28
1.38. Photoredox-catalyzed α -amino C-H arylation.....	29
1.39. Photoredox-catalyzed hydroalkoxymethylation of electron-deficient alkenes.....	29
1.40. Single electron transmetalation in photoredox/nickel cross-coupling.....	30
1.41. Proposed mechanism for single electron transmetalation in photoredox/nickel cross-coupling.....	31
1.42. Ce(IV)-mediated carbon-carbon bond formation.....	31
1.43. Ce(IV)-catalyzed oxidation of alcohols in a dual oxidant system.....	31
1.44. Aerobic oxidation of benzylic alcohols catalyzed by CAN/TEMPO.....	32
1.45. Proposed mechanism for the oxidation of benzylic alcohols via CAN/TEMPO catalysis.....	32
1.46. CAN-catalyzed epoxide opening.....	33
1.47. CAN-catalyzed deprotection of t-butoxycarbonyl compounds.....	33
1.48. CAN-catalyzed oxidation of hydroquinones.....	34
1.49. CAN-catalyzed cyclocondensation using ultrasound.....	34
2.1. Early use of catalytic silver nitrate and potassium persulfate in oxidations.....	40
2.2. Early mechanism proposed for catalytic silver(I)/persulfate oxidation of chromic ion.....	41
2.3. Ag(I)/Persulfate-catalyzed cleavage of glycols.....	42

2.4. Mechanism of Ag(II) oxidation of carboxylic acids by cyclization of the resulting radical.....	42
2.5. Ag(I)/Persulfate-catalyzed oxidation of cyclopropanol.....	42
2.6. Ag(I)/Persulfate-catalyzed decarboxylative C-H arylation of benzoic acids.....	43
2.7. General scheme of Minisci reaction.....	44
2.8. Proposed mechanism of the Minisci reaction.....	44
2.9. General scheme of Minisci acylation reaction.....	44
2.10. Synthesis of 8-Azaergoline Ring System by Minisci-type acylation reaction....	44
2.11. Minisci-type reactions of indoleglyoxylic acids with pyridines.....	45
2.12. Use of N-protected amino acids in Minisci alkylations.....	45
2.13. Use of Minisci reaction in the synthesis of various medicinal compounds.....	46
2.14. Use of Minisci reaction in various total syntheses.....	47
2.15. Cross-coupling reaction of electron-deficient pyridine with arylboronic acid.....	48
2.16. Proposed mechanism for the cross-coupling reaction of electron-deficient pyridine with arylboronic acid.....	48
2.17. Cross-coupling reaction of electron-deficient pyridine with arylboronic acid.....	53
2.18. Cross-coupling reaction of electron-deficient pyridine with aryl trifluoroborate.....	66
2.19. Mechanism of Ag(I)/Persulfate-Catalysis in Coupling of Arylboronic acid and Electron-deficient Pyridine.....	68

2.20. Proposed Mechanism of the Ag(I)/Persulfate-Catalyzed Arylation of Electron-deficient Pyridine.....	70
3.1. Oxidative decarboxylation and coupling of oxalic acid derivatives to quinones.....	75
3.2. Addition of alkyl radicals to naphthoquinones in total synthesis of marmycin A.....	76
3.3. Tandem radical alkylation-cyclization-aromatization reaction sequence to produce carbazole compounds.....	76
3.4. Cross-coupling reaction of quinone with arylboronic acid.....	77
3.5. Cross-coupling reaction of quinone with arylboronic acid for kinetic studies.....	79
3.6. Proposed Mechanism of the Ag(I)/Persulfate-Catalyzed Reaction of Arylboronic acids and Quinones.....	83
3.7. Proposed Catalytic Cycle of the Ag(I)/Persulfate-Catalyzed Reaction of Arylboronic acids and Quinones.....	84
4.1. Glucocorticoid fluorination.....	90
4.2. Fluorination of gypsetin derivative.....	91
4.3. Radiolabeled [¹⁸ F]-fluorination of silyl enol ether.....	91
4.4. Palladium-catalyzed fluorination of (a) phenylpyridines and (b) quinolines.....	93
4.5. Palladium-catalyzed selective fluorination of benzyltriflamides.....	93
4.6. Gold-catalyzed cyclization-fluorination of alkynes.....	94

4.7. Gold-catalyzed hydration-fluorination of alkynes.....	94
4.8. (a) Copper-mediated fluorination of arylboronate esters and (b) fluorination of arenes via C-H borylation.....	95
4.9. Copper-mediated fluorination of (a) aryl stannanes and (b) aryl trifluoroborates.....	95
4.10. Iron-catalyzed benzylic fluorination.....	96
4.11. Palladium-catalyzed fluorination of aryl trifluoroborates.....	96
4.12. Manganese porphyrin-catalyzed C-H fluorination of (a) heptanes, a simple alkane and (b) sclareolide, a sesquiterpene lactone.....	97
4.13. Copper bis-imine catalyzed fluorination of heptanes.....	98
4.14. Decarboxylative radical fluorination using NFSI.....	98
4.15. Photo-fluorodecarboxylation of phenylacetic acid.....	98
4.16. Iron(III)-mediated fluorination of unactivated alkenes.....	99
4.17. Silver-mediated electrophilic fluorination of aryl boronic acid.....	99
4.18. Silver-mediated electrophilic fluorination of aryl stannanes.....	100
4.19. Silver-catalyzed electrophilic fluorination of aryl stannanes.....	100
4.20. Radiolabeled [¹⁸ F]-fluorodestannylation.....	101
4.21. Synthesis of [¹⁸ F]-6-fluoro-L-DOPA.....	102
4.22. Silver-catalyzed vinylogous fluorination.....	102
4.23. Silver-catalyzed difluoromethylation of benzylic C-H bonds.....	103
4.24. Fluorination of pyridines with AgF ₂	103
4.25. Silver-catalyzed decarboxylative fluorination of (a) a tertiary acid, (b) a dehydrolithocholic acid derivative, and (c) a carboxylic acid on a	

radical probe.....	105
4.26. Ag(I)-catalyzed fluorination of aliphatic carboxylic acid 7	
using Selectfluor.....	111
4.27. Ag(I)-catalyzed fluorination of aliphatic carboxylic acid 9a	
using Selectfluor.....	119
4.28. Ag(I)-catalyzed fluorination of aliphatic carboxylic acid 10a	
using Selectfluor.....	123
4.29. Ag(I)-catalyzed fluorination of aliphatic carboxylic acid 11a	
using Selectfluor.....	127
4.30. Mechanistic possibilities for Ag(I)-catalyzed decarboxylation.....	139
4.31. Decarboxylative fluorination reaction with triethylborane.....	141
4.32. Decarboxylative fluorination reaction with Na₂S₂O₈ as additive.....	142
4.43. Proposed catalytic cycle of Ag(I)-catalyzed fluorination using Na₂S₂O₈ and Selectfluor.....	154
4.44. Decarboxylative fluorination reaction with NFSI and Na₂S₂O₈.....	156
4.45. Proposed catalytic cycle of Ag(I)-catalyzed fluorination using NFSI and persulfate.....	156
4.46. Mechanism of Ag(I) oxidation by Selectfluor.....	160
4.47. Proposed catalytic cycle of Ag(I)-catalyzed fluorination using Selectfluor....	163
5.1. Silver-catalyzed intramolecular chloroamination of allenes.....	173
5.2. Intramolecular hydroamination of aminoalkynes with silver-phenanthroline.....	173
5.3. Silver-catalyzed intramolecular amidation of saturated C-H bonds.....	173

5.4. Silver-catalyzed decarboxylative chlorination of aliphatic carboxylic acids.....	174
5.5. Tunable, chemoselective amination via silver-ligand catalysis.....	174
5.6. Ligand-controlled, tunable silver-catalyzed C-H amination.....	175
5.7. Decarboxylative fluorination of 7 with dmp as ligand in acetone/water.....	178
5.8. Decarboxylative fluorination of 7 with dmp as ligand in MeCN.....	179
5.9. Decarboxylative fluorination of 9a using dmp as ligand and AgOTf as catalyst in MeCN.....	181
5.10. Proposed catalytic cycle for decarboxylative fluorination reaction of aliphatic acids in non-aqueous media using N-containing ligand.....	193
5.11. Decarboxylative fluorination of 9a using dmp as ligand and AgNO₃ as catalyst.....	194
5.12. Decarboxylative Fluorination Reaction of 9a with AgOTf-dmp with persulfate.....	197
5.13. Proposed catalytic cycle for decarboxylative fluorination reaction of aliphatic acids in non-aqueous media using N-containing ligand and persulfate.....	204

List of Abbreviations

(2,2,6,6-Tetramethylpiperidin-1-yl)oxy	TEMPO
Ceric ammonium nitrate	CAN
Trifluoroacetic acid	TFA
Acetonitrile	MeCN
Dichloromethane	DCM
N-fluorobenzenesulfonimide	NFSI
Tetra-n-butyl ammonium fluoride	TBAF
Equivalents	equiv
Ethyl acetate	EtOAc

ABSTRACT

Catalytic oxidations that proceed through single-electron transfers are emerging as important approaches towards the formation of C-C and C-F bonds in molecules of pharmaceutical and biological importance. A great deal of recent effort has focused on metal-catalyzed oxidations, in particular silver catalysis combined with the use of a terminal oxidant. In addition, the use of readily available starting materials employed in these reactions can provide a wide range of structures important for screening in medicinal chemistry and for the construction of building blocks important in materials chemistry. The motivation for this research lies in the fundamental understanding of electron transfer in metal-mediated organic reactions. A greater understanding of the mechanistic pathways in these reactions can allow for the optimization of existing methods, as well as opening up the possibility for the development of new synthetic reactions.

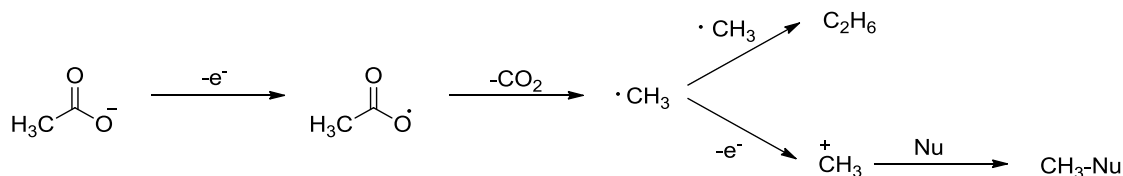
The research presented in this dissertation encompasses the mechanistic studies of several silver-catalyzed reactions of synthetic importance that are thought to go through single electron oxidation. This work has led to a greater understanding of (a) carbon-carbon bond formation between arylboronic acids and heteroarenes mediated by persulfate, (b) the coupling of arylboronic acids to quinones, (c) alkyl fluorinations that proceed through decarboxylation in aqueous media, and (d) the development and mechanistic study of a decarboxylative fluorination in organic media through the use of a sterically-hindered ligand. Investigations of these reactions have revealed considerable

amounts of unexpected mechanistic complexity. The mechanistic studies and method development of these reactions has led to the development of more efficient catalytic single-electron oxidation reactions, and has the potential to influence new areas of synthetic and organometallic chemistry.

Chapter 1. Introduction to catalytic single electron oxidations in organic synthesis

1.1 Origins of single electron oxidation

Single electron transfer involving organic substrates provides access to a number of compounds of synthetic importance. In particular, single electron oxidation processes generate reactive intermediates that can undergo a number of pathways to produce synthetically relevant compounds. One of the earliest examples of single electron oxidation was performed by Faraday in 1834, when he observed the evolution of gas bubbles at the surface of the anode upon electrolysis of a solution of aqueous potassium acetate.¹ Twenty years later, Kolbe showed that the bubbles formed during the electrolysis were caused by the decarboxylation of acetate to produce CO₂ gas and ethane.² The reaction mechanism (Scheme 1.1) involves single electron oxidation of acetate to produce a carboxyl radical which spontaneously evolves CO₂ to form methyl radicals. Methyl radicals can either homocouple to generate ethane,³ or undergo a second single electron oxidation to produce a cation. Nucleophilic attack of this cation can produce various products in solution.⁴ Since the development of this reaction, a number of methods have emerged that take advantage of the powerful intermediates generated through single electron oxidations.



Scheme 1.1. Mechanism of the Kolbe reaction.

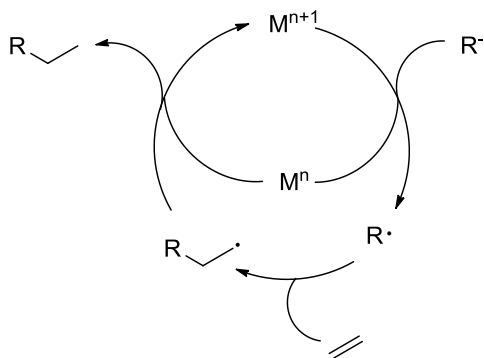
1.2 Mechanism of single electron transfer

The mechanisms of organometallic reactions were largely investigated in the 1960s and 1970s, leading to an increase in development of such reactions. This also corresponded to an increase in radical chemistry, a field that was not considered to be synthetically useful other than in polymer chemistry. However, the mechanistic investigations during this time led to the realization that radicals and single electron transfer were common characteristics of organometallic chemistry, expanding the development of synthetic methods that incorporate these features.

A number of metals can perform single electron transfer through oxidation, the most common of which are Fe(III), Cu(II), Mn(III), Ag(II), and the lanthanide Ce(IV). These metal complexes have been used on a stoichiometric scale for the oxidation of various functional groups, including enolates, silyl enol ethers, enamines, and enols, as well as electron-rich π -systems, and anions, to generate radicals and radical cations. Single electron oxidation using such metals will be discussed in Section 1.4. In addition to transition and lanthanide metals, hypervalent iodine oxidants and electrochemical oxidation provide access to radical and radical cations; however, they will not be the focus of this chapter.

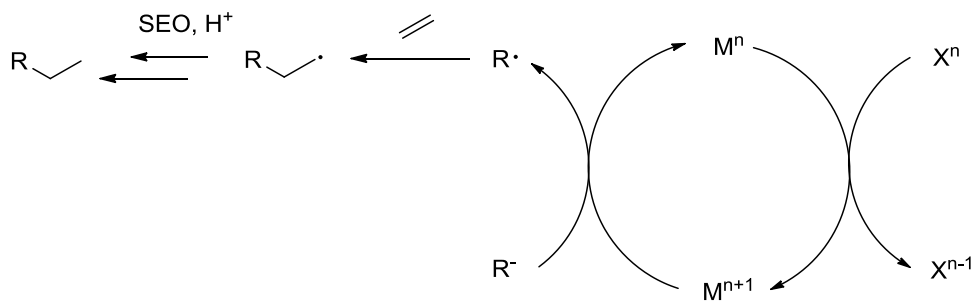
While the stoichiometric oxidation of organic substrates by metal oxidants to generate radicals is common, the development of catalytic reactions has remained infrequent.⁵⁻⁷ Metal-catalyzed single electron oxidations of organic substrates most commonly occur through one of two pathways: chain radical reaction and non-chain single electron transfer reaction. In the chain reaction pathway, the oxidation state of the

metal changes by one during the course of the reaction (Scheme 1.2). The catalyst in this type of reaction is regenerated by a subsequent single electron transfer by a resulting radical in the reaction.



Scheme 1.2. Chain reaction metal-catalyzed reaction by single electron oxidation.

In the non-chain pathway, the catalyst is generated or regenerated by the addition of a stoichiometric oxidant (Scheme 1.3), which will be seen during the course of this dissertation. The research presented in this dissertation involving single electron oxidation relies on the use of silver catalysts. A thorough understanding of the mechanism of single electron transfer in these reactions can lead to the development of improved or even new reaction systems.



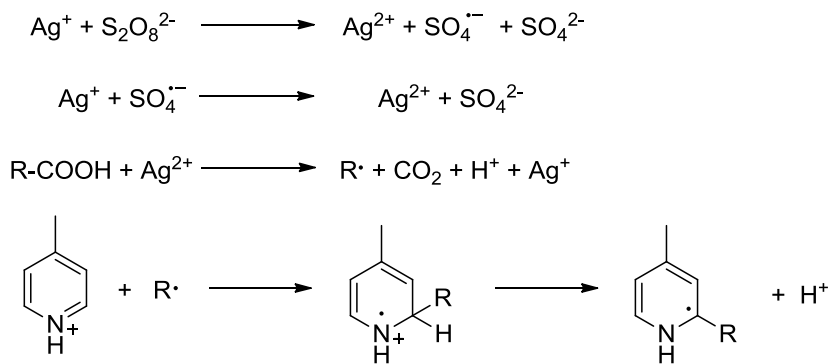
Scheme 1.3. Non-chain metal-catalyzed single electron oxidation mediated by terminal oxidant.

1.3 Terminal oxidants

As mentioned in Section 1.2, a commonly used method of turning over metal complexes in catalytic reactions is through the addition of stoichiometric oxidants. A number of electron sources can be used to either generate or regenerate active metal oxidants, the most common of which are persulfate, peroxides, and molecular oxygen in air. In the following sections, a reaction and mechanism is provided as examples for each of the commonly used oxidants.

1.3.1 Persulfate

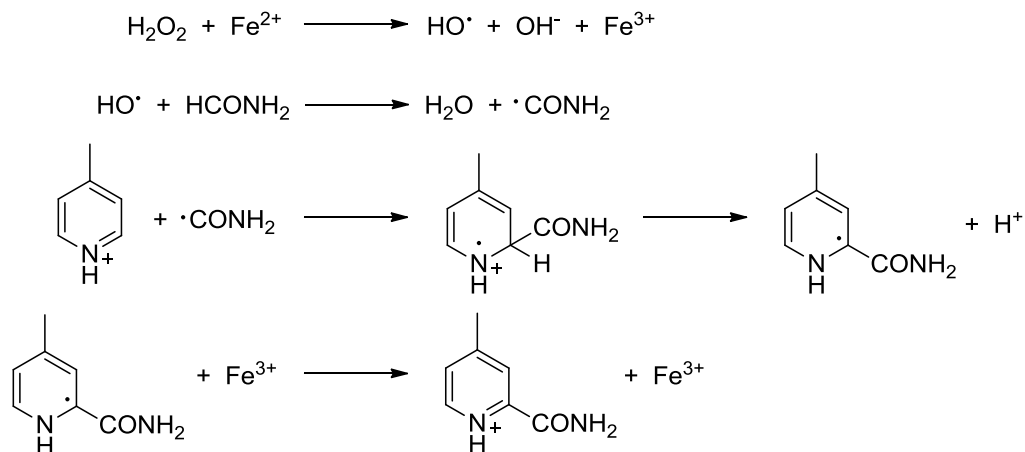
In 1969, Anderson and Kochi investigated the mechanism of decarboxylation of aliphatic carboxylic acids by Ag(I) and persulfate.⁸ They found that the oxidative decarboxylation of these acids was accelerated significantly by the silver ion. Minisci and coworkers expanded on the work by Anderson and Kochi, to develop a new reaction involving the homolytic alkylation of heteroaromatic bases, using a silver-catalyzed persulfate system to oxidatively decarboxylate acids.⁹ Reaction of Ag(I) with persulfate produces Ag(II), sulfate radical anion, and sulfate anion. Cross-coupled products can be made through the generation of an alkyl radical by decarboxylation of carboxylic acids via oxidation by Ag(II), followed by addition to electron-deficient heteroarene rings (Scheme 1.4). The resulting Ag(I) can be turned over to Ag(II) by reaction with sulfate radical anion.



Scheme 1.4. Ag-catalyzed radical addition to heteroarene.

1.3.2 Peroxides

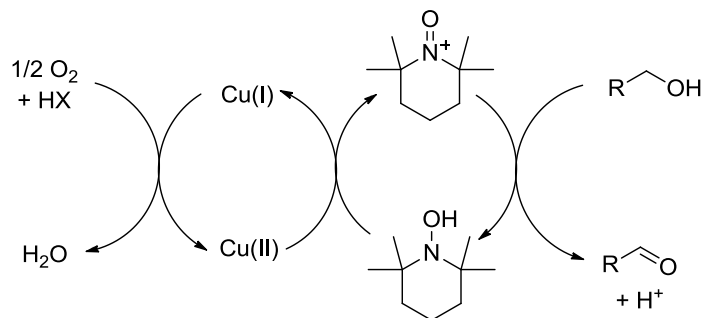
In another attempt to catalyze radical addition to heteroarenes, Minisci found that iron could be coupled with hydrogen peroxide to promote radical formation.¹⁰ Hydrogen peroxide performs a single electron oxidation to produce Fe(III) and a hydroxyl radical, which can abstract a proton from the substrate to produce a radical. Upon addition of the radical to the heteroarene, Fe(III) performs a single electron oxidation to generate the product and regenerate Fe(II) (Scheme 1.5).



Scheme 1.5. Fe-catalyzed radical addition to heteroarene.¹⁰

1.3.3 Molecular oxygen

Oxygen is often used as a cheap source of electrons to turn over catalysts in single electron transfer reactions, either by bubbling through with O₂ gas or simply by exposure to air. It is often used in conjunction with copper, as shown in Scheme 1.6, where Cu(II) promotes the single electron oxidation of TEMPO (2,2,6,6-tetramethylpiperidiny-1-oxyl) or hydroxyl TEMPO to generate Cu(I) and a nitrosonium ion, which can oxidize the alcohol to produce an aldehyde (Scheme 1.6).¹¹ The Cu(II) is regenerated via single electron oxidation of Cu(I) by oxygen. Semmelhack and coworkers showed that this catalytic aerobic system could be used for the oxidation of primary alcohols, including allylic and benzylic alcohols.¹¹

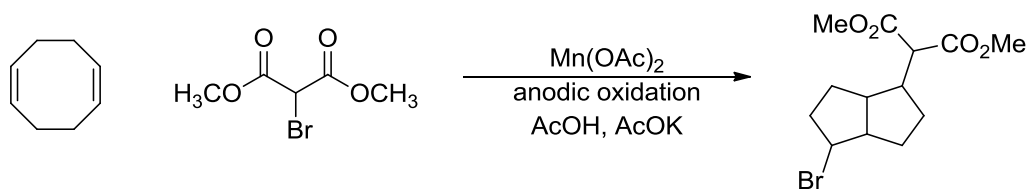


Scheme 1.6. Cu-catalyzed oxidation of alcohols.¹¹

1.3.4 Electrochemical oxidation

A common method of generating or regenerating the active catalyst in a reaction is through the use of electrochemical oxidation. This method was often used in the early development of Mn-catalyzed methods. Nedelec and coworkers showed that they could promote radical addition of dimethyl bromomalonate to olefins via electrochemical regeneration (Scheme 1.7).¹² This reaction is initiated by the electrochemical oxidation of

Mn(II) to produce Mn(III), which is a strong oxidant capable of oxidizing dimethyl bromomalonate to generate a radical. The resulting radical can then add to the olefin to generate the cross-coupled product.



Scheme 1.7. Addition of dimethyl bromomalonate radical to olefins via electrochemical Mn(III) catalysis.¹²

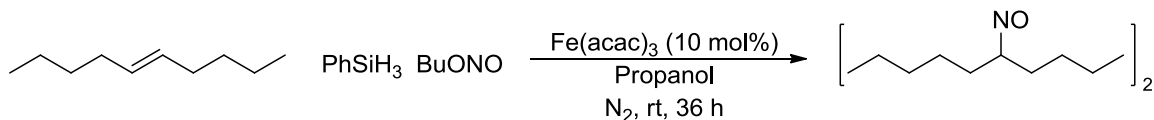
1.4 Metal-catalyzed single electron oxidation

1.4.1. Fe(III) catalysis

Fe(III) salts, which are often used as Lewis acid catalysts, are also efficient single electron oxidants. Stoichiometric quantities of Fe(III) salts can be used for a variety of transformations, an example of which is the oxidative coupling of lithium enolates to generate 1,4-dicarbonyl compounds.^{13,14} Recently, iron has received attention for being a low-toxic and inexpensive substitute for rare metals catalysts, including palladium. While iron is both an economical and pollution-free metal source, the development of iron-catalyzed reactions has been limited.

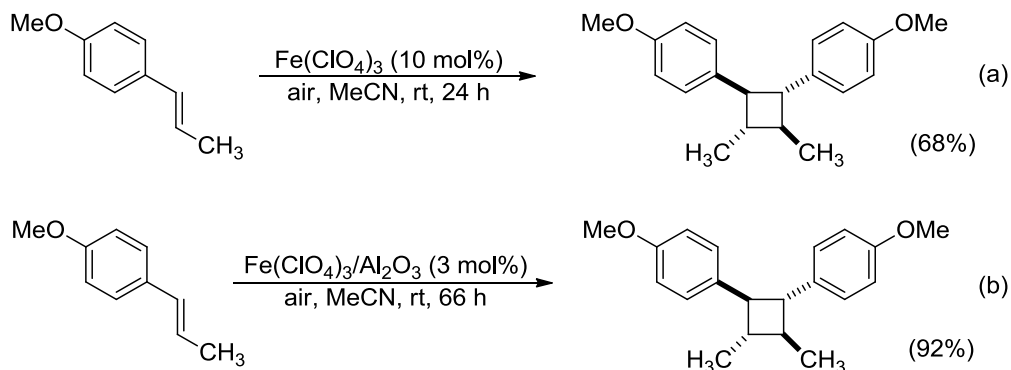
Mukaiyama and coworkers found that tris(acetylaceto)iron(III) (Fe(acac)₃) was an efficient catalyst for the nitrosation of terminal and 1,2-disubstituted olefins to form nitroso alkane dimers (Scheme 1.8).¹⁵ When bubbling N₂ during the course of the reaction, they found that the nitrosation of 5-decene yielded dimer in 73% yield, compared to the reaction without N₂ which yielded dimer in 54%. They hypothesized that

constant bubbling of N₂ replaced nitrogen monoxide, generated by the gradual decomposition of butyl nitrite, which can deactivate the catalyst. This hypothesis was tested by running the nitrosation reaction under nitrogen monoxide, which yielded no product.



Scheme 1.8. Fe(III)-catalyzed nitrosation of olefins to form dimers.¹⁵

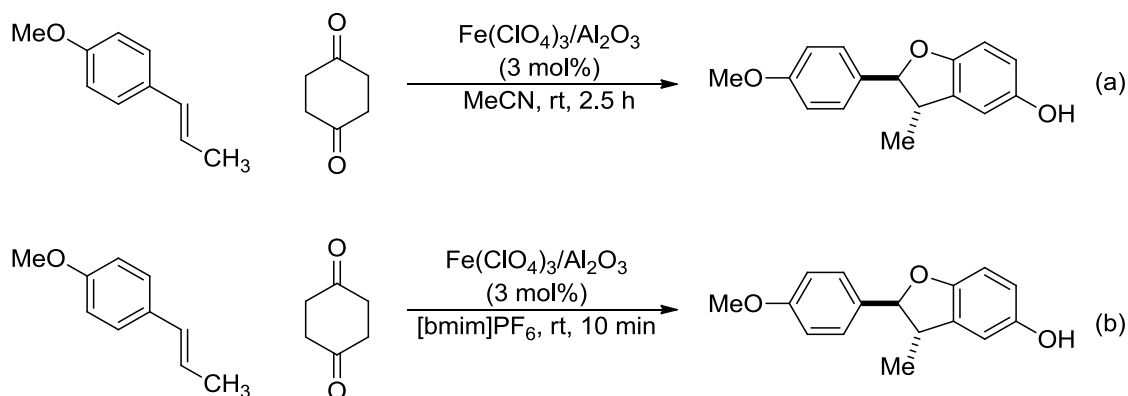
Itoh and coworkers reported a [2+2]-cycloaddition of styrene derivatives using Fe(ClO₄)₃ to produce cyclobutanes with stereospecificity (Scheme 1.9).¹⁶ Alumina supported Fe(III) catalyst gave excellent results, though requiring a long reaction time (Scheme 1.9b). The reaction mechanism involves the oxidation of styrene by Fe(III) to generate a radical cation, which then undergoes dimerization.



Scheme 1.9. Fe(III)-catalyzed [2+2]-cycloaddition of styrene derivatives.¹⁶

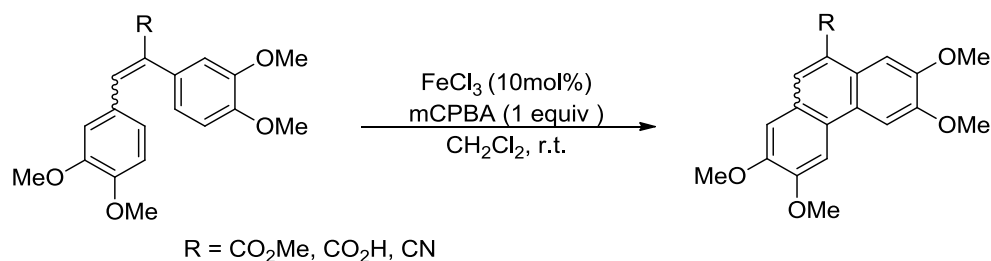
The following year, they reported the synthesis of 2,3-dihydrobenzofuran derivatives through the Fe(III)-catalyzed reaction of styrene derivatives with 1,4-benzoquinone (Scheme 1.10).¹⁷ The cross-coupling reaction proceeded smoothly in MeCN; however, further studies showed that the reaction was greatly accelerated in ionic

liquids. Desired cycloadduct products were obtained in 10 min when run in butylmethylimidazolium hexafluorophosphate as a solvent, compared to 2.5 h when run in MeCN. It is hypothesized that the reaction proceeded more rapidly in the polar solvent system. The proposed reaction mechanism involves the oxidation of styrene by Fe(III) to generate a radical cation and Fe(II). Fe(III) is regenerated by oxidation of Fe(II) by quinone.



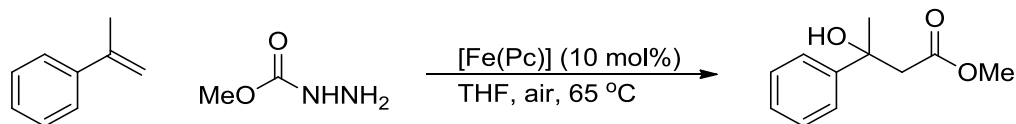
Scheme 1.10. Fe(III)-catalyzed cycloaddition of styrene derivatives with quinone.¹⁷

Wang and coworkers reported a FeCl₃-catalyzed intramolecular oxidative coupling of acceptor-substituted stilbenes, in which meta-chloroperbenzoic acid (mCPBA) is used as the stoichiometric oxidant (Scheme 1.11).¹⁸ They also extended this reaction system to the intermolecular oxidative coupling of 2-naphthols and phenol ether. ESR (electron spin resonance) studies showed the generation of a radical species upon reaction of stilbene with FeCl₃. The proposed reaction mechanism involves the single electron transfer from stilbene to Fe(III), to form a radical cation and Fe(II). The radical cation undergoes electrophilic attack onto another phenyl ring to form a C-C bond. The reduced catalyst is regenerated by reaction with mCPBA.



Scheme 1.11. Fe(III)-catalyzed intramolecular oxidative coupling.¹⁸

Taniguchi and coworkers reported an Fe(III)-catalyzed intermolecular oxidative addition of alkylcarbonyl radicals to alkenes, in which the radicals are generated from carbazates.¹⁹ When using iron(II) phthalocyanine ([Fe(Pc)] in air, cross-coupled products were obtained in good yields (Scheme 1.12). A proposed mechanism for this reaction involves the single electron oxidation of methyl carbazate by Fe(III), which is produced upon oxidation of Fe(II) by molecular oxygen in air.

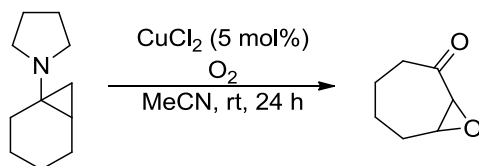


Scheme 1.12. Fe(III)-catalyzed oxidative addition of alkoxy carbonyl radicals to alkenes.¹⁹

1.4.2 Cu(II) catalysis

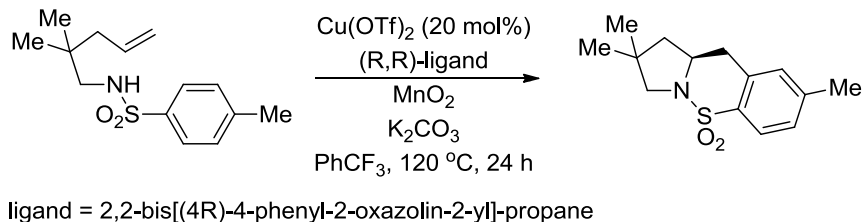
High-valent copper reagents are used in a number of carbon-carbon bond forming reactions. Copper-catalyzed processes can be found in a number of chemical disciplines ranging from material science to biochemistry to organic synthesis. Itoh and coworkers reported a CuCl₂-catalyzed oxygenation of bicyclic bridgehead cyclopropylamines to cyclic epoxy ketones (Scheme 1.13).²⁰ The reaction was performed under constant bubbling of oxygen over the course of 24 hours. When performing ESR studies, they

found that equimolar addition of cyclopropylamine to a solution of CuCl_2 cleanly quenches the Cu(II) paramagnetic signals. Based on this result, Itoh suggests the occurrence of a single electron transfer reaction from cyclopropylamine to Cu(II) . The single electron oxidation of the tertiary amine to generate a cyclopropylamine radical cation results in facile ring opening of the cyclopropyl functionality. The resulting Cu(I) can be regenerated to Cu(II) by O_2 .



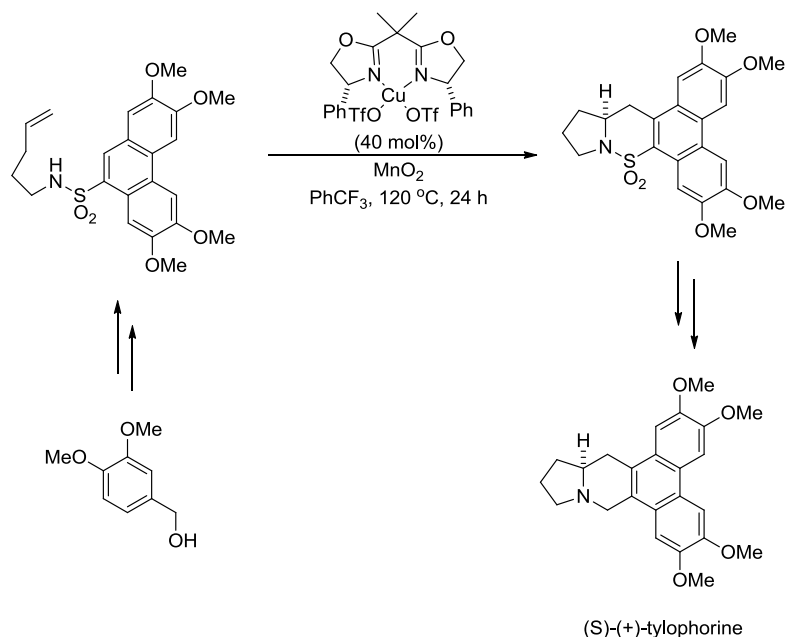
Scheme 1.13. Cu(II) -catalyzed oxygenolysis of cyclopropylamines to epoxy ketones.²⁰

Chemler and coworkers reported a number of methods on Cu -mediated cyclization of amides.^{21–23} In their first catalytic report, they developed a Cu(II) -catalyzed asymmetric carboamination reaction that involves intramolecular addition of arylsulfonamides across terminal alkenes to provide chiral sultams (Scheme 1.14).²⁴ Carboamination reactions that are stoichiometric in Cu(II) often form Cu(0) , likely caused by the disproportionation of Cu(I) to Cu(II) and Cu(0) . They proposed that ligands on the copper would stabilize Cu(I) and Cu(II) in preference to Cu(0) in the catalytic reaction. In addition, a number of stoichiometric oxidants were screened, including O_2 , MnO_2 , PhI(OAc)_2 , and oxone. Of these, MnO_2 , which functions as a stoichiometric oxidant for the resulting Cu(I) , provided the highest conversion of starting material.



Scheme 1.14. Cu(II)-catalyzed enantioselective intramolecular carboamination of alkenes.²⁴

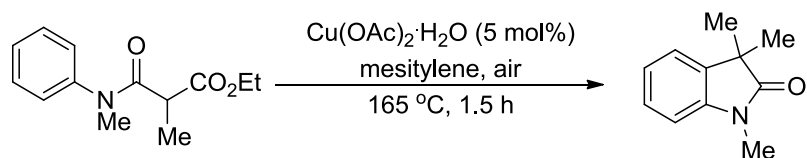
The following year, the same group also applied their method to an eight step total synthesis of (*S*)-(+)-tylophorine, a cancer cell growth inhibitor, from the commercially available 3,4-dimethoxybenzyl alcohol (Scheme 1.15).²⁵



Scheme 1.15. Total synthesis of (*S*)-(+)-tylophorine via enantioselective intramolecular alkene carboamination.²⁵

In 2009, a stoichiometric Cu(II)-mediated route to oxindoles from intramolecular coupling of anilides was developed.²⁶ A similar reaction was developed by the Kundig group the same year using CuCl₂.²⁷ The following year, the Taylor group showed that

these cyclization reactions can be carried out using Cu(II) in catalytic quantities by utilizing a stoichiometric oxidant in the form of atmospheric oxygen (Scheme 1.16).²⁸



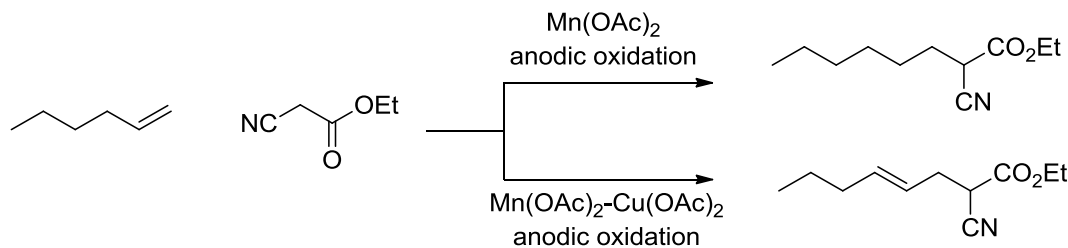
Scheme 1.16. Cu(II)-catalyzed synthesis of oxindoles via C-H activation.²⁸

1.4.3 Mn(III) catalysis

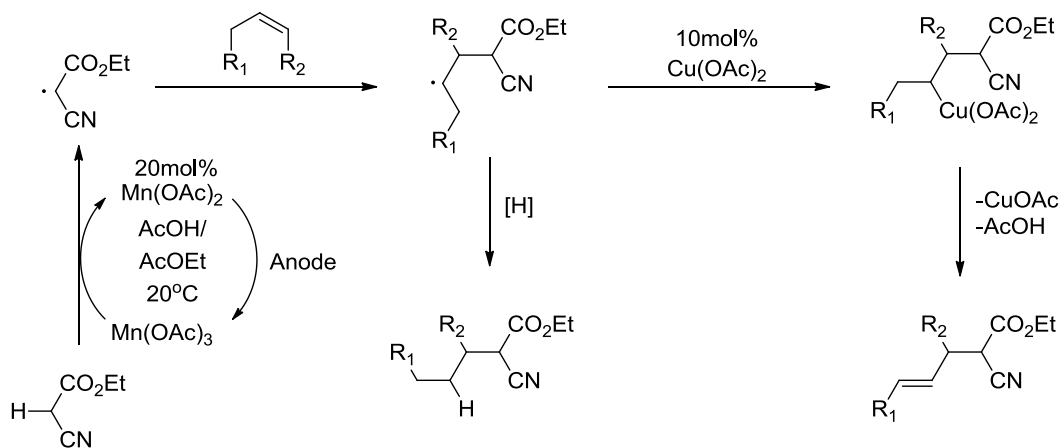
Manganese(III) acetate is the most frequently used Mn(III) oxidant in organic synthesis.²⁹ A large majority of stoichiometric Mn(III)-mediated reactions involve intramolecular cyclizations, occurring through single electron oxidation of dicarbonyl substrates. While Mn(III) salts such as Mn(OAc)₃ have high potential for use in oxidative coupling reactions, their use is limited due to their instability and requirement of at least 2 stoichiometric equivalents based on substrates in synthetic reactions. As a result of these limitations, a number of methods were developed involving Mn(III) catalysis coupled with electrochemical regeneration.

Nishiguchi and coworkers showed that anodic oxidation of Mn(OAc)₂·4H₂O in the presence of olefins and ethyl cyanoacetate resulted in cross-coupling.³⁰ When run in the presence of catalytic amount of Cu(OAc)₂, unsaturated cross-coupling products were obtained (Scheme 1.17). The proposed mechanism of this reaction involves the electrochemical oxidation of Mn(II) to Mn(III), followed by single electron oxidation of ethyl cyanoacetate to produce a methane radical and Mn(II) (Scheme 1.18). Addition of the radical to the olefin produces a subsequent radical, which can abstract a hydrogen

from solvent to generate product. However, in the presence of Cu(II), further oxidation of the resulting addition radical, followed by β -elimination can generate the unsaturated product (Scheme 1.18).



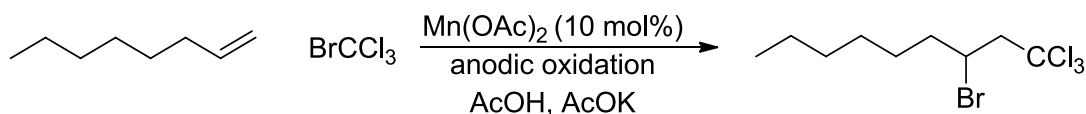
Scheme 1.17. Electrochemical Mn(III)-catalyzed carbon-carbon bond formation.³⁰



Scheme 1.18. Proposed mechanism of electrochemical Mn(III)-catalyzed carbon-carbon bond formation.

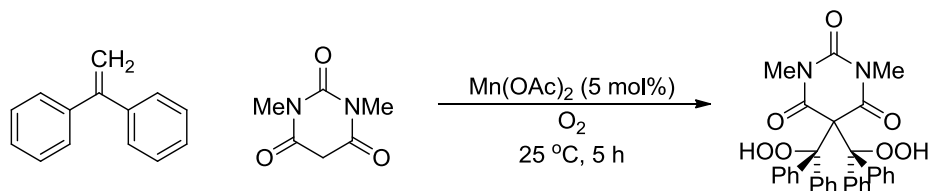
Nedelec and coworkers found that combining electrochemically generated Mn(III) with dimethyl bromomalonate and olefins resulted in efficient free-radical chain addition, as described in Section 1.3.4.¹² The following year, they reported a Mn(III)-catalyzed electrochemical C-C bond formation involving radical addition of polyhalomethanes to olefins (Scheme 1.19).³¹ This research was an extension of earlier

studies, in which dialkyl bromomalonate radicals add to olefins. The Mn(III) in this reaction is formed through constant anodic oxidation of Mn(II).



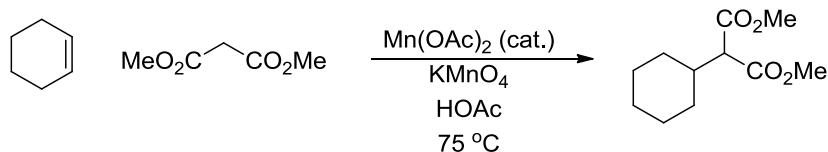
Scheme 1.19. Mn(III)-catalyzed radical addition of polybromomethane to olefin.³¹

Kurosawa and coworkers reported the reaction of 1,1-disubstituted ethenes with barbituric acid derivatives in the presence of Mn(OAc)₂ and air to yield addition products (Scheme 1.20).³² The reaction produced similar yield when using Mn(OAc)₃, but performed poorly with substitution of the catalyst for ceric ammonium nitrate. The proposed reaction mechanism involves the oxidation of Mn(II) by the molecular oxygen in air to produce Mn(III), which can oxidize the ethane to produce a radical that adds to barbituric acid.



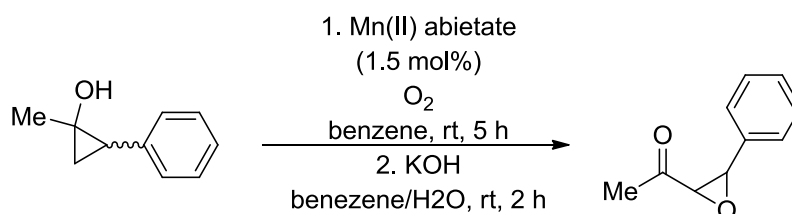
Scheme 1.20. Mn-catalyzed hydroperoxyalkylations of barbituric acid derivatives.³²

The Linker group reported a dimethyl malonate radical addition to olefins to synthesize diesters, in which Mn(III) catalysis was coupled with the use of potassium permanganate as a stoichiometric oxidant (Scheme 1.21).³³



Scheme 1.21. Mn(III)-catalyzed radical addition of dimethyl malonate to olefins.³³

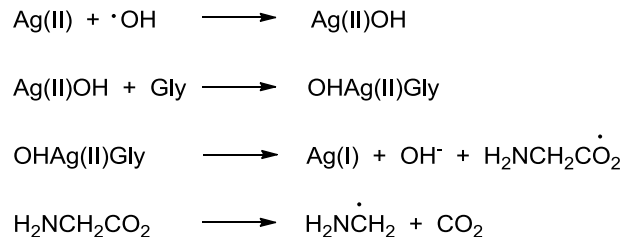
The Kulinkovich group prepared a number of aliphatic and arylaliphatic α,β -epoxy ketones by Mn-catalyzed ring cleavage of 1-substituted and 1,2-disubstituted cyclopropanols with oxygen, followed by dehydration of the resulting cyclic peroxides with base (Scheme 1.22).³⁴ The oxidation of cyclopropanols was performed by stirring in solutions of benzene under an oxygen atmosphere in the presence of Mn(II) abietate or Mn(II) acetylacetonate, followed by treatment with aqueous potassium hydroxide.



Scheme 1.22. Mn-catalyzed synthesis of α,β -epoxy ketones from cyclopropanols.³⁴

1.4.4 Ag(II) catalysis

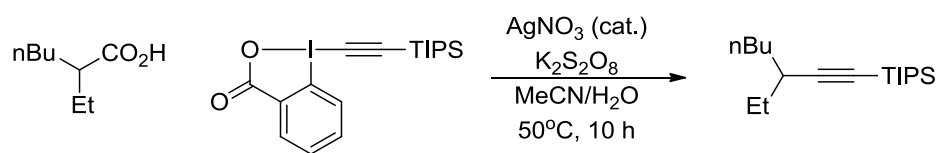
High-valent silver intermediates represent a class of catalysts capable of performing single electron oxidation of a number of substrates due to their high redox potentials. The oxidation of glycine by Ag(II) was investigated by the Neta group.³⁵ Ag(II) was produced in irradiated aqueous solutions by the reaction of Ag(I) with hydroxyl radicals (Scheme 1.23). Kinetic studies showed that glycine complexes to the metal before undergoing single electron oxidation to produce Ag(I) and radical.



Scheme 1.23. Ag-catalyzed oxidation of glycine.³⁵

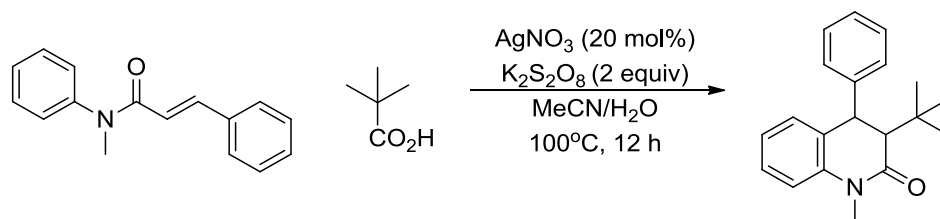
Oxidations by silver in conjunction with persulfate encompass the bulk of Ag(II)-catalyzed oxidations. In addition, this oxidative system is often used for the decarboxylation of carboxylic acids, as shown in the Minisci reaction described in Section 1.3.1.⁹ Much of this research will be presented in Chapters 2 and 3. In this section, examples from the last three years will be presented.

Recently, Li and coworkers developed a silver-catalyzed decarboxylative alkylation of carboxylic acids in aqueous solution (Scheme 1.24).³⁶ In the presence of silver nitrate and potassium persulfate, aliphatic carboxylic acids underwent decarboxylative alkylation with ethynylbenziodoxolones, in particular the triisopropylsilyl(TIPS)-substituted derivative.



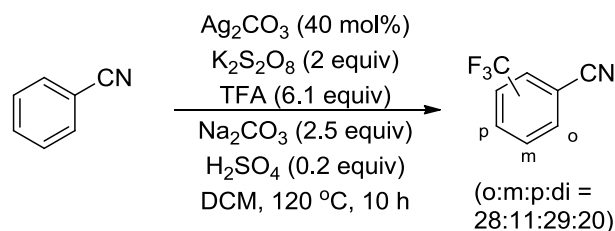
Scheme 1.24. Ag-catalyzed decarboxylative alkylation.³⁶

Mai and coworkers used similar reaction conditions for the decarboxylative 6-endo-trig radical cyclization of *N*-arylcinnamamides (Scheme 1.25).³⁷ Later that year, they expanded this method to the synthesis of 3-acyl-4-arylquinolin-2(1*H*)-ones.³⁸



Scheme 1.25. Tandem radical addition/cyclization via silver catalysis.³⁷

The traditional Minisci reaction was expanded to perform trifluoromethylations.³⁹ The Zhang group found that trifluoroacetic acid was an efficient source of trifluoromethyl radicals, which could add to various arenes (Scheme 1.26). A mixture of mono- and di-substituted products was obtained.



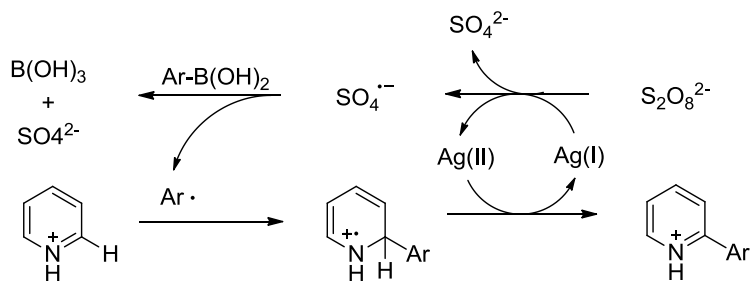
Scheme 1.26. Trifluoromethylation of arenes with TFA via silver catalysis.³⁹

In 2010, Baran and coworkers developed a variation on the Minisci reaction, involving the coupling of various arylboronic acids with several heteroarenes to generate 2-pyridyl products, as shown in Scheme 1.27.⁴⁰ Their reaction involved the addition of a catalytic amount of silver nitrate and an excess of potassium persulfate in a heterogeneous system requiring 1:1 parts water:organic solvent. Halfway through the reaction, a second addition of 20 mol% silver nitrate and 3 equivalents of potassium persulfate are required to obtain the product in 81% isolated yield. In addition, the reaction was done in an open flask which was exposed to air.



Scheme 1.27. Reaction conditions for oxidative addition of arylboronic acid to heteroarene.⁴⁰

They proposed a reaction mechanism which involved the reduction of persulfate to form a sulfate radical anion and Ag^{2+} . They suggested that it is the sulfate radical anion that oxidizes the arylboronic acid to form an aryl radical, which then adds to the heteroarene (Scheme 1.28). Work done in our group on this reaction has led to the proposal that $\text{Ag}(\text{II})$ performs a single electron oxidation of the boronic acid to generate an aryl radical. The mechanism of this reaction will be the subject of Chapter 2.



Scheme 1.28. Proposed mechanism involving oxidative addition of arylboronic acid to heteroarene.

1.4.5 Photoredox catalysis

Visible light-mediated photoredox catalysis represents a relatively new class of reagents that can transform substrates via single electron transfer. These transformations can be performed using both ruthenium and iridium catalysts, where the ligands bound to the metal centers can change the redox properties of the catalysts (Figure 1.1).⁴¹ The most

commonly used of these reagents is $\text{Ru}(\text{bpy})_3\text{Cl}_2$, which is a versatile photoredox catalyst due to its ease of synthesis and overall stability.^{42,43} It has had applications in energy storage,⁴⁴ photoinduced water splitting,⁴⁵ and photovoltaic cells.⁴⁶ Despite its applications, photoredox chemistry has only recently gained widespread recognition within the synthetic organic community.⁴⁷

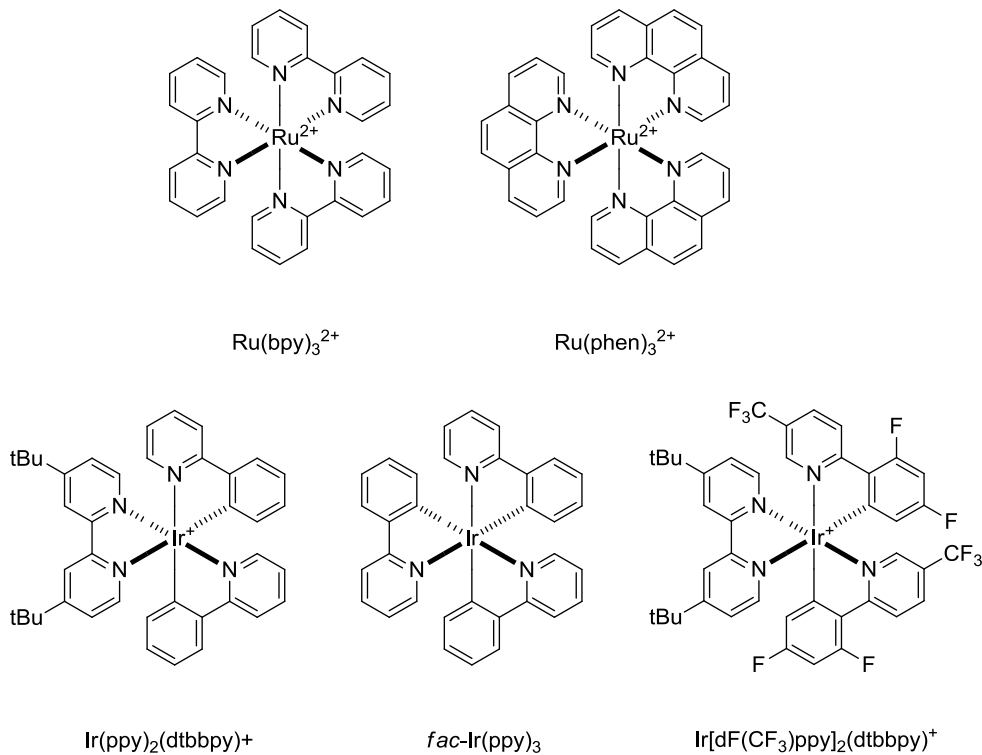
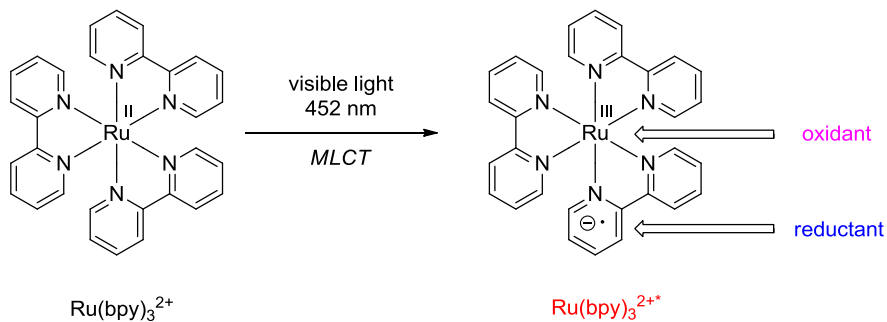


Figure 1.1. Examples of commonly used photoredox catalysts in organic synthesis.

Light-promoted chemical synthesis must first begin with the excitation of a photon by the catalyst, which generates a high energy excited state species. Irradiation of $\text{Ru}(\text{bpy})_3^{2+}$ with visible light ($\lambda = 452\text{nm}$) excites the photocatalyst to $\text{Ru}^*(\text{bpy})_3^{2+}$, through metal to ligand charge transfer (MLCT). When this occurs, the metal center of

the excited state complex functions as an oxidant, and the ligand functions as a reductant, as shown in Scheme 1.29.



Scheme 1.29: Excitation of $\text{Ru}(\text{bpy})_3^{2+}$ to $\text{Ru}^*(\text{bpy})_3^{2+}$ using visible light.

The excited state intermediate can easily be reduced or oxidized by going through the reductive quenching cycle or the oxidative quenching cycle to generate $\text{Ru}(\text{bpy})_3^+$ or $\text{Ru}(\text{bpy})_3^{3+}$, respectively. The reduction of $\text{Ru}(\text{bpy})_3^{2+}$ to $\text{Ru}(\text{bpy})_3^+$ generates a strong reducing agent, while the oxidation to $\text{Ru}(\text{bpy})_3^{3+}$ generates a strong oxidant, as shown in Figure 1.2.

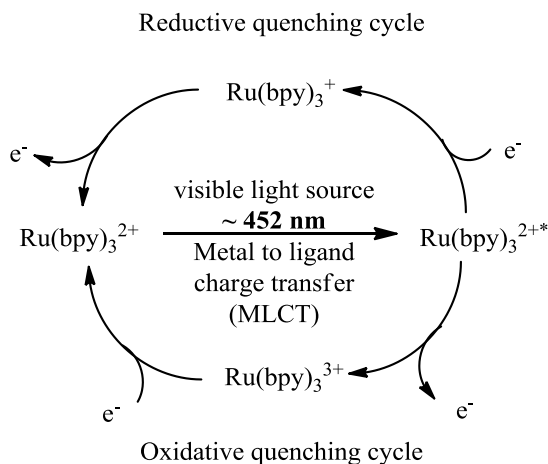
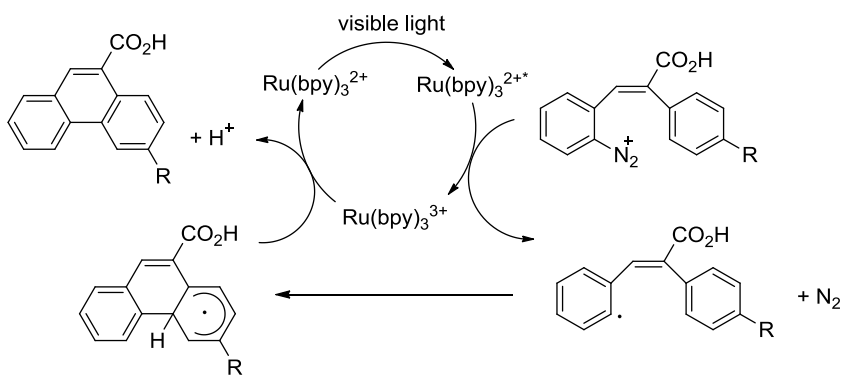


Figure 1.2 Reductive and oxidative quenching cycle of $\text{Ru}(\text{bpy})_3^{2+*}$.

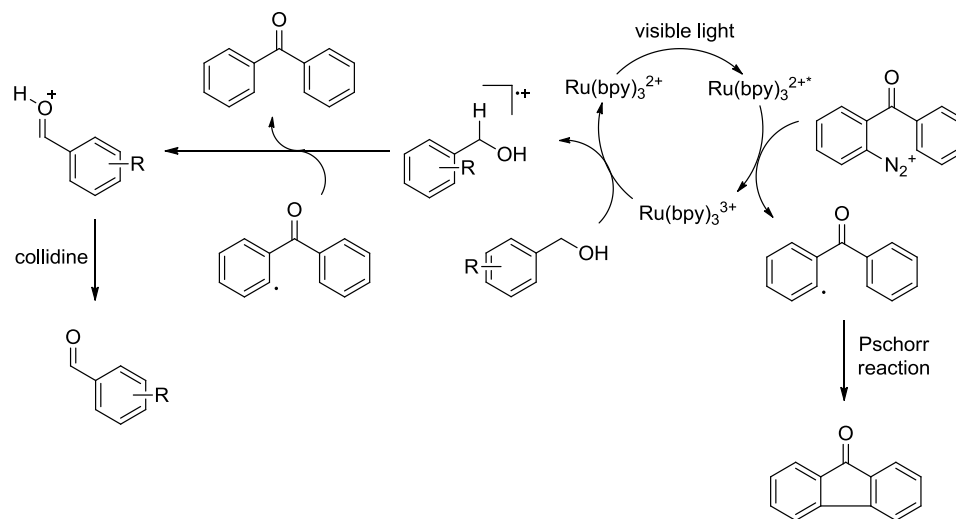
The $\text{Ru}(\text{bpy})_3^{3+}$ intermediate can be utilized to perform single electron oxidations of organic substrates. Various oxidants can be used to transform $\text{Ru}(\text{bpy})_3^{2+}$ to $\text{Ru}(\text{bpy})_3^{3+}$, including persulfates, aromatic nitro groups, various viologens, and iron(III) salts.

In 1984, Cano-Yelo and Deronzier developed a reaction involving the transformation of aryldiazonium compounds to phenanthrenes in a photocatalytic Pschorr reaction using $\text{Ru}(\text{bpy})_3^{2+}$ as the photocatalyst.⁴⁸ They found that the Pschorr reaction took place with high quantum yield upon photoexcitation of a catalytic amount of $\text{Ru}(\text{bpy})_3^{2+}$. This allowed them to suggest that the reaction proceeded at least in part by a photo-induced electron transfer process. Diazonium tetrafluoroborate salts absorb light strongly in acetonitrile. When the substrates were irradiated with light in the absence of the photocatalyst, they obtained the Pschorr reaction product in only 10-20% yields. However, in the presence of $\text{Ru}(\text{bpy})_3^{2+}$, the phenanthrene product was obtained in 100% yield. Their proposed mechanism is shown in Scheme 1.30.



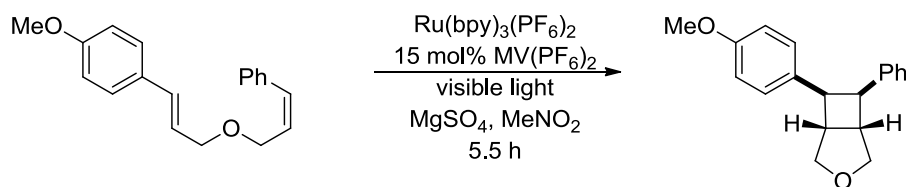
Scheme 1.30. Proposed reaction mechanism for the transformation of aryldiazonium salts to phenanthrenes using $\text{Ru}(\text{bpy})_3^{2+}$.⁴⁸

They then developed a reaction involving the oxidation of benzylic alcohols to aldehydes, in which the Pschorr reaction was used to oxidize the excited state of $\text{Ru}(\text{bpy})_3^{2+*}$ to generate $\text{Ru}(\text{bpy})_3^{3+}$ (Scheme 1.31).⁴⁹



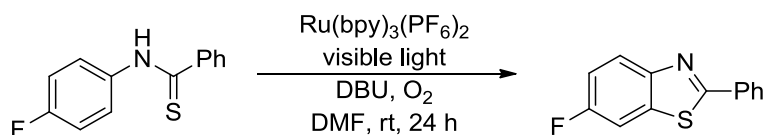
Scheme 1.31. Proposed reaction mechanism for the oxidation of benzylic alcohols to aldehydes using RuL_3^{2+} .⁴⁹

Yoon and workers explored [2+2] cycloadditions by oxidative photocatalysis. Once exposed to visible light, $\text{Ru}(\text{bpy})_3^{2+}$ is converted to the excited state, $\text{Ru}^*(\text{bpy})_3^{2+}$, which can react with methyl viologen (MV^{2+}), an electron acceptor to produce $\text{Ru}(\text{bpy})_3^{3+}$.⁵⁰ The higher oxidation state can oxidize electron-rich styrenes to generate a radical cation that can undergo [2+2] cycloaddition (Scheme 1.32). They showed that a bis(styrene) can undergo efficient intramolecular cycloaddition in the presence of catalytic $\text{Ru}(\text{bpy})_3^{2+}$ and methyl viologen upon irradiation by visible light.



Scheme 1.32. Photoredox-catalyzed [2+2] cycloaddition.⁵⁰

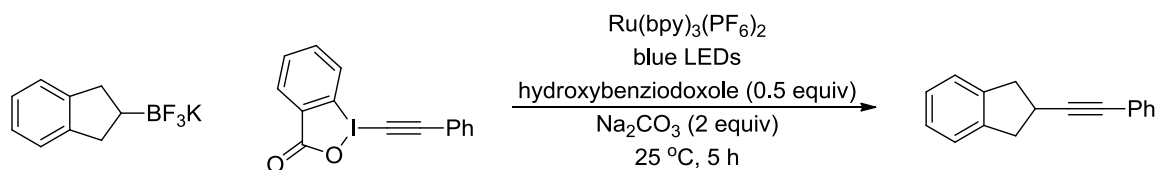
The Li group has developed an aerobic visible-light photoredox synthesis of 2-substituted benzothiazoles (Scheme 1.33).⁵¹ They reported a green reaction mixture at the beginning of the reaction, an observation they claim is consistent with the formation of $\text{Ru}(\text{bpy})_3^{3+}$, via oxidation of $\text{Ru}^*(\text{bpy})_3^{2+}$ by molecular oxygen. A proposed reaction mechanism involves the deprotonation of thioanilide to form an anion, which is then reduced to form a radical via single electron oxidation by $\text{Ru}(\text{bpy})_3^{3+}$. While an oxidative quenching mechanism is proposed for this reaction, a reductive quenching mechanism cannot be ruled out, in which $\text{Ru}^*(\text{bpy})_3^{2+}$ is reduced to $\text{Ru}(\text{bpy})_3^+$ by the benzothiazole anion, followed by regeneration of $\text{Ru}(\text{bpy})_3^{2+}$ through oxidation of $\text{Ru}(\text{bpy})_3^+$ by molecular oxygen.



Scheme 1.33. Photoredox-catalyzed synthesis of 2-substituted benzothiazoles.⁵¹

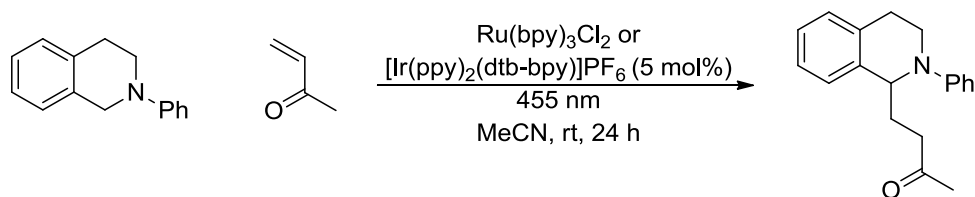
The Chen group presented a visible-light-mediated deboronative alkylation, in which the mild oxidant hydroxybenziodoxole (BI-OH) mediated the reaction (Scheme 1.34).⁵² Primary, secondary, and tertiary alkyl trifluoroborates or boronic acids could be used. Luminescence quenching studies showed a decrease of $\text{Ru}(\text{bpy})_3(\text{PF}_6)_2$

luminescence in the presence of BI-OH, but not in the presence of trifluoroborates or BI-alkyne. This suggests that BI-OH interacts with $\text{Ru}^*(\text{bpy})_3^{2+}$ to produce $\text{Ru}(\text{bpy})_3^{3+}$.



Scheme 1.34. Photoredox induced deboronative alkylation.⁵²

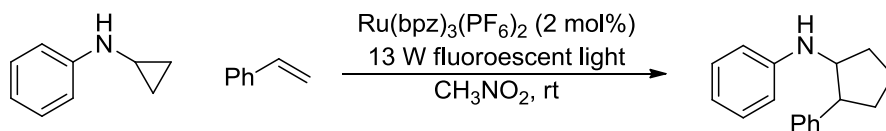
In addition to utilizing the high-valent Ru^{3+} oxidation state, the Ru^{*2+} complex is also capable of generating radicals and radical cations through single electron oxidation. Reiser and coworkers reported the coupling of tertiary amines and α,β -unsaturated carbonyl compounds in conjugate additions (Scheme 1.35).⁵³ In addition to $\text{Ru}(\text{bpy})_3^{2+}$, $[\text{Ir}(\text{ppy})_2(\text{dtb-bpy})]\text{PF}_6$ was also tested as a photocatalyst, which proved to be more effective in some cases. The excited $\text{Ru}^*(\text{bpy})_3^{2+}$ can oxidize the tertiary amine to generate a radical cation and $\text{Ru}(\text{bpy})_3^+$. Upon loss of a proton, the radical can add to the unsaturated compound. The resulting radical can oxidize $\text{Ru}(\text{bpy})_3^+$ to regenerate $\text{Ru}(\text{bpy})_3^{2+}$.



Scheme 1.35. Photoredox-catalyzed addition of α -amino radicals to Michael acceptors.⁵³

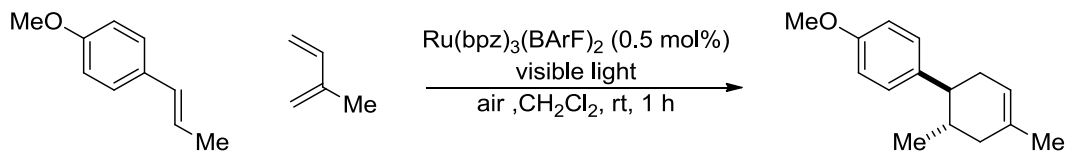
Zheng and coworkers reported an intermolecular [3+2] cycloaddition of olefins with mono- and bicyclic cyclopropylanilines via visible light photocatalysis (Scheme 1.36).⁵⁴ The excited $\text{Ru}^*(\text{bpy})_3^{2+}$ can oxidize the cyclopropylamine to generate a radical

cation and $\text{Ru}(\text{bpy})_3^+$. After ring opening, the resulting β -carbon radical iminium ion can add to the olefin. The resulting radical can oxidize $\text{Ru}(\text{bpy})_3^+$ to regenerate $\text{Ru}(\text{bpy})_3^{2+}$.



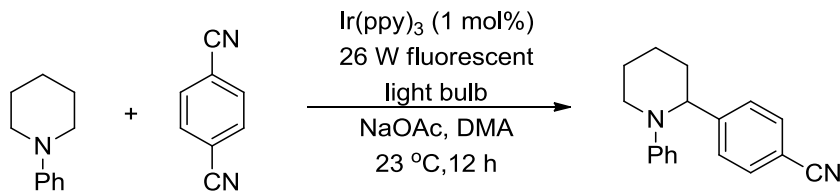
Scheme 1.36. Photoredox-catalyzed [3+2] cycloaddition of cyclopropylamines with olefins.⁵⁴

The Yoon group expanded the photocatalytic [2+2] cycloadditions to radical cation Diels-Alder cycloadditions (Scheme 1.37).⁵⁵ The excited state $\text{Ru}^*(\text{bpy})_3^{2+}$ can oxidize anethole to produce a radical cation, which is activated toward [4+2] cycloaddition.



Scheme 1.37. Photoredox-catalyzed radical cation Diels-Alder cycloadditions.⁵⁵

The MacMillan group found that they could utilize photoredox catalysis for α -amino C-H arylation reaction (Scheme 1.38).⁵⁶ Their proposed mechanism involves the single electron reduction of the arene by $\text{Ir}^*(\text{III})$ to generate an arene radical anion and $\text{Ir}(\text{IV})$, which is a strong oxidant. $\text{Ir}(\text{IV})$ can then oxidize the amine to generate a radical cation. Following radical coupling and loss of a CN^- , the cross-coupling product is generated.



Scheme 1.38. Photoredox-catalyzed α -amino C-H arylation.⁵⁶

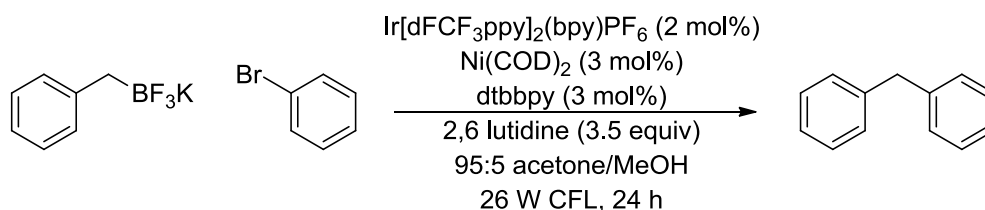
Akita and coworkers reported the first photocatalytic generation of alkyl, allyl, benzyl, and aryl radicals via oxidation of organoborates.⁵⁷ This method was applied to the catalytic coupling of organoborates with TEMPO and olefins containing electron-withdrawing groups. The following year, they showed that their method could be expanded to the hydroalkoxymethylation of electron-deficient alkenes (Scheme 1.39).⁵⁸ A proposed reaction mechanism involves single electron oxidation of the organotrifluoroborate by Ir*(III) to produce an alkoxymethyl radical and Ir(II), followed by radical addition to the olefin.



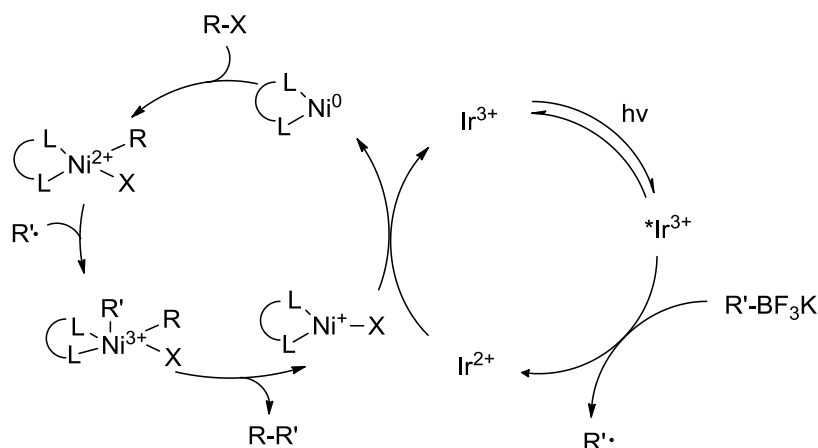
Scheme 1.39. Photoredox-catalyzed hydroalkoxymethylation of electron-deficient alkenes.⁵⁸

The Molander group presented a photoredox cross-coupling method where visible light photoredox catalysis was coupled with nickel catalysis.⁵⁹ This dual catalysis allowed for the cross-coupling of potassium alkoxyalkyl- and benzyltrifluoroborates with a number of aryl bromides under mild reaction conditions (Scheme 1.40). The combination of Ni(0) and aryl halide results in rapid oxidative addition, generating a Ni(II) intermediate (Scheme 1.41). The single electron oxidation of organotrifluoroborates by

Ir*(III) generates Ir(II) and an alkyl radical. Capture of the alkyl radical by Ni(II) can generate a Ni(III) intermediate, which can undergo reductive elimination to produce the cross-coupled product and Ni(I). Reduction of this species by the resulting Ir(II) complex regenerates both Ni(0) and Ir(III). The MacMillan group also presented a similar method where aryl halides were coupled to amino acids as well as substituted carboxylic acids via photoredox/nickel dual catalysis.⁶⁰



Scheme 1.40. Single electron transmetalation in photoredox/nickel cross-coupling.⁵⁹

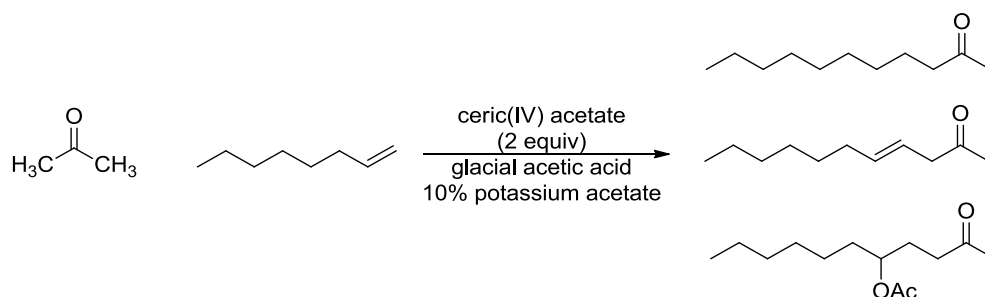


Scheme 1.41. Proposed mechanism for single electron transmetalation in photoredox/nickel cross-coupling

1.4.7 Ce(IV) catalysis

One of the first examples of Ce(IV)-mediated carbon-carbon formation was performed by Heiba and coworkers in the early 1970s (Scheme 1.42).⁶¹ They found that

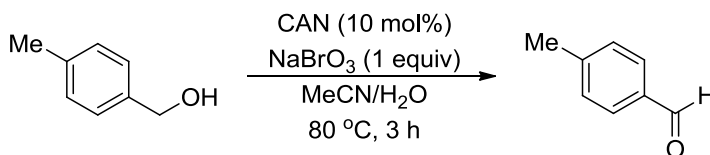
enolizable ketones could react with olefins in the presence of metal oxidants such as Mn(III), Cu(II), and Ce(IV). Reaction of 1-octene in excess acetone with 2 equivalents of Ce(IV) salt produced three products, including the saturated ketone undecanone, an unsaturated ketone, and a keto acetate.



Scheme 1.42. Ce(IV)-mediated carbon-carbon bond formation.⁶¹

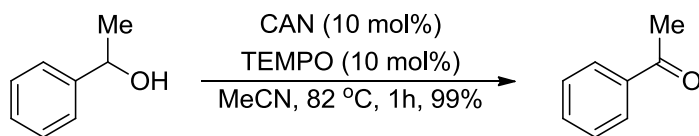
Although Ce(IV) is an effective oxidant for a diverse range of substrates, a major disadvantage of its use is the need for large amount of Ce(IV)-containing reagents due to their high molecular weights (eg. CAN, MW = 548 g/mol). As a result, a number of catalytic Ce(IV) methods have been developed, in which the resulting Ce(III) is converted to Ce(IV) through the addition of a stoichiometric oxidant.⁶²

One of the earliest examples in which CAN was used as a catalytic oxidant was shown by the Ho group (Scheme 1.43).⁶³ In this reaction, Ce(IV) is made catalytic by reoxidation of *in situ* generated Ce(III) by the bromate ion.

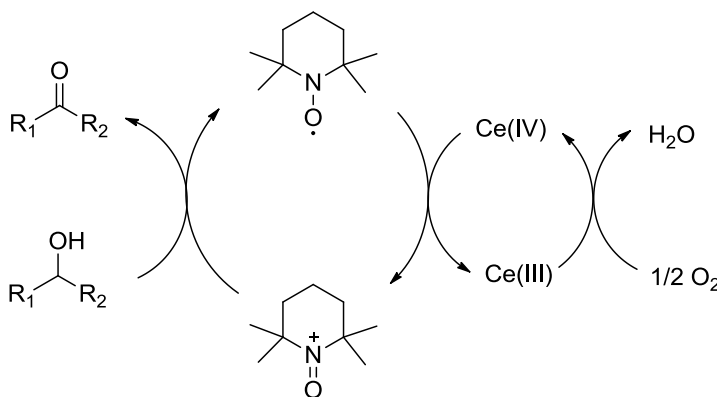


Scheme 1.43. Ce(IV)-catalyzed oxidation of alcohols in a dual oxidant system.⁶³

The Kim group explored the catalytic oxidation of alcohols to produce aldehydes and ketones by coupling CAN catalysis with TEMPO catalysis.⁶⁴ Primary benzylic alcohols reacted smoothly in 2.5 hours to give the corresponding aldehydes. However, secondary benzylic alcohols oxidized much faster, as shown in Scheme 1.44. The mechanism of oxidation is proposed to involve oxidation of TEMPO by Ce(IV) to produce the N-oxoammonium cation and Ce(III), respectively. The cation can oxidize the alcohol to give the carbonyl, and the Ce(IV) can be regenerated by oxidation of Ce(III) by molecular oxygen (Scheme 1.45).



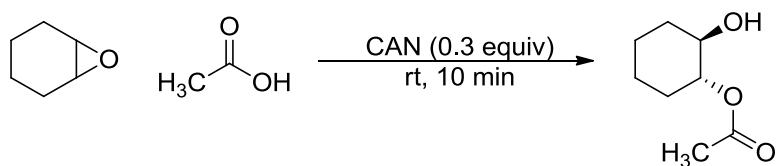
Scheme 1.44. Aerobic oxidation of benzylic alcohols catalyzed by CAN/TEMPO.⁶⁴



Scheme 1.45. Proposed mechanism for the oxidation of benzylic alcohols via CAN/TEMPO catalysis.

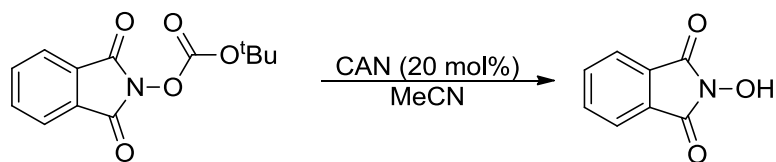
The Iranpoor group investigated the possibility of using Ce(IV) as a catalyst for the regio- and stereoselective ring opening of epoxides in the presence of various nucleophiles.⁶⁵ Reactions of epoxides, in particular cyclohexene oxide, in acetic acid with

catalytic quantities of Ce(IV) occurred rapidly at room temperature (Scheme 1.46). Various other substrates reacted with good yields under reflux conditions. The reaction mechanism is hypothesized to occur via oxidation of the epoxide by Ce(IV) to generate a radical cation and Ce(III), respectively. The radical cation can undergo nucleophilic attack by acetic acid, followed by ring opening to generate a second radical cation. Ce(IV) can be regenerated by single electron transfer from Ce(III) to the radical cation.



Scheme 1.46. CAN-catalyzed epoxide opening.⁶⁵

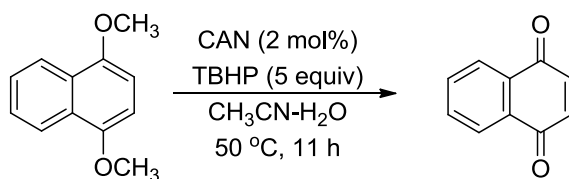
Hwu and coworkers investigated the use of CAN as a catalyst for the efficient removal of the t-BOC group from amino acids and related compounds (Scheme 1.47).⁶⁶ A proposed mechanism for the removal of the t-BOC group involves oxidation of the carbonyl group by Ce(IV) to produce the corresponding radical cation and Ce(III). The radical cation can then fragment to give t-butyl cation and carboxylate radical, which can turn over Ce(III) to Ce(IV) by single electron transfer.



Scheme 1.47. CAN-catalyzed deprotection of t-butoxycarbonyl compounds.⁶⁶

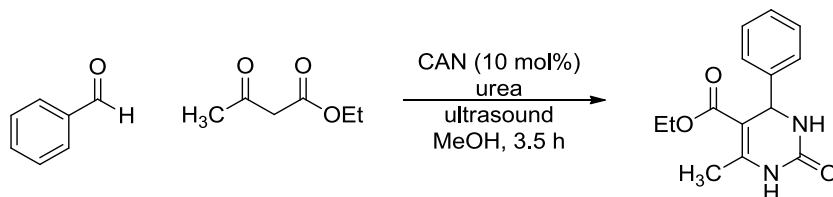
Krohn and coworkers examined the CAN-catalyzed oxidation of hydroquinones and hydroquinone monomethyl ethers to quinones using t-butyl hydroperoxide as the

stoichiometric oxidant (Scheme 1.48).⁶⁷ The mechanism is thought to occur via two successive electron transfer processes from the electron-rich hydroquinone to Ce(IV).



Scheme 1.48. CAN-catalyzed oxidation of hydroquinones.⁶⁷

The Yadav group explored an ultrasound-accelerated three component condensation of aldehyde, β -ketoester, and urea in the presence of CAN to produce dihydropyrimidinones (Scheme 1.49).⁶⁸ A variety of aromatic, aliphatic, and heterocyclic aldehydes were tested.



Scheme 1.49. CAN-catalyzed cyclocondensation using ultrasound.⁶⁸

1.5 Project goals

In addition to the variety of catalysts capable of performing single electron oxidations, a number of substrates can undergo these reactions. This dissertation focuses on the silver-catalyzed oxidation of arylboronic acids and aliphatic carboxylic acids. Chapters 2-5 of this dissertation present research on the following topics involving metal-catalyzed single electron oxidation: 1) the mechanistic study of silver-catalyzed cross-coupling of arylboronic acids with pyridine; 2) the mechanistic study of silver-catalyzed

cross-coupling of arylboronic acids with quinone; 3) the mechanistic study of silver-catalyzed decarboxylative fluorination in aqueous media; and 4) the development and mechanistic study of silver-catalyzed decarboxylative fluorination in organic media through the use of N-containing ligands.

1.6 References

- (1) Faraday, M. "Experimental Researches in Electricity. Seventh Series" *Phil Trans. Royal Soc. London.* **1834**, *124*, 77-122.
- (2) Kolbe, H. *Ausführliches Lehrbuch der Organischen Chemie*, Vol. 1, Braunschweig, Viewig und Sohn, 1854.
- (3) Vijh, A. K.; Conway, B. E. *Chem. Rev.* **1967**, *67*, 623–664.
- (4) Walling, C.: *Free Radicals in Solution*, p 581, New York, Wiley, 1957.
- (5) Jahn, U. *Top. Curr. Chem.* **2012**, *320*, 323–452.
- (6) Jahn, U. *Top. Curr. Chem* **2012**, *320*, 191–322.
- (7) Jahn, U. *Top. Curr. Chem* **2012**, *320*, 121–190.
- (8) Anderson, J. M.; Kochi, J. K. *J. Am. Chem. Soc.* **1970**, *92*, 1651–1659.
- (9) Minisci, F.; Bernardi, R.; Bertini, F.; Galli, R.; Perchinummo, M. *Tetrahedron.* **1971**, *27*, 3575–3579.
- (10) Minisci, F.; Vismara, E.; Fontana, F.; Morini, G.; Serravalle, M.; Giordano, C. *J. Org. Chem.* **1986**, *51*, 4411–4416.
- (11) Semmelhack, M. F.; Schmid, C. R.; Cortes, D. A.; Chou, C. S. *J. Am. Chem. Soc.* **1984**, *106*, 3374–3376.
- (12) Nedelec, J. Y.; Nohair, K. *Synlett.* **1991**, 659–660.
- (13) Baran, P. S.; Hafensteiner, B. D.; Ambhaikar, N. B.; Guerrero, C. A.; Gallagher, J. D. *J. Am. Chem. Soc.* **2006**, *128*, 8678–8693.

- (14) Martin, C. L.; Overman, L. E.; Rohde, J. M. *J. Am. Chem. Soc.* **2010**, *132*, 4894–4906.
- (15) Kato, K.; Mukaiyama, T. *Chem. Lett.* **1992**, 1137–1140.
- (16) Ohara, H.; Itoh, T.; Nakamura, M.; Nakamura, E. *Chem. Lett.* **2001**, 624–625.
- (17) Ohara, H.; Kiyokane, H.; Itoh, T. *Tetrahedron Lett.* **2002**, *43*, 3041–3044.
- (18) Wang, K.; Lu, M.; Yu, A.; Zhu, X.; Wang, Q. *J. Org. Chem.* **2009**, *74*, 935–938.
- (19) Taniguchi, T.; Sugiura, Y.; Zaimoku, H.; Ishibashi, H. *Angew. Chem. Int. Ed.* **2010**, *49*, 10154–10157.
- (20) Itoh, T.; Kaneda, K.; Teranishi, S. *Tetrahedron Lett.* **1975**, *32*, 2801–2804.
- (21) Sherman, E. S.; Chemler, S. R. *Adv. Synth. Catal.* **2009**, *351*, 467.
- (22) Fuller, P. H.; Kim, J.-W.; Chemler, S. R. *J. Am. Chem. Soc.* **2008**, *130*, 17638–17639.
- (23) Sequeira, F. C.; Turnpenny, B. W.; Chemler, S. R. *Angew. Chem. Int. Ed.* **2010**, *49*, 6365–6368.
- (24) Zeng, W.; Chemler, S. R. *J. Am. Chem. Soc.* **2007**, *129*, 12948–12949.
- (25) Zeng, W.; Chemler, S. R. *J. Org. Chem.* **2008**, *73*, 6045–6047.
- (26) Perry, A.; Taylor, R. J. K. *Chem. Commun.* **2009**, 3249–3251.
- (27) Jia, Y. X.; Kündig, E. P. *Angew. Chem. Int. Ed.* **2009**, *48*, 1636–1639.
- (28) Klein, J. E. M. N.; Perry, A.; Pugh, D. S.; Taylor, R. J. K. *Org. Lett.* **2010**, *12*, 3446–3449.
- (29) Snider, B. B. *Tetrahedron.* **2009**, *65*, 10738–10744.
- (30) Shundo, R.; Nishiguchi, I.; Matsubara, Y.; Hirahima, T. *Tetrahedron.* **1991**, *47*, 831–840.
- (31) Nohair, K.; Lachaise, I.; Paugam, J.-P.; Nedelec, J.-Y. *Tetrahedron Lett.* **1992**, *33*, 213–216.

- (32) Qian, C.-Y.; Nishino, H.; Kurosawa, K.; Korp, J. D. *J. Org. Chem.* **1993**, *58*, 4448–4451.
- (33) Linker, T.; Kersten, B.; Linker, U.; Peters, K.; Peters, E.-M.; Schnering, H. G. von. *Synlett.* **1996**, 468–469.
- (34) Kulinkovich, O. G.; Astashko, D. A.; Tyvorskii, V. I.; Ilyina, N. A. *Synthesis.* **2001**, 1453–1455.
- (35) Kumar, A.; Neta, P. *J. Am. Chem. Soc.* **1980**, *102*, 7284–7289.
- (36) Liu, X.; Wang, Z.; Cheng, X.; Li, C. *J. Am. Chem. Soc.* **2012**, *134*, 14330–14333.
- (37) Mai, W.-P.; Wang, J.-T.; Yang, L.-R.; Yuan, J.-W.; Xiao, Y.-M.; Mao, P.; Qu, L.-B. *Org. Lett.* **2014**, *16*, 204–207.
- (38) Mai, W.-P.; Sun, G.-C.; Wang, J.-T.; Song, G.; Mao, P.; Yang, L.-R.; Yuan, J.-W.; Xiao, Y.-M.; Qu, L.-B. *J. Org. Chem.* **2014**, *79*, 8094–8102.
- (39) Shi, G.; Shao, C.; Pan, S.; Yu, J.; Zhang, Y. *Org. Lett.* **2015**, *17*, 38–41.
- (40) Seiple, I. B.; Su, S.; Rodriguez, R. A.; Gianatassio, R.; Fujiwara, Y.; Sobel, A. L.; Baran, P. S. *J. Am. Chem. Soc.* **2010**, *132*, 13194–13196.
- (41) Prier, C. K.; Rankic, D. A.; MacMillan, D. W. C. *Chem. Rev.* **2013**, *113*, 5322–5363.
- (42) Tucker, J. W.; Stephenson, C. R. J. *J. Org. Chem.* **2012**, *77*, 1617–1622.
- (43) Narayanam, J. M. R.; Stephenson, C. R. J. *Chem. Soc. Rev.* **2011**, *40*, 102–113.
- (44) Gray, H. B.; Maverick, A. W. *Science.* **1981**, *214*, 1201.
- (45) Alstrum-Acevedo, J. H.; Brennaman, M. K.; Meyer, T. J. *Inorg. Chem.* **2005**, *44*, 6802–6827.
- (46) O'Regan, B.; Gratzel, B. *Nature* **1991**, *353*, 737.
- (47) Nicewicz, D. A.; Macmillan, D. W. C. *Science.* **2008**, *322*, 77–80.
- (48) Cano-Yelo, H.; Deronzier, A. *J. Chem. Soc. Perkin Trans. 2* **1984**, 1093–1098.
- (49) Cano-Yelo, H.; Deronzier, A. *Tetrahedron Lett.* **1984**, *25*, 5517–5520.

- (50) Ischay, M. a; Lu, Z.; Yoon, T. P. *J. Am. Chem. Soc.* **2010**, *132*, 8572–8574.
- (51) Cheng, Y.; Yang, J.; Qu, Y.; Li, P. *Org. Lett.* **2012**, *14*, 98–101.
- (52) Huang, H.; Zhang, G.; Gong, L.; Zhang, S.; Chen, Y. *J. Am. Chem. Soc.* **2014**, *136*, 2280–2283.
- (53) Kohls, P.; Jadhav, D.; Pandey, G.; Reiser, O. *Org. Lett.* **2012**, *14*, 672–675.
- (54) Maity, S.; Zhu, M.; Shinabery, R. S.; Zheng, N. *Angew. Chem. Int. Ed. Engl.* **2012**, *51*, 222–226.
- (55) Lin, S.; Ischay, M. A.; Fry, C. G.; Yoon, T. P. *J. Am. Chem. Soc.* **2011**, *133*, 19350–19353.
- (56) McNally, A.; Prier, C. K.; Macmillan, D. W. C. *Science* **2011**, *334*, 1114–1118.
- (57) Yasu, Y.; Koike, T.; Akita, M. *Adv. Synth. Catal.* **2012**, *354*, 3414–3420.
- (58) Miyazawa, K.; Yasu, Y.; Koike, T.; Akita, M. *Chem. Commun.* **2013**, *49*, 7249–7251.
- (59) Tellis, J. C.; Primer, D. N.; Molander, G. a. *Science*. **2014**, *345*, 433–436.
- (60) Zuo, Z.; Ahneman, D. T.; Chu, L.; Terrett, J. A.; Doyle, A. G.; Macmillan, D. W. C. *Science (80-.)*. **2014**, *345*, 437–440.
- (61) Heiba, E. I.; Dessau, R. M. *J. Am. Chem. Soc.* **1971**, *93*, 524–527.
- (62) Sridharan, V.; Menéndez, J. C. *Chem. Rev.* **2010**, *110*, 3805–3849.
- (63) Ho, T.-L. *Synthesis* **978**, *78*, 936.
- (64) Kim, S. S.; Jung, H. C. *Synthesis*, **2003**, 2135–2137.
- (65) Iranpoor, N.; Baltork, I. M.; Zardaloo, F. S. *Tetrahedron* **1991**, *47*, 9861–9866.
- (66) Hwu, J. R.; Jain, M. L.; Tsay, S. C.; Hakimelahi, G. H. *Tetrahedron Lett.* **1996**, *37*, 2035–2038.
- (67) Krohn, K.; Vitz, J. *J. für Prakt. Chemie.* **2000**, *342*, 825–827.
- (68) Yadav, J. S.; Reddy, B. V. S.; Bhaskar Reddy, K.; Sarita Raj, K.; Prasad, A. R. *J. Chem. Soc. Perkin Trans. 1* **2001**, *2*, 1939–1941.

Chapter 2. Mechanistic Studies of Ag(I)/Persulfate-Catalyzed Cross-Coupling of Arylboronic Acids to Electron-Deficient Pyridines

2.1 Background and Significance

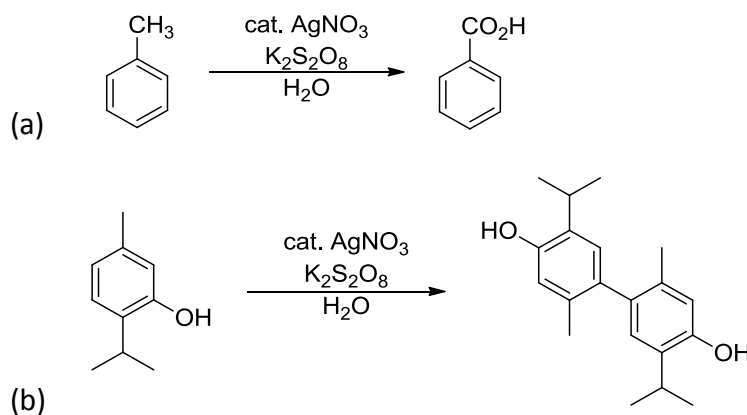
2.1.1 Catalytic Single Electron Oxidation

Catalytic oxidations that proceed through single electron transfer are becoming one of the most important approaches for the formation of C-C bonds in molecules of pharmaceutical and biological importance. A great deal of recent effort has focused on two general methods: 1) visible light photoredox catalysis and 2) metal-catalyzed oxidations. In both approaches, the use of a terminal oxidant is often required. In addition, the use of readily available starting materials employed in these reactions can provide a wide range of related structures important for screening in medicinal chemistry and for the construction of building blocks important in materials chemistry. The mechanistic studies and method development of these reactions could allow for the development of more efficient metal-catalyzed single electron transfer reactions.

2.1.2 Silver(I)-Persulfate Catalysis

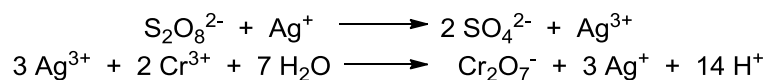
The persulfate ion is a good oxidant for a range of organic compounds due to its high oxidation potential.¹ However, many oxidations by persulfate do not generally occur at room temperature due to the rate limiting homolysis to generate two sulfate radical anions, which has an activation energy of approximately 30 kcal/mol. Because of this limitation, persulfate is often used as an oxidant thermally, or in conjunction with strong mineral acids or metal ions, such as Ag(I). The interaction between silver nitrate and

persulfate has been investigated as early as 1900, when Marshall observed the formation of a black precipitate upon mixing aqueous solutions of silver nitrate and potassium persulfate.² It was assumed that the product of this reaction was silver persulfate, which would then undergo rapid decomposition with water. Austin later investigated the product of this decomposition, identifying it as silver oxide.³ In addition to this key discovery, he also investigated the catalytic effect of silver nitrate in oxidations with persulfate, observing the oxidation of toluene to benzoic acid, and dimerization of thymol to dithymol (Scheme 2.1).



Scheme 2.1. Early use of catalytic silver nitrate and potassium persulfate in oxidations

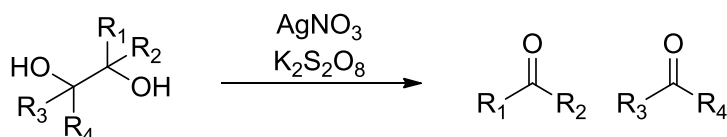
Yost and coworkers studied the kinetics of the Ag(I)/persulfate-catalyzed oxidation of the chromic ion and proposed that Ag(I) underwent a two-electron oxidation by persulfate to form an unstable Ag(III) intermediate in the rate determining step of the reaction (Scheme 2.2).⁴ Yost reasoned this mechanism because for every equivalent of silver that is precipitated from the reaction of silver salt and potassium persulfate, two oxidation equivalents of potassium persulfate were consumed.



Scheme 2.2. Early mechanism proposed for catalytic silver(I)/persulfate oxidation of chromic ion

Since then, however, experimental evidence has pointed toward the formation of Ag(II) intermediates in this reaction, through the oxidation of Ag(I) to Ag(II) by persulfate, followed by the oxidation of Ag(I) by the sulfate radical anion, overall forming two equivalents of sulfate anion, as Yost had also observed.

Greenspan and Woodburn observed the oxidation of glycols by silver-catalyzed persulfate (Scheme 2.3).⁵ The oxidation products of their reactions with a variety of glycols were aldehydes and ketones in good to moderate yields (40-100%). They also found that silver-catalyzed persulfate was not specific only to glycols, but also effective in the oxidation of primary and secondary alcohols to aldehydes and ketones, respectively, as well as the oxidation of water soluble aldehydes, such as acetaldehyde.



R = alkyl, aryl, cycloalkyl, or H

Scheme 2.3. Ag(I)/Persulfate-catalyzed cleavage of glycols

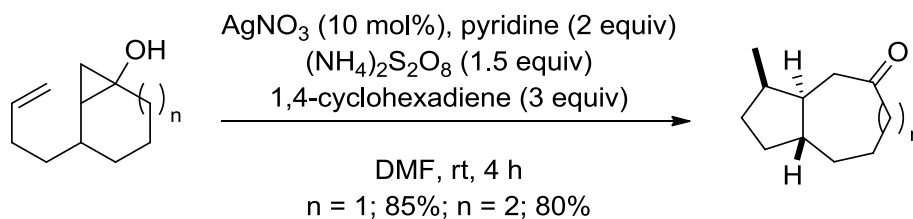
In 1969, Anderson and Kochi investigated the mechanism of decarboxylation of aliphatic carboxylic acids by Ag(I) and persulfate.⁶ They found that the oxidative decarboxylation of these acids was accelerated significantly by the silver ion. Kinetic studies showed that the reaction was first order in both Ag(I) and persulfate, and zero order in carboxylic acid, which allowed them to suggest that the rate limiting step was the

oxidation of Ag(I) by persulfate, and the oxidation of carboxylic acid occurs after this step. In addition, they suggested that it was Ag(II), formed by the oxidation of Ag(I) by persulfate in the rate limiting oxidation step, and not sulfate radical anions that were the reactive intermediates responsible for the oxidation of carboxylic acids. To test this hypothesis, they prepared stable Ag(II) salts, which are stabilized by nitrogen containing ligands such as picolinic acid and bipyridine. Using a bisbipyridine-silver(II) complex, they saw that carboxylic acids could be oxidized in a stoichiometric manner to produce the same products as the catalytic reaction of Ag(I) and persulfate (Scheme 2.4).

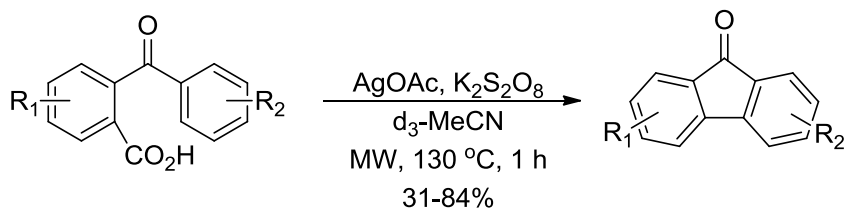


Scheme 2.4. Mechanism of Ag(II) oxidation of carboxylic acids

Recent applications of silver-catalyzed persulfate oxidation include the ring-opening of cyclopropanols (Scheme 2.5).⁷ In this reaction, Narasaka and coworkers catalytically ring opened cyclopropanol with the use of pyridine as ligand. Another application includes the oxidation of benzoic acids to form radicals (Scheme 2.6), in which Greaney and coworkers successfully decarboxylate benzoic acids, followed by cyclization of the resulting radical.⁸



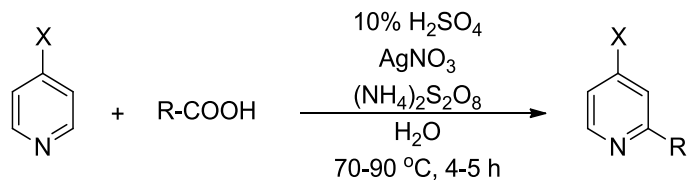
Scheme 2.5. Ag(I)/Persulfate-catalyzed oxidation of cyclopropanol



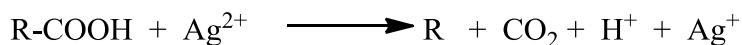
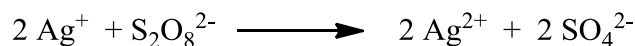
Scheme 2.6. Ag(I)/Persulfate-catalyzed decarboxylative C-H arylation of benzoic acids

2.1.3 Minisci Reaction

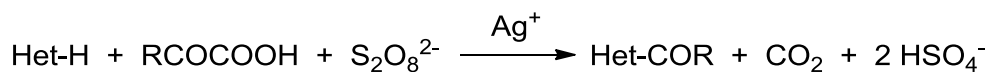
Minisci and coworkers expanded on the work by Anderson and Kochi by developing a new reaction involving the homolytic alkylation of heteroaromatic bases using a silver-catalyzed persulfate system (Scheme 2.7).⁹ The original Minisci reaction involves the silver-catalyzed oxidative decarboxylation of alkyl carboxylic acids by persulfate, followed by addition of the resulting radical to heterocycles (Scheme 2.8). Heteroaromatic bases are electron deficient aromatic substrates which readily react with radicals. Therefore, cross-coupled products can be made through the generation of an alkyl radical by decarboxylation of carboxylic acids, as shown in the work by Kochi, followed by addition to electron-deficient heteroarene rings. In addition to the alkylation of heteroarenes, Minisci was also successful in applying the Ag(I)/persulfate-catalyzed reaction to the acylation of pyridines and pyrazines (Scheme 2.9).¹⁰ This reaction was successfully employed in the last step in the synthesis of 8-azaergoline, an ergoline, which is a group of natural products that have shown significant pharmacological activity (Scheme 2.10).¹¹



Scheme 2.7. General scheme of Minisci reaction

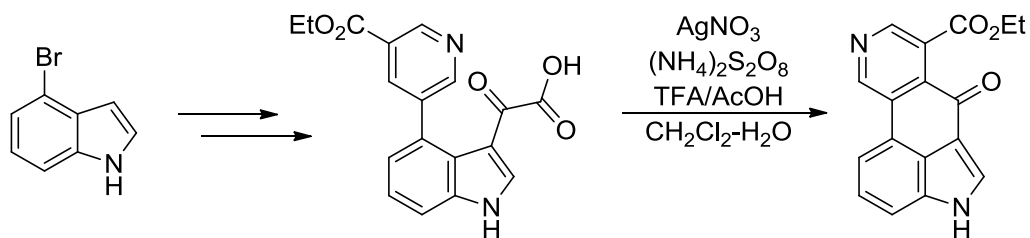


Scheme 2.8. Proposed mechanism of the Minisci reaction



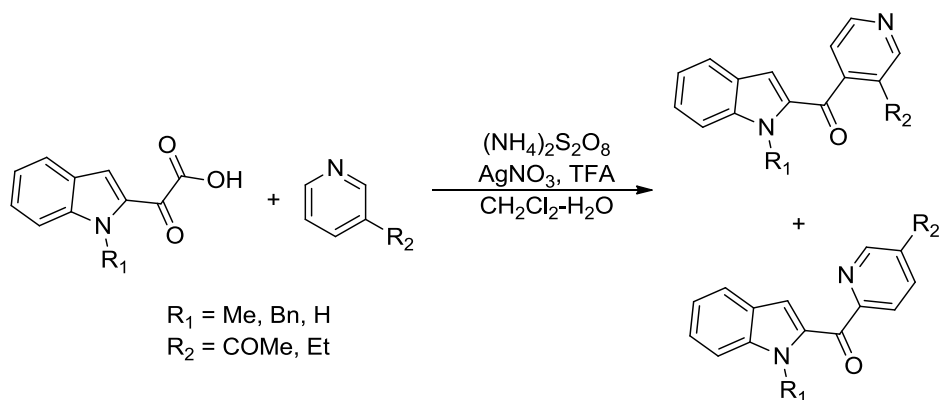
Het = Pyridine, pyrazine
R = Me, Et, Pr, Ph

Scheme 2.9. General scheme of Minisci acylation reaction

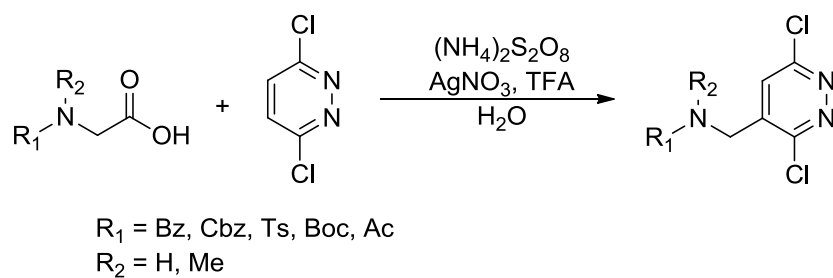


Scheme 2.10. Synthesis of 8-Azaergoline Ring System by Minisci-type acylation reaction

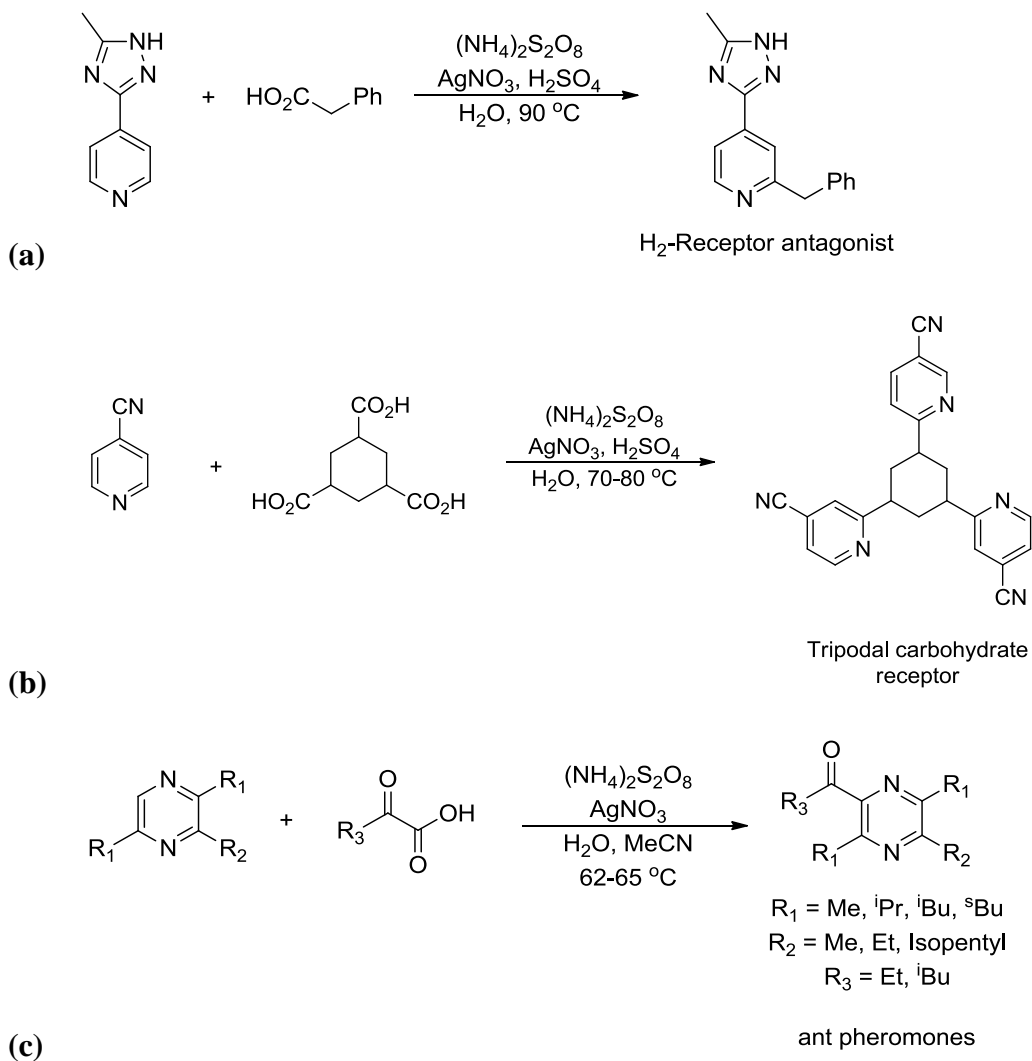
Minisci reactions are extremely valuable C-H functionalization methods that allow for the synthesis of a variety of organic compounds important in biological and medicinal chemistry. Since the development of this reaction by Minisci, this method has been applied to the synthesis of various compounds (Schemes 2.11, 2.12, 2.13)¹²⁻¹⁶ and total syntheses (Scheme 2.14).¹⁷⁻¹⁹



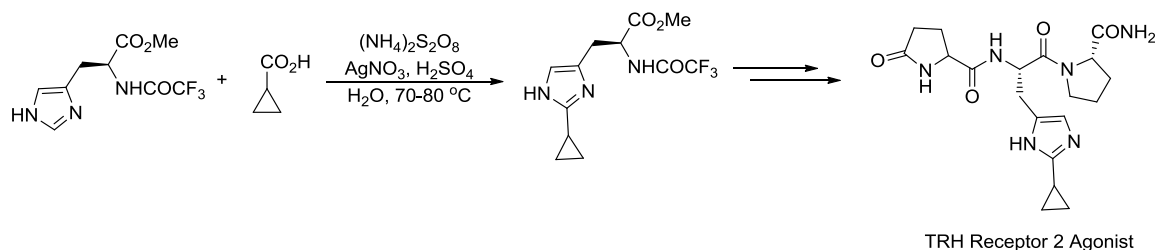
Scheme 2.11. Minisci-type reactions of indoleglyoxylic acids with pyridines



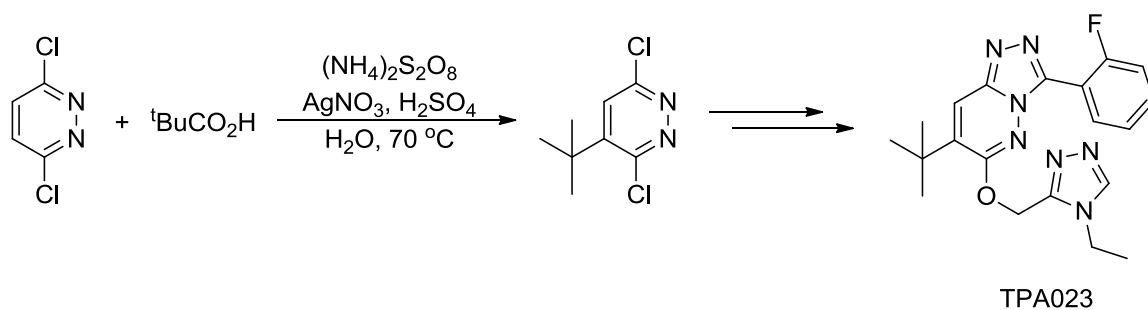
Scheme 2.12. Use of N-protected amino acids in Minisci alkylations



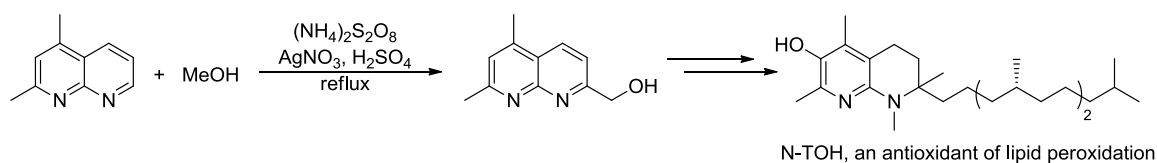
Scheme 2.13. Use of Minisci reaction in the synthesis of various medicinal compounds



(a)



(b)



(c)

Scheme 2.14. Use of Minisci reaction in various total syntheses

2.1.4 Silver(I)/Persulfate-Catalyzed Cross-Coupling of Arylboronic Acids and Heteroarenes

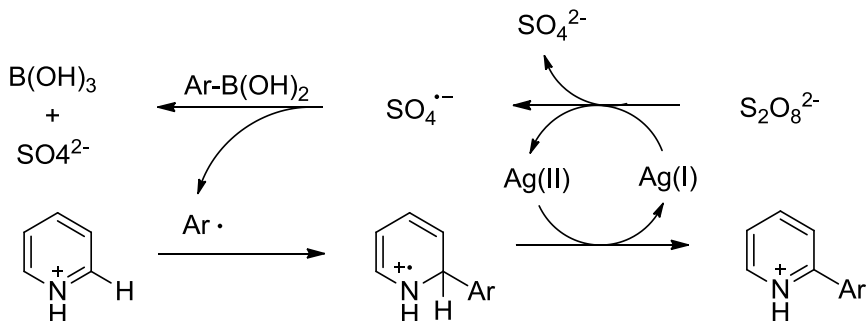
The recent work of Baran and coworkers on the Ag(I)/persulfate cross-coupling of arylboronic acids with electron-deficient pyridines is of fundamental importance.²⁰ In 2010, Baran and coworkers developed a variation on the Minisci reaction, involving the coupling of various arylboronic acids with several heteroarenes to generate 2-pyridyl

products, as shown in Scheme 2.15. The direct arylation of electron-deficient pyridines under mild conditions allows for simple access to a variety of arylated heteroarenes.

Their reaction involved the addition of a catalytic amount of silver nitrate and an excess of potassium persulfate in a heterogeneous system requiring 1:1 parts water to organic solvent. Halfway through the reaction, a second addition of 20 mol% silver nitrate and 3 equivalents of potassium persulfate were required to obtain the product in 81% isolated yield. In addition, the reaction was done in an open flask which was exposed to air. They proposed a reaction mechanism, which involved the reduction of persulfate to form a sulfate radical anion and Ag^{2+} . They suggested that it is the sulfate radical anion that oxidizes the arylboronic acid to form an aryl radical, which then adds to the heteroarene, as shown in Scheme 2.16.



Scheme 2.15. Cross-coupling reaction of electron-deficient pyridine with arylboronic acid



Scheme 2.16. Proposed mechanism for the cross-coupling reaction of electron-deficient pyridine with arylboronic acid

The approach developed by Baran overcomes several of the shortcomings of the traditional Minisci reaction, most importantly the addition of aryl radicals to an aromatic heterocycle. The products of this reaction generate compounds containing the 2-pyridyl subunit, which are found in various chemical compounds including pharmaceuticals,²¹ natural products,²² unnatural nucleotides,²³ and fluorescent probes,²⁴ as shown in Figure 2.1.

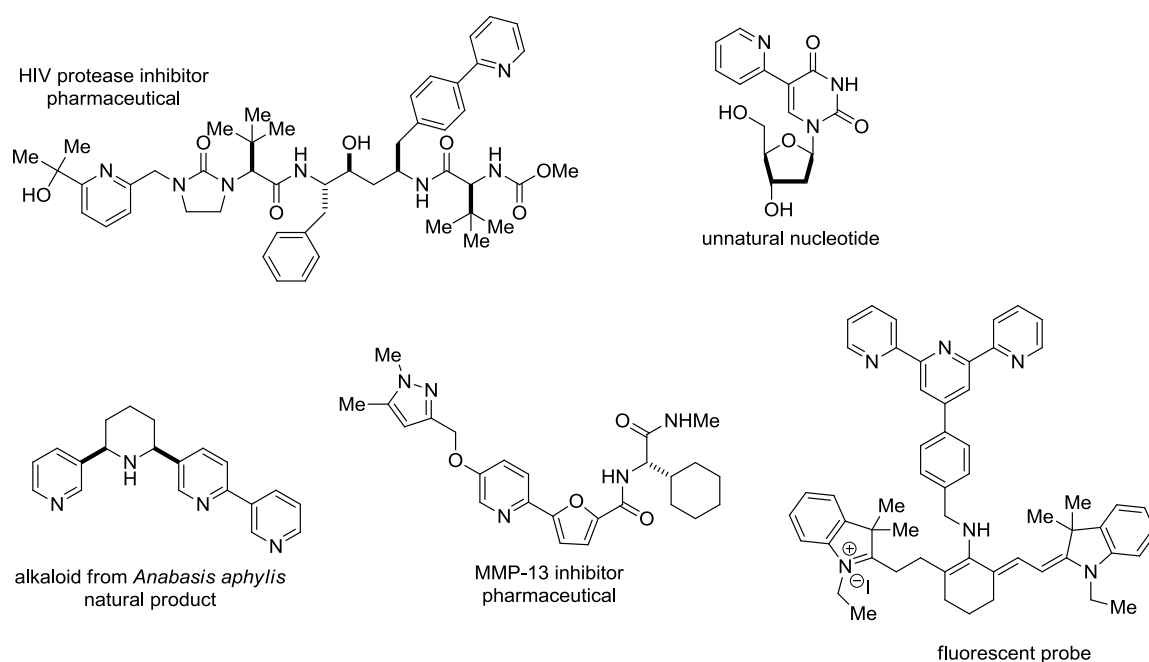


Figure 2.1: Example of important compounds containing the 2-pyridyl subunit

The method developed by Baran and coworkers is procedurally elegant and has broad substrate scope. Although the reaction provides access to a variety of substituted heteroarenes, a second addition of silver catalyst and stoichiometric persulfate oxidant are often required. Given the importance of this bond-forming reaction, it is hypothesized

that a detailed mechanistic study of the system would facilitate a more efficient approach to reaction design using the Ag(I)/persulfate catalytic system. Herein, mechanistic data defining the role of the individual components in the reaction are presented that reveal a great degree of mechanistic complexity, that once understood provides a more effective approach to this catalytic system, thus extending its utility.

2.2 Experimental

2.2.1 Materials

AgNO₃, K₂S₂O₈, Na₂S₂O₈ were purchased from Acros Organics. **1** was purchased from Oakwood Products, Inc. **2** was purchased from TCI Fine Chemicals. TFA and **4** was purchased from Alfa Aesar. All chemicals were used without further purification.

2.2.2 Instrumentation

GC analyses were done using a Shimadzu Gas Chromatograph GC-14B. Proton, carbon, and boron NMR were recorded on a Bruker 500 MHz spectrometer. GC-MS analyses were done with an HP 5890 Series II Gas Chromatograph with an HP Mass Selector Detector. Column chromatography was performed using the automated CombiFlash® Rf system from Teledyne Isco, Inc. Products were separated using prepacked silica gel columns with a gradient elution of ethyl acetate and hexanes.

2.2.3 Methods

2.2.3.1 Procedure for degassing solvents

CH₂Cl₂ was purified by a Solvent Purification system (Innovative Technology Inc.; MA). H₂O was degassed by bubbling through with argon overnight.

2.2.3.2 Procedure for synthesis of **3**

In a 25 mL round bottom flask with a magnetic stirring bar, **1**, TFA, and **2** were dissolved in 10 mL CH₂Cl₂. To the flask, 5 mL degassed H₂O was added. AgNO₃ was dissolved in 5 mL degassed water and added to the reaction. K₂S₂O₈ was added to the reaction as a solid. The flask was then evacuated of air, a septum was attached, and was back-filled with Ar. The reaction was allowed to stir overnight. Reaction workup involved diluting the reaction with 10 mL CH₂Cl₂ and quenching with 10 mL saturated bicarbonate solution. The organic layer was separated and run through a plug of neutral alumina. The alumina was washed with ethyl acetate. Product formation was confirmed by GC-MS. The organic layer was rotary evaporated to dryness. Crude product formation was observed by ¹H NMR in CDCl₃. Product was purified via automated flash chromatography and characterized by ¹H NMR and ¹³C NMR.

2.2.3.3 Procedure for Reaction Progress Kinetic Analysis Studies

In a 100 mL round bottom flask with a magnetic stirring bar, **1**, TFA, and **2** were dissolved in 30 mL CH₂Cl₂. To the flask, 15 mL degassed H₂O was added. AgNO₃ was dissolved in 15 mL degassed water and added to the reaction. K₂S₂O₈ was added to the reaction as a solid. The flask was then evacuated of air, a septum was attached, and was back-filled with Ar. The reaction was stopped and 0.5 mL aliquots were taken from the organic layer during the course of the reaction. Aliquots taken were quenched with 1.0 mL saturated bicarbonate solution, and 0.5 mL of biphenyl in ethyl acetate solution was added as an internal standard. The organic layer was extracted and analyzed by GC.

2.2.3.4 Procedure for Pyridine ^1H NMR studies

^1H NMR spectra were obtained for four solutions: 1) In a vial, 28.75 μL (0.25 mmol) of **1** was dissolved in 1.0 mL CDCl_3 . 2) In a vial, 28.75 μL (0.25 mmol) of **1** and 18.575 μL (0.25 mmol) of TFA was dissolved in 1.0 mL CDCl_3 . 3) In a vial, 28.75 μL (0.25 mmol) of **1**, 18.575 μL (0.25 mmol) of TFA, and 42.475 mg (0.25 mmol) of AgNO_3 were dissolved in 1.0 mL CDCl_3 . 4) In a vial, 28.75 μL (0.25 mmol) of **1** and 42.475 mg (0.25 mmol) of AgNO_3 were dissolved in 1.0 mL CDCl_3 .

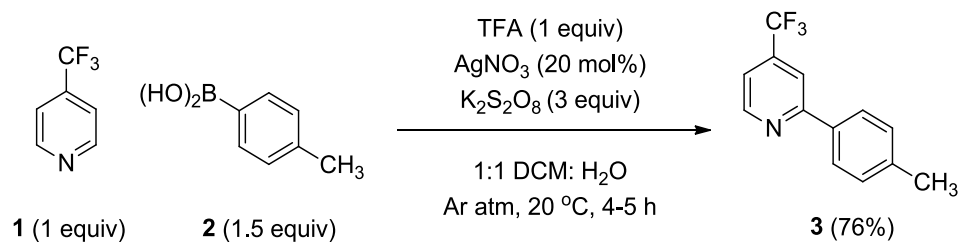
2.2.3.5 Procedure for ^{11}B NMR studies

^{11}B NMR studies were done using quartz NMR tubes. Spectra were obtained for the following solutions: 1) **2** dissolved in D_2O . 2) In a vial, 0.15 mmol of **4**, 0.1 mmol of **1**, 0.1 mmol of TFA, and 0.02 mmol of AgNO_3 was dissolved in 1 mL D_2O . The solution was then transferred to a quartz NMR tube. A ^{11}B NMR spectrum was immediately obtained. After letting the previous sample sit for 4h, a ^{11}B NMR spectrum was obtained again, showing some hydrolysis of **4** to **2**. 3) In a vial, 0.15 mmol of **4**, 0.1 mmol of TFA, and 0.02 mmol of AgNO_3 was dissolved in 1 mL D_2O . The solution was then transferred to a quartz NMR tube. A ^{11}B NMR spectrum was immediately obtained. After letting the previous sample sit for 4h, a ^{11}B NMR spectrum was obtained again, showing some hydrolysis of **4** to **2**.

2.3 Results

2.3.1 Solvent and Solubility Studies

To study this reaction developed by the Baran group, the cross-coupling reaction of 4-trifluoromethyl pyridine (**1**) and *p*-tolylboronic acid (**2**) containing 20 mol% AgNO₃ (with respect to **1**), potassium persulfate and trifluoroacetic acid (TFA) in a 1:1 solution of DCM and water was examined (Scheme 17).



Scheme 2.17. Cross-coupling reaction of electron-deficient pyridine with arylboronic acid

The use of water as a solvent was found to be critical for reaction success. In the absence of water, in only dichloromethane (DCM) solvent, no product formation is observed by gas-chromatography (GC). When done in only water, in the absence of DCM, **3** was isolated in 59% yield.

A variety of organic solvents were screened in conjunction with water. It was found that a biphasic organic-aqueous solvent system was necessary to obtain significant amount of product **3**. When run in DCM/water, **3** was obtained in 76% yield. When run in ethyl acetate/water, **3** was obtained in 70% yield. However, when run in miscible solvents, including tetrahydrofuran/water, methanol/water, and acetonitrile/water, no product formation was observed by GC.

Next, because AgNO_3 and $\text{K}_2\text{S}_2\text{O}_8$ have limited solubility in organic solvents, the use of organic soluble silver salts and persulfates, in the form of AgPF_6 and tetrabutylammonium persulfate, were probed in the cross-coupling reaction. In DCM/water mixture, cross-coupled product **3** was obtained in 12% yield. When done in the absence of water, in only DCM, no product formation was observed.

2.3.2 Kinetic Analysis

To study the mechanism of this catalytic system, the reaction of **1** and **2** containing 20 mol% AgNO_3 (with respect to **1**), potassium persulfate and trifluoroacetic acid (TFA) in a 1:1 solution of DCM and water was examined (Scheme 2.17). The cross-coupled product was formed in high yield, without any other substitution side-products forming.

Protonation of pyridine by TFA produces a better radicophile and enhances selectivity of the 2-position.²⁵ To maintain controlled reaction conditions, solvents were degassed and the reaction was carried out under an atmosphere of argon as shown in Scheme 17. The exclusion of air from the reaction resulted in a 76% isolated yield, compared to the 81% yield reported by Baran and coworkers, which required a second addition of $\text{K}_2\text{S}_2\text{O}_8$ and AgNO_3 . Additionally, toluene was obtained as a side product in roughly 30% yield (with respect to **2**). Removal of oxygen and the subsequent increased yield is consistent with the previously proposed free-radical mechanism.²⁰ These higher-yielding conditions were suitable for thorough mechanistic studies.

2.3.2.1 Catalyst Stability Experiments

Kinetic studies were performed in which either the loss of starting material (**1**) or growth of product was followed over time via GC. A catalyst stability experiment was initiated to determine the stability of catalytic AgNO₃ during the course of the reaction.²⁶⁻²⁹ Two reactions were performed, the 100% run in which initial concentrations were set based on synthetic conditions, and the 50% run, in which the concentrations were adjusted so that they were one half of the initial concentrations of the 100% run, maintaining the same excess of each reagent, as shown in Table 1. In these kinetic studies, “excess” is defined as the difference in initial stoichiometric concentrations of a reagent (**2** or K₂S₂O₈) and the monitored substrate (**1**) (equations 2.1 and 2.2).

$$[\text{excess}] = [\mathbf{2}] - [\mathbf{1}] \quad (2.1)$$

$$[\text{excess}] = [\text{K}_2\text{S}_2\text{O}_8] - [\mathbf{1}] \quad (2.2)$$

Table 2.1. Catalyst stability experiment reaction conditions

Run	1 (M)	2 (M)	excess (M)	K ₂ S ₂ O ₈ (M)	excess (M)	AgNO ₃ (M)
1-100%	0.10	0.15	0.050	0.30	0.20	0.020
2-50%	0.050	0.10	0.050	0.25	0.20	0.020

If total catalyst concentration remains constant during the course of the reaction, the rates of both reactions would be identical; the concentration of catalyst halfway through a reaction should be the same as in the beginning of the reaction. Therefore, when both the 100% run and 50% run are plotted together, both rate plots would overlay. However, if the concentration of the catalyst was decreasing as the reaction proceeded, the reaction rates would not be identical; both rate plots would not overlay. When rate

profiles of Runs 1 and 2 are compared, the decays do not overlay, consistent with a decrease in the concentration of AgNO_3 during the course of the reaction (Figure 2.2).

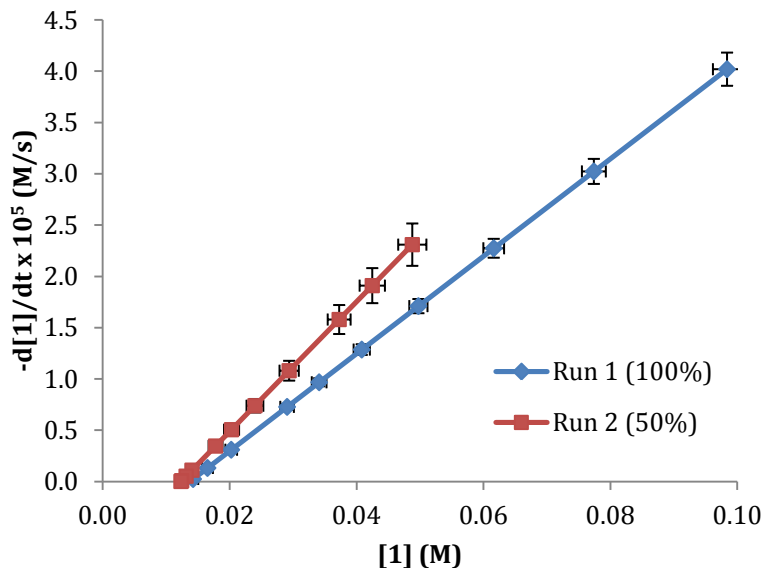


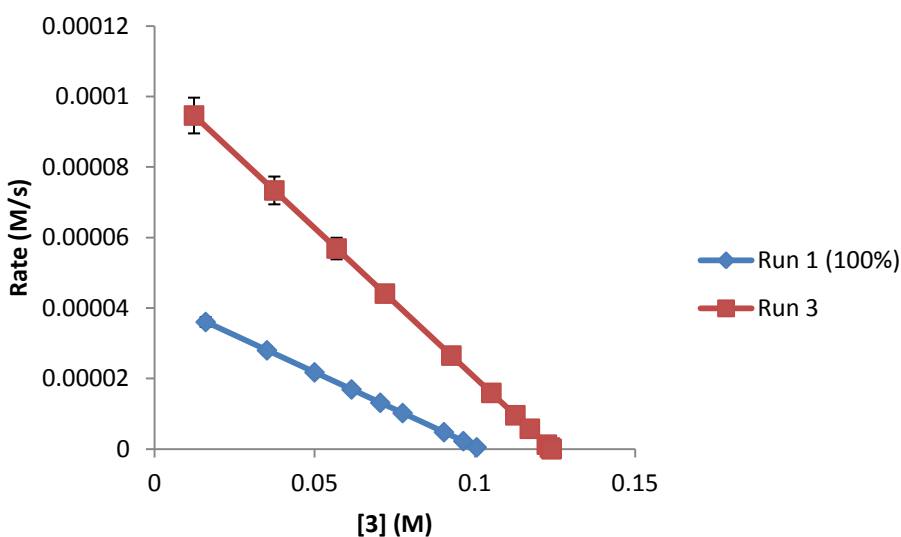
Figure 2.2. Rate vs. [1] for same excess experiments.

2.3.2.2 Kinetic Order Experiments

To determine the rate order of each of the reactants in the reaction, experiments were designed and performed to be compared to the 100% run. Concentrations of each substrate were increased individually to determine its effect on the reaction rate while all other substrate concentrations were kept constant, as shown in Table 2.2. To determine the order of **1**, the rate plots of Runs 1 and 3 were plotted together. When doubling the concentration of **1**, the rate of the reaction was shown to approximately double as shown in Figure 2.3, indicating a rate order of 1 for substrate **1**.

Table 2.2. Rate order experiment reaction conditions

Run	1 (M)	2 (M)	excess (M)	K ₂ S ₂ O ₈ (M)	excess (M)	AgNO ₃ (M)
1-100%	0.10	0.15	0.05	0.30	0.20	0.020
Run 3	0.20	0.15	0.05	0.30	0.20	0.020
Run 4	0.10	0.15	0.05	0.30	0.20	0.040
Run 5	0.10	0.15	0.05	0.60	0.50	0.020
Run 6	0.10	0.30	0.20	0.30	0.20	0.020

**Figure 2.3.** Rate vs. [3] for different excess experiments for **1**.

Similarly, the rate order of AgNO₃ was found by doubling the loading of catalyst from 20 mol% (Run 1) to 40 mol% (Run 4), as shown in Table 2. The rate of the reaction was shown to increase upon doubling of silver catalyst concentration (Figure 2.4). In order to determine the rate order of the catalyst, the rate plot was normalized by dividing the rate by the concentration of AgNO₃ in each experiment. When plotted together, overlay was seen, indicating a 1st order dependence on AgNO₃ in the reaction (Figure 2.5).

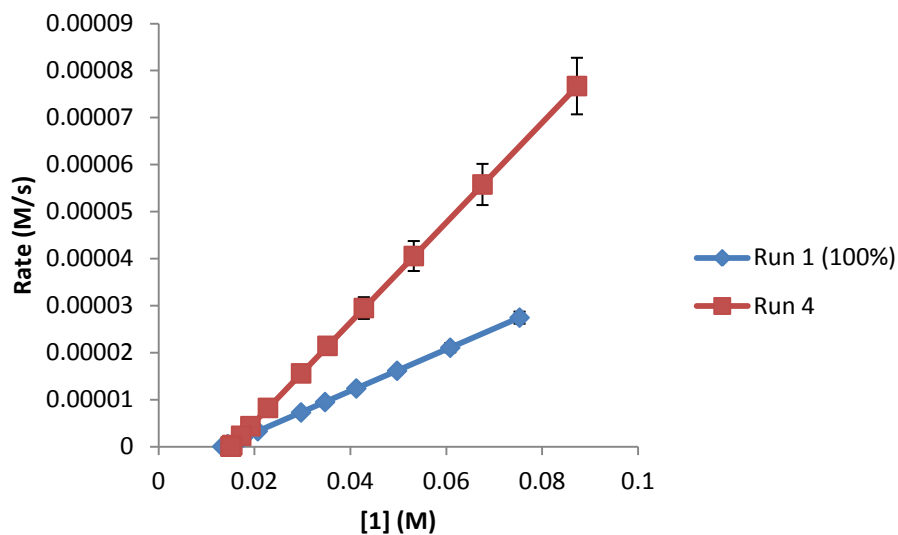


Figure 2.4. Rate vs. [1] for different excess experiments for AgNO_3 .

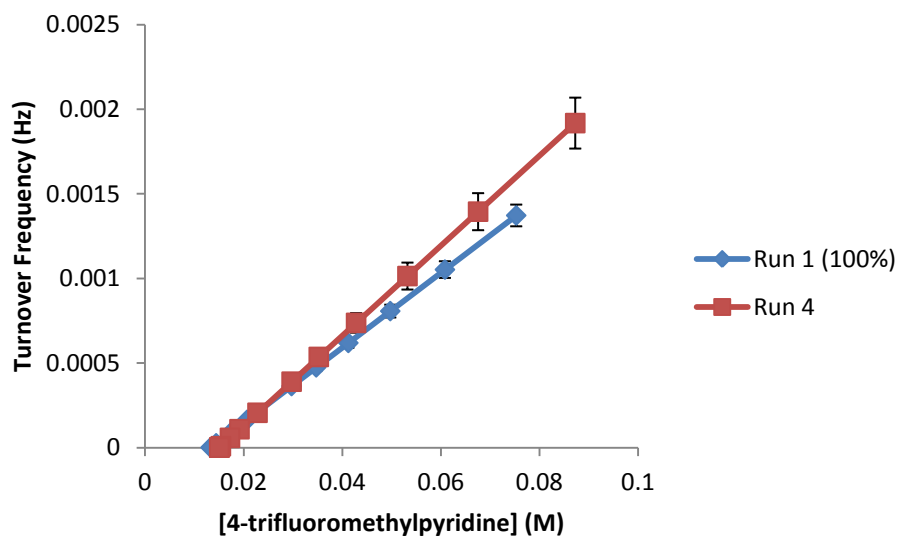


Figure 2.5. Normalized Rate vs. [1] for different excess experiments for AgNO_3 .

To determine the rate order of $\text{K}_2\text{S}_2\text{O}_8$, the concentration of oxidant was doubled (Table 2). Surprisingly, the increase in persulfate did not affect the rate of the reaction,

suggesting an order of zero (Figure 6). It was suspected that the true order of the oxidant was being masked by its low solubility (4.72 g/100 mL at 20 °C).³⁰ In order to investigate this physical process, Na₂S₂O₈ was used, which has more than ten-fold higher solubility (54.6 g/100mL) than K₂S₂O₈.³⁰ Upon doubling of Na₂S₂O₈ concentration, the rate of the reaction approximately doubled (Figure 2.7), indicating an order of one for persulfate.

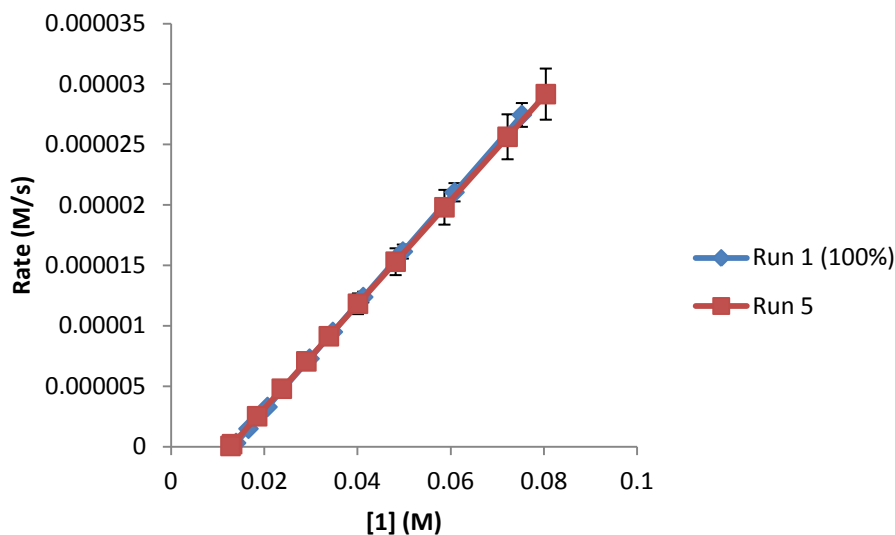


Figure 2.6. Rate vs. [1] for different excess experiments for K₂S₂O₈.

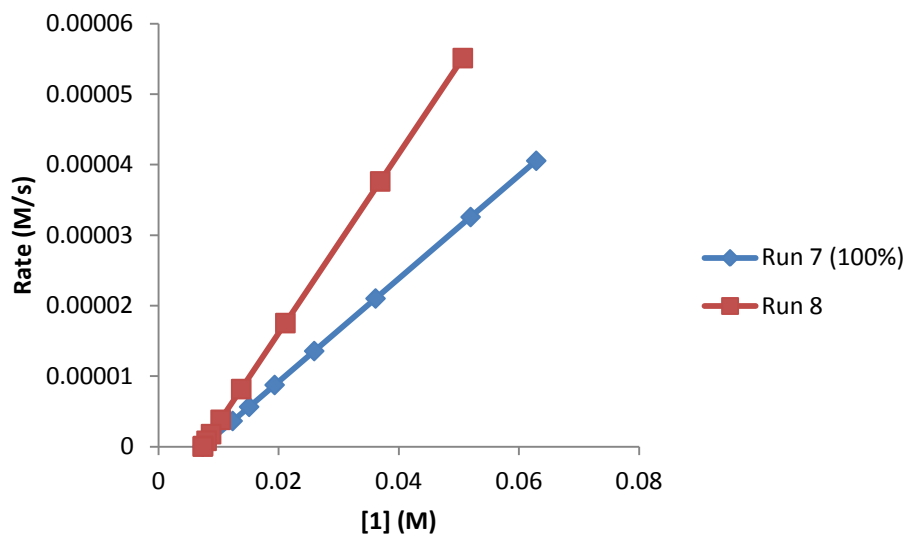


Figure 2.7. Rate vs. [1] for different excess experiments for $\text{Na}_2\text{S}_2\text{O}_8$.

The concentration of **2** was doubled (Run 6) to determine its role in the reaction (Table 2.2). Surprisingly, an increase in the initial concentration of **2** resulted in an overall decrease in reaction rate (Figure 2.8). The order of **2** was determined through normalization of $-\text{d}[\mathbf{1}]/\text{dt}$, defined by equation 2.3

$$-\frac{\frac{d[\mathbf{1}]}{dt}}{[\mathbf{2}]^x} = k_{obs}[\mathbf{1}] \quad (2.3)$$

where x is the order of **2**. Overlay of the two reaction profiles is observed when $x = -0.5$, indicative of an inverse half order for **2** (Figure 2.9).

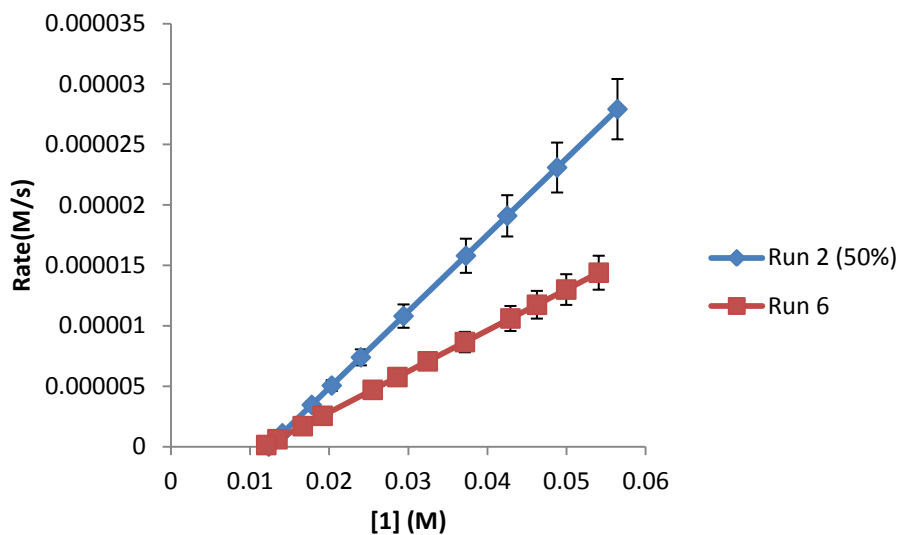


Figure 2.8. Rate vs. [1] for different excess experiments for 2.

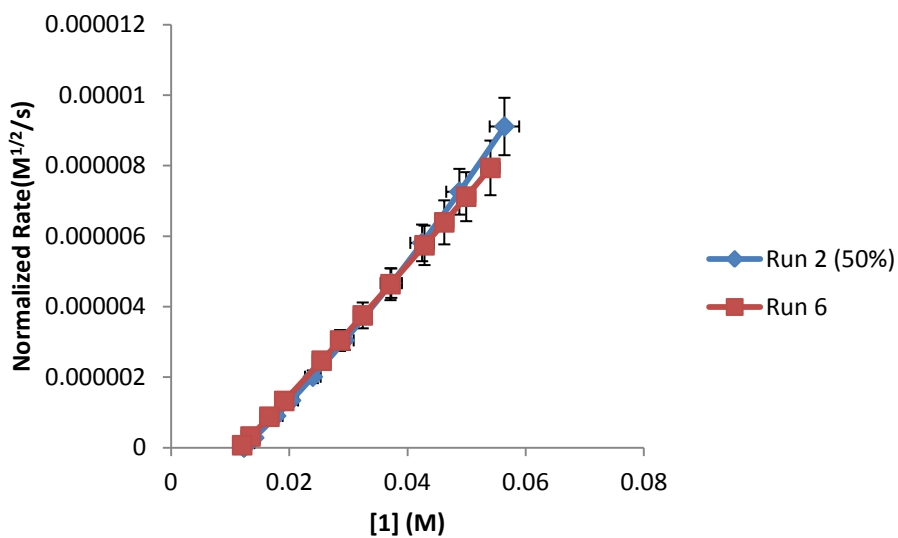


Figure 2.9. Normalized Rate vs. [1] for different excess experiments for 2.

The rate orders for all reaction components are shown in Table 3. The rate orders of persulfate and AgNO_3 are consistent with a process where catalytic Ag(I) is oxidized by

persulfate. The orders obtained for **1** and **2** are surprising. If the reaction is indeed proceeding through initial oxidation of **2** followed by addition to **1**, the first order observed for **1** compared to the inverse half order for **2** suggests a more complicated process. From the kinetic studies, the empirical rate law is shown in Equation 2.4, in which **1**, $S_2O_8^{2-}$, and Ag(I) are first order and **2** is inverse half order.

$$-\frac{d[\mathbf{1}]}{dt} \approx k_{obs} \frac{[\mathbf{1}][S_2O_8^{2-}][Ag^I]_{tot}}{[\mathbf{2}]^{0.5}} \quad (2.4)$$

Table 2.3. Observed Rate Orders of Substrates in Cross-Coupling Reaction of **1** and **2**

1	2	$K_2S_2O_8$	$AgNO_3$
1	-0.5	0*	1

*Due to low solubility of $K_2S_2O_8$ (4.72 g/100 ml at 20 °C)¹⁰; when using $Na_2S_2O_8$ (54.6 g/100mL), rate order shown to be approximately 1.

2.3.3 Pyridine 1H NMR Studies

The formation of silver-pyridine complexes is well-established in the literature.³¹⁻
³³ In addition, there is literature precedence describing the activation of Ag(I) by amines toward oxidation by persulfate.^{34,35} Bonchev and Aleksiev showed that the addition of suitable nitrogen-containing neutral ligands, such as phenanthroline, ethylenediamine, and pyridine, to Ag(I)/persulfate reactions resulted in the acceleration in the oxidation of Ag(I) to Ag(II).^{34,35} This activating effect was attributed to a lowering of the Ag(II)/Ag(I) couple.

To investigate the possible interaction between **1** and $AgNO_3$, 1H NMR studies were carried out in D_2O to mimic reaction conditions (Figure 2.10). Downfield shifts of

aromatic protons were observed upon addition of TFA (Figure 2.10b) or AgNO₃ (Figure 2.10d) to **1** in D₂O. Upon addition of TFA and AgNO₃ to **1** (Figure 2.10c), a slight upfield shift of aromatic protons is observed compared to the mixture of **1** and TFA (Figure 2.10b).

The shifts in the proton NMR spectra are shown in Table 2.4. The lack of overlay of the spectra is consistent with equilibrium complexation between **1** and Ag(I) under reaction conditions.

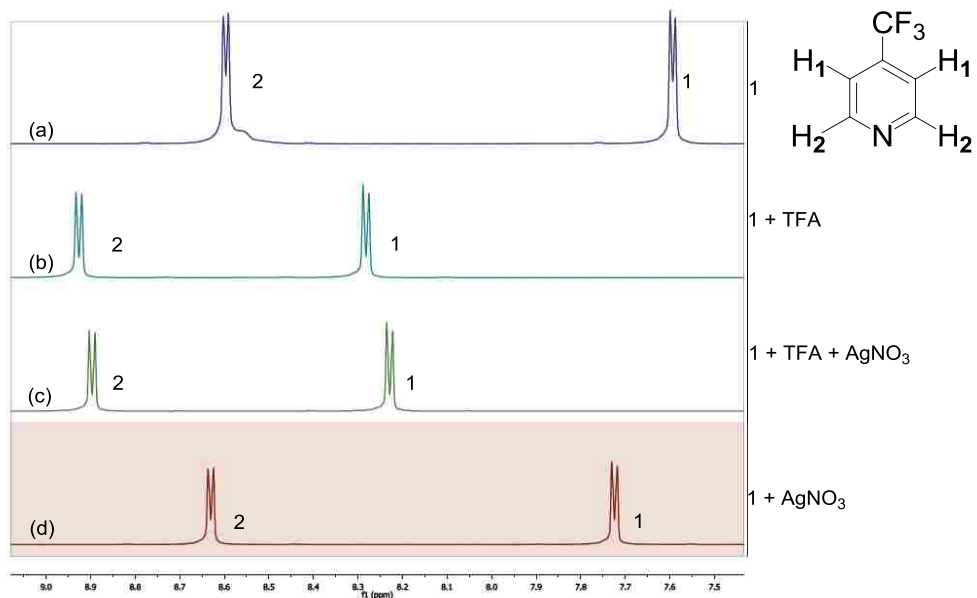


Figure 2.10. ¹H NMR spectra of **1** with additives

Table 2.4. ^1H NMR shifts of **1** with additives

	$\Delta 1$ (ppm)	$\Delta 2$ (ppm)
1	8.60	7.59
1 + TFA	8.92	8.28
1 + TFA + AgNO_3	8.89	8.23
1 + AgNO_3	8.63	7.72

2.3.4 AgNO_3 -Boronic Acid Studies

With some insight into the possible role of **1**, the mechanistic role of **2** was probed next. An inverse rate order is typically indicative of two possible scenarios: 1) the presence of the reaction component shifts an equilibrium, decreasing the concentration of the intermediate prior to a rate determining step, or 2) the component behaves as an antagonist acting outside the desired pathway that leads to product. Given the long history of the Ag(I) /persulfate oxidation system, it is instructive to examine the literature carefully for possible precedent to explain the unusual observations obtained from the kinetic studies. Studies on the interaction between AgNO_3 and boronic acids in ammoniacal solution date back to the 1880s.³⁶⁻³⁸ These early investigations showed that while alkyl boronic acids reduce Ag(I) through an intermediate Ag-alkyl , aromatic boronic acids form an insoluble salt. Heating of this salt led to hydrolytic cleavage producing an arene, boric acid and Ag_2O .

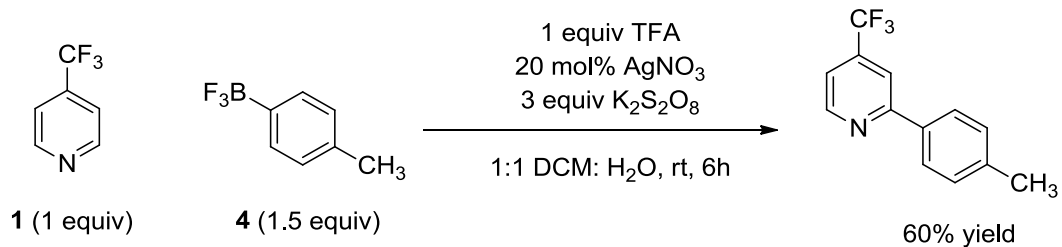
To examine the Ag(I)-initiated hydrolysis under reaction conditions, stoichiometric quantities of **2** and AgNO₃ were stirred in 1:1 DCM:H₂O solution. After approximately five minutes, the formation of a gray/silver colored precipitate was observed consistent with silver oxide described in previous studies. The formation of toluene as a by-product of this reaction was confirmed by gas chromatography-mass spectrometry (GC-MS). To further probe the system, two reactions were carried out. The first involved reacting 1.5 mmol of **2** with 1.0 mmol AgNO₃ in 1:1 DCM:H₂O solution. A second reaction was run under the same conditions with 3.0 mmol of **1**. Approximately 0.84 mmol of toluene formed when **1** was included in the reaction mixture, compared to 0.23 mmol of toluene formed when **1** was excluded, a finding consistent with inhibition of AgNO₃ and consumption of **2** outside of the desired reaction pathway. The increase in toluene formation in the presence of **1** is also consistent with interaction between **1** and AgNO₃ and the classic studies on the reaction of AgNO₃ and boronic acids in ammoniacal solutions.³⁶⁻³⁸

2.3.5 ¹¹B NMR Studies

The question that still remains unanswered is: which species is oxidizing the boronic acid after the rate determining step, the Ag(II) or SO₄²⁻? The classic work of Kochi and others has shown that metastable Ag(II) is responsible for decarboxylation of carboxylic acids to produce radicals by Ag(I)/persulfate.^{6,39} This work was applied by Minisci and coworkers, in which the alkyl radical, generated from decarboxylation of an acid adds to a heteroarene to form substituted heterocycles.⁹ In the present reaction,

Baran proposed that persulfate radical anion addition to the aryl boronic acid was responsible for intermediate aryl radical formation.²⁰

To test the question posed above, the use of potassium 4-methylphenyl trifluoroborate (**4**) in place of **2** (Scheme 2.18) was first examined. The reaction was performed under the unoptimized conditions shown in Scheme 1 and provided a 60% isolated yield of **3**. Aryl trifluoroborates are known to hydrolyze under basic conditions.^{40,41} The stability of **4** under reaction conditions was examined in aqueous acidic media by monitoring the ¹¹B NMR spectrum as described by Lloyd-Jones. Minimal hydrolysis of **4** to **2** was observed. The results of this reaction show that **4** is not hydrolyzed (*i.e.* remains quaternized) under reaction conditions, and it is unlikely for the sulfate radical to add to the trifluoroborate or boronic acid.



Scheme 2.18. Cross-coupling reaction of electron-deficient pyridine with aryl trifluoroborate

2.3.6 Allyl Acetate Studies

Next, the reaction with **2** was carried out in the presence of allyl acetate, a well-known radical trap for SO₄^{•-}.⁴² If SO₄^{•-} is acting as the oxidizing agent in the reaction, the addition of allyl acetate would be deleterious to reaction progress. Interestingly, addition of 6 equiv of allyl acetate had no impact on yield and the rate of reaction increased slightly (Figure 2.11).

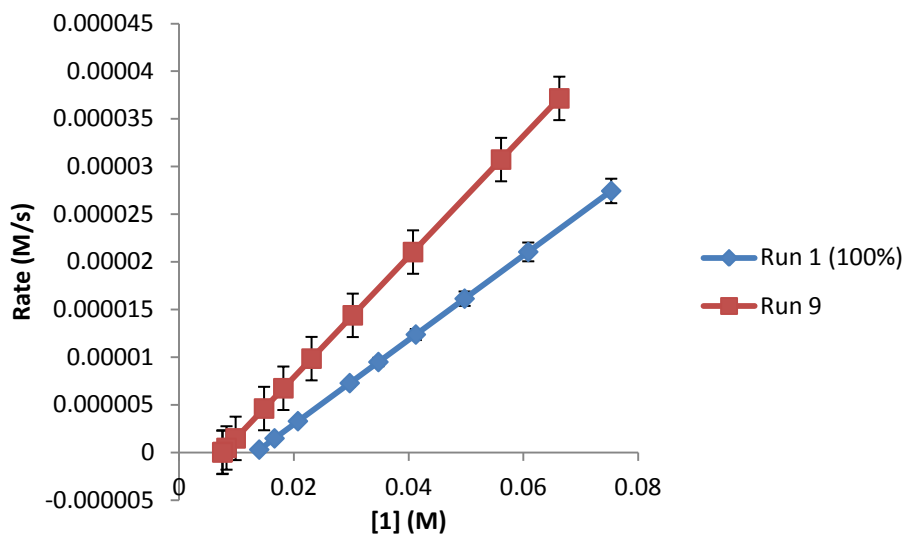


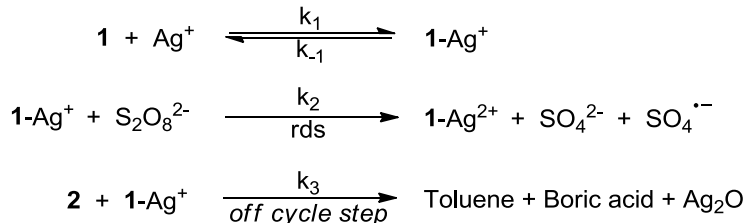
Figure 2.11. Rate vs. [1] plot comparing reaction with and without allyl acetate

This observation suggests that by decreasing the concentration of SO_4^- through capture by allyl acetate, the reaction is being driven forward toward the formation of product, presumably through the reduction of $\text{S}_2\text{O}_8^{2-}$ by Ag(I) producing Ag(II). These additional experiments show that reactions with **2** proceed even when SO_4^- is sequestered by allyl acetate. As a consequence, these experiments are consistent with a process where the oxidation proceeds through a Ag(II)-mediated process. Since quaternized boron is more susceptible to single electron oxidation,⁴³ it is proposed that water (solvent) or pyridine interacts with the aryl boronic acid to facilitate oxidation by Ag(II). A proposed mechanism for the reaction is shown in Scheme 2.20.

2.3.7 Proposed Mechanism for the Ag(I)/Persulfate-Catalyzed Cross-Coupling of Arylboronic acids and Electron-deficient Pyridines

2.3.7.1 Proposed Mechanism

Based on the observed kinetic and spectroscopic data, the proposed reaction mechanism involves: i) a pre-equilibrium step in which **1** and Ag(I) form a complex, ii) the reduction of $S_2O_8^{2-}$ by the Ag(I)-**1** complex, which is the rate-determining step, and iii) an off-cycle step involving protodeboronation of **2** accelerated by the Ag(I)-**1** complex (Scheme 2.19).



Scheme 2.19. Mechanism of Ag(I)/Persulfate-Catalysis in Coupling of Arylboronic acid and Electron-deficient Pyridine

2.3.7.2 Derivation of Rate Equation

Rate equation based on the rate determining step of the reaction:

$$-\frac{d[CF_3C_5H_4N]}{dt} = k_2[CF_3C_5H_4N - Ag^I][S_2O_8] \quad (2.5)$$

The interaction between silver(I) and pyridine was assumed to be at steady state:

$$[CF_3C_5H_4N - Ag^I] = \frac{k_1[CF_3C_5H_4N][Ag^I]}{k_{-1} + k_2[S_2O_8^{2-}] + k_3[Ar-B(OH)_2]} \quad (2.6)$$

$$-\frac{d[CF_3C_5H_4N]}{dt} = \frac{k_1k_2[CF_3C_5H_4N][Ag^I][S_2O_8]}{k_{-1} + k_2[S_2O_8^{2-}] + k_3[Ar-B(OH)_2]} \quad (2.7)$$

A mass balance was written for the silver complexes in the system:

$$[Ag^I]_{tot} = [Ag^I] + [CF_3C_5H_4N - Ag^I] \quad (2.8)$$

$[Ag^I]$ was solved for:

$$[Ag^I] = \left(\frac{[Ag]_{tot}(k_{-1} + k_2[S_2O_8^{2-}] + k_3[Ar-B(OH)_2])}{k_{-1} + k_2[S_2O_8^{2-}] + k_3[Ar-B(OH)_2] + k_1[CF_3C_5H_4N]} \right) \quad (2.9)$$

$[Ag^I]$ was inserted into the rate law:

$$-\frac{d[CF_3C_5H_4N]}{dt} = \left(\frac{k_1 k_2 [CF_3C_5H_4N][S_2O_8]}{k_{-1} + k_2[S_2O_8^{2-}] + k_3[Ar-B(OH)_2]} \right) \left(\frac{[Ag]_{tot}(k_{-1} + k_2[S_2O_8^{2-}] + k_3[Ar-B(OH)_2])}{k_{-1} + k_2[S_2O_8^{2-}] + k_3[Ar-B(OH)_2] + k_1[CF_3C_5H_4N]} \right) \quad (2.10)$$

The equation simplifies to:

$$-\frac{d[CF_3C_5H_4N]}{dt} = \left(\frac{k_1 k_2 [CF_3C_5H_4N][S_2O_8][Ag]_{tot}}{k_{-1} + k_2[S_2O_8^{2-}] + k_3[Ar-B(OH)_2] + k_1[CF_3C_5H_4N]} \right) \quad (2.11)$$

Assuming $k_2 \ll k_{-1}$, $k_2 \ll k_3$, $k_2 \ll k_1$, and that Ag^I is the resting state of the catalyst ($k_1 \ll k_{-1}$, $k_3 \gg k_1$):

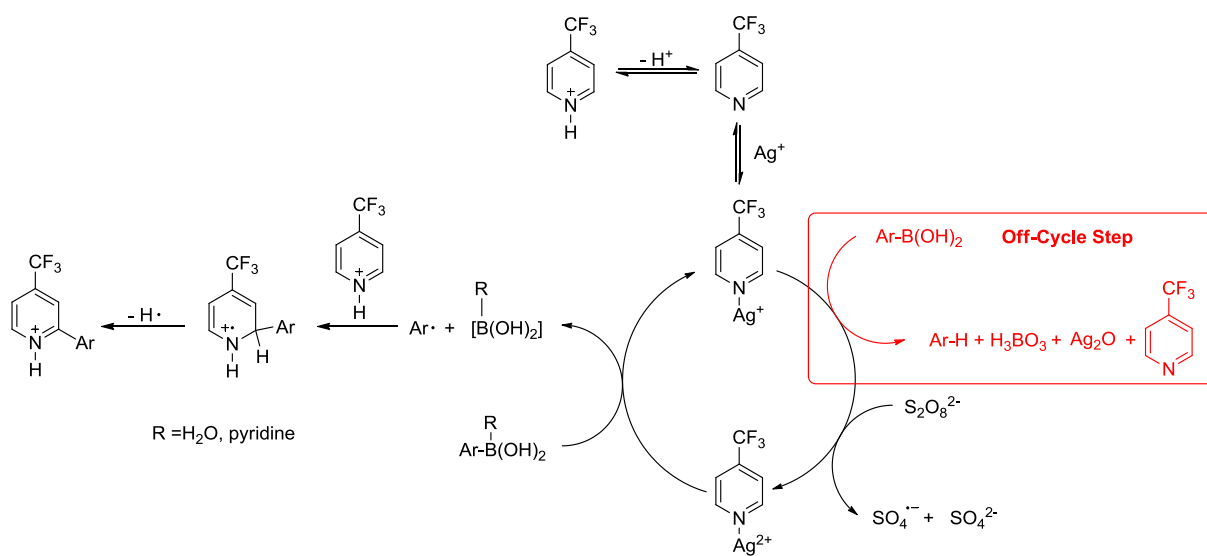
$$-\frac{d[CF_3C_5H_4N]}{dt} = \frac{k_1 k_2 [CF_3C_5H_4N][Ag^I]_{tot} [S_2O_8^{2-}]}{k_{-1} + k_3[Ar-B(OH)_2]} \approx k_{obs} \frac{[CF_3C_5H_4N][S_2O_8^{2-}][Ag^I]_{tot}}{[Ar-B(OH)_2]^{0.5}} \quad (2.12)$$

For the rate law to be valid, $[Ag(I)]_{tot}$ must be constant. However, the proposed mass balance does not account for the change in $[Ag(I)]_{tot}$ as the reaction progresses. The proposed off-cycle mechanism explains the slight deactivation seen in the same excess plots as well as the toluene produced; however, under these conditions the rate law does not apply. If the rate law applies, the negative order seen for $[Ar-B(OH)_2]$ can be

explained, but requires a new proposal to bring the Ag(I) back into the catalytic cycle so that the mass balance is correct.

2.3.7.3 Proposed Catalytic Cycle

Under the conditions of the reaction, pyridine coordinates to Ag(I), followed by persulfate oxidation in the turnover-limiting step (Scheme 2.20). The resulting Ag(II)-pyridine complex oxidizes the arylboronic acid, producing an aryl radical, which can then add to the pyridinium ion leading to product. An off-cycle step is also involved outside of the desired pathway, in which the arylboronic acid is protodeboronated, leading to unwanted side products.



Scheme 2.20. Proposed Mechanism of the Ag(I)/Persulfate-Catalyzed Arylation of Electron-deficient Pyridine

2.3.8 Optimization of Reaction Conditions

Aside from providing insight into the reaction mechanism, these results provide a means to optimize reaction conditions and increase the yield of the reaction. The inverse

half order of **2** indicates that increasing its concentration is deleterious to reaction progress. Furthermore, addition of a reagent capable of preventing formation of catalytically inactive Ag(I) to its active form should be beneficial to reaction progress. To test this supposition, a reaction was initiated using 0.5 M HNO₃ to prevent the formation of catalytically inactive Ag(I).³⁷ Employing these modified conditions enabled the reduction of catalyst and oxidant loading to 10 mol% AgNO₃ and 2 equiv of persulfate, respectively in a 1:1 solution of DCM and water under Ar atmosphere overnight, leading to an isolated yield of 90%. Additionally, toluene side-product formation was reduced to 9% (with respect to **2**).

2.4 Conclusions

The mechanistic experiments described herein show an unexpected degree of complexity in the Ag(I)/persulfate-catalyzed cross-coupling of arylboronic acids and pyridines, information that could not otherwise be extracted from the use of simple empirical models or studies based on product distributions. The mechanism derived from spectroscopic and kinetic studies shows that Ag(I) is activated for reduction of persulfate and an off-cycle protodeboronation by pyridine. These results provide the key mechanistic insight that enables control of the off-cycle process thus providing higher efficiency and yield. In addition, literature precedent and evidence provided herein demonstrate that Ag(II) is the likely oxidant responsible for formation of aryl radicals from aryl boronic acids. While the studies presented clarify several mechanistic details of the Ag(I)/persulfate catalyzed cross-coupling of arylboronic acids and pyridines, the

results may have impact in the design and refinement of other radical-based additions proceeding through catalytic oxidations mediated by Ag(I)/persulfate.

2.5 References

- (1) House, D. *Chem. Rev.* **1962**, *62*, 185–203.
- (2) Marshall, H. *Proc. Roy. Soc. Edin.* **1900**, *23*, 163.
- (3) Austin, P. C. *J. Chem. Soc., Trans.* **1911**, *99*, 262–266.
- (4) Yost, D. M. *J. Am. Chem. Soc.* **1926**, *48*, 152–164.
- (5) Greenspan, F. P.; Woodburn, H. M. *J. Am. Chem. Soc.* **1954**, *76*, 6345–6349.
- (6) Anderson, J. M.; Kochi, J. K. *J. Org. Chem.* **1970**, *35*, 986–989.
- (7) Chiba, S.; Cao, Z.; El Bialy, S. A. A.; Narasaka, K. *Chem. Lett.* **2006**, *35*, 18–19.
- (8) Seo, S.; Slater, M.; Greaney, M. F. *Org. Lett.* **2012**, *14*, 2650–2653.
- (9) Minisci, F.; Bernardi, R.; Bertini, F.; Galli, R.; Perchinummo, M. *Tetrahedron* **1971**, *27*, 3575–3579.
- (10) Fontana, F.; Minisci, F.; Barbosa, M. C. N.; Vismara, E. *J. Org. Chem* **1991**, *56*, 2866–2869.
- (11) Doll, M. K. H. *J. Org. Chem.* **1999**, *64*, 1372–1374.
- (12) Bennasar, M. L.; Roca, T.; Griera, R.; Bosch, J. *Org. Lett.* **2001**, *3*, 1697–1700.
- (13) Cowden, C. J. *Org. Lett.* **2003**, *5*, 4497–4499.
- (14) Lipinski, C. A.; Lamattina, J. L.; Hohnke, L. A. *J. Med. Chem.* **1985**, *28*, 1628–1636.
- (15) Palde, P. B.; Gareiss, P. C.; Miller, B. L. *J. Am. Chem. Soc.* **2008**, *130*, 9566–9573.
- (16) Sato, N.; Matsuura, T. *J. Chem. Soc., Perkin Trans. 1* **1996**, 2345–2350.
- (17) Kaur, N.; Lu, X.; Gershengorn, M. C.; Jain, R. *J. Med. Chem.* **2005**, *48*, 6162–6165.

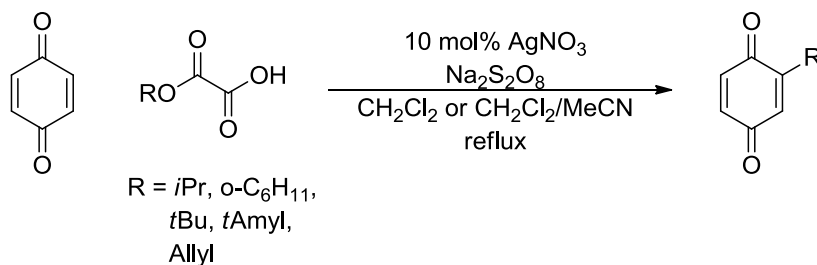
- (18) Carling, R. W.; Madin, A.; Guiblin, A.; Russell, M. G. N.; Moore, K. W.; Mitchinson, A.; Sohal, B.; Pike, A.; Cook, S. M.; Ragan, I. C.; Mckernan, R. M.; Quirk, K.; Ferris, P.; Marshall, G.; Thompson, S. A.; Wafford, K. A.; Dawson, G. R.; Atack, J. R.; Harrison, T.; Castro, L.; Street, L. J. *J. Med. Chem.* **2005**, *48*, 7089–7092.
- (19) Nam, T.; Rector, C. L.; Kim, H.; Sonnen, A. F.-P.; Meyer, R.; Nau, W. M.; Atkinson, J.; Rintoul, J.; Pratt, D. A.; Porter, N. A. *J. Am. Chem. Soc.* **2007**, *129*, 10211–10219.
- (20) Seiple, I. B.; Su, S.; Rodriguez, R. A.; Gianatassio, R.; Fujiwara, Y.; Sobel, A. L.; Baran, P. S. *J. Am. Chem. Soc.* **2010**, *132*, 13194–13196.
- (21) Degoe, D. A.; Grampovnik, D. J.; Flentge, C. a; Flosi, W. J.; Chen, H.-J.; Yeung, C. M.; Randolph, J. T.; Klein, L. L.; Dekhtyar, T.; Colletti, L.; Marsh, K. C.; Stoll, V.; Mamo, M.; Morfitt, D. C.; Nguyen, B.; Schmidt, J. M.; Swanson, S. J.; Mo, H.; Kati, W. M.; Molla, A.; Kempf, D. J. *J. Med. Chem.* **2009**, *52*, 2571–2586.
- (22) Aida, W.; Ohtsuki, T.; Li, X.; Ishibashi, M. *Tetrahedron* **2009**, *65*, 369–373.
- (23) Gutierrez, A. J.; Terhorst, T. J.; Matteucci, M. D.; Froehler, B. C. *J. Am. Chem. Soc.* **1994**, *116*, 5540–5544.
- (24) Tang, B.; Yu, F.; Li, P.; Tong, L.; Duan, X.; Xie, T.; Wang, X. *J. Am. Chem. Soc.* **2009**, *131*, 3016–3023.
- (25) Minisci, F.; Vismara, E.; Fontana, F.; Morini, G.; Serravalle, M.; Giordano, C. *J. Org. Chem.* **1986**, *51*, 4411–4416.
- (26) Blackmond, D. G. *Angew. Chem. Int. Ed.* **2005**, *44*, 4302–4320.
- (27) Mathew, J. S.; Klussmann, M.; Iwamura, H.; Valera, F.; Futran, A.; Emanuelsson, E. a C.; Blackmond, D. G. *J. Org. Chem.* **2006**, *71*, 4711–4722.
- (28) Devery, J. J.; Conrad, J. C.; MacMillan, D. W. C.; Flowers, R. A. *Angew. Chem. Int. Ed.* **2010**, *49*, 6106–6110.
- (29) Choquette, K. A.; Sadasivam, D. V.; Flowers, R. A., II. *J. Am. Chem. Soc.* **2011**, *133*, 10655–10661.
- (30) Apelblat, A.; Korin, E.; Manzurola, E. *J. Chem. Thermodyn.* **2001**, *33*, 61–69.
- (31) Bruehlman, R.; Verhoek, F. *J. Am. Chem. Soc.* **1948**, *70*, 1401–1404.

- (32) Bjerrum, J. *Acta Chem. Scand* **1972**, 26, 2734–2742.
- (33) Vosburgh, W. C.; Cogswell, S. A. *J. Am. Chem. Soc.* **1943**, 65, 2412–2413.
- (34) Alexiev, A.; Bonchev, P. R. *Mikrochim. Acta.* **1970**, 13–19.
- (35) Bonchev, P. R.; Aleksiev, A. A. *Theor. Exp. Chem.* **1973**, 9, 144–147.
- (36) Michaelis, A.; Becker, P. *Ber. Dtsch. Chem. Ges.* **1882**, 15, 180–185.
- (37) Seaman, W.; Johnson, J. *J. Am. Chem.* **1931**, 53, 711–723.
- (38) Johnson, J. R.; M. G. Van Campen, J.; Grummitt, O. *J. Am. Chem. Soc.* **1938**, 60, 111–115.
- (39) Anderson, J. M.; Kochi, J. K. *J. Am. Chem. Soc.* **1970**, 92, 1651–1659.
- (40) Lennox, A. J. J.; Lloyd-Jones, G. C. *J. Am. Chem. Soc.* **2012**, 134, 7431–7441.
- (41) Butters, M.; Harvey, J. N.; Jover, J.; Lennox, A. J. J.; Lloyd-Jones, G. C.; Murray, P. M. *Angew. Chem. Int. Ed.* **2010**, 49, 5156–5160.
- (42) Kalb, A.; Allen, T. *J. Am. Chem. Soc.* **1964**, 86, 5107–5112.
- (43) Shundrin, L. A.; Bardin, V. V.; Frohn, H.-J. *Zeitschrift für Anorg. und Allg. Chemie* **2004**, 630, 1253–1257.

Chapter 3. Mechanistic Studies of Ag(I)/Persulfate-Catalyzed Cross-Coupling of Arylboronic Acids to Quinones

3.1 Background and Significance

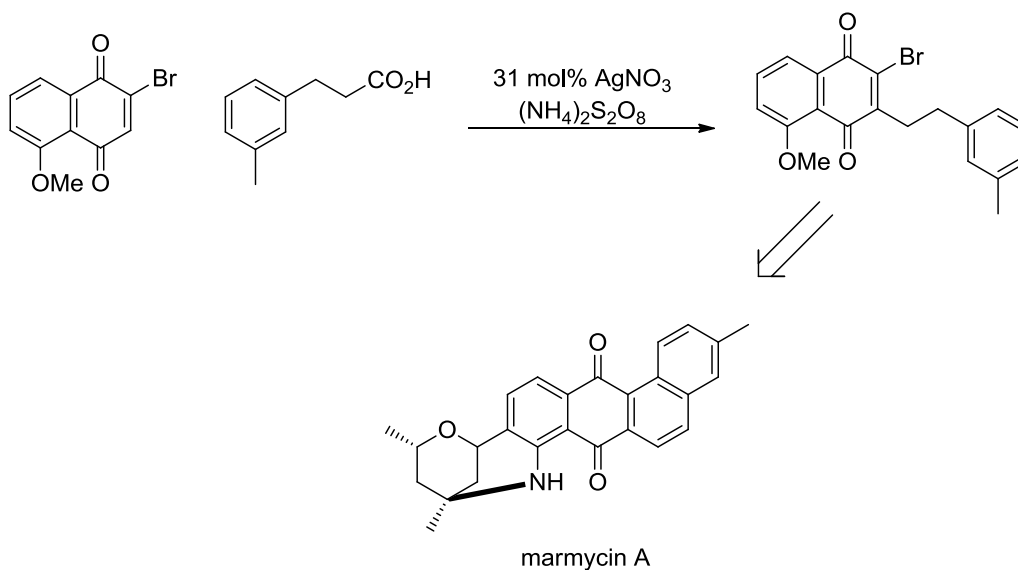
The work done by the Minisci group on the Ag/persulfate system spanned beyond the coupling of carboxylic acids to heteroarenes. They were also successful in developing a reaction involving the radical alkylation of benzoquinones by alkyl oxalates (Scheme 3.1).¹ The reaction involves oxidative decarboxylation of oxalic acid monoesters by Ag(II), followed by the addition of the resulting carbon centered radical to the quinone ring. Carboxylate or alkyl radicals can be generated by the initial oxidation by Ag(II). The double decarboxylation to form an alkyl radical only works if a stable radical can form.



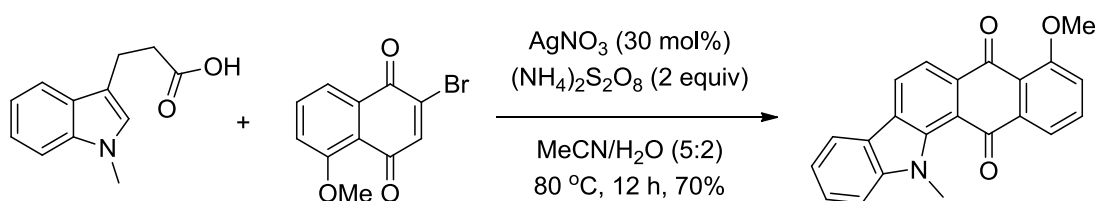
Scheme 3.1. Oxidative decarboxylation and coupling of oxalic acid derivatives to quinones

Aliphatic carboxylic acids have also been shown to couple with quinones.² Zhang and coworkers were successful in alkylating 2-bromonaphthoquinone using catalytic silver nitrate and ammonium persulfate (Scheme 3.2). This step was later used in the overall total synthesis of marmycin A. This group was later able to perform a tandem radical alkylation-cyclization-aromatization reaction of quinones and carboxylic acids to

form complex carbazole compounds using 30 mol% silver acetate and ammonium persulfate (Scheme 3.3).³



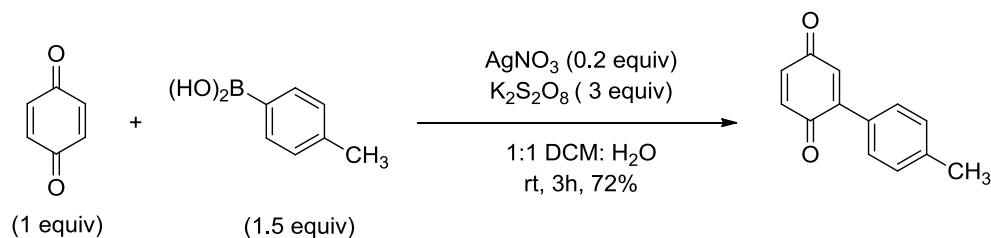
Scheme 3.2. Addition of alkyl radicals to naphthoquinones in total synthesis of marmycin A



Scheme 3.3. Tandem radical alkylation-cyclization-aromatization reaction sequence to produce carbazole compounds

3.1.1 Silver(I)/Persulfate-Catalyzed Cross-Coupling of Arylboronic Acids and Quinones

In addition to the cross-coupling of heteroarenes with arylboronic acids, Baran and coworkers were also successful in coupling the acids with quinones using the Ag(I)/persulfate oxidative system (Scheme 3.4).⁴



Scheme 3.4. Cross-coupling reaction of quinone with arylboronic acid

In chapter 2 of this dissertation, the effect of nitrogen coordination to silver was apparent in the inverse order seen in boronic acid, through the increased ability of Ag(I) to protodeboronate the acid. The aim of this chapter is to see how the reaction mechanism involving quinones differed from that of the electron-deficient pyridine, due to the absence of nitrogen-containing compounds to form complexes with silver in this reaction.

3.2 Experimental

3.2.1 Materials

AgNO₃ and K₂S₂O₈ were purchased from Acros Organics. **5** was purchased from Alfa Aesar. **2** was purchased from TCI Fine Chemicals. All chemicals were used without further purification.

3.2.2 Instrumentation

GC analyses were done using a Shimadzu Gas Chromatograph GC-14B. Proton and carbon NMR were recorded on a Bruker 500 MHz spectrometer. GC-MS analyses were done with an HP 5890 Series II Gas Chromatograph with an HP Mass Selector Detector. Column chromatography was performed using the automated CombiFlash® Rf system from Teledyne Isco, Inc. Products were separated using prepacked silica gel columns with a gradient elution of ethyl acetate and hexanes.

3.2.3 Methods

3.2.3.1 Procedure for degassing solvents

CH₂Cl₂ was purified by a Solvent Purification system (Innovative Technology Inc.; MA). H₂O was degassed by bubbling through with argon overnight.

3.2.3.2 Procedure for synthesis of 4-methyl-[1,1'-biphenyl]-2,5-dione (6)

In a 25 mL round bottom flask with a magnetic stirring bar, **5** and **2** were dissolved in 10 mL CH₂Cl₂. To the flask, 5 mL degassed H₂O was added. AgNO₃ was dissolved in 5 mL degassed water and added to the reaction. K₂S₂O₈ was added to the reaction as a solid. The flask was then evacuated of air, a septum was attached, and was back-filled with Ar. The reaction was allowed to stir overnight. Reaction workup involved diluting the reaction with 10 mL CH₂Cl₂ and quenching with 10 mL saturated bicarbonate solution. The organic layer was separated and run through a plug of neutral alumina. The alumina was washed with ethyl acetate. Product formation was confirmed by GC-MS. The organic layer was rotary evaporated to dryness. Crude product formation was observed by ¹H NMR in CDCl₃. Product was purified via automated flash chromatography and characterized by ¹H NMR and ¹³C NMR.

3.2.3.3 Procedure for Reaction Progress Kinetic Analysis studies

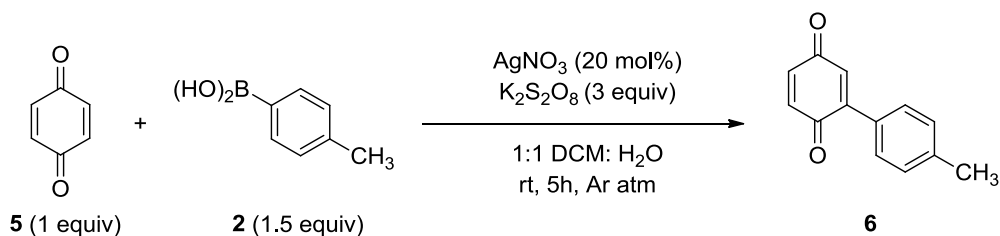
In a 100 mL round bottom flask with a magnetic stirring bar, **5** and **2** were dissolved in 30 mL CH₂Cl₂. To the flask, 15 mL degassed H₂O was added. AgNO₃ was dissolved in 15 mL degassed water and added to the reaction. K₂S₂O₈ was added to the reaction as a solid. The flask was then evacuated of air, a septum was attached, and was back-filled with Ar. The reaction was stopped and 0.5 mL aliquots were taken from the

organic layer during the course of the reaction. Aliquots taken were quenched with 1.0 mL saturated bicarbonate solution, and 0.5 mL of biphenyl in ethyl acetate solution was added as an internal standard. The organic layer was extracted and analyzed by GC.

3.3 Results

3.3.1 Kinetic Analysis

To study this catalytic system, the reaction of 1,4-benzoquinone (**5**) and *p*-tolylboronic acid (**2**) using catalytic silver nitrate (20 mol%) and excess potassium persulfate (3 equiv) in dichloromethane/water was examined (Scheme 3.5). Studies of this reaction were done at room temperature, under argon atmosphere for 5 hours.



Scheme 3.5. Cross-coupling reaction of quinone with arylboronic acid for kinetic studies

3.3.1.1 Kinetic Order Experiments

In order to determine the kinetic orders of the substrates in this reaction, a 100% run was first done under the conditions shown in Table 3.1. The loss of **5** was monitored over time. Surprisingly, the loss of starting material over time was not exponential but linear (Figure 3.1). The linear portion of the decay was fit to a straight line, in which the slope is equal to $-k_{\text{obs}}$ (Figure 3.2). A linear decay resulting from a concentration vs. time plot suggests that the reaction is zero order in the substrate being monitored. Since the

loss of **5** was being monitored, this suggests that the cross-coupling reaction of quinone and boronic acid is zero order in **5**.

Table 3.1. Conditions for different excess experiments for rate order of **2**

Run	[5] (M)	[2] (M)	[K ₂ S ₂ O ₈] (M)	[AgNO ₃] (M)
10-100%	0.1	0.15	0.3	0.02
11	0.1	0.3	0.3	0.02

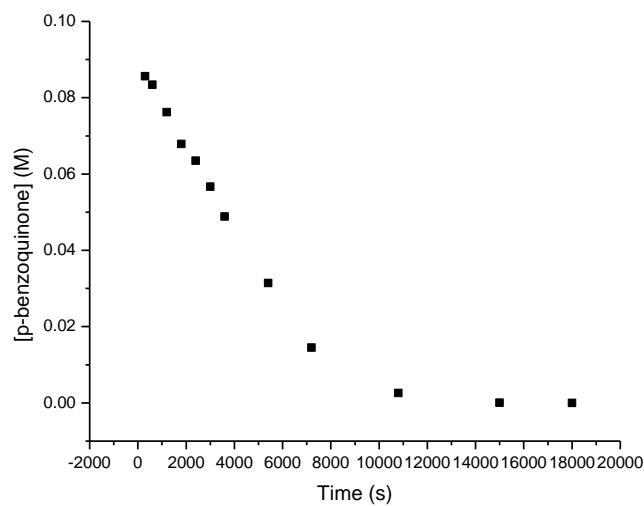


Figure 3.1. Decay plot of Run 10

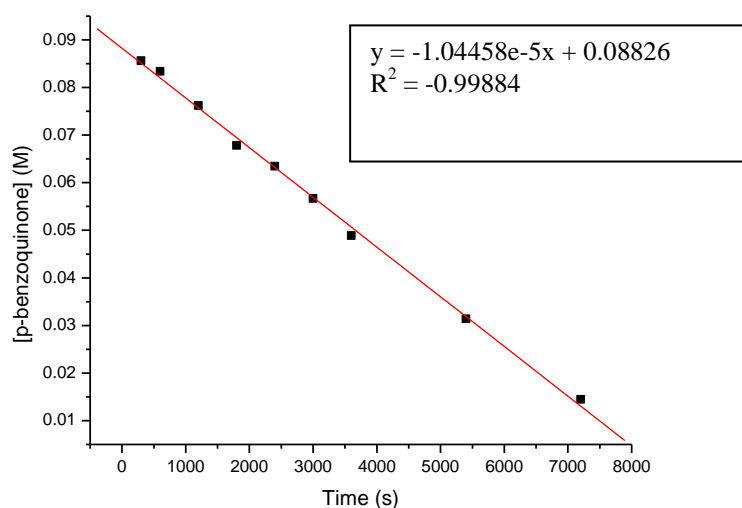


Figure 3.2. Linear fit of Run 10

To determine the order of **2**, a kinetic reaction was run under the conditions shown in Run 11 (Table 3.1), in which the [**2**] was doubled compared to that of Run 10. Once again, the loss of **5** was linear over time (Figure 3.3). The linear portion of this decay was fit to a straight line, as shown in Figure 3.4. The linear fits of Runs 10 and 11 were used to produce a $-d[\mathbf{5}]/dt$ vs. time plot (Figure 3.5) comparing both reactions. The resulting plot produces a horizontal line, suggesting that increasing concentrations of **5** does not affect the rate of the reaction. This confirms the zero order dependence suggested for **5**. When Runs 10 and 11 are plotted together, there is graphical overlay, suggesting that **2** is also zero order in this reaction.

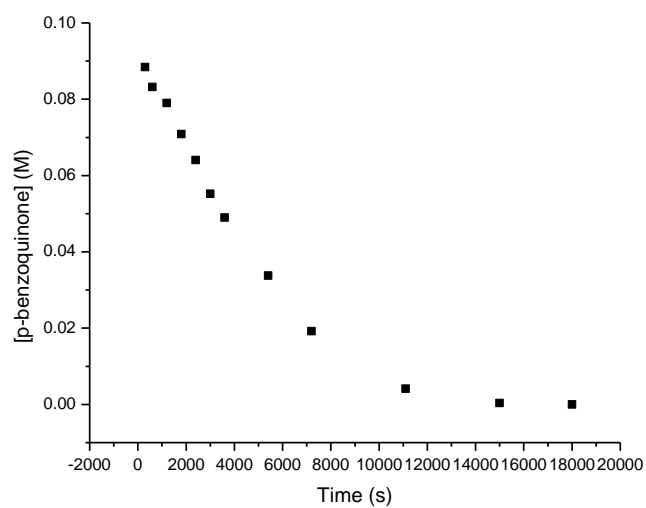


Figure 3.3. Decay plot of Run 11

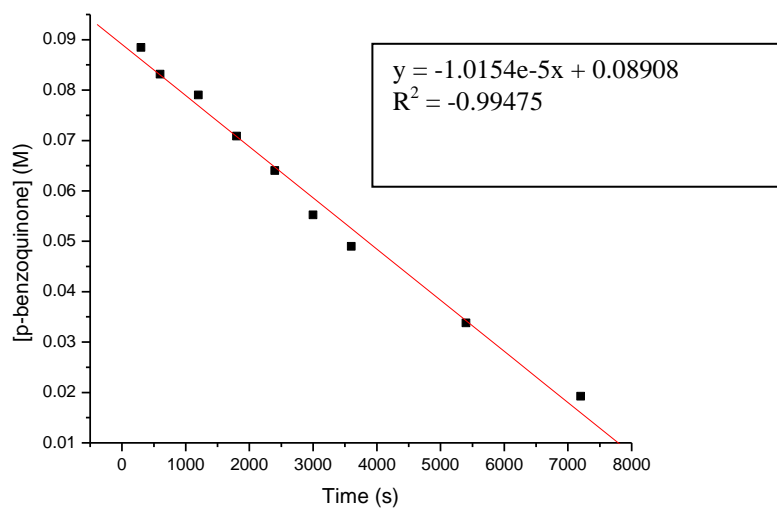


Figure 3.4. Linear fit of Run 11

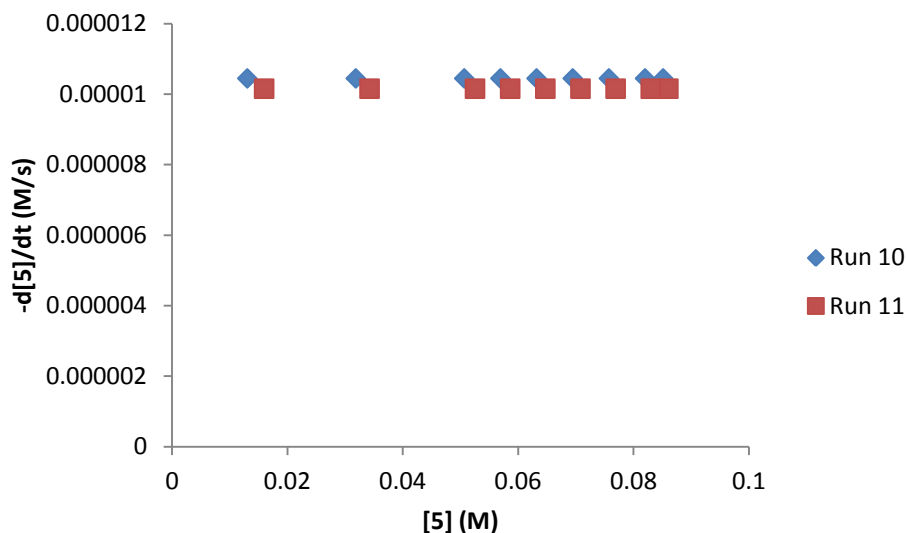
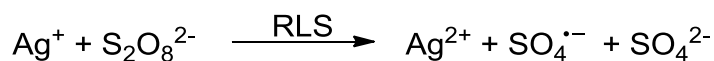


Figure 3.5. Plot of rate vs. [4] for rate order for 2

3.3.2 Proposed Mechanism for the Ag(I)/Persulfate-Catalyzed Cross-Coupling of Arylboronic acids and Quinones

3.3.2.1 Proposed Mechanism

Based on the kinetic data, it is proposed that the mechanism of the reaction of **5** and **2** in the presence of catalytic silver nitrate and potassium persulfate involves the reduction of $S_2O_8^{2-}$ by Ag(I) as the first and rate limiting step of the reaction (Scheme 3.6), following classic Ag(I)/persulfate chemistry.

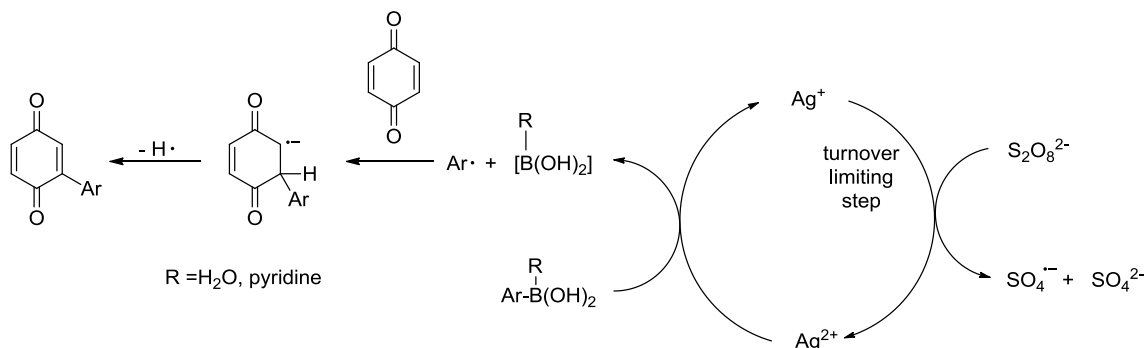


Scheme 3.6. Proposed Mechanism of the Ag(I)/Persulfate-Catalyzed Reaction of Arylboronic acids and Quinones

3.3.2.2 Proposed Catalytic Cycle

From this proposed mechanism, an overall catalytic cycle for this reaction involves the oxidation of Ag(I) to Ag(II) by persulfate, followed by the oxidation of

boronic acid to produce an aryl radical. This radical can then add to the quinone, and upon loss of a proton produces the cross-coupled product.



Scheme 3.7. Proposed Catalytic Cycle of the Ag(I)/Persulfate-Catalyzed Reaction of Arylboronic acids and Quinones

3.4 Conclusion

The kinetic studies, in conjunction with those shown in Chapter 2, suggest that mechanism of the reaction of arylboronic acids and quinones varies significantly with that of the electron-deficient pyridines. The absence of a nitrogen-containing ligand in this reaction affects the orders of substrates in this reaction, in which both substrates were found to be zero. These results suggest that the mechanism of this reaction goes through classic Ag/persulfate chemistry, in which Ag(I) is oxidized by persulfate in the rate limiting step of the reaction.

3.5 References

- (1) Coppa, F.; Fontana, F.; Lazzarini, E.; Minisci, F. *Chem. Lett.* **1992**, 1299–1302.
- (2) Ding, C.; Tu, S.; Li, F.; Wang, Y.; Yao, Q.; Hu, W.; Xie, H.; Meng, L.; Zhang, A. *J. Org. Chem* **2009**, *74*, 6111–6119.
- (3) Ding, C.; Tu, S.; Yao, Q.; Li, F.; Wang, Y.; Hu, W.; Zhang, A. *Adv. Synth. Catal.* **2010**, *352*, 847–853.
- (4) Fujiwara, Y.; Domingo, V.; Seiple, I. B.; Gianatassio, R.; Del Bel, M.; Baran, P. S. *J. Am. Chem. Soc.* **2011**, *133*, 3292–3295.

4. Mechanistic Studies of Ag(I)-Catalyzed Decarboxylative Fluorination

4.1 Background and Significance

4.1.1 Importance of Carbon-Fluorine Bonds

Carbon-fluorine bond formation is becoming increasingly prevalent in the chemical industry due to the presence of these bonds in a large number of compounds of pharmaceutical^{1,2} and biological importance.³⁻⁵ Approximately 20% of commercially available pharmaceuticals and 30% of agrochemicals contain fluorine.⁶ Fluorination of pharmaceuticals can increase the lipophilicity and metabolic stability of the drug compound, enhancing the efficacy and bioavailability of a drug compound.^{1,7} In addition to pharmaceutical and agrochemical compounds, the presence of fluorine is vital in polymers,⁸ materials,^{9,10} and for molecular positron emission tomography (PET) imaging (Figure 4.1).^{11,12} Despite the abundance of fluorine in nature, as well as the vast utility of this functional group, there are only a small number of naturally occurring organic compounds.¹³ For these reasons, the development of facile and versatile fluorination methods is essential.

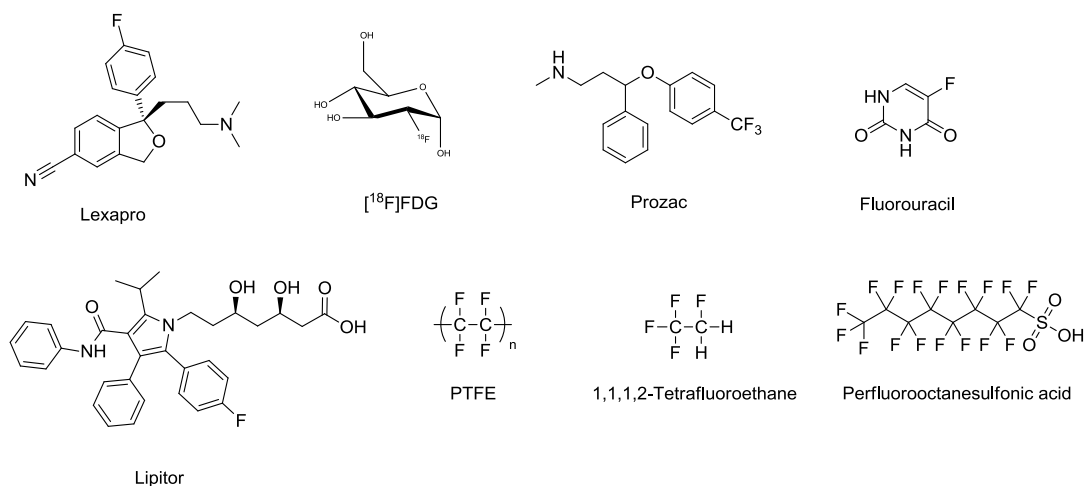


Figure 4.1. Examples of important fluorinated compounds

In recent years, significant progress has been made in the synthesis of C-F bonds through transition metal-catalyzed methods,^{6,14,15} and in particular, a great emphasis has been placed on the use of electrophilic fluorinating reagents in conjunction with metal catalysts. The understanding of metal-catalyzed fluorinations is critical for the optimization of existing methods, expansion of substrate scope, enhancement of chemoselectivity, as well as the development of new synthetic reactions.

4.1.2 Fluorinating Reagents

4.1.2.1 Nucleophilic fluorinating reagents

The use of fluoride ions as fluorinating reagents tends to be difficult due to their lack of solubility, as well as their dual reactivity as both a nucleophile and a base.¹⁵ Nucleophilic fluorinating reagents were developed as sources of fluoride ions, which have better solubility and better reactivity. The corrosive and reactive nature of HF can be controlled for use in nucleophilic fluorination by the use of amines, by reducing its

nucleophilicity (eg. TREAT·3HF and hydrogen fluoride pyridine). Another approach to increasing the nucleophilicity of fluoride, which is a hard Lewis base, is to pair it with a soft Lewis acid, such as S-F reagents (eg. DAST and DeoxoFluor). A number of nucleophilic reagents are shown in Figure 4.2.

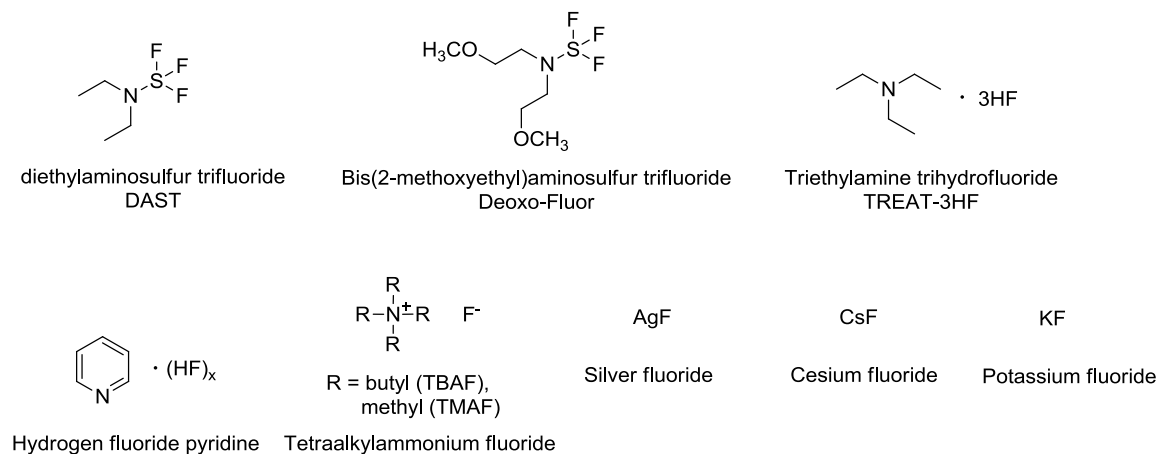


Figure 4.2. Examples of commonly used nucleophilic fluorinating reagents

4.1.2.2 Electrophilic fluorinating reagents

The majority of electrophilic fluorinating reagents are derived from fluorine gas, the strongest elemental oxidant. Elemental fluorine was isolated by Moissan in 1886, which later earned him a Nobel Prize.³ For years, F_2 was the only reagent available for electrophilic fluorinations. However, high reactivity, lack of selectivity, and toxicity are all properties that make it difficult to work with the reagent. Diluting F_2 with inert gases such as argon and nitrogen greatly expanded the scope of fluorinations with the reagent. In 1968, the first electrophilic fluorinating reagent, fluoroxytrifluoromethane (CF_3OF), was reported by Barton and coworkers.¹⁶ The use of this reagent was quickly followed by the development and use of perchloryl fluoride (FClO_3), as well as acyl and perfluoroacyl

hypofluorites (RC(O)OF and $\text{R}_\text{F}\text{C(O)OF}$). While these reagents have proven effective in the fluorination of a number of organic compounds, they have many drawbacks, including high reactivity and lack of selectivity. Xenon difluoride (XeF_2) was developed as a more stable alternative, but its high oxidation potential still limits its use as an electrophilic fluorinating source.

The difficulties associated with direct fluorination have stimulated the development of alternative sources of electrophilic fluorine in the form of N-F reagents. The lower electronegativity of nitrogen compared to oxygen, as well as the stronger bond of N-F compared to O-F, allow for the N-F reagents to be stable and easy to handle. The N-F fluorinating reagents are either neutral R_2NF compounds or quaternary ammonium $\text{R}_3\text{N}^+\text{F}^- \text{X}^-$ salts, where X^- is a non-nucleophilic anion (Figure 4.3). The organonitrogen fragments are designed to be good leaving groups, promoting the reactivity of the bound fluorine with nucleophiles in an $\text{S}_\text{N}2$ type reaction.¹⁷ Umemoto and coworkers were the first to isolate N-fluoropyridinium salts, which showed good reactivity on organic molecules.¹⁸ The development of Selectfluor® (1-chloromethyl-4-fluoro-1,4-diazoniabicyclo[2.2.2]octane bis(tetrafluoroborate, F-TEDA- BF_4) presented a major advance for electrophilic fluorination because the reagent is mild, stable, and commercially available.¹⁹

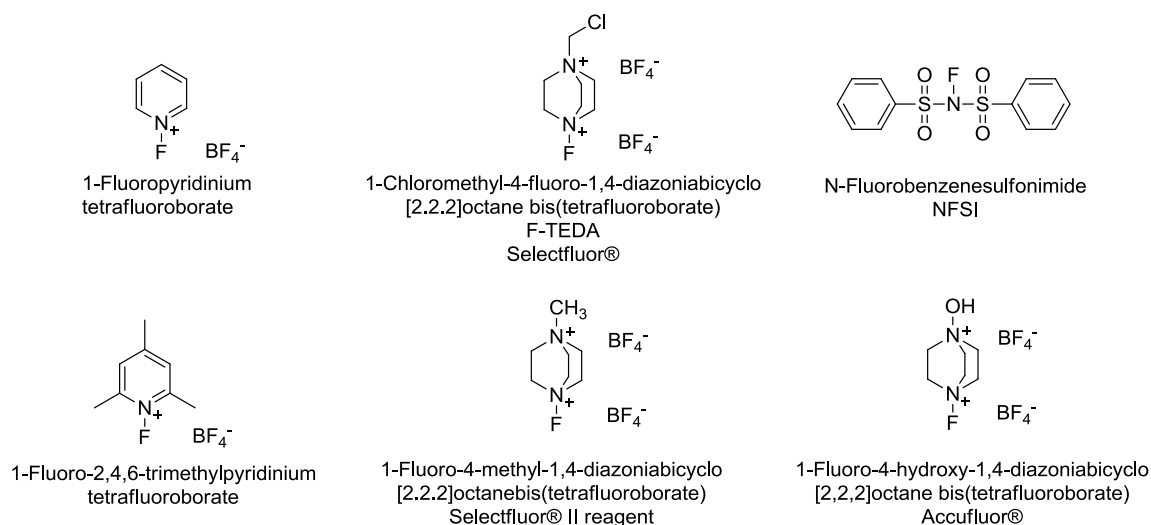
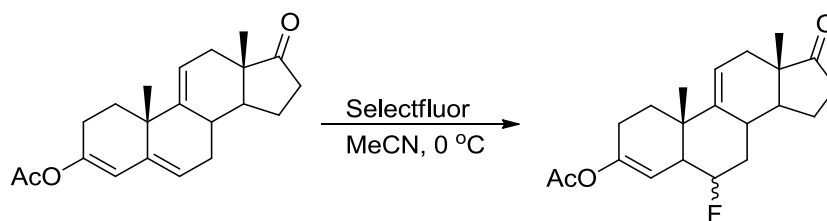


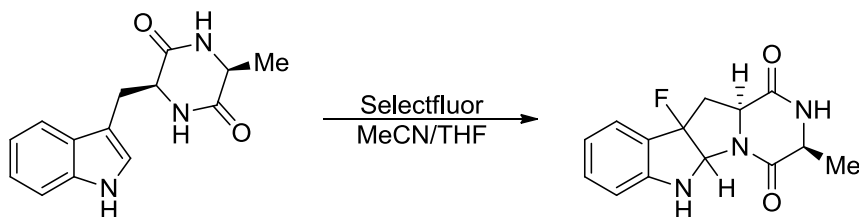
Figure 4.3. Examples of commonly used N-F electrophilic fluorinating reagents

Herrington and coworkers examined the reaction of steroid 3,5-dienol acetates with electrophilic fluorinating reagents for the purpose of selecting a reagent for use in commercial scale synthesis.²⁰ They reported that Selectfluor was the best reagent for the conversion of glucocorticoids to fluorinated products (Scheme 4.1).



Scheme 4.1. Glucocorticoid fluorination

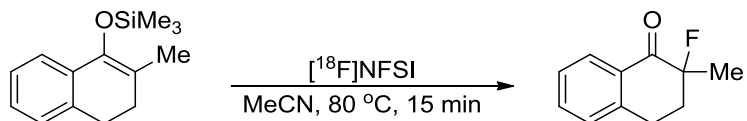
The indole moiety is present in a variety of natural products including gypsetin. The fluorination of this biologically relevant molecule was presented by Wong and coworkers, who developed a Selectfluor-mediated fluorination method (Scheme 4.2).²¹



Scheme 4.2. Fluorination of gypsetin derivative

Electrophilic fluorinating reagents can also be used in radiolabeling. The conditions required for the preparation of ^{18}F -radiotracers used for PET imaging are very different from that of conventional ^{19}F -fluorination. The ^{18}F isotope has a short-lived half-life of 110 minutes.¹¹ As a result, all manipulations for the synthesis of ^{18}F -labeled compounds, including purification, must be completed in approximately 1-2 hours to ensure sufficient active material for clinical use. In addition, it is necessary to introduce the radioisotope as late as possible in synthesis to achieve maximum efficiency. To aid in these syntheses, a number of ^{18}F -electrophilic fluorinating reagents have been produced and used and tested in synthesis.

The Gouverneur group has done a significant amount of work in this area, beginning with the synthesis of $[\text{}^{18}\text{F}]\text{-NFSI}$.²² They showed the reactivity of this compound by performing the radiofluorination of silyl enol ether, which produced the fluorinated product in the absence of radiofluorinated side-products (Scheme 4.3). In addition, the reaction was complete in 15 min. This reagent was suitable for the radiolabeling of various other silyl enol ethers and allylsilanes.

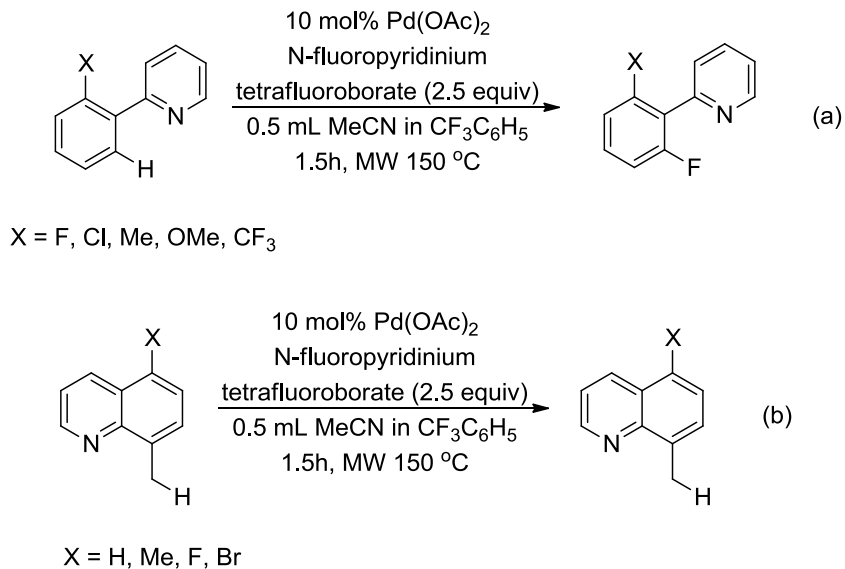


Scheme 4.3. Radiolabeled $[\text{}^{18}\text{F}]$ -fluorination of silyl enol ether

There are many hypotheses on the mechanism of reaction of electrophilic fluorinating reagents.^{17,19} Reaction with Selectfluor may proceed through S_N2 displacement, with nucleophilic attack at the fluorine. However, other competing pathways are also possible, such as single-electron transfer. Fluorine atom abstraction from Selectfluor is possible, resulting in an organonitrogen radical cation. Hu and coworkers used electron momentum spectroscopy to confirm that the lone pairs of electrons on the two nitrogens of 1,4-diazabicyclo[2.2.2]octane (DABCO) do not occupy the expected orbitals according to classical valence bond theory,²³ a theory that had been proposed by Hoffman in the 1960s.²⁴ The radical cation of DABCO, as a result, is very stable. This finding provides support to a single electron transfer mechanism.

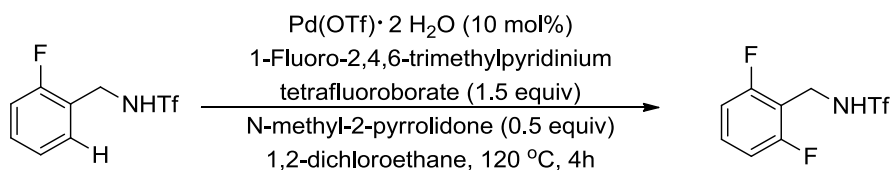
4.1.3 Transition-Metal Mediated Electrophilic Fluorination

In 2006, Sanford and coworkers developed the first palladium-catalyzed method for the formation of aromatic and benzylic C-F bonds.²⁵ A catalytic amount of Pd(OAc)₂ in conjunction with the electrophilic fluorinating reagent N-fluoropyridinium tetrafluoroborate under microwave conditions was efficient for the fluorination of a variety of C-H bonds (Scheme 4.4). The method was found to be useful for a wide range of starting materials, and showed broad substrate scope due to its tolerance of many functional groups, including aryl halides, nonenolizable ketones and esters, trifluoromethyl substituents, and methyl ethers. This reaction was effective in the benzylic C-H fluorination of a number of substituted quinolines, as shown in Scheme 4.4.



Scheme 4.4. Palladium-catalyzed fluorination of (a) phenylpyridines and (b) quinolines

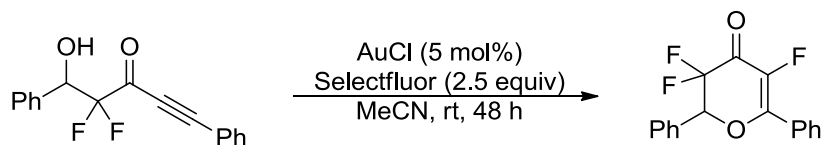
The Yu group then developed a synthetically versatile ortho-C-H fluorination method with triflamide-protected benzylamines using N-fluoro-2,4,6-trimethylpyridinium triflate, a palladium catalyst, and N-methylpyrrolidinone (NMP) (Scheme 4.5).²⁶ The use of 0.5 equiv of NMP was found to be critical for success of the reaction. They propose that the combination of triflamine substrate and a substoichiometric amount of NMP as a promoter is crucial for the formation of a cationic pentacoordinated Pd(IV) complex, formed upon the oxidation of a Pd-intermediate by the electrophilic fluorinating source.



Scheme 4.5. Palladium-catalyzed selective fluorination of benzyltriflamides

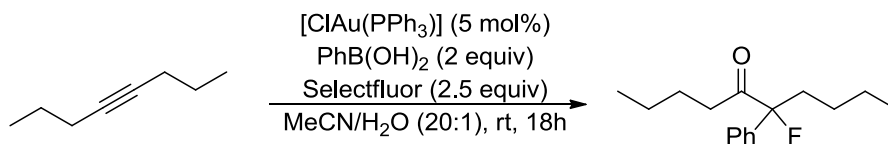
In 2008, Gouverneur and coworkers reported the feasibility of Au(I)-catalyzed alkoxyhalogenation of β -hydroxy- α,α -difluoroyrones, including a cyclization-

fluorination cascade.²⁷ Exposure of ynones to a mixture of AuCl and Selectfluor gave cyclized-fluorinated products (Scheme 4.6). This was the first example of a reaction combining a gold catalyst and an electrophilic fluorination source, as well as the first example of oxidative fluorination of an organogold intermediate.



Scheme 4.6. Gold-catalyzed cyclization-fluorination of alkynes

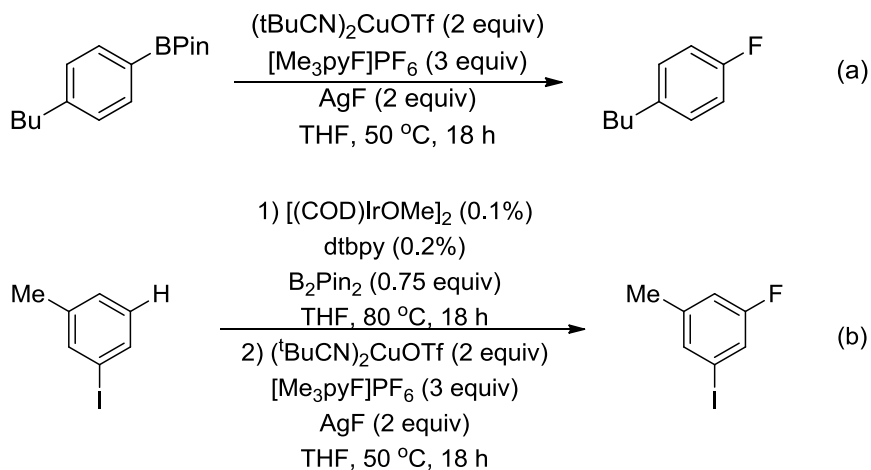
In 2010, Hammond and Xu revealed the hydration of alkynes to give α -substituted α -fluoroketones in one pot, under mild conditions (Scheme 4.7).²⁸ In addition, the formation of a Au(III) intermediate was confirmed by X-ray photoelectron spectroscopy (XPS) studies. This paper was the first to experimentally show the oxidation of Au(I) to Au(III) by Selectfluor.



Scheme 4.7. Gold-catalyzed hydration-fluorination of alkynes

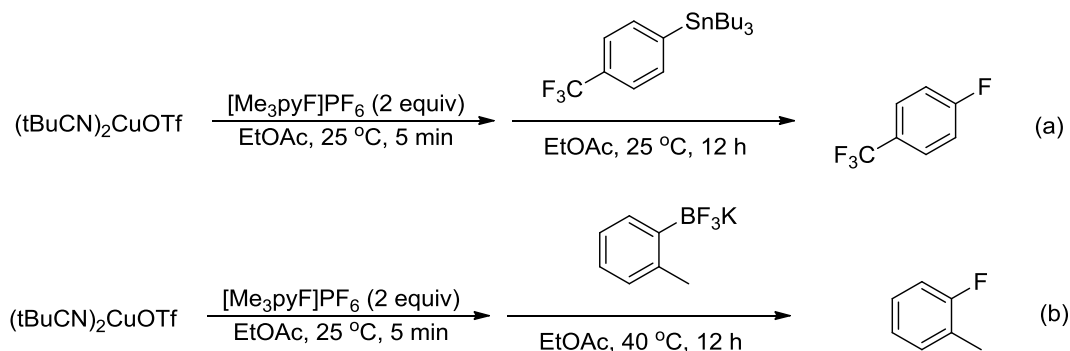
The Hartwig group presented a copper-mediated fluorination of arylboronate esters that proceeds under mild conditions and shows broad substrate scope (Scheme 4.8a).²⁹ Electron-rich, electron-deficient, ortho-substituted, and diversely functionalized arylboronate esters undergo fluorination in good yield. In addition, sequential, one-pot processes allow the fluorination of arenes to occur through arylboronate ester intermediates generated in situ (Scheme 4.8b). Mechanistic studies of this reaction suggest that the fluorination of arylboronate esters occurs by the initial formation of a

Cu(III) fluoride complex from the oxidation of Cu(I) by $[\text{Me}_3\text{pyF}]\text{PF}_6$, which was identified by NMR and ESI-MS spectroscopy.



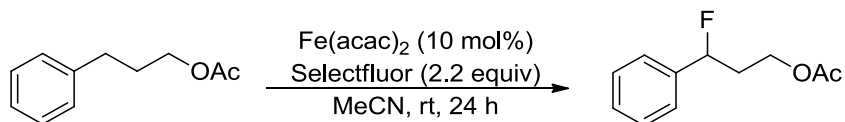
Scheme 4.8. (a) Copper-mediated fluorination of arylboronate esters and (b) fluorination of arenes via C-H borylation

The Sanford group later developed a similar method in which they also used copper and $[\text{Me}_3\text{pyF}]\text{PF}_6$ to perform the fluorination of aryl stannanes and aryl trifluoroborates (Scheme 4.9).³⁰ Substrates bearing aryl aldehydes, ketones, amides, and esters produced the aryl fluorides in good yields.



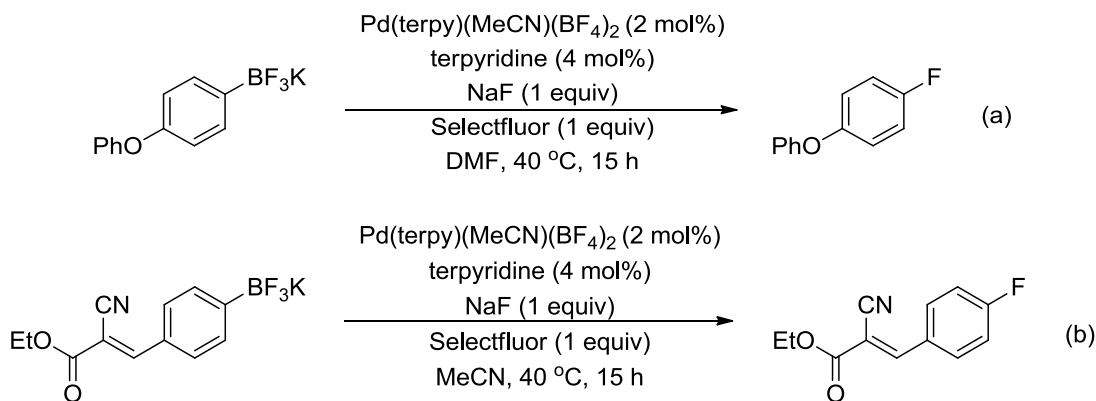
Scheme 4.9. Copper-mediated fluorination of (a) aryl stannanes and (b) aryl trifluoroborates

Lectka and coworkers performed studies using an iron(II) catalyst and Selectfluor to promote the fluorination of benzylic substrates (Scheme 4.10).³¹ Electron-poor or more neutral alkyl benzenes proved most promising, whereas electron-rich aromatic systems led to varying quantities of polyfluorinated products, often ring fluorination adducts.



Scheme 4.10. Iron-catalyzed benzylic fluorination

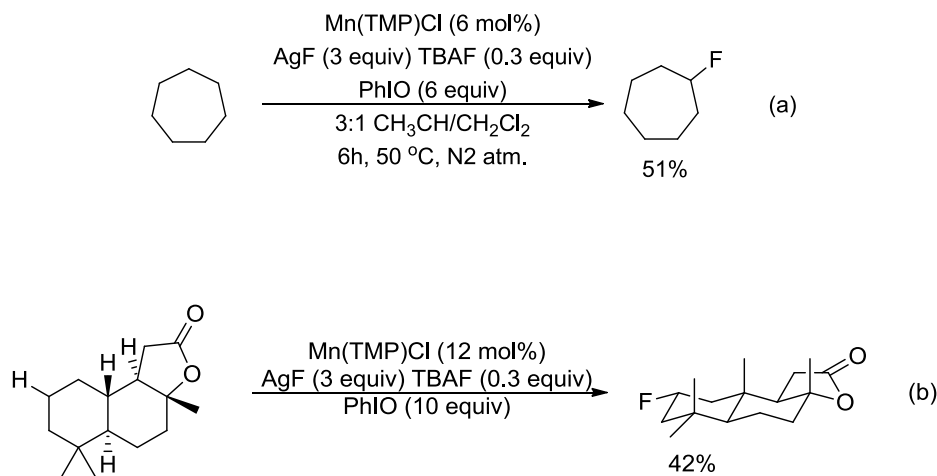
Ritter and coworkers developed the first metal-catalyzed method for the fluorination of arylboronic acid derivatives utilizing a terpyridyl Pd(II) complex (Scheme 4.11).³² The reaction proceeds under mild conditions, and is tolerant toward moisture and air. Mechanistic studies of this reaction suggest a single electron transfer mechanism involving a Pd(III)-intermediate, which was isolated and characterized by x-ray crystallography. This intermediate is formed upon the oxidation of Pd(II) in the turnover-limiting step of the reaction.



Scheme 4.11. Palladium-catalyzed fluorination of aryl trifluoroborates

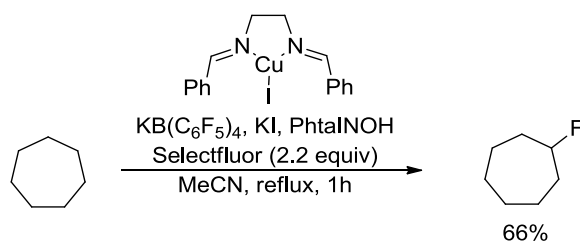
4.1.4 Aliphatic Carbon-Fluorine Bond Forming Reactions

The number of aliphatic C-F bond forming reactions has increased significantly in the past few years. Groves and coworkers developed a method involving the oxidative fluorination of a number of aliphatic C-H bonds by using catalytic manganese porphyrin, a commercially available fluoride salt as the fluoride ion source, and iodosylbenzene as a stoichiometric oxidant.³³ Simple alkanes (Scheme 4.12a), terpenoids (Scheme 4.12b), and steroids were found to undergo oxidative fluorination.



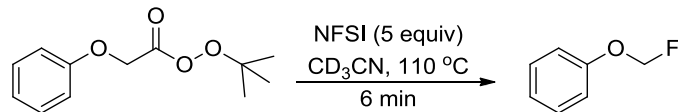
Scheme 4.12. Manganese porphyrin-catalyzed C-H fluorination of (a) heptanes, a simple alkane and (b) sclareolide, a sesquiterpene lactone

Similar fluorinations were achieved by the Lectka group, in which they were able to use a catalytic amount of a copper(I) bisimine complex, Selectfluor, *N*-hydroxyphthalimide as a radical precursor, and KB(C₆F₅)₄ as a anionic phase-transfer catalyst to fluorinate a series of aliphatic (Scheme 4.13), benzylic, and allylic substrates.³⁴



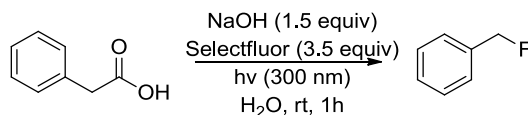
Scheme 4.13. Copper bis-imine catalyzed fluorination of heptanes

Sammis and coworkers also investigated the potential for fluorine atom transfer to alkyl radicals.³⁵ They found that peroxyesters could undergo decarboxylation and subsequent fluorination using common electrophilic fluorinating reagents, such as NFSI and Selectfluor (Scheme 4.14). This method proved efficient for a broad range of alkyl radicals, including tertiary, benzylic, and heteroaromatic-stabilized radicals. These experiments represented the first examples of fluorine transfer from an organic reagent to an alkyl radical.



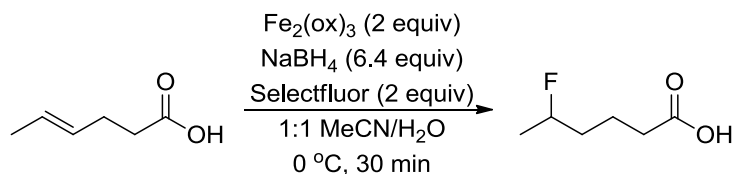
Scheme 4.14. Decarboxylative radical fluorination using NFSI

In addition to the decarboxylation of peroxyesters, the Sammis group was also successful in performing the fluorodecarboxylation of 2-aryloxy and 2-aryl carboxylic acids through UV irradiation.³⁶ They found that fluorinated products were generated in the absence of transition metals when an alkaline solution and Selectfluor were combined with the substrate and irradiated at 300 nm (Scheme 4.15).



Scheme 4.15. Photo-fluorodecarboxylation of phenylacetic acid

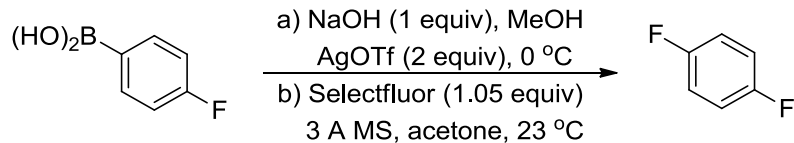
The Boger group developed a method involving the hydrofluorination of unactivated alkenes using stoichiometric quantities of $\text{Fe}_2(\text{ox})_3$ and NaBH_4 , with Selectfluor as a fluorine source (Scheme 4.16).³⁷ They propose the generation of an alkyl radical from the unactivated alkene, followed by free radical fluorination by Selectfluor. This method shows broad alkene scope, excellent functional group tolerance, exclusive Markovnikov regioselectivity, and is tolerant to air and moisture.



Scheme 4.16. Iron(III)-mediated fluorination of unactivated alkenes

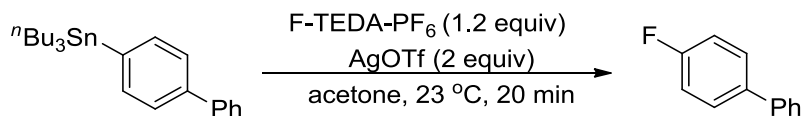
4.1.5 Silver-Mediated Fluorinations

In 2009, the Ritter group developed the first practical reaction sequence for the conversion of arylboronic acids to aryl fluorides (Scheme 4.17).³⁸ A benefit of this reaction is the commercial availability of the substrates, as well as the ability to perform this reaction on a multigram scale. This silver-mediated reaction was also useful for the fluorination of aryl- and alkenylboronic acids and esters.



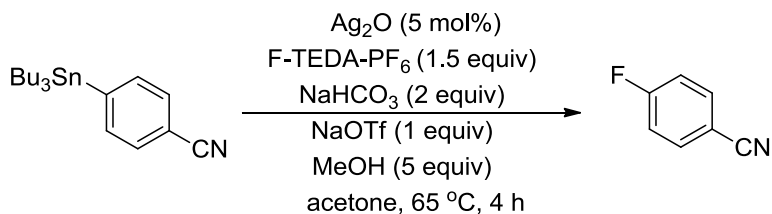
Scheme 4.17. Silver-mediated electrophilic fluorination of aryl boronic acid

The same group also developed a silver-mediated fluorination method for the functionalization of aryl stannanes (Scheme 4.18).³⁹ This reaction proved to be applicable to the late-stage fluorination of complex molecules such as quinine and camptothecin.



Scheme 4.18. Silver-mediated electrophilic fluorination of aryl stannanes

Later, Ritter and coworkers reported the first use of silver to form carbon heteroatom bonds by cross-coupling catalysis, in which they developed a catalytic method for fluorination of aryl stannanes (Scheme 4.19).⁴⁰ They applied silver catalysis to late stage fluorination, in which a number of complex small molecules were fluorinated from their stannane precursors, including polypeptides, polyketides, and alkaloids, a few of which are shown in the examples of flavanone, estrone, and DOPA in Figure 4.4.

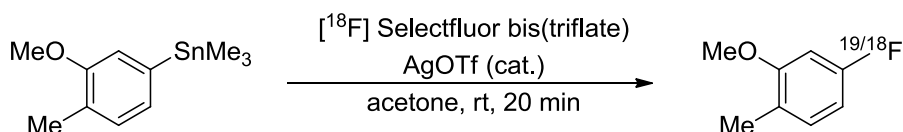


Scheme 4.19. Silver-catalyzed electrophilic fluorination of aryl stannanes



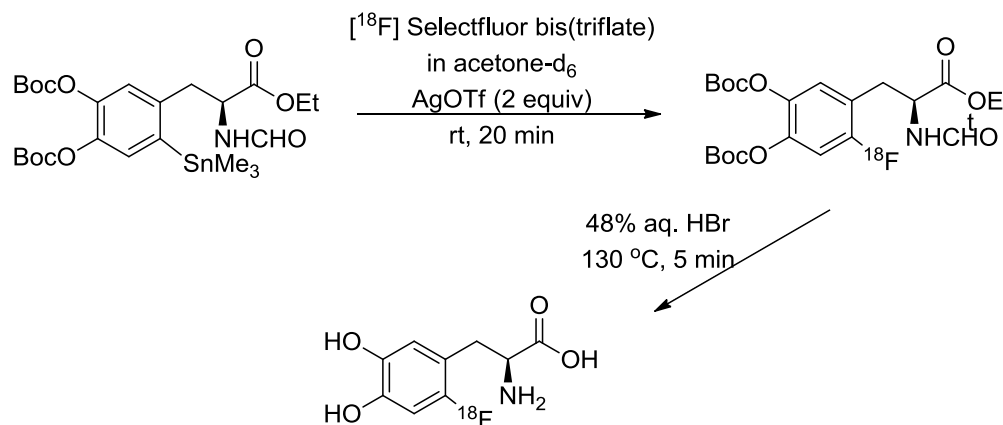
Figure 4.4. Silver-catalyzed fluorination of complex small molecules by Ritter

This work was expanded on by the Gouverneur group for the synthesis of [^{18}F]-labeled materials.⁴¹ In addition to the synthesis and application of [^{18}F]-NFSI mentioned in Section 4.1.2, the Gouverneur group also synthesized [^{18}F]-Selectfluor, and showed its reactivity with silver salts. In order to avoid the problems that arise from isotopic exchange, they chose to synthesize [^{18}F]-Selectfluor bis(triflate) as opposed to the bis(tetrafluoroborate) compound. They found that this new reagent could be successfully utilized for the synthesis of ^{18}F -labeled materials. Aryl stannanes were successfully fluorinated using catalytic AgOTf in 20 min under mild conditions (Scheme 4.20).



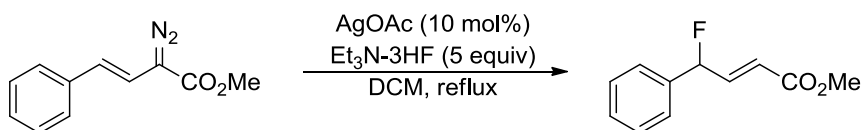
Scheme 4.20. Radiolabeled [^{18}F]-fluorodestannylation

Dopamine metabolism can be monitored by ^{18}F -labeled L-DOPA, a technique that is useful in neurological diseases, such as schizophrenia and Parkinson's disease.¹⁹ The scope of [^{18}F]-Selectfluor bis(triflate) was extended by proving to be a suitable reagent for the generation of [^{18}F]-6-fluoro-L-DOPA.⁴² This reaction can be performed on arylstannanes (Scheme 4.21), as well as protected arylboronic esters in the presence of catalytic AgOTf.



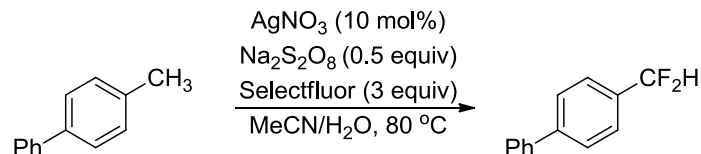
Scheme 4.21. Synthesis of [^{18}F]-6-fluoro-L-DOPA

Davies and coworkers were able to apply silver catalysis to the fluorination of vinyl diazoacetates to generate γ -fluoro- α,β -unsaturated carbonyls (Scheme 4.22).⁴³ The scope of the reaction was examined with a variety of vinyldiazo derivatives. The reaction was found to be general, and the size of the ester group did not affect the efficiency of the reaction.



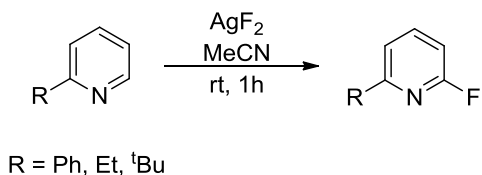
Scheme 4.22. Silver-catalyzed vinylogous fluorination

The Tang group was the first to use silver catalysis for the activation of benzylic C-H bonds to prepare difluoromethylated arenes.⁴⁴ Under mild reaction conditions, they used silver nitrate, Selectfluor, and a substoichiometric amount of persulfate to produce difluoromethylated arenes (Scheme 4.23). Although the use of persulfate was not required in this reaction, the use of the oxidant led to a higher conversion of starting material.



Scheme 4.23. Silver-catalyzed difluoromethylation of benzylic C-H bonds

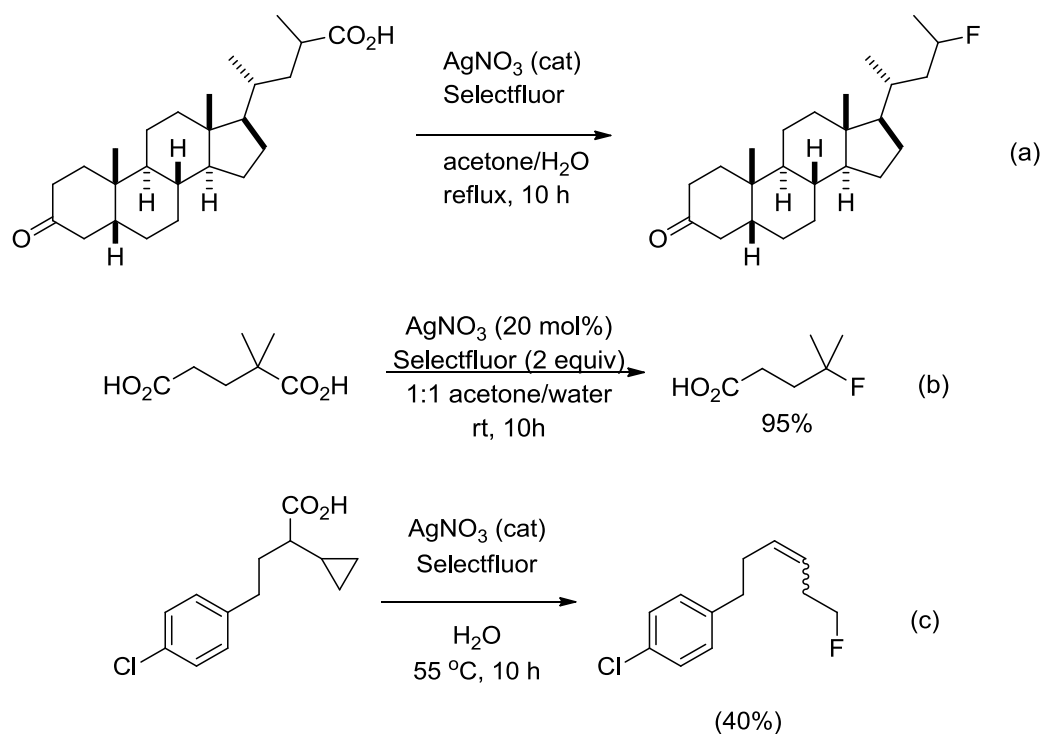
A broadly applicable method for the site-selective C-H fluorination of pyridines and diazines using AgF_2 was developed by the Hartwig group (Scheme 4.24).⁴⁵ The appeal of this reaction stems from the use of a commercially available silver salt as the fluorinating reagent, as well as the mild synthetic conditions. This reaction was designed based on the mechanism of the Chichibabin reaction, in which pyridines react with NaNH_2 to form 2-aminopyridines. The fluorination occurs on a broad range of substituted pyridines with both electron-donating and electron-withdrawing groups at each position of the ring. Pyridines containing ketones, esters, amides, acetals, protected alcohols and amines, nitriles, alkyl tosylates, and enolizable carbonyls underwent fluorination in good yield, while keeping those functionalities unreacted. In addition, pyridines containing bromide and chloride substituents in the 2-position of the pyridine remained intact, even though they are susceptible to nucleophilic displacement.



Scheme 4.24. Fluorination of pyridines with AgF_2

Li and coworkers reported the silver-catalyzed decarboxylative fluorination of aliphatic carboxylic acids with Selectfluor in aqueous solution.⁴⁶ This method showed tolerance for a number of functional groups, including amides, esters, carbonyls, halides,

ethers, and aryl groups. The functional group tolerance of this reaction is depicted in Scheme 4.25a, where a dehydrolithocholic acid derivative undergoes decarboxylative fluorination. The reactivity of carboxylic acids in this reaction decreases in the order tertiary > secondary > primary >> aromatic, which can allow for the successful implementation of chemoselective fluorodecarboxylation. In the example of 2,2-dimethylglutaric acid (Scheme 4.25b), the tertiary carboxylic acid is selectively decarboxylated and fluorinated at room temperature, leaving the primary carboxylic acid unreacted. In addition, the reactivities of carboxylic acids suggest that this reaction proceeds by an oxidative radical mechanism. To investigate this mechanistic feature, they used a cyclopropylacetic acid radical probe (Scheme 4.25c). When reacted with silver nitrate and Selectfluor, the ring opened fluorinated product was produced in 40% yield, suggesting alkyl radical generation during the course of the reaction.



Scheme 4.25. Silver-catalyzed decarboxylative fluorination of (a) a dehydrolithocholic acid derivative, (b) a tertiary acid, and (c) a carboxylic acid on a radical probe.

4.2 Experimental

4.2.1 Materials

AgNO_3 , Selectfluor, 2,2-dimethylglutaric acid, 2,2-dimethylbutyric acid, isobutyric acid, BET_3 (1 M in THF), and NFSI were purchased from Alfa Aesar. Sodium persulfate was purchased from Sigma-Aldrich. All chemicals were used without further purification. Reagent grade acetone and deionized water were used.

4.2.2 Instrumentation

Proton, carbon, and fluorine NMR were recorded on a Bruker 500 MHz spectrometer. GC-MS analyses were done with an HP 5890 Series II Gas Chromatograph with an HP Mass Selector Detector. Column chromatography was performed using the

automated CombiFlash® Rf system from Teledyne Isco, Inc. Products were separated using prepacked silica gel columns with a gradient elution of ethyl acetate and hexanes. The pH of the reaction was monitored using a Vernier pH sensor PH-BTA and Logger Lite 4.1 software.

4.2.3 Methods

4.2.3.1 Procedure for synthesis of fluorinated products

The decarboxylative fluorination reaction was performed in open air without the need for degassed solvents. In a vial equipped with a magnetic stir bar was added carboxylic acid (1 mmol), Selectfluor (708 mg, 2 mmol), and AgNO₃ (34 mg, 0.2 mmol). Acetone (5 mL) and DI water (5 mL) were added, and the mixture was allowed to react between 2-4 h (depending on carboxylic acid). Reaction mixture was extracted thrice with dichloromethane. Organic layer was dried with magnesium sulfate and concentrated to obtain fluorinated product.

4.2.3.2 Procedure for synthesis of 2,2-dimethyl-3-phenylpropanoic acid

To a round bottom flask equipped with a stir bar was added diisopropylamine and 30 mL dry THF under argon. The solution was stirred and cooled to approximately 0°C. A solution of 2.2 M n-BuLi in hexanes was added over 30 min via syringe pump and allowed to stir. Isobutyric acid was added over 10 min via syringe. The solution was allowed to warm to room temperature and stirred for 1.5 h. The stirred solution was cooled to approximately 15°C. Benzyl chloride was added over 30 min via syringe pump maintaining temperature below 5°C. The resulting mixture was allowed to warm to

ambient temperature and stirred under Ar overnight. The reaction mixture was partitioned between 200 mL diethyl ether and 200 mL water. The aqueous layer was acidified by addition of conc. HCl (36%, ca. 10 mL). The resulting mixture was extracted with 3 x 50 mL diethyl ether. The combined organic phase was dried (Na_2SO_4), filtered and concentrated. The colorless oil was then solidified under high vac.

4.2.3.3 Procedure for kinetic studies

For kinetic studies, the concentration of reagents was kept at synthetically relevant conditions. In an NMR tube, carboxylic acid and F-TEDA- BF_4 were combined. To the tube was added 0.5 mL acetone and 0.5 mL of AgNO_3 solution (in water), and α,α,α -trifluoromethyltoluene (10 μL , internal standard). The tube was shaken and inserted into the NMR. Reactions were monitored in situ by ^{19}F NMR on a Bruker 500 NMR (470 MHz) spectrometer. All reactions were performed at 23°C. Peak integrations were analyzed using MestReNova software. Concentrations at each time point were determined with respect to the internal standard. Concentration (M) vs. time (sec) plots were generated based on this data and fit to the best exponential fit, in this case, single exponential fits. The use of 4th and 5th order polynomials also provided the same results. The rate of each time point was found by calculating the derivative of the trendline. To normalize rate plots, plots of $\text{rate}/[\text{substrate}]^n$ were determined, in which n is the order of the substrate.

4.2.3.4 Procedure for IR studies

2,2-dimethylglutaric acid and AgNO_3 were allowed to react overnight, forming a small amount of precipitate. The precipitate was isolated, washed with water, and allowed to dry under vacuum. An FTIR spectrum was obtained.

4.2.3.5 Procedure for Ag- Selectfluor NMR studies

In one NMR tube, Selectfluor was dissolved in 1:1 acetone- d_6 : D_2O . In a second NMR tube, AgNO_3 (0.1 mmol) and Selectfluor (0.1 mmol) were combined and dissolved in 1:1 acetone- d_6 : D_2O (0.25 mL each), shaken, and allowed to sit overnight. Proton, carbon-13, and fluorine-19 NMR were obtained.

4.2.3.6 Procedure for BEt_3 reaction of 2,2-dimethylglutaric acid

In an NMR tube was added carboxylic acid (0.1 mmol), NFSI (63.1 mg, 0.2 mmol), and BEt_3 (0.02 mmol, 1M soln in THF). Acetone (0.5 mL) and DI water (0.5 mL) were added, and the mixture was allowed to react overnight. Product yield was determined by fluorine-19 NMR using α,α,α -trifluoromethyltoluene internal standard.

4.2.3.7 Procedure for reaction using sodium persulfate

The decarboxylative fluorination reaction was performed in open air without the need for degassed solvents. In a vial equipped with a magnetic stir bar was added carboxylic acid (1 mmol), Selectfluor (708 mg, 2 mmol), $\text{Na}_2\text{S}_2\text{O}_8$ (119 mg, 0.05 mmol), and AgNO_3 (34 mg, 0.2 mmol). Acetone (5 mL) and DI water (5 mL) was added, and the mixture was allowed to react for 15 min. Reaction mixture was extracted thrice with dichloromethane. Organic layer was dried with magnesium sulfate and concentrated to obtain fluorinated product.

4.2.3.8 Procedure for reaction using NFSI and sodium persulfate

In an NMR tube was added carboxylic acid (0.1 mmol), NFSI (63.1 mg, 0.2 mmol), Na₂S₂O₈ (11.9 mg, 0.05 mmol), and AgNO₃ (3.4 mg, 0.02 mmol). Acetone (0.5 mL) and DI water (0.5 mL) was added, and the mixture was allowed to react overnight. Product yield was determined by fluorine-19 NMR using α,α,α -trifluoromethyltoluene internal standard.

4.2.3.9 Procedure for pH studies

A pH probe was referenced with two buffer solutions of pH 4 and 7. In a vial was added 2,2-dimethylglutaric acid (160.17mg, 1 mmol), AgNO₃ (34 mg, 0.2mmol), and Selectfluor (708 mg, 2 mmol). The pH probe was inserted and acetone (5 mL) and H₂O (5 mL) was added, then the reaction vial was sealed. The pH of the reaction was monitored over the course of 2 hours. The pH of acetone/water without any additives was also monitored for 2 hours. No change in pH was observed.

4.2.3.10 Procedure for synthesis of 1-(chloromethyl)-1,4-diazabicyclo[2.2.2]octane tetrafluoroborate (TEDA-BF₄)

DABCO (10 g) and dichloromethane (50 mL) were combined in a round bottom flask with acetone (50 mL) and allowed to stir for 3 days to form a solid precipitate (1-(chloromethyl)-1,4-diazabicyclo[2.2.2]octane chloride). The resulting precipitate was filtered and washed with acetone, then recrystallized in hot ethanol. The recrystallization solution was diluted with acetone to produce a precipitate. The solid was collected and allowed to dry under reduced pressure. The dry precipitate (5.026 g, 25 mmol) was then reacted with NaBF₄ (2.744 g, 25 mmol) in dry MeCN. The mixture was allowed to stir

overnight under argon. The precipitated NaCl was removed by filtration and then washed with dry MeCN. The resulting solution was concentrated under reduced pressure and then recrystallized in an ethanol/ethyl acetate mixture. The resulting crystals were dried under reduced pressure to yield 1-(chloromethyl)-1,4-diazabicyclo[2.2.2]octane tetrafluoroborate.

4.2.3.11 Procedure for crystallization of AgNO₃-TEDA-BF₄ complex

To a round bottom flask was added AgNO₃ (170 mg, mmol) and TEDA-BF₄ (248 mg, 1 mmol). The contents were dissolved in a mixture of acetone and water (9 mL and 1 mL, respectively). Slow evaporation in open air over the course of days was allowed for crystal formation.

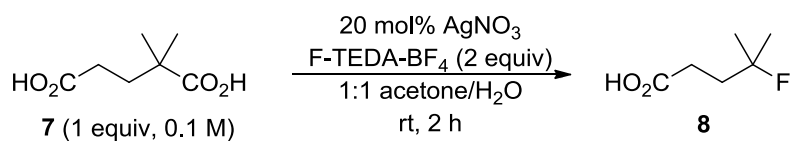
4.3 Results

4.3.1 Determination of Reaction Conditions

The recent development of a silver-catalyzed decarboxylative fluorination reaction using the electrophilic fluorinating reagent 1-chloromethyl-4-fluoro-1,4-diazoniabicyclo[2.2.2]octane bis(tetrafluoroborate) (Selectfluor®, F-TEDA-BF₄) is of significant importance due to its procedural ease, mild reaction conditions, and extensive substrate scope.⁴⁶ The mechanistic understanding of this reaction has the potential to aid synthetic chemists in the design of improved or possibly new protocols that proceed through single electron oxidation.

The goal of this research project was to explore the role of silver catalyst and Selectfluor as fluorinating reagents in organic reactions. To do so, we chose to study the silver-catalyzed fluorination of aliphatic carboxylic acids using Selectfluor, a reaction

recently developed by the Li group.⁴⁶ In the original report, fluorination of secondary and tertiary acid proceeded in moderate to excellent yield. The reactions generally call for the use of 20 mol% catalyst and 2 equivalents of Selectfluor in 1:1 acetone/water media (Scheme 4.26). Fluorination of the compound 2,2-dimethylglutaric acid (**7**), a dicarboxylic acid, displayed selectivity of the tertiary carboxylic acid over the primary acid moiety at room temperature. Under the conditions of the original reaction, there was difficulty in observing product formation by ¹⁹F NMR. As a result, we attempted to determine whether the same reaction could be performed at higher concentration to make the system suitable for monitoring by ¹⁹F NMR. Not only did this change result in complete conversion, the time required for reaction decreased significantly. While originally reacted for 10 hours, we found that by increasing the concentration of the reaction from 0.05 M to 0.1 M (with respect to **7**), the reaction went to completion in 2 hours. Using these synthetic reaction conditions, kinetic studies were performed on the decarboxylative fluorination reaction of **7**.



Scheme 4.26. Ag(I)-catalyzed fluorination of aliphatic carboxylic acid **7** using Selectfluor

4.3.2 Kinetic Analysis

4.3.2.1 Catalyst Stability Studies

To study the mechanism of this system, we sought to first do a thorough kinetic study of each component in the system. All kinetic studies were done under synthetically

relevant conditions.⁴⁷⁻⁵² Reaction progress was monitored by observing the growth of product **[8]** over time using ^{19}F NMR (Figure 4.5). A significant amount of initiation was observed (approximately 600 seconds, Figure 4.5) in the reaction, a feature that will be discussed *vide infra*.

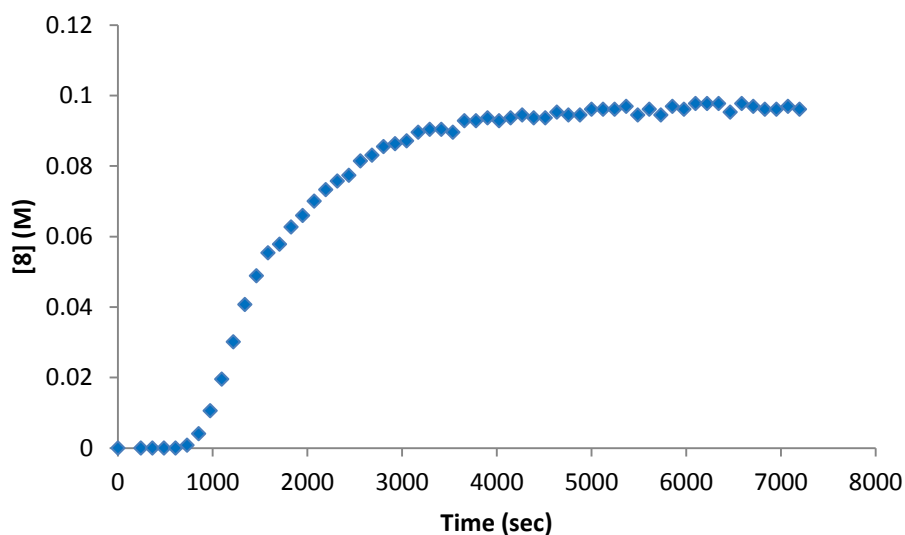


Figure 4.5. Growth of fluorinated product **8** over time monitored by ^{19}F NMR in decarboxylative fluorination reaction of **7**

We first wanted to determine catalyst stability of AgNO_3 during the course of the reaction. To do so, we monitored the reaction described in Scheme 4.26, under the conditions shown in Table 4.1, Run 1. A second reaction was initiated at the half-way point of Run 1 (Table 4.1, Run 2). To do this, **[7]** was decreased to 0.05 M, one-half of that in Run 1, and **[Selectfluor]** was adjusted by an equivalent amount with respect to **[7]**, decreased from 0.2 M to 0.15 M. The $[\text{AgNO}_3]$ in Run 2 remained the same as in Run 1.

Table 4.1. Reaction conditions for catalyst stability studies in decarboxylative fluorination reaction of **7**

Run	[7] (M)	[AgNO ₃] (M)	[Selectfluor] (M)	Excess [Selectfluor] (M)
1 - 100%	0.1	0.02	0.2	0.1
2 - 50%	0.05	0.02	0.15	0.1

In an ideal catalytic system, the concentration of catalyst remains constant over the course of the reaction. If [AgNO₃] remained constant during the course of the reaction, the rates of both Runs 1 and 2 would be the same. If [AgNO₃] decreased as the reaction proceeded through catalyst deactivation, the rates of Runs 1 and 2 would be different and their rate profiles would not overlay. To determine catalyst stability, **8** is converted to **7** (to be able to compare the rate profiles of both reactions on the same concentration scale) and Runs 1 and 2 are plotted together (Figure 4.6). When time-adjusted, both rate profiles show graphical overlay, consistent with constant [AgNO₃] over the course of the reaction (Figure 4.7).^{53,54} Catalyst stability during the course of the reaction suggested that AgNO₃ loading could be lowered in this reaction. We were able to lower AgNO₃ loading from 20 mol% to 5 mol% to generate **8** in 90% yield by increasing concentration from 0.1 M to 0.2 M (with respect to **7**) upon reaction overnight.

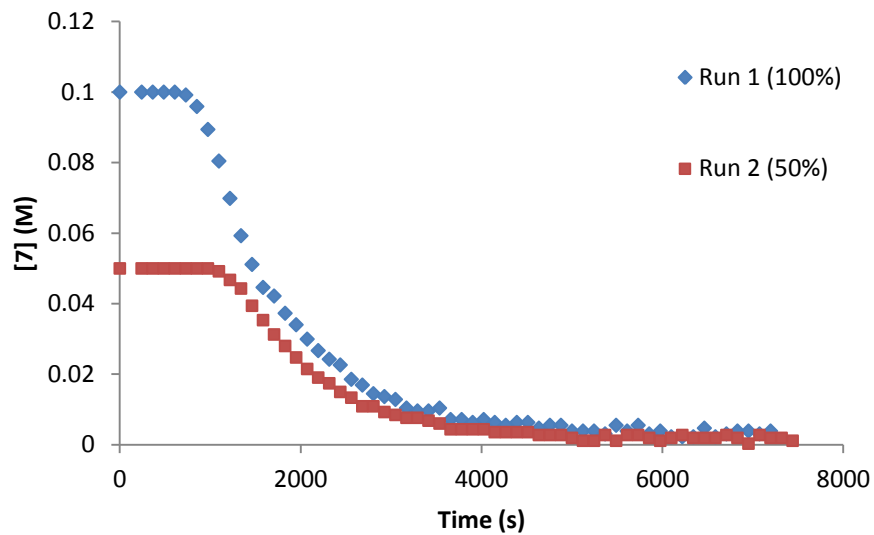


Figure 4.6. Plot of [7] vs. time for Runs 1 and 2 for catalyst stability studies in decarboxylative fluorination reaction of **7**

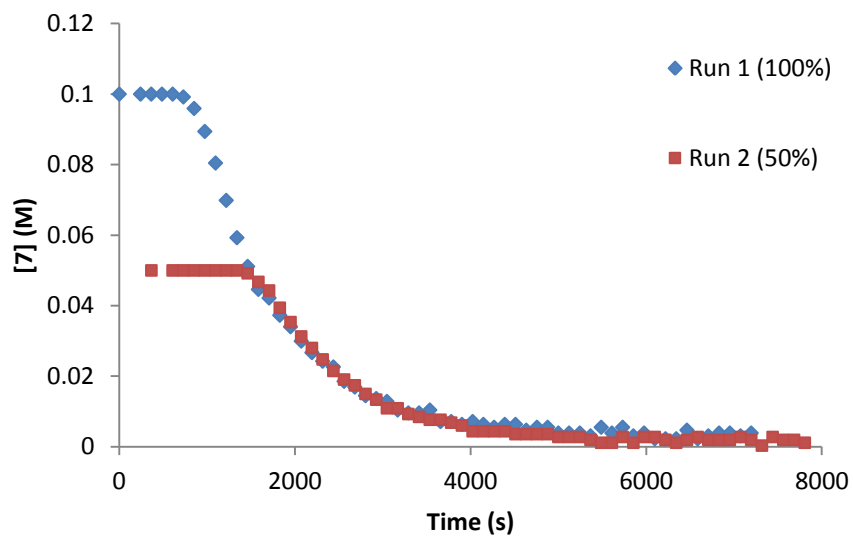


Figure 4.7. Time-adjusted profiles showing overlay of Runs 1 and 2 in decarboxylative fluorination reaction of **7**

4.3.2.2 Kinetic Order Studies for 2,2-dimethylglutaric acid

Next, the role of each substrate in the reaction was elucidated by determining their rate orders. Kinetic orders of substrates were found by varying the concentration of each substrate individually to observe its effect on the rate of reaction.

Table 4.2. Reaction conditions for kinetic order studies for fluorination of **7**

run	[7] (M)	[AgNO ₃] (M)	[Selectfluor] (M)	Excess [Selectfluor] (M)
1 - 100%	0.1	0.02	0.2	0.1
3	0.1	0.04	0.2	0.1
4	0.1	0.02	0.15	0.05
5	0.075	0.02	0.2	0.125

The order of AgNO₃ was found by increasing the catalyst loading from 20 mol% (Table 4.2, Run 1) to 40 mol% (Table 4.2, Run 3). This increase in catalyst loading resulted in an increase in the reaction rate (Figure 4.8). The turnover frequency of the catalyst is found by normalizing $(-d[\mathbf{2}]/dt)/[\text{AgNO}_3]$ (Figure 4.9). Overlay of Runs 1 and 3 suggest first order rate dependence on silver nitrate.

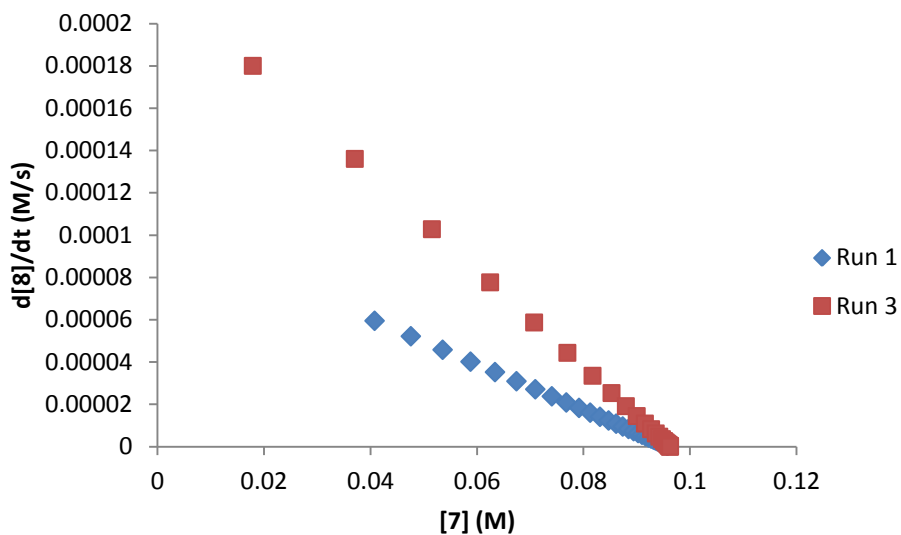


Figure 4.8. $-d[2]/dt$ vs. $[2]$ plot for order of AgNO_3 in decarboxylative fluorination reaction of **7**

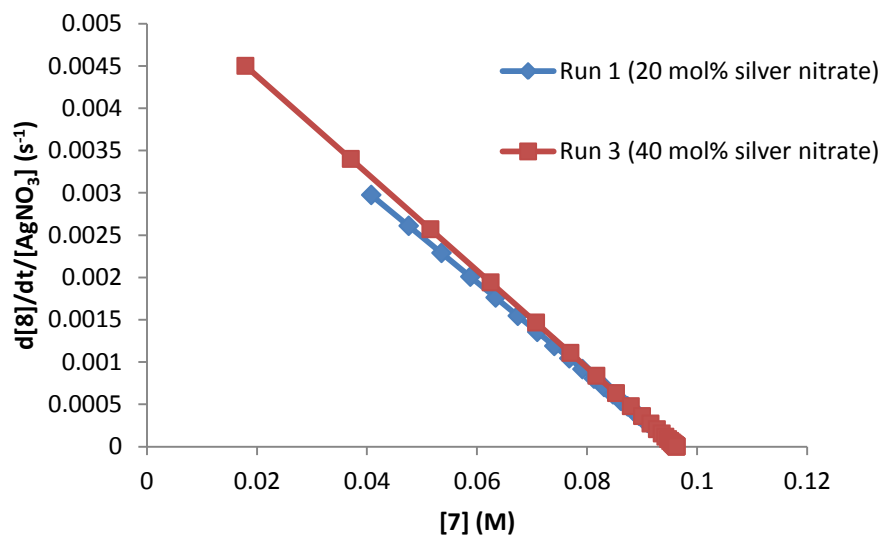


Figure 4.9. Turnover frequency of AgNO_3 in decarboxylative fluorination reaction of **7**

To determine the rate order of Selectfluor, its concentration was adjusted to 0.15 M (Table 4.2, Run 4), while keeping the concentration of all other reactants constant. Decreasing [Selectfluor] resulted in a decrease of overall reaction rate (Figure 4.10).

When plotting $(-d[7]/dt)/[Selectfluor]$, we observed overlay of Runs 1 and 4, indicative of first order rate dependence on Selectfluor (Figure 4.11).

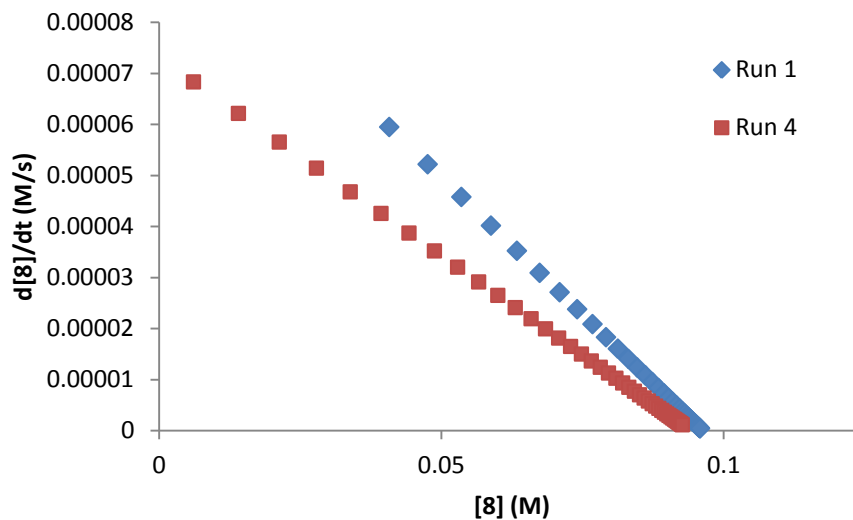


Figure 4.10. $-d[2]/dt$ vs. $[2]$ plot for order of Selectfluor in decarboxylative fluorination reaction of **7**

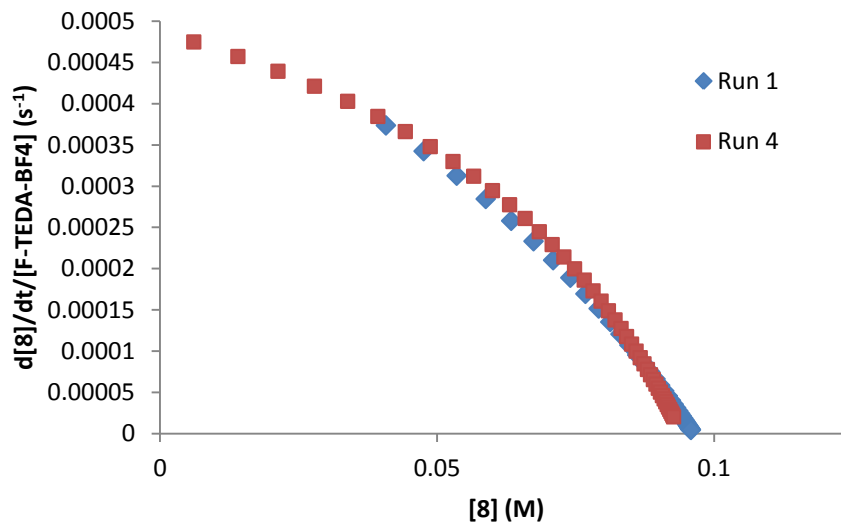


Figure 4.11. Normalized rate vs. $[8]$ plot showing first order rate dependence on Selectfluor in decarboxylative fluorination reaction of **7**

The order of **7** proved to be more complex. When lowering the amount of **1** from 0.1 M to 0.075 M (Table 4.2, Runs 1 and 5, respectively), an increase of reaction rate was observed (Figure 4.12). The rate plots of each reaction were fit to straight lines, in which the slope was equal to the rate. When using Equation 1, we observed -1.5 order dependence on **7**, suggesting that the substrate was inhibiting reaction progress.

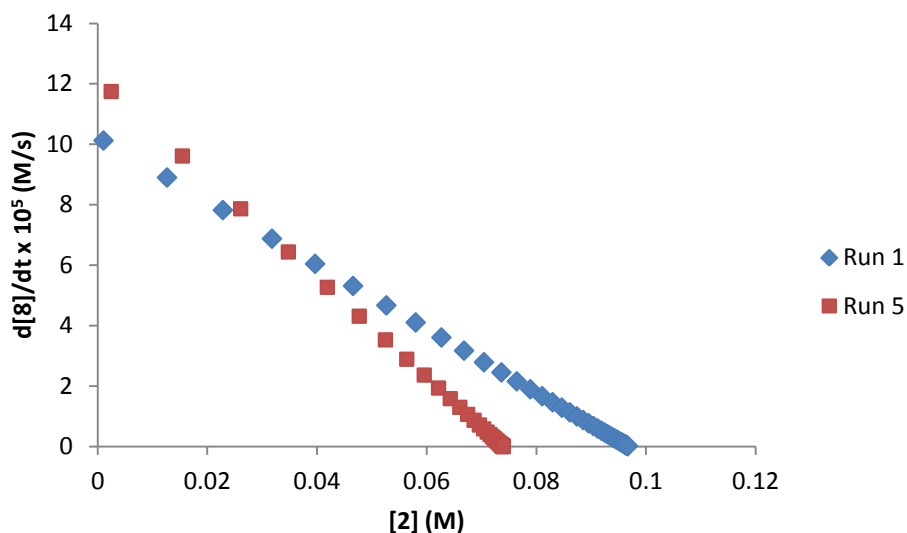


Figure 4.12. $-d[8]/dt$ vs. $[8]$ plot for order of 7 in decarboxylative fluorination reaction of **7**

$$\log\left(\frac{\text{slope}_a}{\text{slope}_b}\right) = x \log\left(\frac{[7]_a}{[7]_b}\right) \quad (1)$$

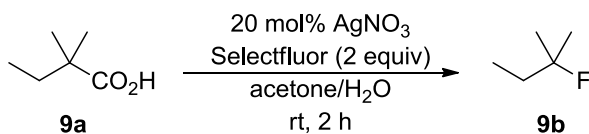
The rate orders for the reaction shown in Scheme 4.26 are summarized in Table 4.3. Carboxylic acid was found to be inverse order, and silver catalyst and Selectfluor showed first order rate dependence.

Table 4.3. Rate Orders for each component in Ag(I)-catalyzed fluorination of **7**

7	AgNO ₃	Selectfluor
-1.5	1	1

4.3.2.3 Kinetic Order Studies for 2,2-dimethylbutyric acid

Kinetic studies were also performed on additional substrates to determine whether the inverse order observed for **7** was a result of an additional carboxylic acid moiety on the compound.



Scheme 4.27. Ag(I)-catalyzed fluorination of aliphatic carboxylic acid **9a** using Selectfluor

The substrate studied was 2,2-dimethylbutyric acid (**9a**) to form product **9b** in excellent yield (Scheme 4.27). Kinetic order studies were repeated on this substrate, under the conditions shown in Table 4.4. As shown in Figures 4.13 and 4.14, AgNO₃ was found to be approximately first order. Figures 4.15 and 4.16 show approximate first order rate dependence on Selectfluor. In addition, Figure 4.17 shows the inverse order found for substrate **9a**. The inverse orders observed for this mono-carboxylic acid suggest that the order of **7** is not a result of the presence of an additional carboxylic acid moiety, but rather is indicative of a more complex mechanistic feature.

Table 4.4. Reaction conditions for kinetic order studies for fluorination of **9a**

Run	[9a] (M)	[AgNO ₃] (M)	[Selectfluor] (M)	Excess [Selectfluor] (M)
6 - 100%	0.1	0.02	0.2	0.1
7	0.1	0.04	0.2	0.1
8	0.1	0.02	0.15	0.05
9	0.075	0.02	0.2	0.125

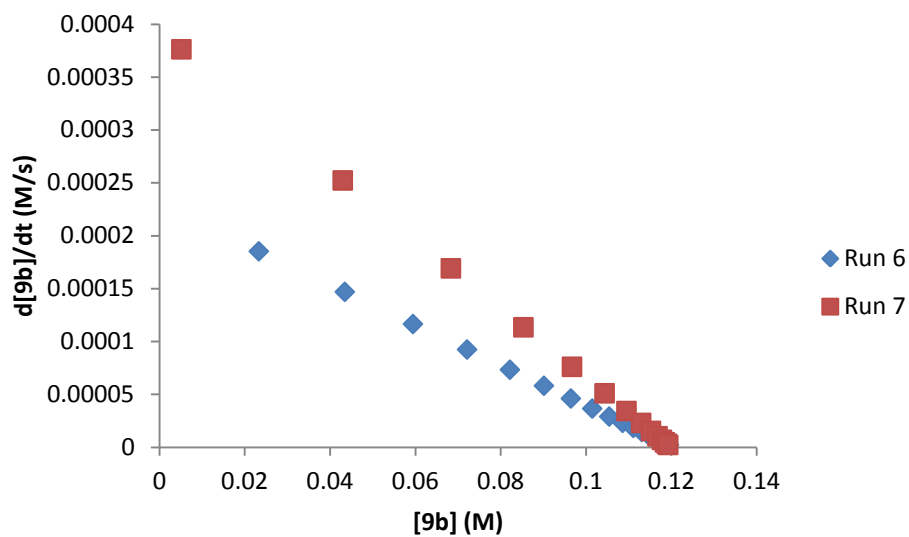


Figure 4.13. $-d[9b]/dt$ vs. $[9b]$ plot for order of AgNO₃ in decarboxylative fluorination reaction of **9a**

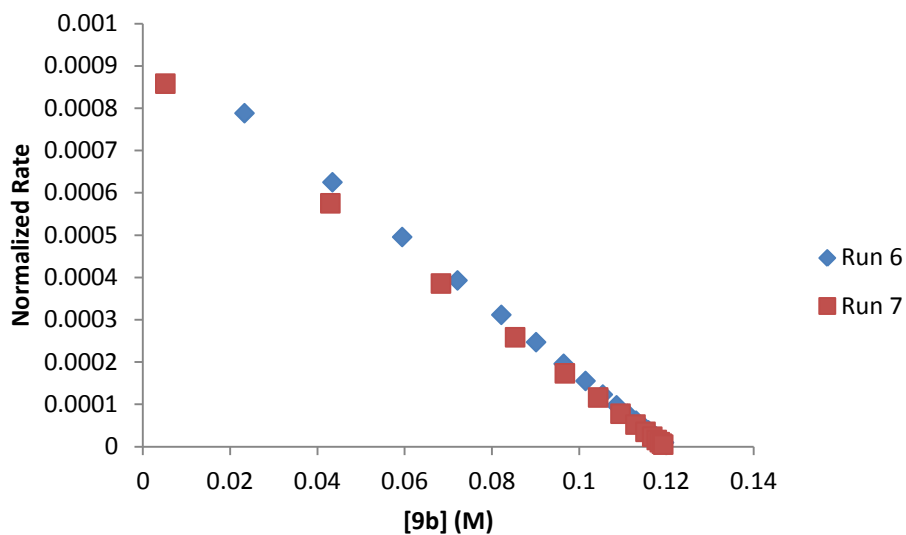


Figure 4.14. Normalized rate plot showing rate order of AgNO_3 in decarboxylative fluorination reaction of **9a**

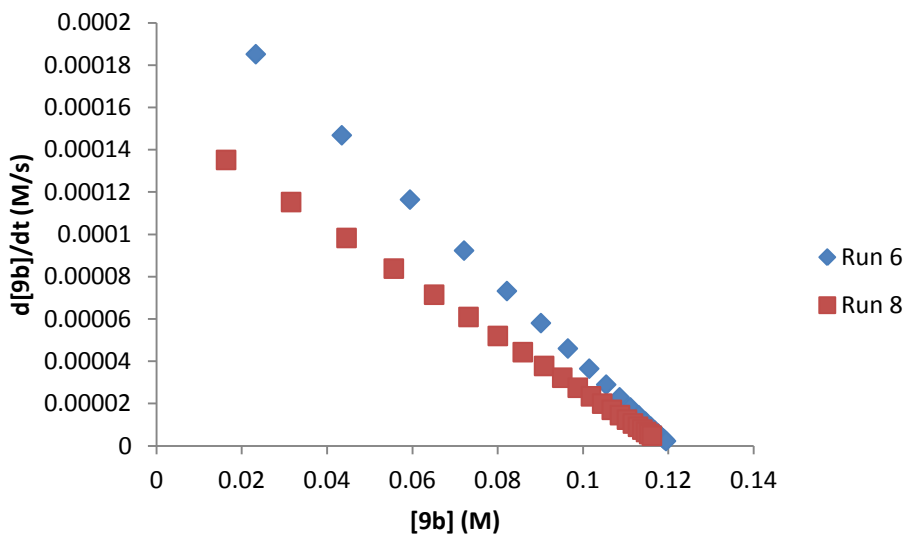


Figure 4.15. $-\text{d}[\text{9b}]/\text{dt}$ vs. $[\text{9b}]$ plot for order of Selectfluor in decarboxylative fluorination reaction of **9a**

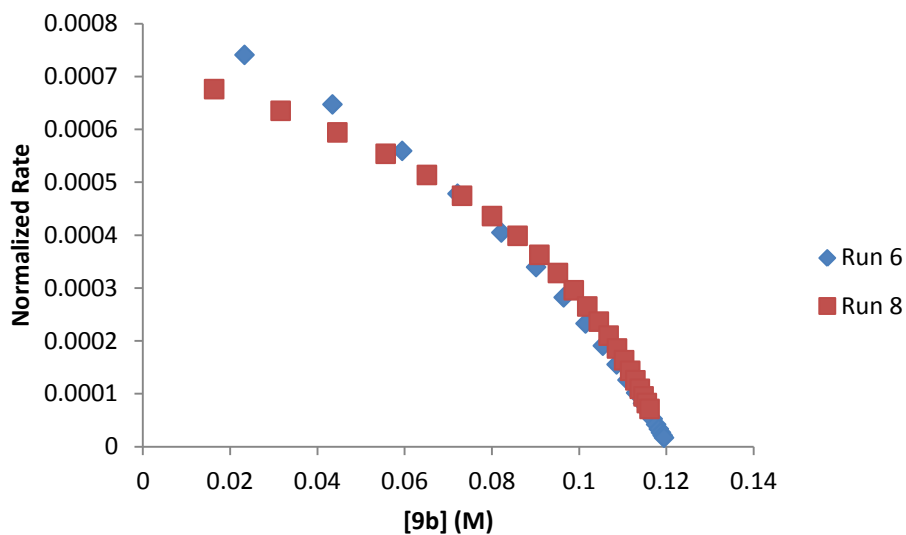


Figure 4.16. Normalized rate plot showing rate order of Selectfluor in decarboxylative fluorination reaction of **9a**

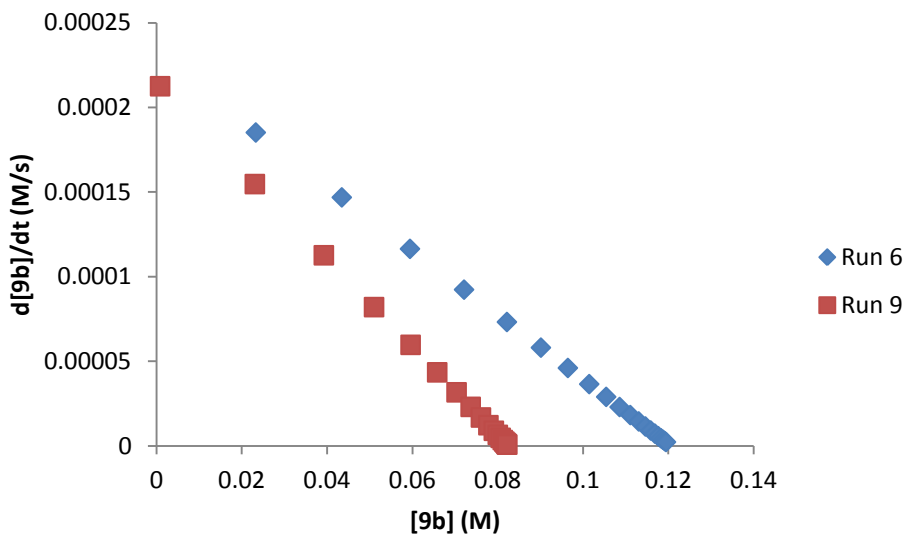


Figure 4.17. $-d[9b]/dt$ vs. $[9b]$ plot for order of **9a** in decarboxylative fluorination reaction of **9a**

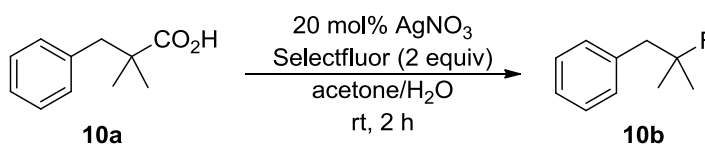
The rate orders for the reaction shown in Scheme 4.27 are summarized in Table 4.5. Carboxylic acid was found to be inverse order, and silver catalyst and Selectfluor showed approximate first order rate dependence.

Table 4.5. Rate Orders for each component in Ag(I)-catalyzed fluorination of **9a**

9a	AgNO ₃	Selectfluor
-0.9	0.9	0.8

4.3.2.4 Kinetic Order Studies for 2,2-dimethylphenylpropanoic acid

The next substrate studied was 2,2-dimethyl-3-phenylpropanoic acid (**10a**) to form product **10b**.



Scheme 4.28. Ag(I)-catalyzed fluorination of aliphatic carboxylic acid **10a** using Selectfluor

Kinetic order studies were repeated on this substrate, under the conditions shown in Table 4.6. As shown in Figures 4.18 and 4.19, AgNO₃ was found to be approximately first order. Figures 4.20 and 4.21 show approximate first order rate dependence on Selectfluor. In addition, Figure 4.22 shows the inverse order found for substrate **10a**.

Table 4.6. Reaction conditions for kinetic order studies for fluorination of **10a**

run	[10a] (M)	[AgNO ₃] (M)	[Selectfluor] (M)	Excess [Selectfluor] (M)
10 - 100%	0.1	0.02	0.2	0.1
11	0.1	0.04	0.2	0.1
12	0.1	0.02	0.15	0.05
13	0.075	0.02	0.2	0.125

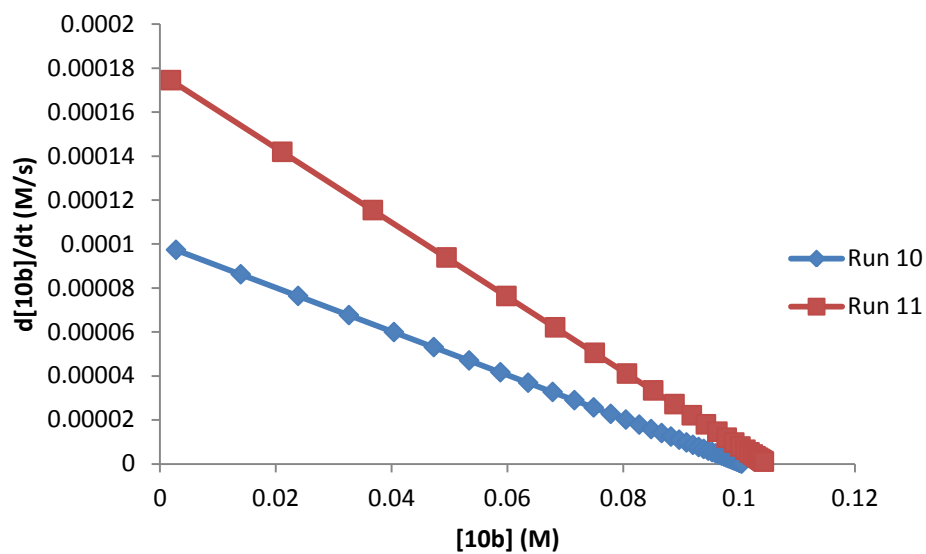


Figure 4.18. $-d[10b]/dt$ vs. $[10b]$ plot for order of AgNO₃ in decarboxylative fluorination reaction of **10a**

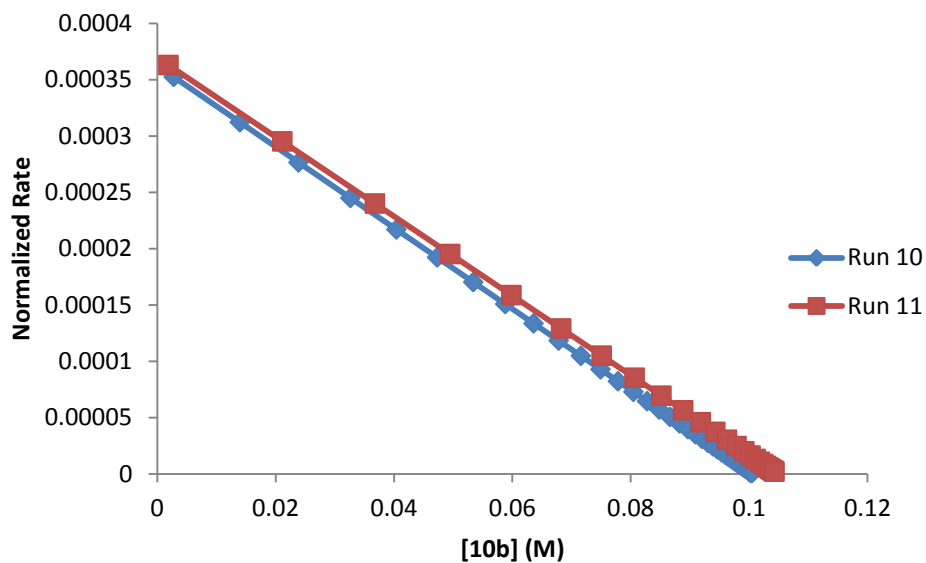


Figure 4.19. Normalized rate plot showing rate order of AgNO_3 in decarboxylative fluorination reaction of **10a**

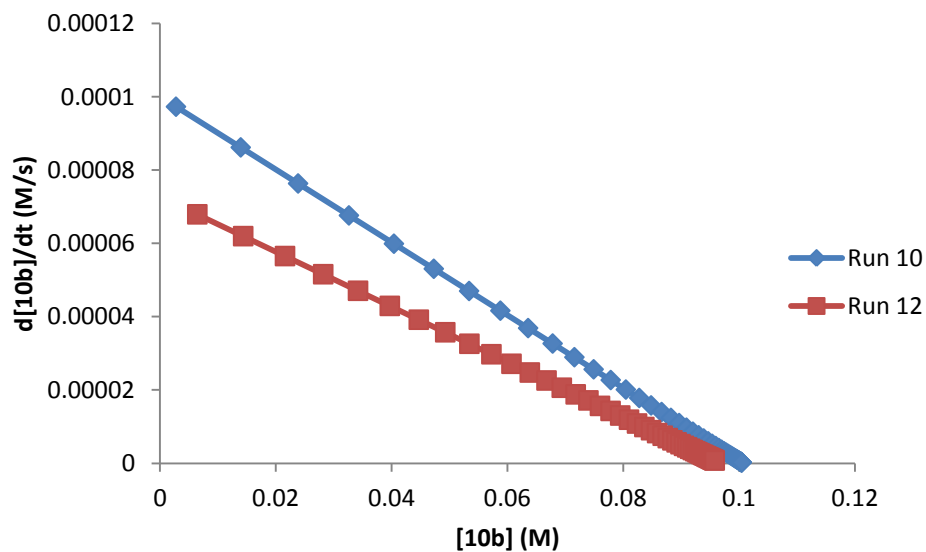


Figure 4.20. $-\text{d}[10\text{b}]/\text{dt}$ vs. $[10\text{b}]$ plot for order of Selectfluor in decarboxylative fluorination reaction of **10a**

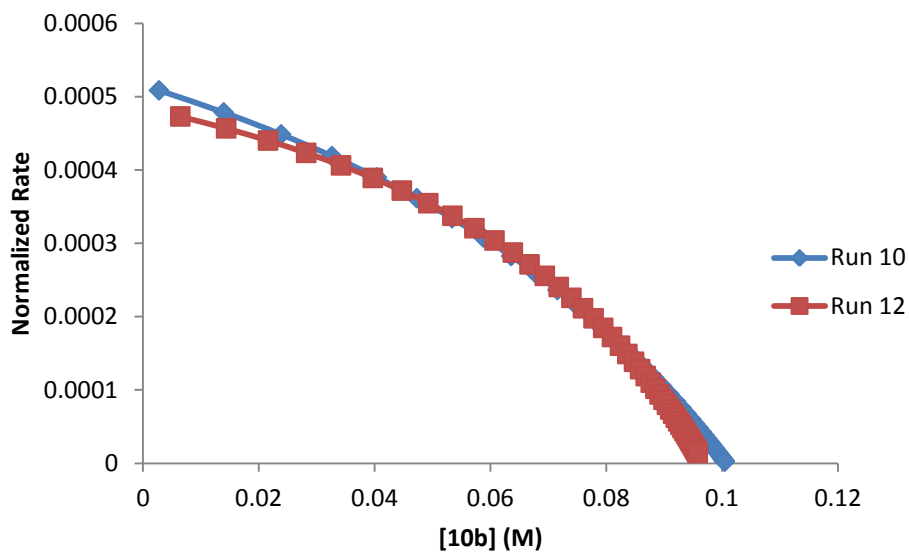


Figure 4.21. Normalized rate plot showing rate order of Selectfluor in decarboxylative fluorination reaction of **10a**

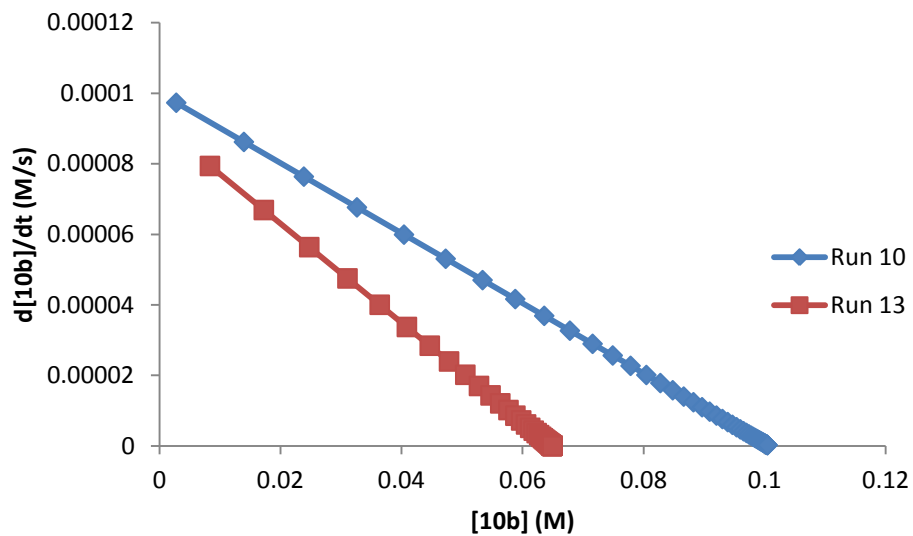


Figure 4.22. $-d[10b]/dt$ vs. $[10b]$ plot for order of **10a** in decarboxylative fluorination reaction of **10a**

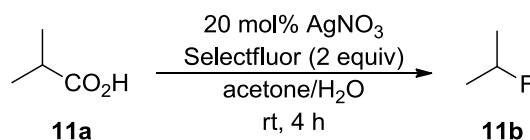
The rate orders for the reaction shown in Scheme 4.28 are summarized in Table 4.7. Carboxylic acid was found to be inverse order, and silver catalyst and Selectfluor showed approximate first order rate dependence.

Table 4.7. Rate Orders for each component in Ag(I)-catalyzed fluorination of **10a**

10a	AgNO ₃	Selectfluor
-0.97	0.8	1

4.3.2.5 Kinetic Order Studies for isobutyric acid

The next substrate studied was isobutyric acid (**11a**) to form product **11b**.

**Scheme 4.29.** Ag(I)-catalyzed fluorination of aliphatic carboxylic acid **11a** using Selectfluor

Kinetic order studies were repeated on this substrate, under the conditions shown in Table 4.8. As shown in Figures 4.23 and 4.24, AgNO₃ was found to be approximately first order. Figures 4.25 and 4.26 show approximate first order rate dependence on Selectfluor. In addition, Figure 4.27 shows the inverse order found for substrate **11a**.

Table 4.8. Reaction conditions for kinetic order studies for fluorination of **11a**

run	[11a] (M)	[AgNO ₃] (M)	[Selectfluor] (M)	Excess [Selectfluor] (M)
14 - 100%	0.1	0.02	0.2	0.1
15	0.1	0.04	0.2	0.1
16	0.1	0.02	0.15	0.05
17	0.075	0.02	0.2	0.125

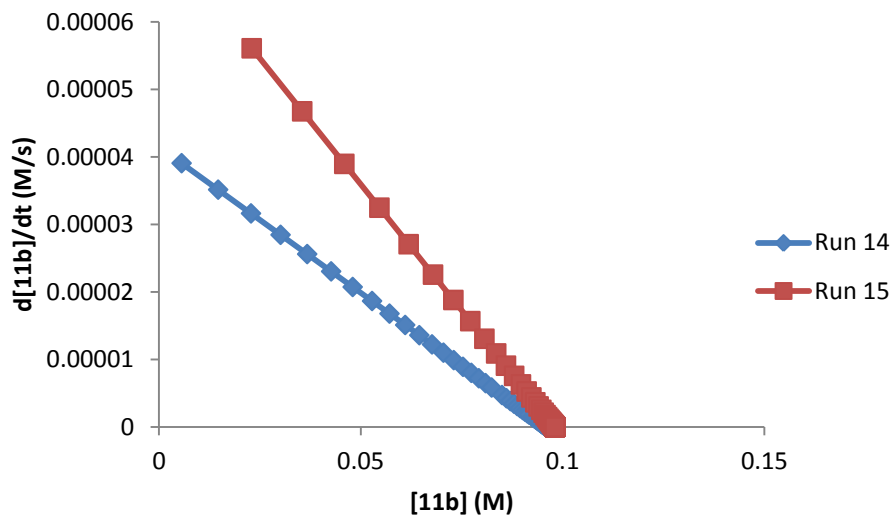


Figure 4.23. $-d[11b]/dt$ vs. $[11b]$ plot for order of AgNO_3 in decarboxylative fluorination reaction of **11a**

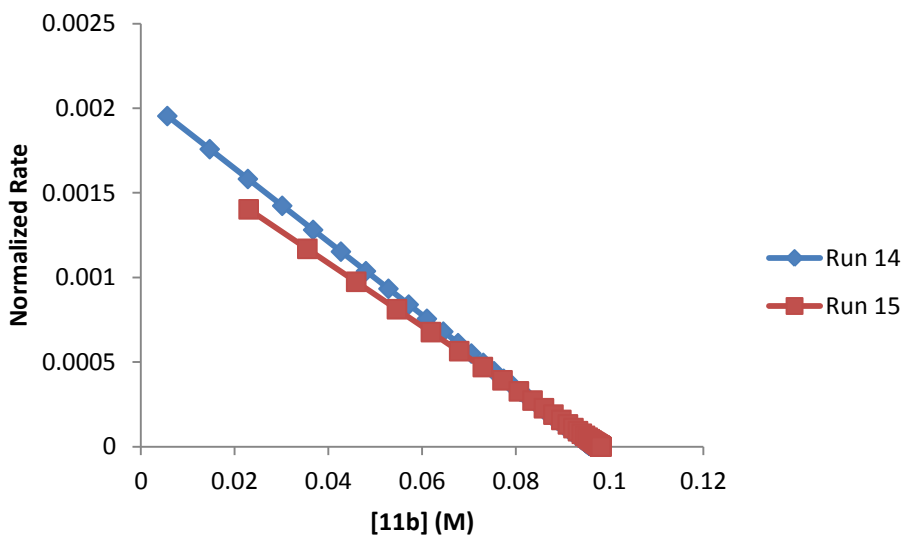


Figure 4.24. Normalized rate plot showing rate order of AgNO_3 in decarboxylative fluorination reaction of **11a**

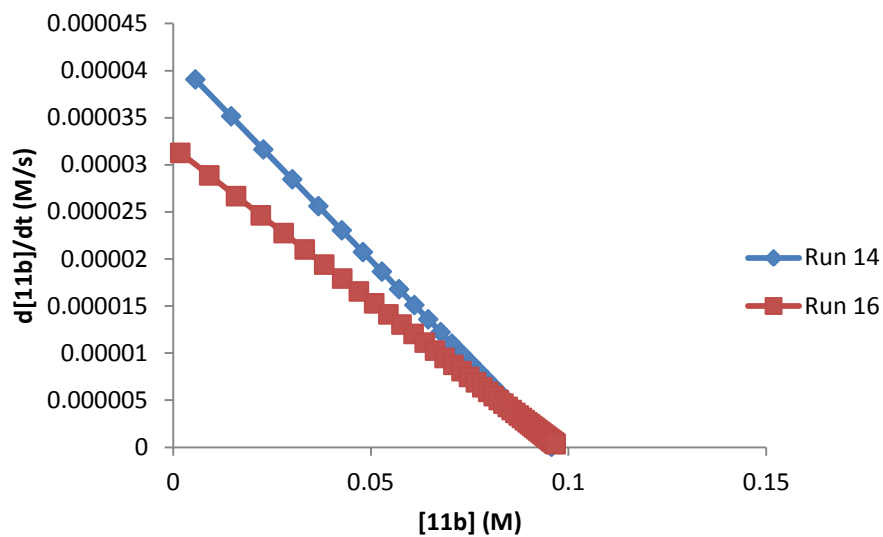


Figure 4.25. $-d[11b]/dt$ vs. $[11b]$ plot for order of Selectfluor in decarboxylative fluorination reaction of **11a**

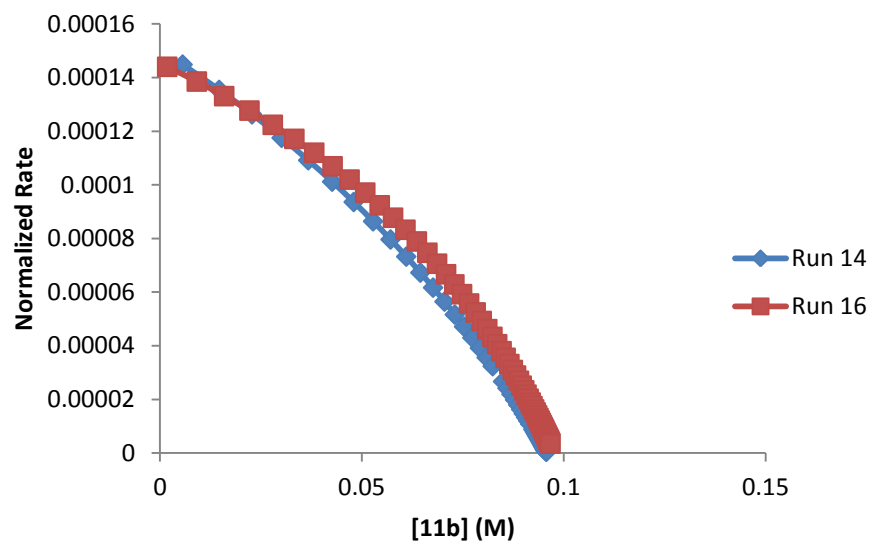


Figure 4.26. Normalized rate plot showing rate order of Selectfluor in decarboxylative fluorination reaction of **11a**

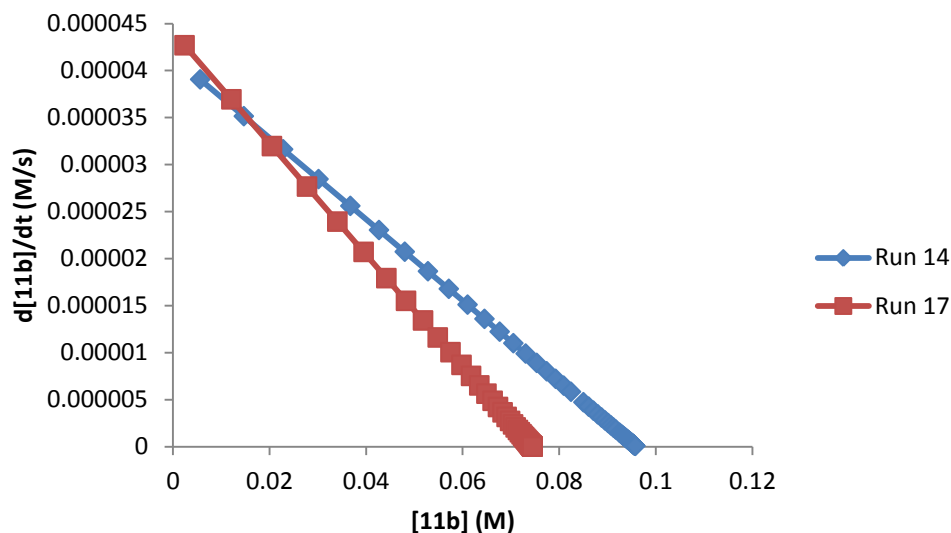


Figure 4.27. $-d[11b]/dt$ vs. $[11b]$ plot for order of 11a in decarboxylative fluorination reaction of 11a

The rate orders for the reaction shown in Scheme 4.29 are summarized in Table 4.9. Carboxylic acid was found to be inverse order, and silver catalyst and Selectfluor showed approximate first order rate dependence.

Table 4.9. Rate Orders for each component in Ag(I)-catalyzed fluorination of 11a

11a	AgNO ₃	Selectfluor
-1.09	1	0.8

4.3.2.6 Activation Parameters

To gain more insight into the transition state of the rate-limiting step of the catalytic cycle, activation parameters were obtained for the reaction of **7** under synthetic conditions at temperatures ranging between 23-40°C (Figure 4.28). The data were fit to the linear form of the Eyring equation (Equation 2), where k_{obs} is the observed decay rate constant, h is Planck's constant, k_B is the Boltzmann constant, R is the universal gas

constant, T is temperature in Kelvin, ΔH^\ddagger is the enthalpy of activation, and ΔS^\ddagger is the entropy of activation.

$$\ln\left(\frac{k_{obs}h}{k_B T}\right) = -\frac{\Delta H^\ddagger}{RT} + \frac{\Delta S^\ddagger}{R} \quad (2)$$

The Gibb's free energy of activation is calculated from $\Delta G^\ddagger = \Delta H^\ddagger - T\Delta S^\ddagger$. The following activation parameters were found: $\Delta H^\ddagger = 6.2$ kcal/mol, $\Delta S^\ddagger = -51.2$ cal/K·mol, and $\Delta G^\ddagger = 21.4$ kcal/mol (at 23 °C). The small transition enthalpy (ΔH^\ddagger) and the large negative transition entropy (ΔS^\ddagger) are indicative of a highly ordered, early transition state.

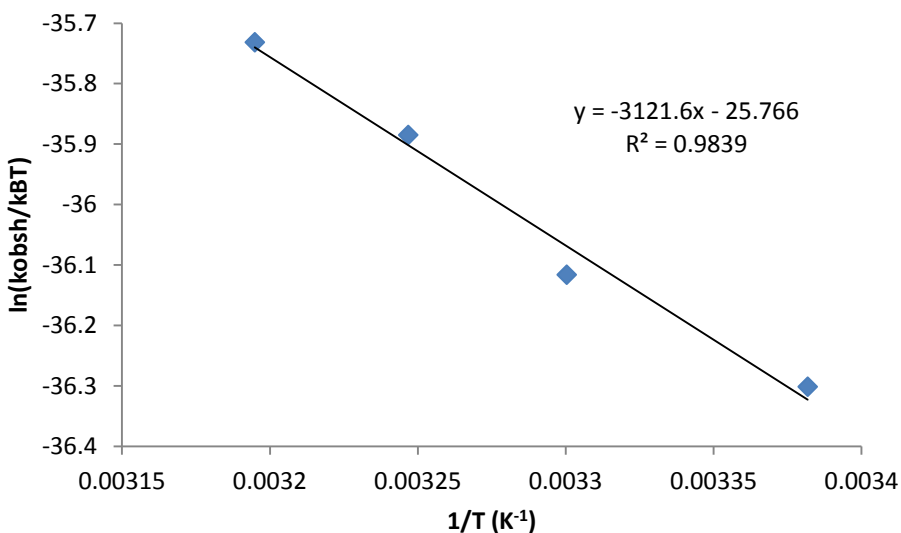


Figure 4.28. Activation parameters of fluorination reaction of **7**

4.3.3 Interaction of Carboxylic Acid with AgNO₃ via IR Studies

The formation of silver-carboxylates is well-established in the literature.⁵⁵ To investigate whether the inverse order found in carboxylic acids could be due to an interaction resulting in silver-carboxylate formation, **7** was mixed with silver nitrate and

allowed to stir overnight, forming a solid precipitate. An FTIR spectrum of the precipitate showed the loss of the –OH peak and shift of the carbonyl peak to lower wavenumbers, indicative of a silver-carboxylate (Figure 4.29).⁵⁵ The formation of this product, along with results found in the catalyst stability study and the inverse order found for the carboxylic acid, suggest that silver interacts with the substrate in a manner that is deleterious to catalytic efficiency, though it does not result in deactivation of silver.

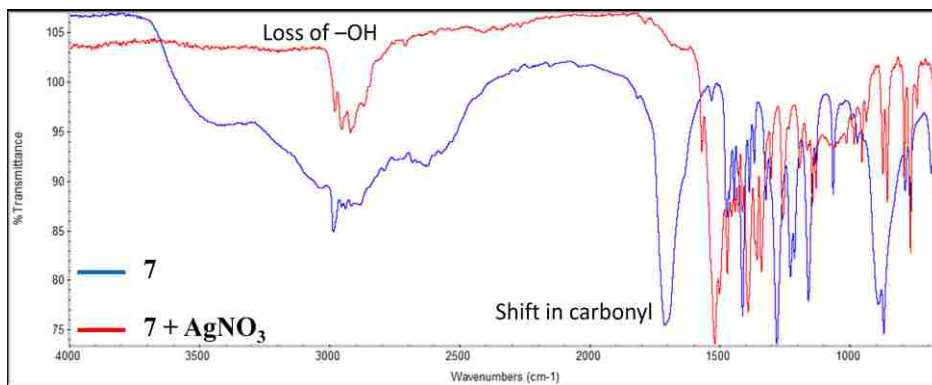


Figure 4.29. FTIR spectra comparing **7** to product of **7** and AgNO₃

4.3.4 Interaction of Selectfluor with AgNO₃ via NMR Studies

The oxidation of Ag(I) to high-valent complexes is often the rate-limiting step in silver-catalyzed reactions.^{52,56} To probe the role of Selectfluor as both a fluorinating reagent as well as an oxidant, the interaction of silver nitrate and Selectfluor was investigated by NMR. Upfield shifts of Selectfluor protons and carbons were observed in the ¹H (Figure 4.30, Table 4.10) and ¹³C NMR (Figure 4.31, Table 4.11) spectra, respectively, upon addition of an equivalent of silver nitrate to Selectfluor in acetone-d₆/D₂O.

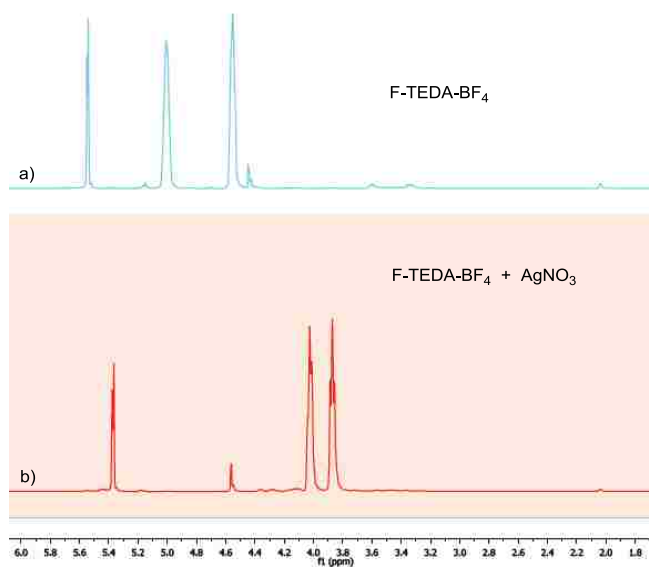


Figure 4.30. ^1H NMR spectra showing shifts of Selectfluor upon addition of AgNO_3

Table 4.10. ^1H NMR shifts of Selectfluor with AgNO_3

	$\Delta 1$ (ppm)	$\Delta 2$ (ppm)	$\Delta 3$ (ppm)
Selectfluor	5.52	5.09	4.45
Selectfluor+ AgNO_3	5.36	4.01	3.85

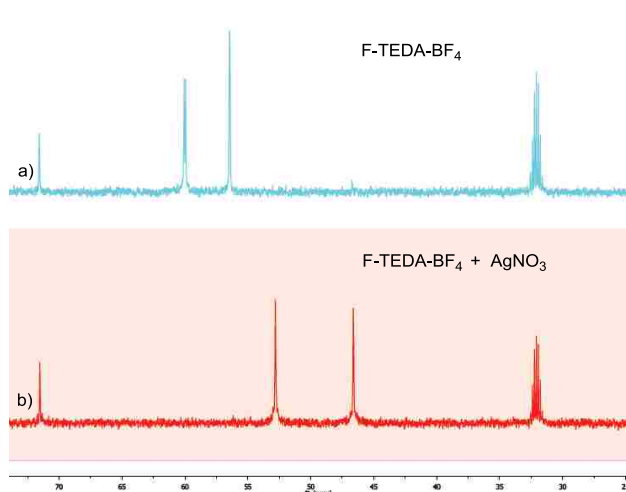


Figure 4.31. ^{13}C NMR spectra showing shifts of Selectfluor upon addition of AgNO_3

Table 4.11. ^{13}C NMR shifts of Selectfluor with AgNO_3

	$\Delta 1$ (ppm)	$\Delta 2$ (ppm)	$\Delta 3$ (ppm)
Selectfluor	71.57	60.01	56.45
Selectfluor+ AgNO_3	71.53	52.82	46.63

In addition to shifts seen by proton and carbon-13 NMR, a disappearance of the N-F peak of Selectfluor at +48.06 ppm was observed by ^{19}F NMR under the same conditions (Figure 4.32). Collectively, these spectroscopic results are consistent with a gain in electron density in the compound, and thus the oxidation of Ag(I) to a high-valent silver complex. While the loss of the N-F signal was observed in the ^{19}F NMR, the appearance of another signal was not observed, likely due to the formation of paramagnetic complexes (eg. Ag^{2+} , d^9) in the reaction. However, due to the transient

nature of the intermediate in this reaction, characterization of the proposed high-valent silver complex was not possible by XPS, LC-MS, or x-ray crystallography.

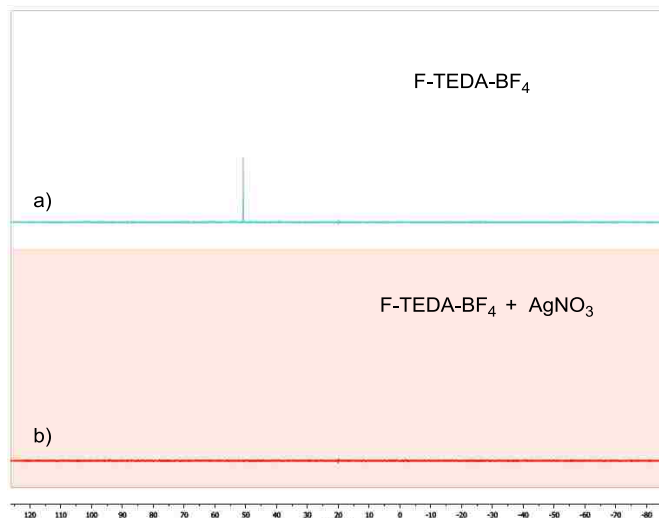


Figure 4.32. ^{19}F NMR spectra showing loss of N-F signal of Selectfluor upon addition of AgNO_3

4.3.5 Role of Water

In the original report, it was reported that water was essential for reaction success. When run in only acetone, **8** is formed in 9% yield (Table 4.12); as shown in Scheme 4.26, **8** is formed in 95% yield when run in a 50:50 ratio of acetone:water. When using increasing amounts of water, it was found that only a 9:1 ratio of acetone:water was necessary to produce **8** in 95% yield.

Table 4.12. Fluorination of **7** using increasing amounts of water

Water added	% Yield (by ^{19}F NMR)
100% acetone	9
100% dry acetone	9
100% acetone + 0.1 mmol H_2O	12
99.1/0.9 (acetone/water)	17
98.2/1.8 (acetone/water)	34
96.4/3.6 (acetone/water)	57
94.6/5.4 (acetone/water)	65
90/10 (acetone/water)	95
80/20 (acetone/water)	94
50/50 (acetone/water)	95

In addition, when adding AgNO_3 to a 9:1 ratio of acetone- d_6 : D_2O , a downfield shift in the water signal from 3.85 ppm to 3.88 ppm was observed by proton NMR, suggesting that water could potentially be acting as a ligand to silver, thus solvating the metal center (Figure 4.33). In addition, the small amount of water could be necessary to solubilize Selectfluor, which has limited solubility in acetone.

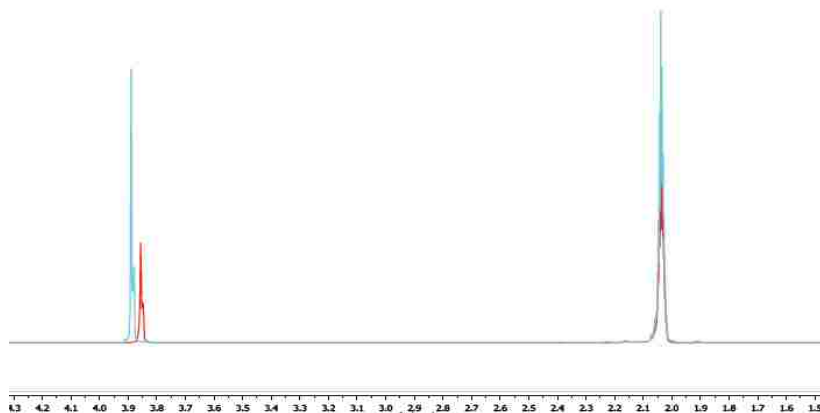


Figure 4.33. Proton NMR spectra suggesting coordination of water to AgNO_3

4.3.6 pH Studies

The pH of the reaction was monitored. Because the decarboxylation of a carboxylic acid was proposed to be occurring, the formation of an alkyl radical, CO_2 , and H^+ should be generated, and thus the pH of the reaction should decrease as acidity increased. When monitored over the course of 2 hours, the pH was found to decrease (Figure 4.34). However, during the initial 600 seconds of the reaction, the pH was found to increase. Interestingly, the time that the pH increases in the beginning of the reaction correlates to the time required for initiation. This result suggests that there is the formation of a more basic complex during the initiation of the reaction.

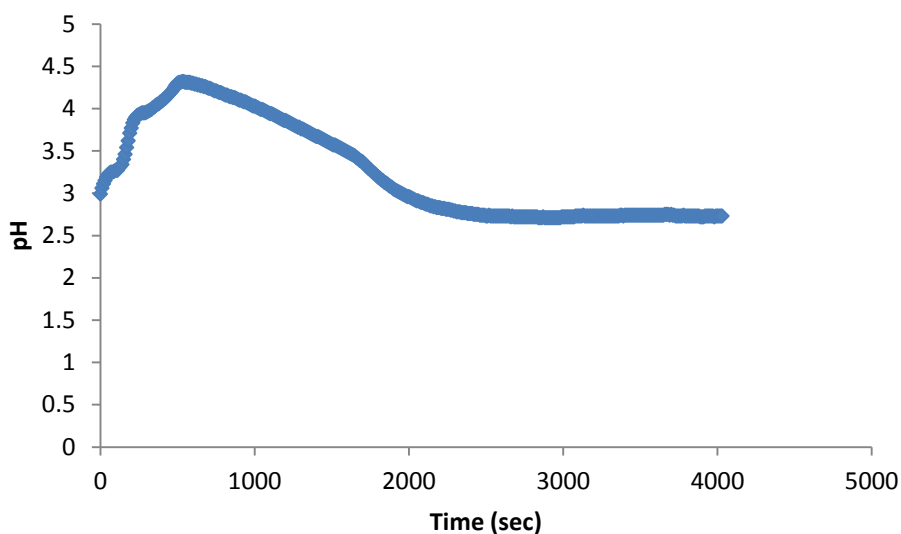
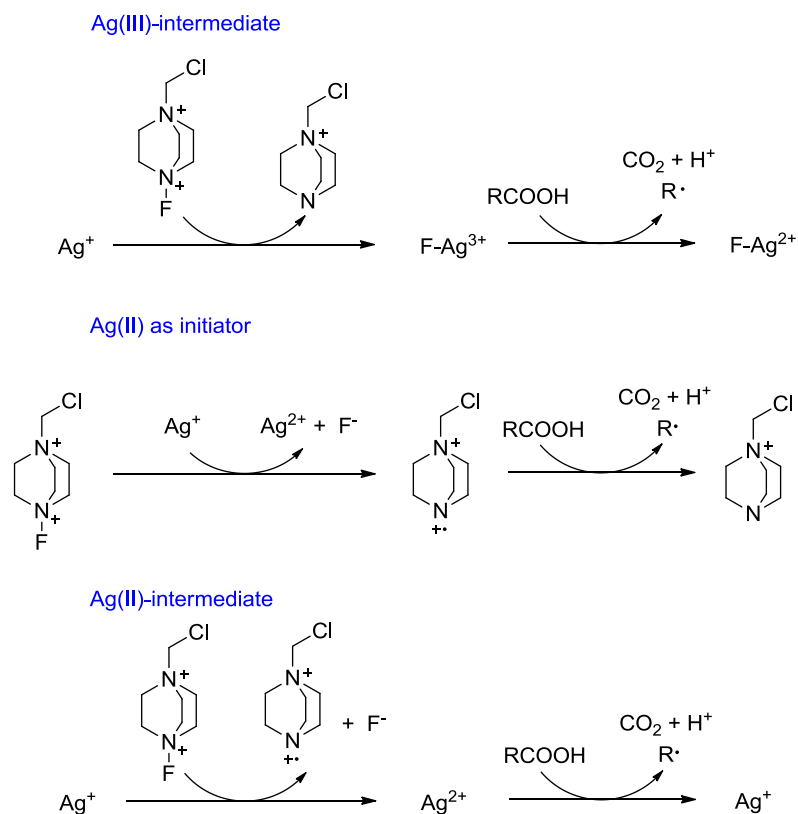


Figure 4.34. pH vs. time plot of decarboxylative fluorination reaction of **7**

4.3.7 Identification of Intermediates and Mechanistic Proposals after Rate-Limiting Step.

Beyond substrate inhibition of the carboxylic acid by the silver nitrate and the oxidation of Ag(I) by Selectfluor, it was vital to explore the reaction mechanism after the

rate-limiting step. The questions that arise are: (A) what intermediates are generated upon oxidation of Ag(I) by Selectfluor, and (B) which of those intermediate species oxidize the carboxylic acid to generate an alkyl radical after the rate-limiting step? It is hypothesized that the reaction mechanism could proceed through one of three pathways: (1) the two-electron oxidation of Ag(I) to Ag(III) by Selectfluor, where Ag(III) oxidizes a carboxylic acid to produce an alkyl radical, (2) single electron oxidation of Ag(I) to Ag(II) by Selectfluor to also generate TEDA-BF₄ radical cation, in which Ag(I) acts only as an initiator in the reaction and the radical cation oxidizes the carboxylic acid, or (3) the oxidation of Ag(I) by Selectfluor to generate Ag(II) and TEDA-BF₄ radical cation, where Ag(II) oxidizes the carboxylic acid to produce a radical (Scheme 4.30). We probed each of these hypotheses to determine the active oxidant in this reaction.



Scheme 4.30. Mechanistic possibilities for Ag(I)-catalyzed decarboxylation

4.3.8 Ag(III)-Catalysis

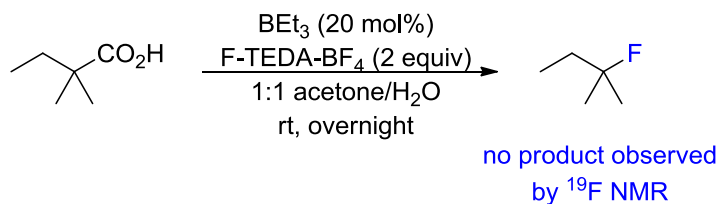
In the original report by the Li group, the reaction mechanism is proposed to proceed through the oxidation of Ag(I) by Selectfluor to form Ag(III), followed by decarboxylation of an acid to produce an alkyl radical through single electron oxidation.⁴⁶ Though Ag(III) is capable of oxidizing carboxylic acids ($E^0 = 1.8 \text{ V}$, $\text{Ag}^{3+}/\text{Ag}^{2+}$),⁵⁷ such complexes are rare and difficult to generate. Known complexes require specific ligands,⁵⁸ including biguanidines,^{59,60} carbaporphyrins,^{61–63} and N-heterocyclic carbenes,⁶⁴ forcing the complexes to be stabilized in the Ag(III) state, or generation under highly basic

conditions.⁶⁵ Due to the rare nature of these complexes, and the lack of ligands other than TEDA-BF₄ in this case, the generation of Ag(III) is unlikely in this reaction.

4.3.9 Ag(II) as Initiator

Several recent papers involving Selectfluor mediated fluorination propose generation of TEDA-BF₄ radical cation through single electron reduction.⁶⁶⁻⁶⁸ In these cases, it is proposed that this species performs oxidation of aliphatic C-H bonds to form alkyl radicals. In the recent paper investigating the mechanism of Cu(I)-catalyzed alkyl fluorination, the Leckta group revealed the role of Cu(I) as an initiator, and TEDA-BF₄ radical cation as the species performing an H-atom abstraction of an alkane to generate the radical.⁶⁶

To probe whether TEDA-BF₄ radical cation could function as an oxidant in the reaction, we used triethylborane as an initiator to generate TEDA-BF₄ radical cation in the absence of AgNO₃. When using a catalytic amount of triethylborane, in the absence of water, and in acetone/water without removing oxygen from the solvent and reaction, no fluorination product was observed by ¹⁹F NMR after letting the reaction sit overnight (Scheme 4.31). This result suggests that Selectfluor is most likely not functioning as the oxidant of carboxylic acid in this reaction, and that AgNO₃ is critical for the success of the decarboxylative fluorination.



Scheme 4.31. Decarboxylative fluorination reaction with triethylborane

4.3.10 Ag(II) as Catalytic Oxidant Studies

4.3.10.1 Persulfate Studies

Since TEDA- BF_4 radical cation is most likely not acting as an oxidant in this reaction, we sought to probe whether Ag(II) could be performing the oxidation. Ag(I)-persulfate catalysis is well-established in the literature, in which Ag(II) is generated upon oxidation of Ag(I).^{56,69} Work done by Kochi and coworkers in the early 1970s on the Ag(I)-persulfate-catalyzed oxidation of aliphatic carboxylic acids to produce alkyl radicals revealed that Ag(II) was the active oxidant rather than sulfate radical anion.^{56,70} We sought to probe the effect that persulfate would have on the decarboxylative fluorination. Addition of $\text{Na}_2\text{S}_2\text{O}_8$ resulted in acceleration of the reaction rate. The addition of $\text{Na}_2\text{S}_2\text{O}_8$ was monitored between 0.1-1.0 equivalents (with respect to **7**), and saturation was observed at concentrations higher than 0.5 equivalents (Figure 4.35). Based on this observation, further studies were done using 0.5 equivalents of persulfate.

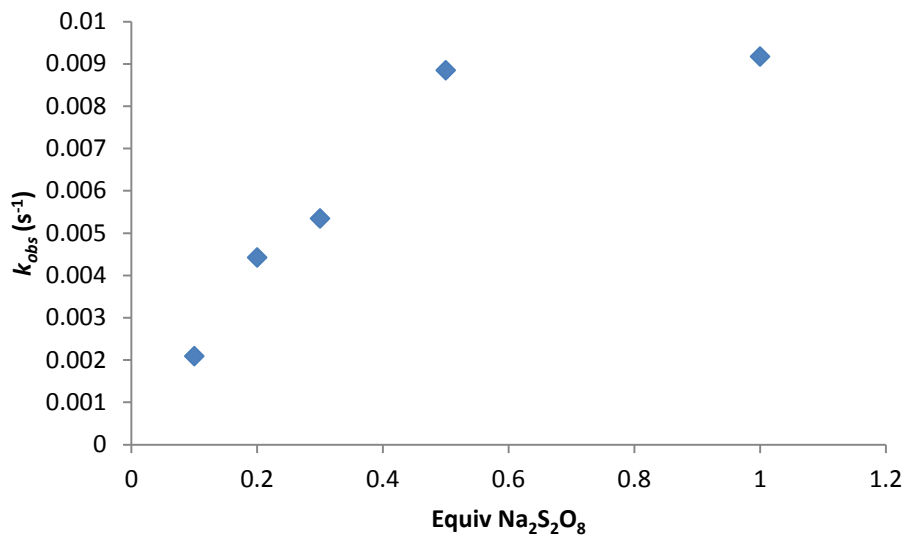
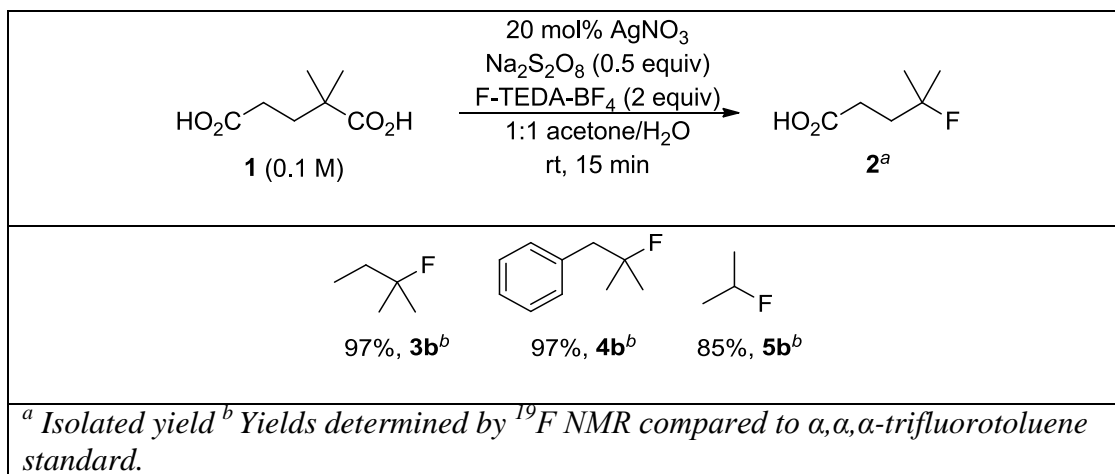


Figure 4.35. Equivalent of Na₂S₂O₈ vs. k_{obs} for the fluorination of **7**

When using 0.5 equivalents of Na₂S₂O₈, combined with 2 equivalents of Selectfluor and 20 mol% AgNO₃, reaction time decreased from 2 hours to 15 minutes, forming alkyl fluorides in excellent yields (Scheme 4.32).



Scheme 4.32. Decarboxylative fluorination reaction with Na₂S₂O₈ as additive

4.3.10.2 Kinetic Studies of 2,2-dimethylglutaric acid using persulfate

Kinetic studies were performed on the reaction of **7** to determine the role of persulfate in the reaction mechanism. Catalyst stability studies performed under the conditions shown in Table 4.13 showed that there was no deactivation of AgNO_3 catalyst during the course of the reaction (Figures 4.36 and 4.37).

Table 4.13. Reaction conditions for catalyst stability studies for fluorination of **7** using sodium persulfate

run	[7] (M)	[AgNO_3] (M)	[Selectfluor] (M)	$\text{Na}_2\text{S}_2\text{O}_8$ (M)
18 - 100%	0.1	0.02	0.2	0.5
19 - 50%	0.05	0.02	0.15	0.5

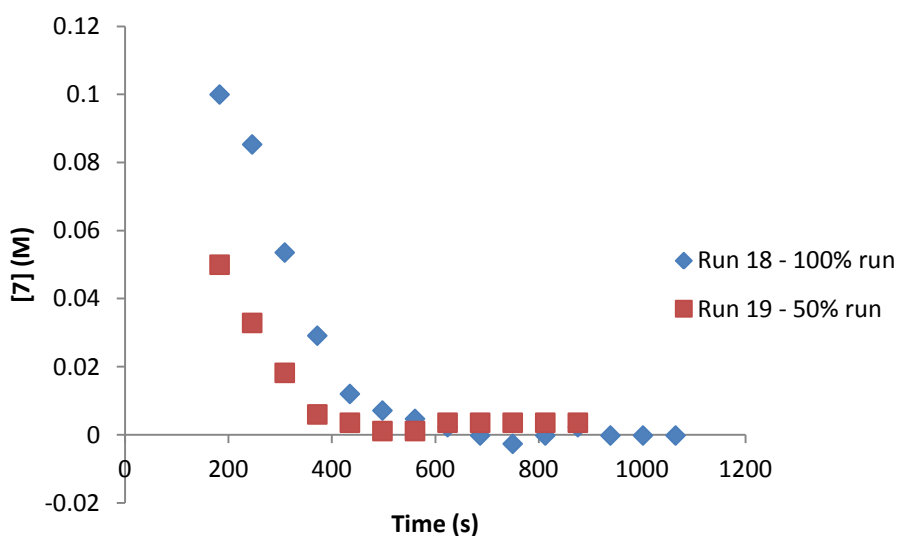


Figure 4.36. Plot of [7] vs. time for Runs 18 and 19 for catalyst stability studies in decarboxylative fluorination reaction of **7** with sodium persulfate

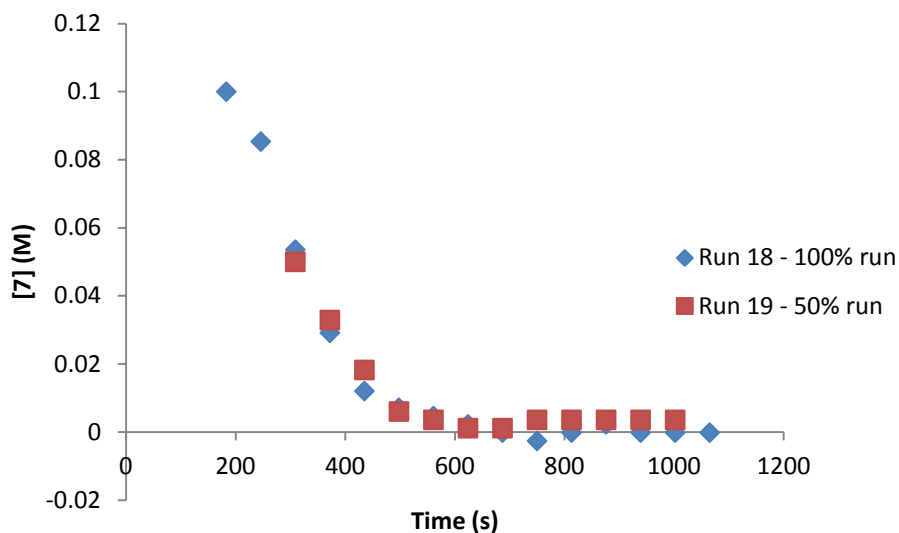


Figure 4.37. Time-adjusted profiles showing overlay of Runs 18 and 19 in decarboxylative fluorination reaction of **7** with sodium persulfate

Next, kinetic order studies were performed under the conditions shown in Table 4.14. These studies showed that AgNO_3 was first order (Figures 4.38 and 4.39), Selectfluor was zero order (Figure 4.40), **7** was -0.5 order (Figure 4.41), and $\text{Na}_2\text{S}_2\text{O}_8$ was approximately first order (Figures 4.42 and 4.43). The -0.5 order observed for **7** implies that in the presence of persulfate, silver-carboxylate formation is slower than Ag(I) oxidation by persulfate, and therefore does not result in substrate inhibition. The approximate first order rate dependence on silver and persulfate suggest that Ag(I) is oxidized to Ag(II) by persulfate. The zero order dependence in Selectfluor not only suggests that it does not play a role before the rate-limiting step, but also that it is no longer oxidizing Ag(I) to Ag(II) ; therefore, its role is likely that of a fluorine atom source after the alkyl radical is produced. The generation of Ag(II) by persulfate, along with the zero-order rate dependence on Selectfluor, suggests that Ag(II) , not TEDA-BF_4 radical cation, is the active oxidant in decarboxylative fluorination reaction.

Table 4.14. Reaction conditions for kinetic order studies for fluorination of **7** using sodium persulfate

Run	[7] (M)	[AgNO ₃] (M)	[Selectfluor] (M)	Na ₂ S ₂ O ₈ (M)
18 - 100%	0.1	0.02	0.2	0.5
20	0.1	0.04	0.2	0.5
21	0.1	0.02	0.15	0.5
22	0.075	0.02	0.2	0.5
23	0.1	0.02	0.2	0.3

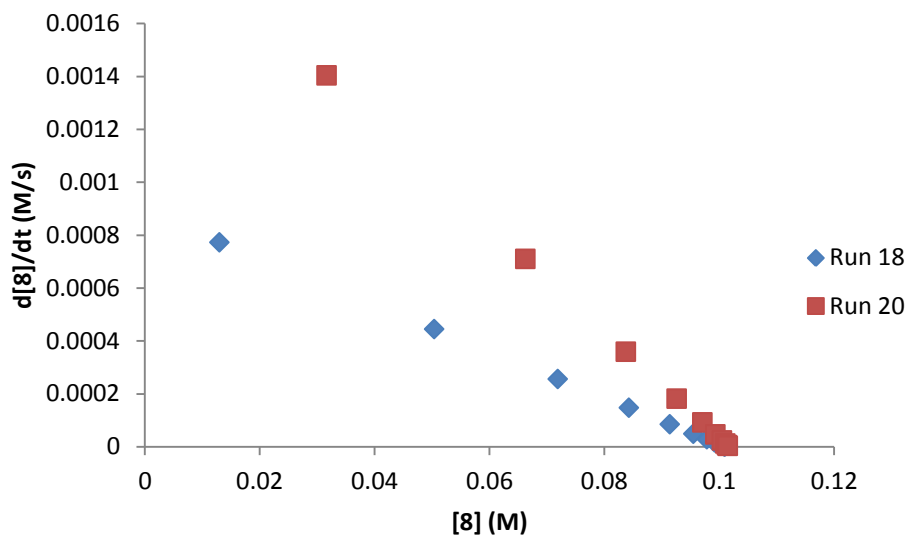


Figure 4.38. $-d[8]/dt$ vs. $[8]$ for rate order of AgNO₃ in decarboxylative fluorination reaction of **7** with sodium persulfate

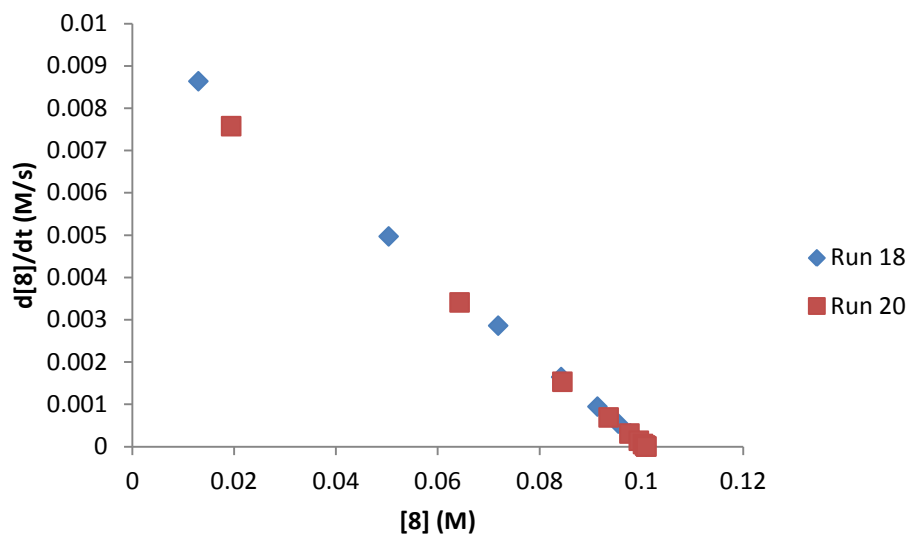


Figure 4.39. Normalized rate plot showing rate order of AgNO_3 in decarboxylative fluorination reaction of **7** with sodium persulfate

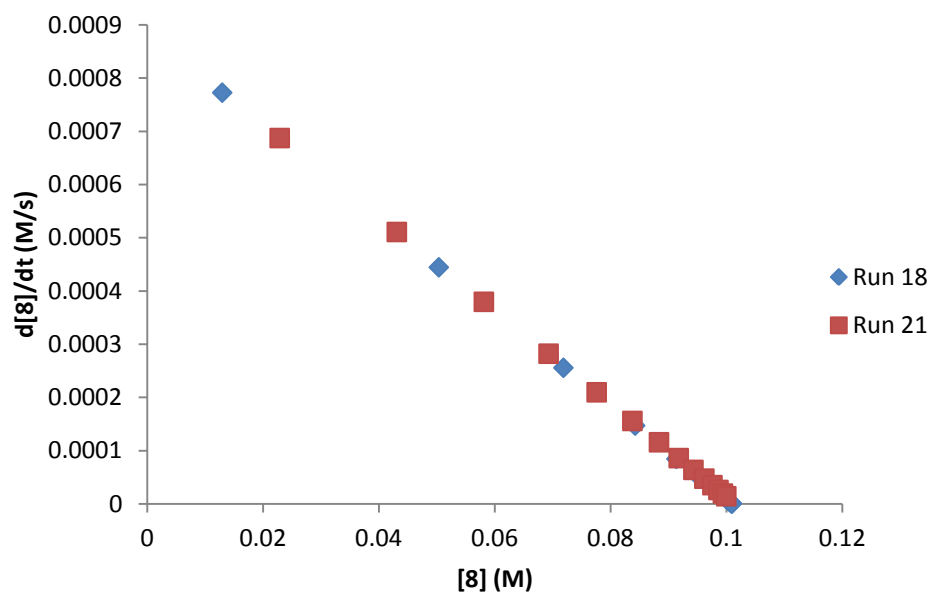


Figure 4.40. $-d[8]/dt$ vs. $[8]$ for rate order of Selectfluor in decarboxylative fluorination reaction of **7** with sodium persulfate

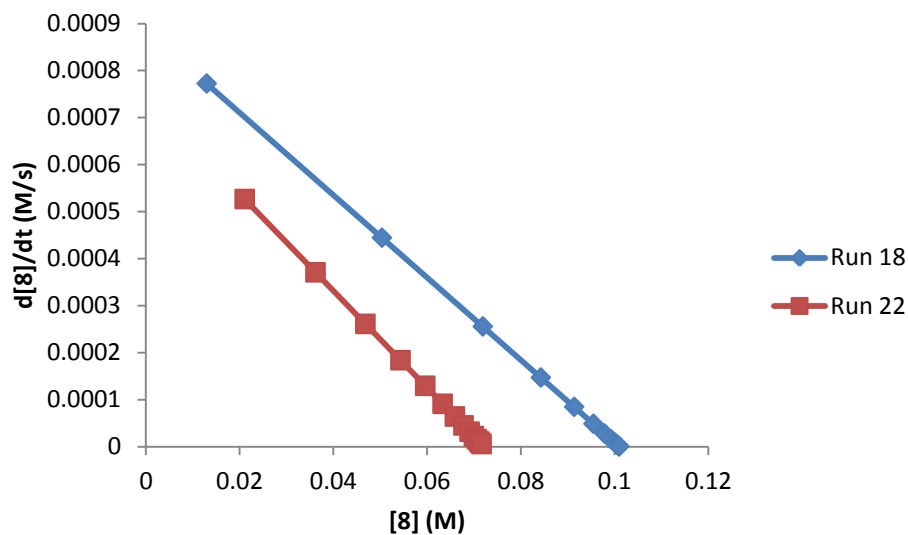


Figure 4.41. $-d[8]/dt$ vs. $[8]$ for rate order of 7 in decarboxylative fluorination reaction of 7 with sodium persulfate

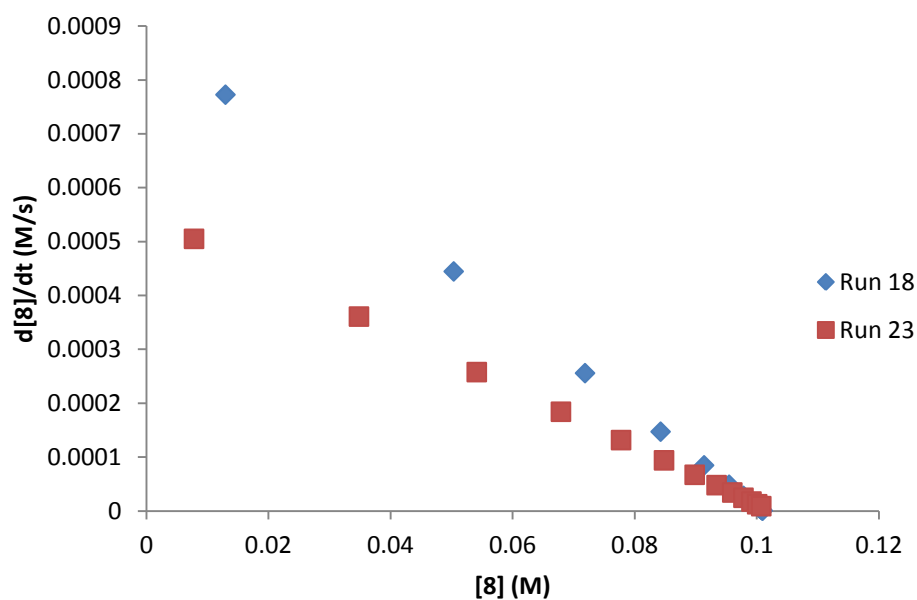


Figure 4.42. $-d[8]/dt$ vs. $[8]$ for rate order of sodium persulfate in decarboxylative fluorination reaction of 7 with sodium persulfate

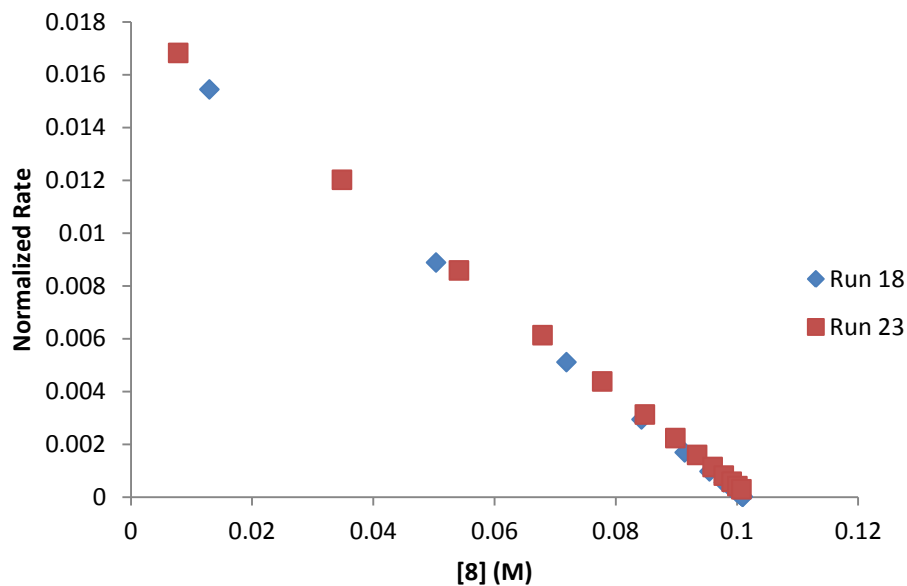


Figure 4.43. Normalized rate plot showing rate order of sodium persulfate in decarboxylative fluorination reaction of **7** with sodium persulfate

The orders found for this system are summarized in Table 4.15. Silver catalyst and sodium persulfate are first order, Selectfluor is zero order, and **7** is inverse half order.

Table 4.15. Rate orders for each component in Ag(I)-Selectfluor-persulfate-mediated fluorination reaction

7	AgNO ₃	Selectfluor	Na ₂ S ₂ O ₈
-0.5	1	0	1

4.3.10.3 Kinetic Studies of 2,2-dimethylbutyric acid using persulfate

Kinetic studies were performed on the reaction of **9a** to determine the role of persulfate in the reaction mechanism. Catalyst stability studies were performed under the

conditions shown in Table 4.16. These studies showed that there was no deactivation of AgNO_3 catalyst during the course of the reaction (Figures 4.44 and 4.45).

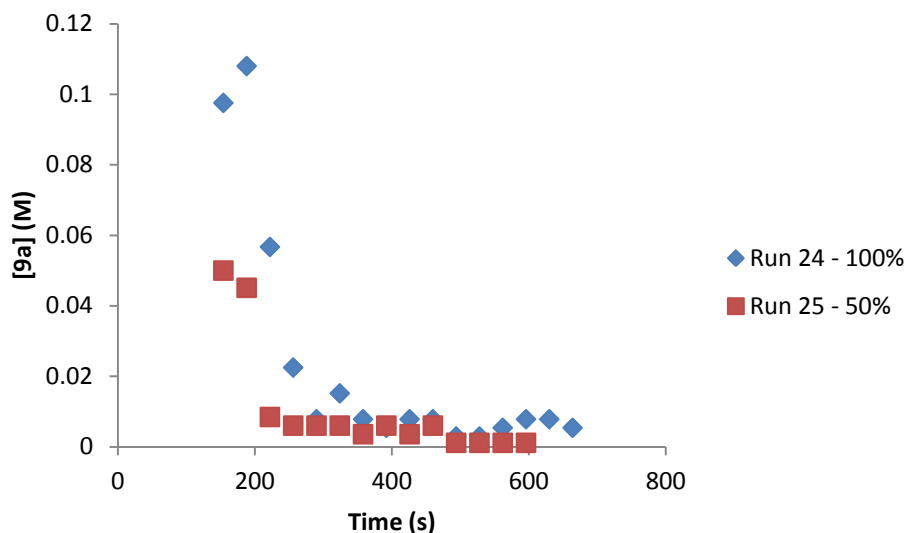


Figure 4.44. Plot of $[9a]$ vs. time for Runs 24 and 25 for catalyst stability studies in decarboxylative fluorination reaction of $9a$ with sodium persulfate

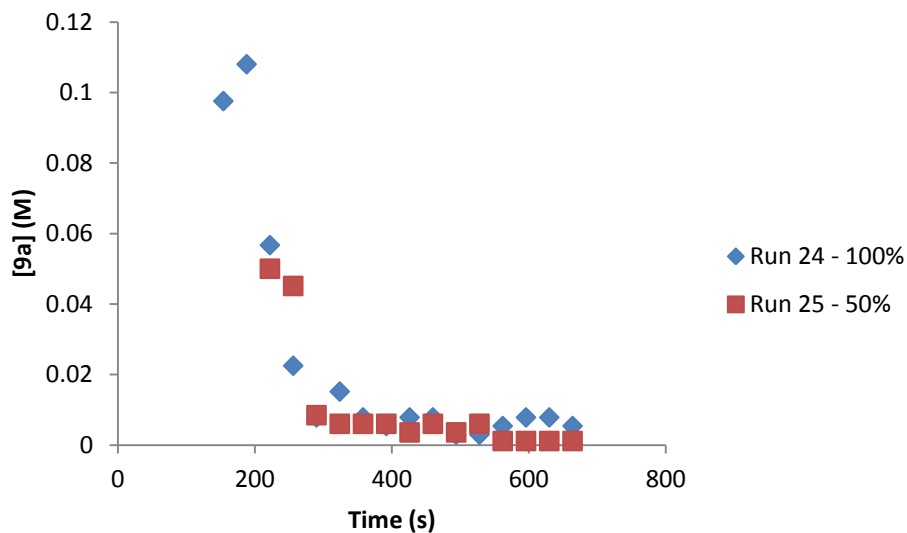


Figure 4.45. Time-adjusted profiles showing overlay of Runs 24 and 25 in decarboxylative fluorination reaction of $9a$ with sodium persulfate

Table 4.16. Reaction conditions for catalyst stability studies for fluorination of **9a** using sodium persulfate

run	[9a] (M)	[AgNO ₃] (M)	[Selectfluor] (M)	Na ₂ S ₂ O ₈ (M)
24 – 100%	0.1	0.02	0.2	0.05
25 - 50%	0.05	0.02	0.15	0.05

Kinetic order studies were performed under the conditions shown in Table 4.17. These studies showed that AgNO₃ was first order (Figures 4.46 and 4.47), Selectfluor was zero order (Figure 4.48), **9a** was zero order (Figure 4.49), and Na₂S₂O₈ was approximately first order (Figures 4.50 and 4.51). The zero order observed for **9a** implies that in the presence of persulfate, silver-carboxylate formation is slower than Ag(I) oxidation by persulfate, and therefore does not result in substrate inhibition. The order of the substrates in this reaction are consistent with those found for the reaction of **7** in Section 4.3.10.2.

Table 4.17. Reaction conditions for kinetic order studies for fluorination of **9a** using sodium persulfate

Run	[9a] (M)	[AgNO ₃] (M)	[Selectfluor] (M)	Na ₂ S ₂ O ₈ (M)
24 - 100%	0.1	0.02	0.2	0.05
26	0.1	0.04	0.2	0.05
27	0.1	0.02	0.15	0.05
28	0.075	0.02	0.2	0.05
29	0.1	0.02	0.2	0.03

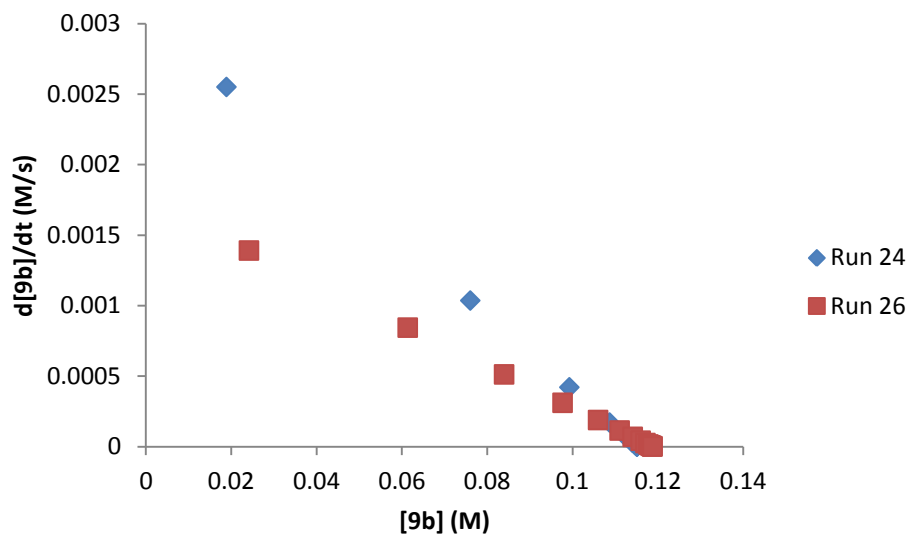


Figure 4.46. $-d[9b]/dt$ vs. $[9b]$ for rate order of $AgNO_3$ in decarboxylative fluorination reaction of **9a** with sodium persulfate

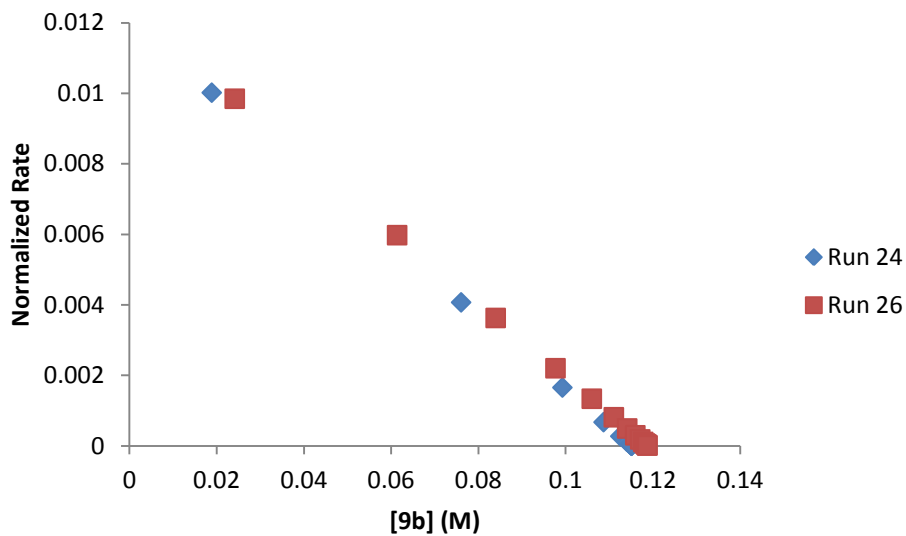


Figure 4.47. Normalized rate plot showing rate order of $AgNO_3$ in decarboxylative fluorination reaction of **9a** with sodium persulfate

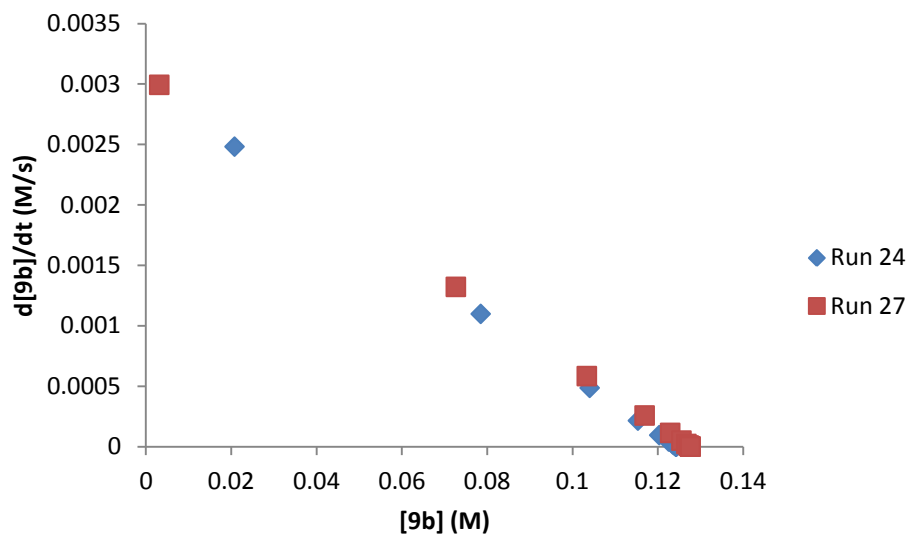


Figure 4.48. $-d[9b]/dt$ vs. $[9b]$ for rate order of Selectfluor in decarboxylative fluorination reaction of **9a** with sodium persulfate

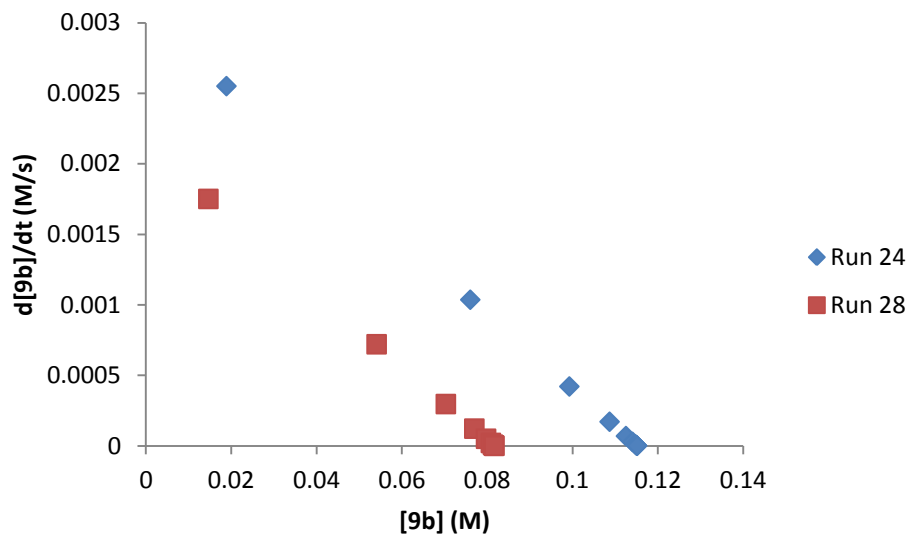


Figure 4.49. Normalized rate plot showing rate order of **9a** in decarboxylative fluorination reaction of **9a** with sodium persulfate

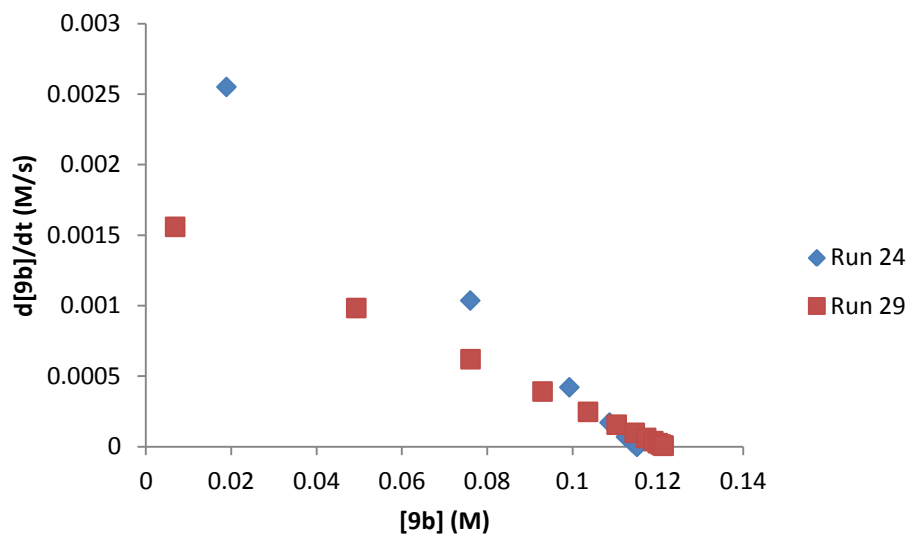


Figure 4.50. $-d[9b]/dt$ vs. $[9b]$ for rate order of sodium persulfate in decarboxylative fluorination reaction of **9a** with sodium persulfate

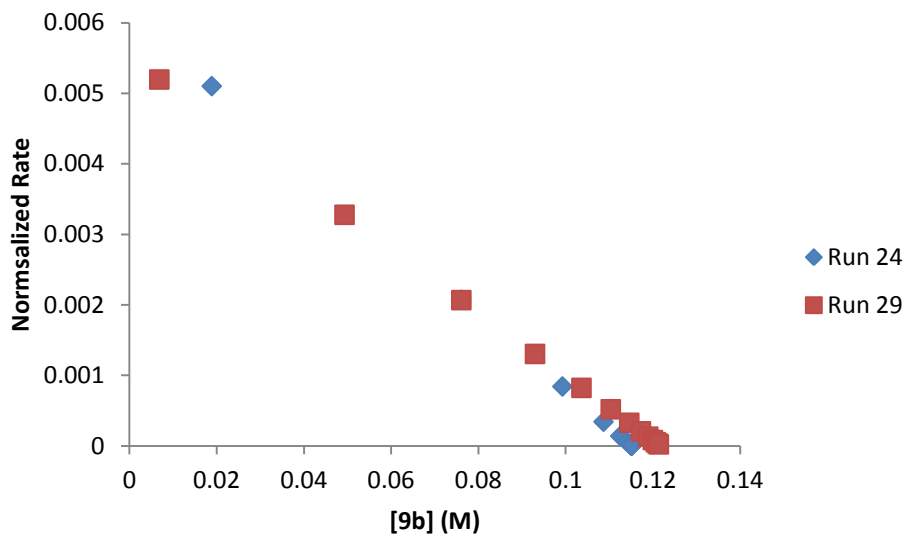


Figure 4.51. Normalized rate plot showing rate order of sodium persulfate in decarboxylative fluorination reaction of **9a** with sodium persulfate

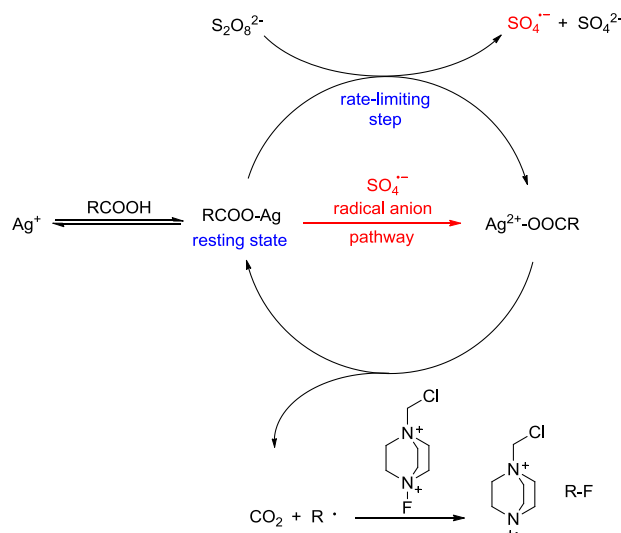
The orders found for this system are summarized in Table 4.18. Silver catalyst and sodium persulfate are first order, Selectfluor is zero order, and **9a** is zero order.

Table 4.18. Rate orders for each component in Ag(I)-Selectfluor-persulfate-mediated fluorination reaction

9a	AgNO ₃	Selectfluor	Na ₂ S ₂ O ₈
0	0.85	0	1

4.3.10.4 Proposed Mechanism of Persulfate Reaction

Based on the kinetic and spectroscopic studies on the reaction with persulfate, a reaction mechanism can be proposed (Scheme 4.43). In the presence of persulfate, the mechanism of the decarboxylative fluorination reaction involved the oxidation of Ag(I)-carboxylate to Ag(II) by persulfate in the rate-limiting step of the reaction. This initial oxidation is followed by the decarboxylation and oxidation of a carboxylic acid by Ag(II) to produce an alkyl radical. The resulting radical can abstract a fluorine from Selectfluor to produce a TEDA-BF₄ radical cation and the aliphatic fluorine product. The catalyst is turned over to regenerate Ag(II) by the radical anion to continue the catalytic cycle.

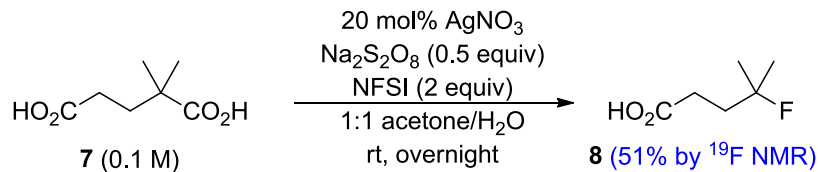


Scheme 4.43. Proposed catalytic cycle of Ag(I)-catalyzed fluorination using Na₂S₂O₈ and Selectfluor

4.3.10.5 NFSI Studies

If Ag(II) is the active oxidant in this reaction, in the presence of persulfate Selectfluor is no longer needed to oxidize Ag(I) to Ag(II), and should only be functioning as a fluorine atom source, as well as producing TEDA-BF₄ radical cation, which can turn over the catalyst to continue the catalytic cycle (Scheme 4.43). If this is the case, the alkyl radical can abstract fluorine from another N-F source that normally does not work to produce alkyl fluorides. Li reported that when replacing Selectfluor with N-fluorobenzenesulfonimide (NFSI), no reaction occurred, most likely because it is not a strong enough oxidant to oxidize Ag(I) to Ag(II). However, in the presence of persulfate, a reagent that can readily oxidize Ag(I), the addition of NFSI should result in alkyl fluoride formation through fluorine abstraction by the alkyl radical in the absence of Selectfluor. In addition, the resulting sulfate radical anion from the oxidation of Ag(I) by persulfate can carry out the subsequent oxidation of Ag(I) to Ag(II) after the rate-limiting step, since the resulting benzenesulfonamide radical anion would not be able to turnover the catalyst.

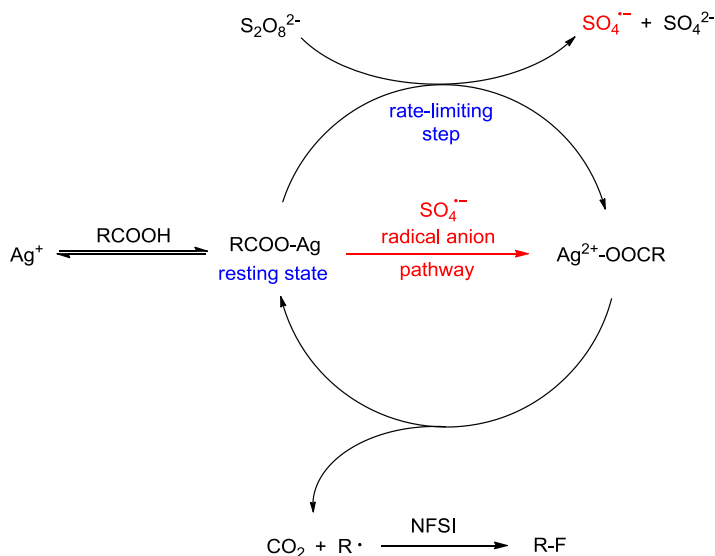
When **7** was allowed to react with a catalytic amount of AgNO₃ in the presence of 0.5 equiv Na₂S₂O₈ and 2 equiv NFSI, fluorinated product **8** was observed in 51% yield by ¹⁹F NMR (Scheme 8). When increasing persulfate from 0.5 equiv to 1.1 equiv, yield of **8** increased to 63%. Based on this result, coupled with those found in the persulfate studies, a mechanism can be proposed in which Ag(II) is the active oxidant in this decarboxylative fluorination reaction.



Scheme 4.44. Decarboxylative fluorination reaction with NFSI and $\text{Na}_2\text{S}_2\text{O}_8$

4.3.10.6 Proposed Mechanism of NFSI Reaction

Based on the studies with NFSI, a reaction mechanism can be proposed which involves the initial oxidation of Ag(I)-carboxylate to Ag(II) by persulfate, followed by the oxidation of carboxylic acid to produce an alkyl radical (Scheme 4.45). The alkyl radical can abstract a fluorine from NFSI to generate the fluorinated product. The Ag(I) can be oxidized to Ag(II) by the sulfate radical anion, which was generated during the initial rate-limiting oxidation.



Scheme 4.45. Proposed catalytic cycle of Ag(I)-catalyzed fluorination using NFSI and Persulfate

4.3.11 Ag-ligand NMR Studies with Selectfluor

4.3.11.1 ^1H NMR Studies of 2,9-dimethyl-1,10-phenanthroline

Since there are no supporting ligands on Ag, it is difficult to characterize the oxidation state of the metal. To probe the oxidation state of Ag and gain further information on the active oxidant in this reaction, a strong donor ligand with a characteristic ^1H NMR signal was employed. If Ag(II) was formed as an intermediate upon mixing with Selectfluor, line broadening should occur in the NMR spectrum, whereas if Ag(III) was generated, no line broadening would occur due to the diamagnetism of a Ag(III) complex (d^8).^{58,61} When an equivalent of Selectfluor was added to a premixed equimolar combination of 2,9-dimethyl-1,10-phenanthroline (dmp) and AgNO_3 (Figure 4.52 and 4.53) significant line broadening was observed in the ^1H NMR spectrum. These findings are consistent with the formation of a paramagnetic (d^9) Ag(II) complex.

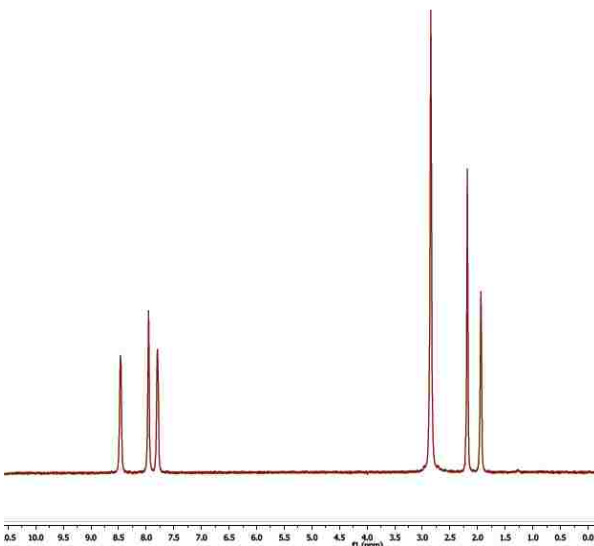


Figure 4.52. ^1H NMR spectrum of dmp with 1 equiv AgNO_3 in MeCN-d_3 .

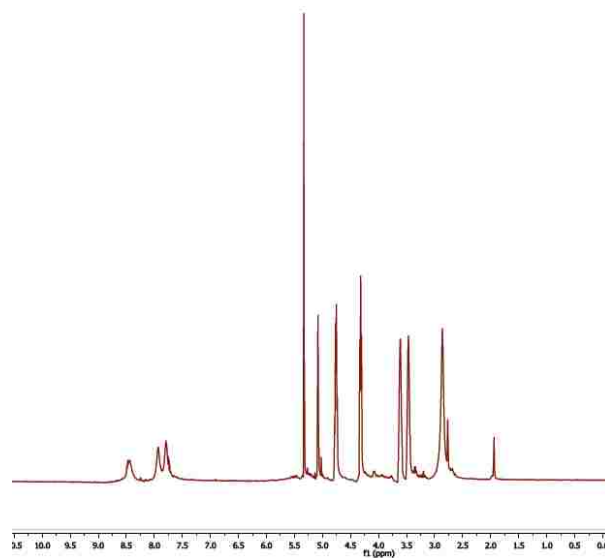


Figure 4.53. ¹H NMR spectrum of dmp with 1 equiv AgNO₃ and Selectfluor in MeCN-d₃.

4.3.11.2 ^1H NMR Studies of Terpyridine

Similar line broadening occurred when terpyridine (terpy) was employed as a donor ligand as well (Figure 4.54). In this case, the line broadening is extremely significant, and the protons of terpy are no longer visible in the spectrum (Figure 4.55).

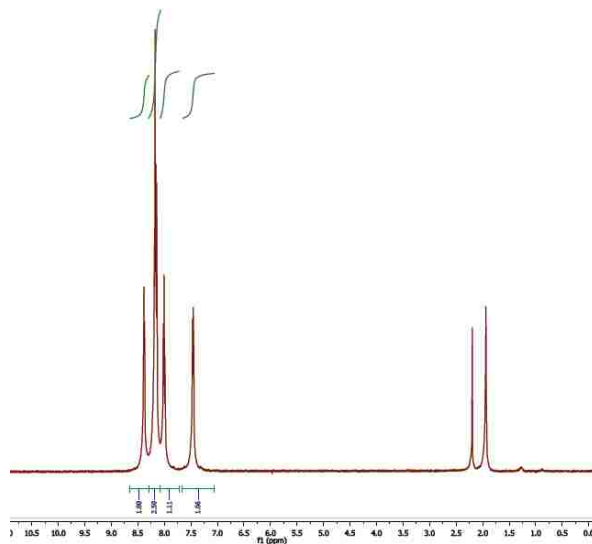


Figure 4.54. ^1H NMR spectrum of terpy with 1 equiv AgNO_3 in MeCN-d_3 .

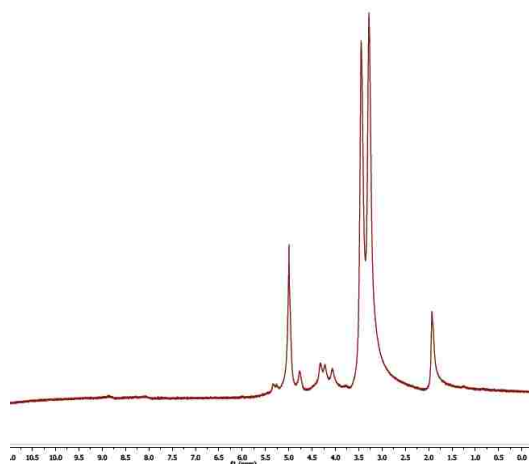
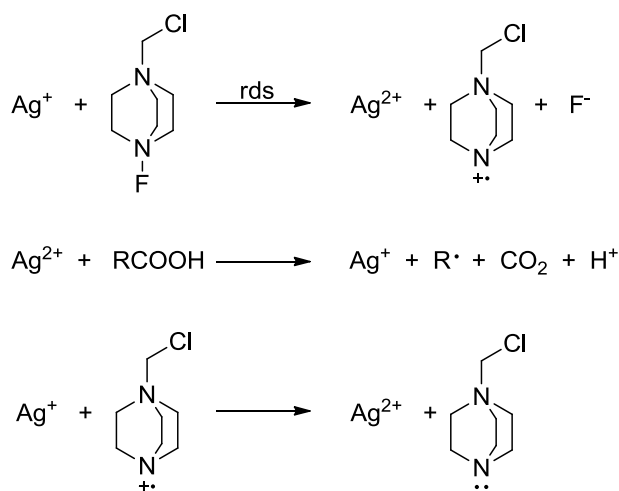


Figure 4.55. ^1H NMR spectrum of terpy with 1 equiv AgNO_3 and Selectfluor in MeCN-d_3 .

4.3.12 AgNO₃-TEDA-BF₄ Studies

4.3.12.1 NMR Studies of AgNO₃-TEDA-BF₄

There is a precedence for silver-amine complexes in the literature.¹⁷ Kinetic studies suggest oxidation of Ag(I) to Ag(II) by Selectfluor in the rate-limiting step of the reaction, also resulting in the formation of TEDA-BF₄ radical cation (Scheme 4.46). Ag(II) can oxidize a carboxylic acid to generate an alkyl radical and regenerate Ag(I). TEDA-BF₄ radical cation can then oxidize Ag(I) to produce Ag(II) to carry on the catalytic cycle, while also generating the free amine TEDA-BF₄.



Scheme 4.46. Mechanism of Ag(I) oxidation by Selectfluor

To investigate whether the amine could be acting as a ligand, we used proton NMR to observe the effect that AgNO₃ has on TEDA-BF₄. A downfield shift of the TEDA-BF₄ protons was observed when an equivalent of AgNO₃ was added in D₂O (Figure 4.56, Table 4.19).

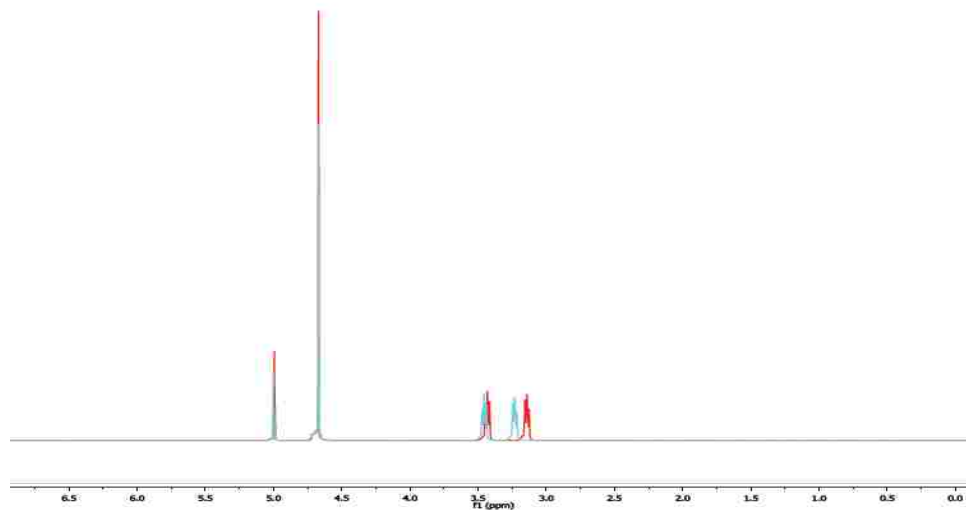


Figure 4.56. Proton NMR spectra suggesting coordination of TEDA-BF₄ to AgNO₃

Table 4.19. ¹H NMR shifts of TEDA-BF₄ with AgNO₃

	Δ1 (ppm)	Δ2 (ppm)	Δ3 (ppm)
TEDA-BF ₄	4.99	3.43	3.15
TEDA-BF ₄ + AgNO ₃	5.01	3.46	3.23

4.3.12.2 Crystallization of AgNO₃-TEDA-BF₄ complex

In addition to the proton NMR studies, crystals of the Ag-amine complex were grown and identified by x-ray crystallography (Figure 4.57). The x-ray crystal structure showed two TEDA-BF₄ ligands coordinated to the silver center, in which the nitrate ion can either be bound or unbound.

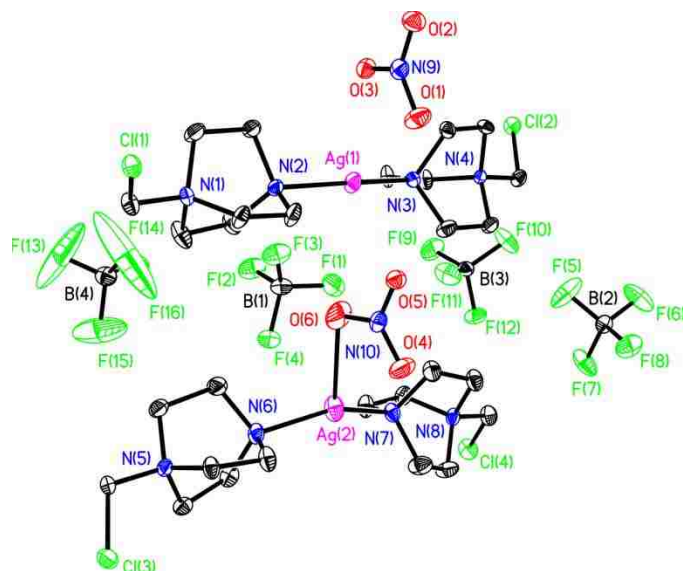
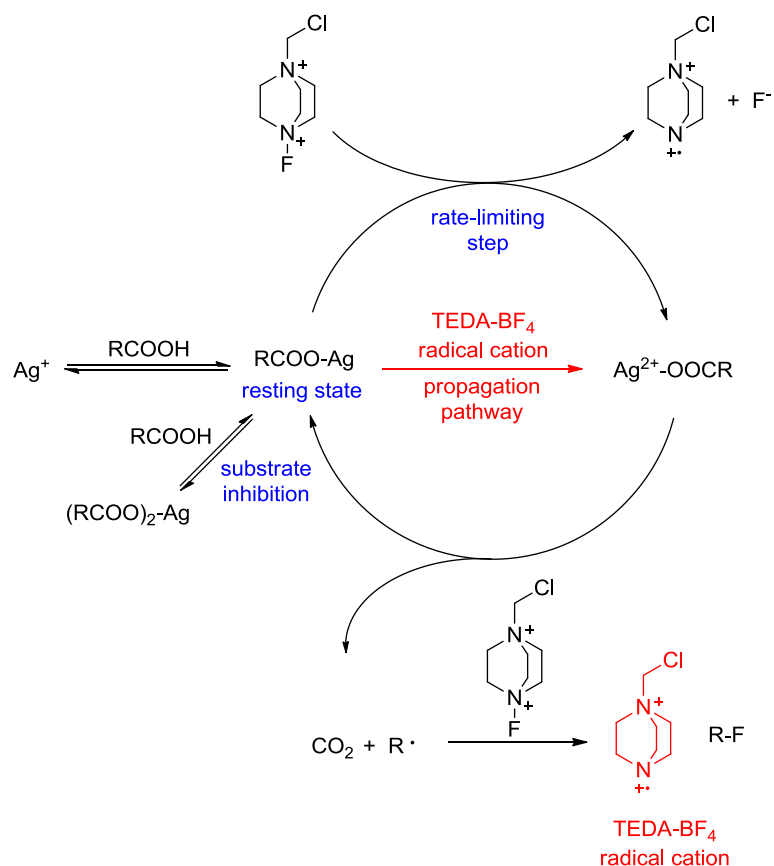


Figure 4.57. X-ray crystal structure showing coordination of TEDA-BF₄ to AgNO₃

4.3.13 Proposed Mechanism of Ag(I)-catalyzed Decarboxylative Fluorination

Based on the kinetic and spectroscopic studies described above, a mechanism is proposed in which Ag(I)-carboxylate, formed in the induction period, is oxidized to Ag(II) by Selectfluor to also generate TEDA-BF₄ radical cation in the rate-limiting step of the reaction (Scheme 4.47). There is also substrate inhibition of acid by the silver catalyst to produce a Ag(carboxylate)₂. Ag(II) oxidizes the carboxylic acid to produce an alkyl radical, which can abstract a fluorine from Selectfluor to yield product and regenerate Ag(I), which can be reoxidized to generate Ag(II) by TEDA-BF₄ radical cation.



Scheme 4.47. Proposed catalytic cycle of Ag(I)-catalyzed fluorination using Selectfluor

4.4 Conclusions

The mechanistic studies described herein show the complex roles of AgNO_3 and Selectfluor in decarboxylative fluorination in acetone:water media. In the rate-limiting step of the reaction, Ag(I)-carboxylate is oxidized to Ag(II) by Selectfluor, also generating TEDA- BF_4 radical cation. In addition, substrate inhibition of the carboxylic acid by the AgNO_3 catalyst was observed through the formation of a $\text{Ag}(\text{carboxylate})_2$, though this step does not affect catalyst stability. Catalyst stability allowed AgNO_3 loading to be decreased significantly, from 20 mol% to 5 mol%. Kinetic studies utilizing

$\text{Na}_2\text{S}_2\text{O}_8$ as an additive suggest that $\text{Ag}(\text{II})$ is the active oxidant in the reaction. As well as uncovering the active oxidant in this reaction, the addition of persulfate was shown to significantly accelerate the rate of decarboxylative fluorination. It is our belief that understanding the mechanism of this reaction through the kinetic and spectroscopic studies described above will aid in the development of improved or novel fluorination methods that proceed through single electron oxidation.

4.5 References

- (1) Müller, K.; Faeh, C.; Diederich, F. *Science* **2007**, *317*, 1881–1886.
- (2) Wang, J.; Sánchez-Roselló, M.; Aceña, J. L.; del Pozo, C.; Sorochinsky, A. E.; Fustero, S.; Soloshonok, V. A.; Liu, H. *Chem. Rev.* **2014**, *114*, 2432–2506.
- (3) Kirk, K. L. *Org. Process Res. Dev.* **2008**, *12*, 305–321.
- (4) Purser, S.; Moore, P. R.; Swallow, S.; Gouverneur, V. *Chem. Soc. Rev.* **2008**, *37*, 320–330.
- (5) Jeschke, P. *Chembiochem* **2004**, *5*, 571–589.
- (6) Furuya, T.; Kamlet, A. S.; Ritter, T. *Nature* **2011**, *473*, 470–477.
- (7) Shimizu, M.; Hiyama, T. *Angew. Chem. Int. Ed.* **2004**, *44*, 214–231.
- (8) Smith, D. W.; Iacono, S. T.; Boday, D. J.; Kettwich, S. C. *Advances in Fluorine-Containing Polymers*; ACS Symposium Series; American Chemical Society: Washington, DC, **2013**; Vol. 1106.
- (9) Cametti, M.; Crousse, B.; Metrangolo, P.; Milani, R.; Resnati, G. *Chem. Soc. Rev.* **2012**, *41*, 31–42.
- (10) Berger, R.; Resnati, G.; Metrangolo, P.; Weber, E.; Hulliger, J. *Chem. Soc. Rev.* **2011**, *40*, 3496–3508.
- (11) Miller, P. W.; Long, N. J.; Vilar, R.; Gee, A. D. *Angew. Chem. Int. Ed.* **2008**, *47*, 8998–9033.
- (12) Ametamey, S. M.; Honer, M.; Schubiger, P. A. *Chem. Rev.* **2008**, *108*, 1501–1516.
- (13) Harper, D. B.; O'Hagan, D. *Nat. Prod. Rev.* **1994**, *11*, 123–133.
- (14) Liang, T.; Neumann, C. N.; Ritter, T. *Angew. Chem. Int. Ed.* **2013**, *52*, 8214–8264.
- (15) Hollingworth, C.; Gouverneur, V. *Chem. Commun.* **2012**, *48*, 2929–2942.
- (16) Barton, D. H. R.; Godinho, L. S.; Hesse, R. H.; Pechet, M. M. *Chem. Commun.* **1968**, 804.
- (17) Lal, G. S.; Pez, G. P.; Syvret, R. G. *Chem. Rev.* **1996**, *96*, 1737–1756.

- (18) Umemoto, T.; Kawada, K.; Tomita, K. *Tetrahedron Lett.* **1986**, *27*, 4465–4468.
- (19) Nyffeler, P. T.; Durón, S. G.; Burkart, M. D.; Vincent, S. P.; Wong, C.-H. *Angew. Chem. Int. Ed.* **2005**, *44*, 192–212.
- (20) Knoechel, D. J.; Herrinton, P. M. *Org. Process Res. Dev.* **1997**, *1*, 217–221.
- (21) Burkart, M. D.; Vincent, S. P.; Düffels, A.; Murray, B. W.; Ley, S. V.; Wong, C.-H. *Bioorg. Med. Chem.* **2000**, *8*, 1937–1946.
- (22) Teare, H.; Robins, E. G.; Arstad, E.; Luthra, S. K.; Gouverneur, V. *Chem. Commun.* **2007**, 2330.
- (23) Wolfe, S.; Shi, Z.; Brion, C. E.; Rolke, J.; Zheng, Y.; Cooper, G.; Chong, D. P.; Hu, C. Y. *Can. J. Chem.* **2002**, *80*, 222–227.
- (24) Hoffmann, R.; Imamura, A.; Hehre, W. J. *J. Am. Chem. Soc.* **1968**, *90*, 1499–1509.
- (25) Hull, K. L.; Anani, W. Q.; Sanford, M. S. *J. Am. Chem. Soc.* **2006**, *128*, 7134–7135.
- (26) Wang, X.; Mei, T.-S.; Yu, J.-Q. *J. Am. Chem. Soc.* **2009**, *131*, 7520–7521.
- (27) Schuler, M.; Silva, F.; Bobbio, C.; Tessier, A.; Gouverneur, V. *Angew. Chem. Int. Ed.* **2008**, *47*, 7927–7930.
- (28) Wang, W.; Jasinski, J.; Hammond, G. B.; Xu, B. *Angew. Chem. Int. Ed.* **2010**, *49*, 7247–7252.
- (29) Fier, P. S.; Luo, J.; Hartwig, J. F. *J. Am. Chem. Soc.* **2013**, *135*, 2552–2559.
- (30) Ye, Y.; Sanford, M. S. *J. Am. Chem. Soc.* **2013**, *135*, 4648–4651.
- (31) Bloom, S.; Pitts, C. R.; Woltornist, R.; Griswold, A.; Holl, M. G.; Lectka, T. *Org. Lett.* **2013**, *15*, 1722–1724.
- (32) Mazzotti, A. R.; Campbell, M. G.; Tang, P.; Murphy, J. M.; Ritter, T. *J. Am. Chem. Soc.* **2013**, *135*, 14012–14015.
- (33) Liu, W.; Huang, X.; Cheng, M.-J.; Nielsen, R. J.; Goddard, W. a; Groves, J. T. *Science* **2012**, *337*, 1322–1325.
- (34) Bloom, S.; Pitts, C. R.; Miller, D. C.; Haselton, N.; Holl, M. G.; Urheim, E.; Lectka, T. *Angew. Chem. Int. Ed.* **2012**, *51*, 10580–10583.

- (35) Rueda-Becerril, M.; Sazepin, C. C.; Leung, J. C. T.; Okbinoglu, T.; Kennepohl, P.; Paquin, J.-F.; Sammis, G. M. *J. Am. Chem. Soc.* **2012**, *134*, 4026–4029.
- (36) Leung, J. C. T.; Chatalova-Sazepin, C.; West, J. G.; Rueda-Becerril, M.; Paquin, J.-F.; Sammis, G. M. *Angew. Chemie. Int. Ed.* **2012**, *124*, 10962–10965.
- (37) Barker, T. J.; Boger, D. L. *J. Am. Chem. Soc.* **2012**, *134*, 13588–13591.
- (38) Furuya, T.; Ritter, T. *Org. Lett.* **2009**, *11*, 2860–2863.
- (39) Furuya, T.; Strom, A. E.; Ritter, T. *J. Am. Chem. Soc.* **2009**, *131*, 1662–1663.
- (40) Tang, P.; Furuya, T.; Ritter, T. *J. Am. Chem. Soc.* **2010**, *132*, 12150–12154.
- (41) Teare, H.; Robins, E. G.; Kirjavainen, A.; Forsback, S.; Sandford, G.; Solin, O.; Luthra, S. K.; Gouverneur, V. *Angew. Chem. Int. Ed.* **2010**, *49*, 6821–6824.
- (42) Stenhagen, I. S. R.; Kirjavainen, A. K.; Forsback, S. J.; Jørgensen, C. G.; Robins, E. G.; Luthra, S. K.; Solin, O.; Gouverneur, V. *Chem. Commun.* **2013**, *49*, 1386–1388.
- (43) Qin, C.; Davies, H. M. L. *Org. Lett.* **2013**, *15*, 6152–6154.
- (44) Xu, P.; Guo, S.; Wang, L.; Tang, P. *Angew. Chem. Int. Ed.* **2014**, *53*, 5955–5958.
- (45) Fier, P. S.; Hartwig, J. F. *Science* **2013**, *342*, 956–960.
- (46) Yin, F.; Wang, Z.; Li, Z.; Li, C. *J. Am. Chem. Soc.* **2012**, *134*, 10401–10404.
- (47) Mathew, J. S.; Klussmann, M.; Iwamura, H.; Valera, F.; Futran, A.; Emanuelsson, E. a C.; Blackmond, D. G. *J. Org. Chem.* **2006**, *71*, 4711–4722.
- (48) Blackmond, D. G. *Angew. Chem. Int. Ed. Engl.* **2005**, *44*, 4302–4320.
- (49) Devery, J. J.; Conrad, J. C.; MacMillan, D. W. C.; Flowers, R. A. *Angew. Chem. Int. Ed.* **2010**, *49*, 6106–6110.
- (50) Choquette, K. A.; Sadasivam, D. V.; Flowers, R. A. *J. Am. Chem. Soc.* **2011**, *133*, 10655–10661.
- (51) Gansäuer, A.; Behlendorf, M.; von Laufenberg, D.; Fleckhaus, A.; Kube, C.; Sadasivam, D. V.; Flowers, R. A. *Angew. Chem. Int. Ed.* **2012**, *51*, 4739–4742.
- (52) Patel, N. R.; Flowers, R. A. *J. Am. Chem. Soc.* **2013**, *135*, 4672–4675.

- (53) Baxter, R. D.; Sale, D.; Engle, K. M.; Yu, J.-Q.; Blackmond, D. G. *J. Am. Chem. Soc.* **2012**, *134*, 4600–4606.
- (54) Devery III, J. J.; Douglas, J. J.; Nguyen, J. D.; Cole, K. P.; Flowers II, R. A.; Stephenson, C. R. *J. Chem. Sci.* **2015**, *6*, 537–541.
- (55) Torroba, J.; Aynsley, J.; Tuzimoto, P. A.; Bruce, D. W. *RSC Adv.* **2012**, *2*, 12866.
- (56) Anderson, J. M.; Kochi, J. K. *J. Am. Chem. Soc.* **1970**, *92*, 1651–1659.
- (57) CRC Handbook of Chemistry and Physics. 86th ed.; CRC Press: Boca Raton, FL; 2005–2006, pp. 8–20.
- (58) Font, M.; Acuna-Pares, F.; Parella, T.; Serra, J.; Luis, Josep, M.; Lloret-Fillol, J.; Costas, M.; Ribas, X. *Nat. Commun.* **2014**, *5*, 4373.
- (59) Simms, M. L.; Atwood, J. L.; Zatko, D. A. *J. Chem. Soc. Chem. Comm.* **1973**, *2*.
- (60) Sen, D. *J. Chem. Soc. A* **1969**, 1304–1305.
- (61) Muckey, M. A.; Szczepura, L. F.; Ferrence, G. M.; Lash, T. D. *Inorg. Chem.* **2002**, *41*, 4840–4842.
- (62) Furuta, H.; Ogawa, T.; Uwatoko, Y.; Araki, K. *Inorg. Chem.* **1999**, *38*, 2676–2682.
- (63) Maeda, H.; Osuka, A.; Ishikawa, Y.; Aritome, I.; Hisaeda, Y.; Furuta, H. *Org. Lett.* **2003**, *5*, 1293–1296.
- (64) Van Veldhuizen, J. J.; Campbell, J. E.; Giudici, R. E.; Hoveyda, A. H. *J. Am. Chem. Soc.* **2005**, *127*, 6877–6882.
- (65) Kirschenbaum, L. J.; Ambrus, J. H.; Atkinson, G. *Inorg. Chem.* **1973**, *12*, 2832–2837.
- (66) Pitts, C. R.; Bloom, S.; Woltornist, R.; Auvenshine, D. J.; Ryzhkov, L. R.; Siegler, M. A.; Lectka, T. *J. Am. Chem. Soc.* **2014**, *136*, 9780–9791.
- (67) Pitts, C. R.; Ling, B.; Woltornist, R.; Liu, R.; Lectka, T. *J. Org. Chem.* **2014**, *79*, 8895–8899.
- (68) Kee, C. W.; Chin, K. F.; Wong, M. W.; Tan, C.-H. *Chem. Commun.* **2014**, *50*, 8211–8214.
- (69) Austin, P. C. *J. Chem. Soc., Trans.* **1911**, *99*, 262–266.

(70) Anderson, J. M.; Kochi, J. K. *J. Org. Chem.* **1970**, *35*, 986–989.

5. Development and Mechanistic Study of Silver-Catalyzed Decarboxylative Fluorination Using a Sterically Hindered N-Containing Ligand in Non-Aqueous Media

5.1 Background and Significance

5.1.1 Silver-ligand complexes

High-valent complexes of silver tend to be unstable due to the powerful oxidizing nature of these compounds in solution.¹ As a result, the Ag(II) and Ag(III) oxidation states are often strongly stabilized by coordination with organic ligands, in particular nitrogen-containing heterocyclic amines, such as pyridines, phenanthrolines, and numerous other macrocycles. These ligands can normally exhibit a coordination number of two or four, as shown in the examples below (py = pyridine; bipy = 2,2'-bipyridine; phen = 1,10-phenanthroline).



Bonchev and Aleksiev have reported a number of examples of silver-persulfate oxidation of sulfanilic acid for the determination of silver.²⁻⁴ They have reported the use of 2,2'-bipyridine (bipy) and ethylenediamine (en) as activators of the reaction. They proposed that the activation of the reactions can be accounted for by the formation of complexes of the amines with the catalyst. In addition, the activating effect is linked with a lowering of the redox potential of the Ag(II)/Ag(I) system.⁴ For example, the redox potential for $\text{Ag(bipy)}_2^{2+}/\text{Ag(bipy)}_2^+$ has been reported to be 1.453 V and the $\text{Ag(phen)}_2^{2+}/\text{Ag(phen)}_2^+$ potential has been reported to be 65 mV less than

$\text{Ag}(\text{bipy})_2^{2+}/\text{Ag}(\text{bipy})_2^+$,¹ while the redox couple of $\text{Ag}(\text{II})/\text{Ag}(\text{I})$ is 1.98 V.⁵ Bonchev and Aleksiev found that the following activating effect of ligands was observed for the oxidation of Ag-ligand by persulfate:⁴



This correlation suggests that the greatest activating effect was put forth by bipy and phen, which are bidentate ligands with a high degree of conjugation. Monodentate ligands, such as pyridines, showed a smaller activating effect than bidentate ones.

Wilkins and coworkers examined the kinetics of complex formation between several transition metals with 1,10-phenanthroline and 2,2'-bipyridine.⁶ In the case of $\text{Ag}(\text{phen})_2$, they found that the coordination of the first phen to $\text{Ag}(\text{I})$ occurred at a rate greater than $5 \times 10^6 \text{ M}^{-1} \text{ sec}^{-1}$. The coordination of the second phenanthroline to form $\text{Ag}(\text{phen})_2^+$, however, could not be measured due its near diffusion-controlled rate constant.

While most ligands typically form 2:1 or 4:1 complexes with silver, a number of sterically hindered diimine complexes, such as 2,2-dimethyl-1,10-phenanthroline (dmp), are known to form 1:1 complexes (Figure 5.1).⁷ Due to the of presence methyl substituents on the ligands, bis-chelate coordination is prevented on the metal center. In addition, the mono-dmp complexes are generally characterized by low solubility in almost all solvents.⁷

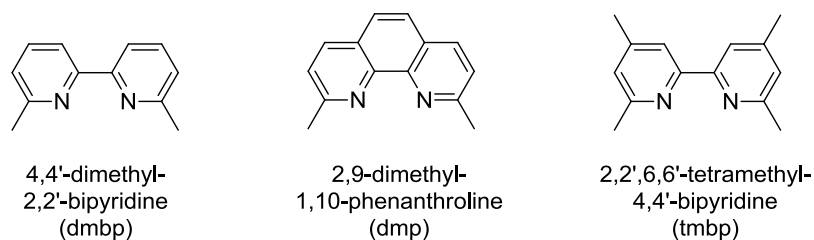
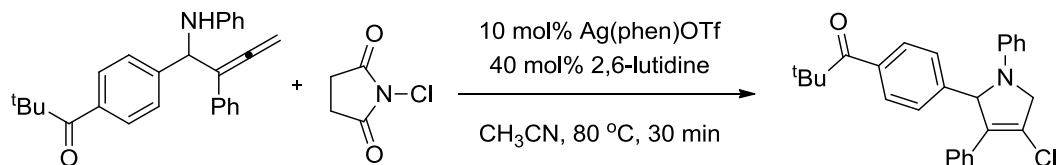


Figure 5.1. Examples of sterically hindered diimine ligands

Rajasekharan and coworkers examined Ag(II) complexes of these hindered N-heterocyclic ligands, in particular with dmbp and dmp.⁸ Unlike $\text{Ag}(\text{bipy})_2^{2+}$, which is stable to reduction in aqueous solution, the Ag(II) complexes formed with dmbp and dmp are unstable even in strong nitric acid solution, implying a redox potential in the range of 1.7-2.0 V. They later reported the first x-ray crystal structure of $\text{Ag}(\text{dmp})\text{NO}_3$, in which they found the structure existing as two complex molecules: a mononuclear $\text{Ag}(\text{dmp})\text{NO}_3$ and a NO_3 bridged dinuclear cation $[\text{Ag}_2(\text{dmp})_2\text{NO}_3]^{2+}$.⁹

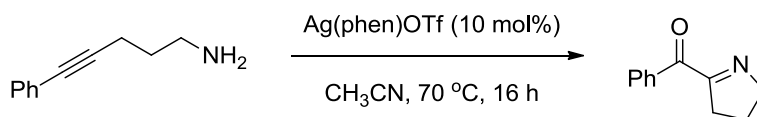
5.1.2 Silver-ligand-catalyzed reactions

A number of silver catalyzed reactions in recent literature utilize various nitrogen-containing ligands to perform a variety of chemistries. Matsubara and coworkers found that a 1,10-phenanthroline-ligated cationic silver complex allowed for the intramolecular chloroamination of allenes with N-chlorosuccinimide using 2,6-lutidine as a base (Scheme 5.1).¹⁰ The process proceeds under mild conditions and can tolerate a variety of functionalities such as keto, ester, cyano, halogen, acetal, and silyl ether groups. They also showed that the chloroamination products are synthetically useful intermediates that can be easily transformed into functionalized 3-pyrroline and pyrrole derivatives.



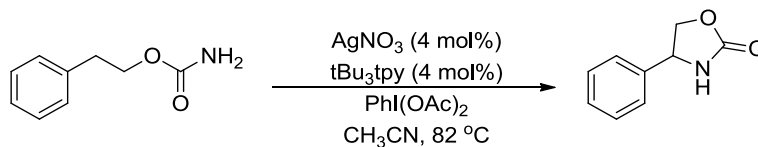
Scheme 5.1. Silver-catalyzed intramolecular chloroamination of allenes

Helquist and coworkers reported an intramolecular hydroamination of aminoalkynes catalyzed by silver-phenanthroline complexes (Scheme 5.2).¹¹ The use of Ag(phen)OTf compared to AgOTf in the absence of ligand dramatically increased the yield of intramolecular hydroaminated product.



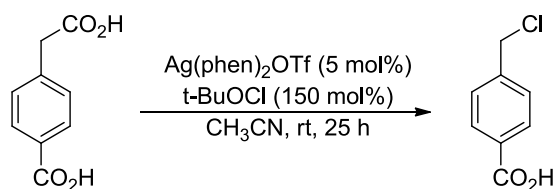
Scheme 5.2. Intramolecular hydroamination of aminoalkynes with silver-phenanthroline

The He group reported an efficient amidation reaction of saturated C-H bonds catalyzed by a disilver complex (Scheme 5.3).¹² When testing a number of ligands, they found that high yield in the absence of side products was obtained only when utilizing *t*Bu₃tpy.



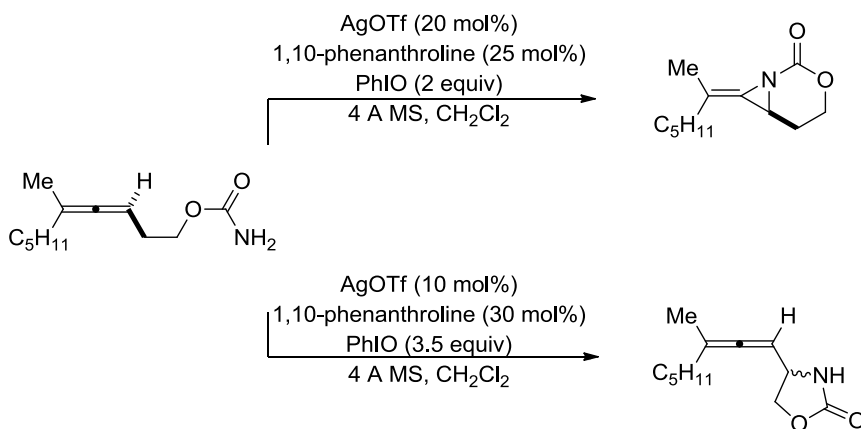
Scheme 5.3. Silver-catalyzed intramolecular amidation of saturated C-H bonds

The Li group reported a catalytic Hunsdiecker reaction of aliphatic carboxylic acids using Ag(phen)₂OTf and *t*-butyl hypochlorite, producing chlorodecarboxylation products in high yields under mild conditions (Scheme 5.4).¹³



Scheme 5.4. Silver-catalyzed decarboxylative chlorination of aliphatic carboxylic acids

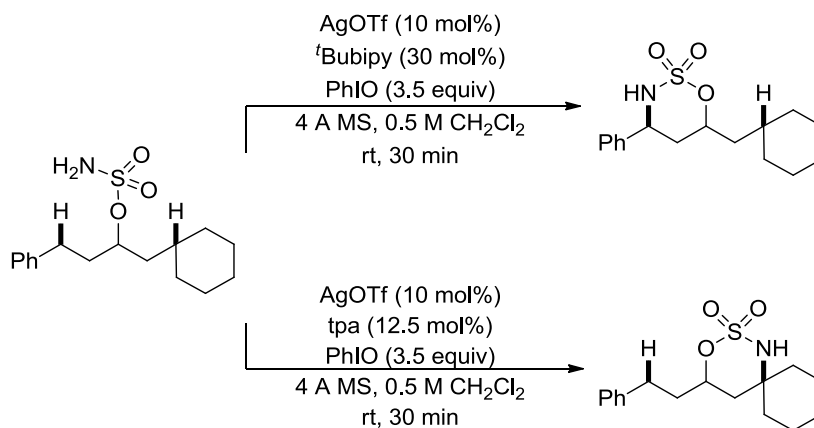
In 2013, the Schomaker group reported a silver-catalyzed chemoselective amination reaction using 1,10-phenanthroline to promote either aziridination or C-H insertion, depending on the coordination geometry of the active catalysts (Scheme 5.5).¹⁴ When using homoallenic carbamates, a 1:1.25 ratio of AgOTf:phen favored aziridination, while a 1:3 ratio yielded mainly C-H insertion (Scheme 5.5). This change in chemoselectivity is attributed to the dramatic steric differences in the coordination geometries of Ag(phen)OTf compared to Ag(phen)₂OTf.



Scheme 5.5. Tunable, chemoselective amination via silver-ligand catalysis

This work was recently followed up by the same group, in a silver-catalyzed C-H amination which was found to be ligand-controlled and tunable.¹⁵ They found that steric effects of a substrate influence the selectivity of (tpa)AgOTf (tpa, tris(2-

pyridylmethyl)amine) to a greater extent than (^tBubipy)₂AgOTf, which promotes reaction at the most electron-rich C-H bond (Scheme 5.6).



Scheme 5.6. Ligand-controlled, tunable silver-catalyzed C-H amination

5.2 Experimental

5.2.1 Materials

AgNO₃, AgOTf, Selectfluor, 2,2-dimethylglutaric acid, 2,2-dimethylbutyric acid, and 2,9-dimethyl-1,10-phenanthroline hemihydrate (dmp) were purchased from Alfa Aesar. Sodium persulfate was purchased from Sigma-Aldrich. All chemicals were used without further purification. Reagent grade acetonitrile was used.

5.2.2 Instrumentation

Proton, carbon, and fluorine NMR were recorded on a Bruker 500 MHz spectrometer. GC-MS analyses were done with an HP 5890 Series II Gas Chromatograph with an HP Mass Selector Detector. GC analyzes were done using a Shimadzu Gas Chromatograph GC-14B. Column chromatography was performed using the automated

CombiFlash® Rf system from Teledyne Isco, Inc. Products were separated using prepacked silica gel columns with a gradient elution of ethyl acetate and hexanes.

5.2.3 Methods

5.2.3.1 Procedure for synthesis of alkyl fluorides in acetonitrile

The decarboxylative fluorination reaction was performed using dry and degassed MeCN. In a vial equipped with a magnetic stir bar was added carboxylic acid (1 mmol), Selectfluor (708 mg, 2 mmol), silver salt (0.2 mmol), and dmp (43.5 mg, 0.2 mmol). MeCN (10 mL) added and the mixture was allowed to react overnight. Reaction mixture was extracted thrice with dichloromethane. The organic layer was dried with magnesium sulfate and concentrated. Column chromatography was performed to obtain fluorinated product.

5.2.3.2 Procedure for kinetic studies

For kinetic studies, the concentration of reagents was kept at synthetically relevant conditions. In an NMR tube, carboxylic acid, Selectfluor, silver salt, and dmp were combined. To the tube was added 1 mL MeCN and α,α,α -trifluoromethyltoluene (10 μ L, internal standard). The tube was shaken and inserted into the NMR. Reactions were monitored *in situ* by ^{19}F NMR on a Bruker 500 NMR (470 MHz) spectrometer. All reactions were performed at 23 °C. Peak integrations were analyzed using MestReNova software. Concentrations at each time point were determined with respect to the internal standard. Concentration (M) vs. time (sec) plots were generated based on these data and fit to the best exponential fit. The rate of each time point was found by calculating the

derivative of the trendline. To normalize rate plots, plots of $\text{rate}/[\text{substrate}]^n$ were determined, in which n is the order of the substrate.

5.2.3.3 Procedure for crystallization of silver-ligand complexes

To a round bottom flask was added AgNO_3 (170 mg, 1 mmol) and 2,9-dimethyl-1,10-phenanthroline hemihydrate (217 mg, 1 mmol). The contents were dissolved in acetonitrile (2 mL). Slow evaporation in open air over the course of days was allowed for crystal formation. The same procedure was used to obtain crystals using AgOTf (256 mg, 1 mmol).

5.2.3.4 Procedure for silver-ligand NMR studies

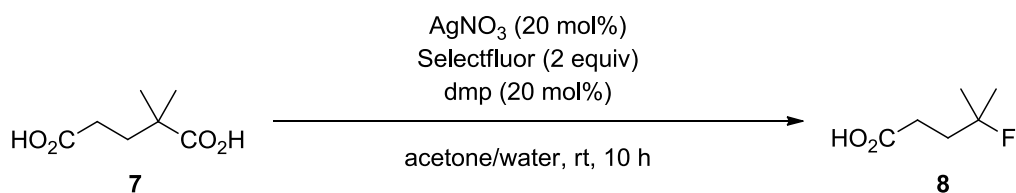
A ^1H NMR spectrum was obtained for 2,9-dimethyl-1,10-phenanthroline hemihydrate (21.7 mg, 0.1 mmol) in MeCN-d_3 . Silver salt was added (1 equiv), shaken, and another ^1H NMR spectrum was obtained.

5.3 Results

5.3.1 Decarboxylative fluorination using ligand in acetone/water

Based on the results presented in Chapter 4 on the mechanism of decarboxylative fluorination, as well as the rich literature on silver-ligand catalysis, the addition of N-containing ligands was investigated in the acetone/water system, which was described in Chapter 4. In the original report on the decarboxylative fluorination reaction, Li and coworkers reported that the reaction was unsuccessful using $\text{Ag}(\text{Phen})_2\text{OTf}$ salt as catalyst.¹⁶ Based on this finding, 2,9-dimethyl-1,10-phenanthroline hemihydrate (dmp) was used as a ligand in this reaction since this compound is known to bind in a 1:1 fashion with silver.^{7,8} Kinetics were performed on the reaction of 2,2-dimethylglutaric

acid in the presence of 2,9-dimethyl-1,10-phenanthroline hemihydrate (dmp) (Scheme 5.7).



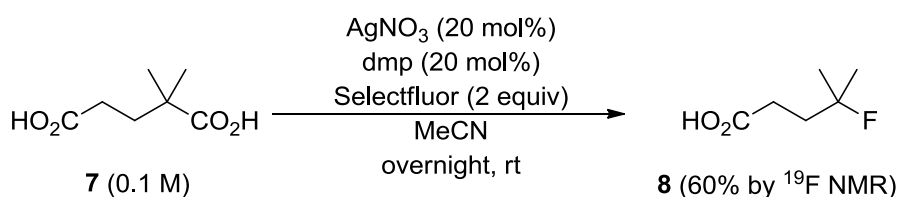
Scheme 5.7. Decarboxylative fluorination of **7** with dmp as ligand in acetone/water

In the absence of the ligand, this reaction goes to completion in approximately 2 hours, as shown in Chapter 4. However, upon addition of the ligand, the reaction takes approximately 10 hours to go to completion. When the loading of only silver nitrate was increased, the rate of the reaction increased. If the active catalyst in this reaction was the silver-ligand complex, the rate of the reaction should not increase upon increase of silver nitrate, but should only increase upon increasing both the loading of silver nitrate and ligand simultaneously. In addition, doubling of the ligand concentration resulted in a slight decrease in the reaction rate, suggesting that the ligand is not contributing to the mechanism of the fluorination reaction in acetone/water, and that addition of a ligand to the reaction is detrimental to reaction success. It is hypothesized that open coordination of the silver catalyst is crucial for reaction success in the acetone/water system.

5.3.2 Optimization of Reaction Conditions in Non-Aqueous Media

In the original report on the decarboxylative fluorination reaction, Li and coworkers reported the necessity for water as a cosolvent in the reaction.¹⁶ Decarboxylative fluorination was not successful in organic solvent alone. This feature was investigated and presented in Chapter 4, in which it was proposed that water was not

required as a cosolvent, but only necessary for solubilizing Selectfluor. Based on these findings, as well as the understanding of the mechanism of decarboxylative fluorination presented in Chapter 4, an attempt was made to perform the fluorination of **7** in the absence of water as a solvent. To do this, we attempted to use nitrogen-containing ligands, due to their activating effect in the Ag(II)/Ag(I) redox couple.⁴ Various solvents were screened, including MeCN, MeOH, EtOAc, DCM, and MeOH/H₂O, yielding no product in the absence of ligands. In addition, various ligands were added in order to stabilize the silver catalyst, including 1,10-dimethylphenanthroline, 2-amino-4-methylpyridine, and 2,9-dimethyl-1,10-phenanthroline hemihydrate (dmp). Of the solvents and ligands screened, the reaction was successful in MeCN with the addition of 20 mol% dmp, yielding **8** in 60% yield (Scheme 5.8). These results imply that the coordination number of ligand to silver is critical for reaction success. When using ligands that occupy all the coordination sites of silver, such as pyridine and phenanthroline, the reaction does not proceed. However, when using a sterically-hindered ligand that binds in a 1:1 fashion with silver, such as dmp, which leaves open coordination sites, the reaction is successful.



Scheme 5.8. Decarboxylative fluorination of **7** with dmp as ligand in MeCN

In order to further optimize the yield, various silver salts were used as catalysts. The best yield of **8** was obtained when using AgOTf at the catalyst (Table 5.1), likely due

to the increased solubility of the silver salt in MeCN compared to AgNO₃. The use of 20 mol% AgOTf instead of AgNO₃, in addition to 20 mol% dmp yielded fluorinated product in 73% yield by ¹⁹F NMR. The reaction was also successful using 2,2-dimethylphenylpropanoic acid and 2,2-dimethylbutyric acid (Table 5.2).

Table 5.1. Yield of fluorinated product **8** with different silver salts

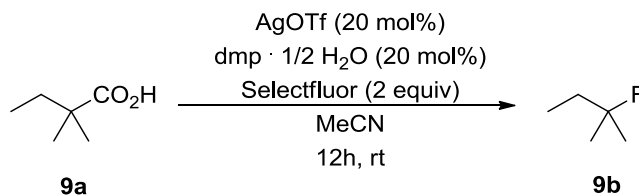
Silver Salt (0.1 M reaction and 20 mol% silver loading except where indicated)	% Yield of 8 (by ¹⁹ F NMR)
AgNO ₃	60.3
AgOTf	73.7
AgOAc	68.4
AgF	30.1
AgSbF ₆	61.9
AgOTf (10 mol%)	45.6
AgOTf (anhydrous dmp)	63.5
AgOTf (0.2 M reaction)	71.6

Table 5.2. Decarboxylative fluorination of other carboxylic acids using AgOTf and dmp in MeCN

R-COOH	Yield (¹⁹ F NMR)
7	73%
9a	85%
10a	53%

5.3.3 Mechanistic study of AgOTf-dmp catalyzed reaction

When using 2,2-dimethylbutyric acid (**9a**), the fluorinated product **9b** was generated in 85% yield. Based on these studies, this substrate was chosen for further mechanistic investigation in order to determine the impact the addition of nitrogen-containing ligand in non-aqueous media has on the reaction mechanism of decarboxylative fluorination (Scheme 5.9).



Scheme 5.9. Decarboxylative fluorination of **9a** using dmp as ligand and AgOTf as catalyst in MeCN

5.3.3.1 NMR Studies of AgOTf-dmp

In order to first determine the interaction between AgOTf and dmp, ¹H NMR studies were performed on the complex in MeCN-d₃. When AgOTf is added to dmp, a downfield shift is observed in the protons of dmp, suggesting coordination of the ligand to the metal (Figure 5.2), consistent with a decrease in electron density (deshielding) of dmp, i.e. the donation of electrons from nitrogen to Ag (Table 5.3). Furthermore, addition of one equivalent of Selectfluor to the AgOTf-dmp reaction mixture resulted in line broadening of the peaks in the proton NMR, suggestive of a paramagnetic (Ag²⁺, d⁹) complex (Figure 5.3).

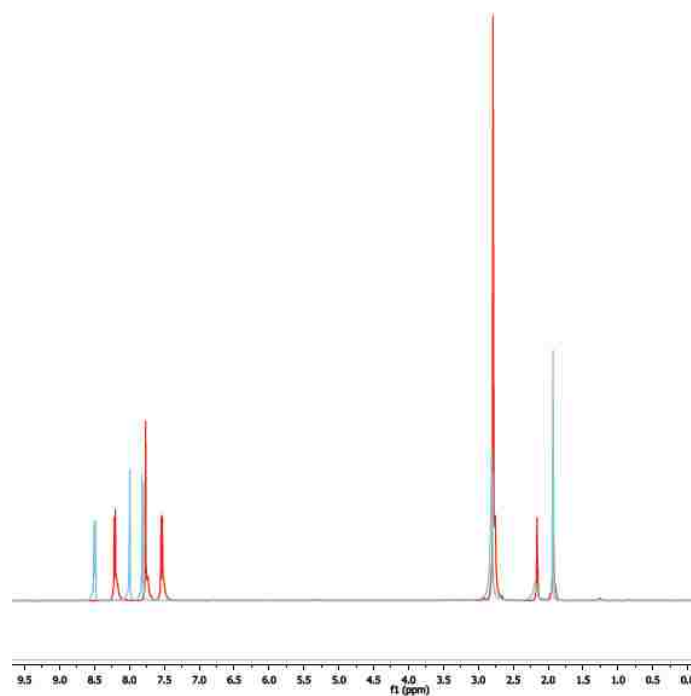


Figure 5.2. ^1H NMR spectra showing downfield shifts in dmp upon addition of AgOTf

Table 5.3. ^1H NMR shifts of dmp with AgOTf

	$\Delta 1$ (ppm)	$\Delta 2$ (ppm)	$\Delta 3$ (ppm)	$\Delta 4$ (ppm)	$\Delta 5$ (ppm)
dmp	8.21	7.77	7.54	2.77	2.16
dmp + AgOTf	8.50	8.00	7.81	2.81	2.19

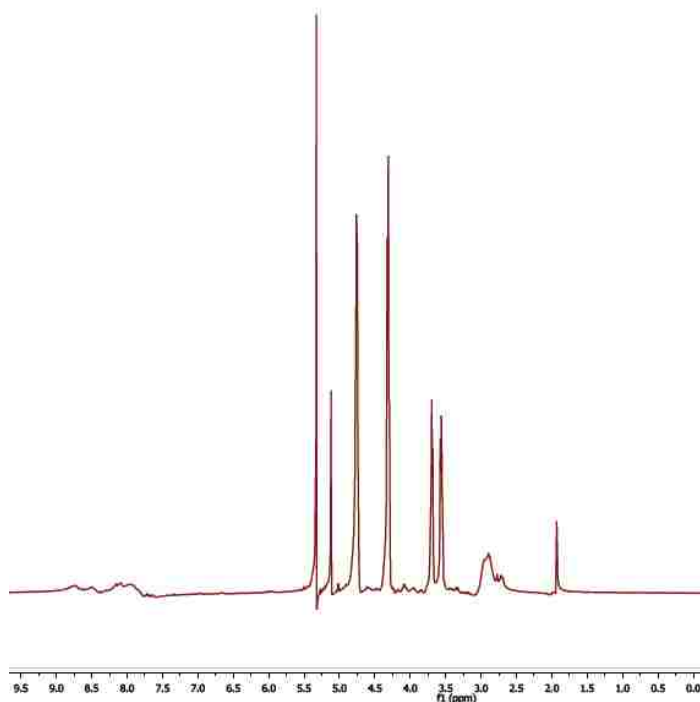


Figure 5.3. ^1H NMR spectra showing paramagnetism upon addition of Selectfluor to AgOTf-dmp

5.3.3.2 Crystallization of AgOTf-dmp complex

Based on the NMR studies presented in Section 5.3.2.1, suggesting the coordination of dmp to AgOTf, an attempt was made to isolate the silver-ligand complex. Crystallization of the intermediate silver-ligand complex was done by stirring silver triflate and 2,9-dimethyl-1,10-phenanthroline (dmp) hemihydrate in acetonitrile for 5 minutes and allowing to crystallize by slow evaporation. The crystal structure of this complex shows the 1:1 coordination of silver and dmp, as well as coordination of one equivalent of acetonitrile to the metal center (Figure 5.4). The triflate anion is in the outer sphere.

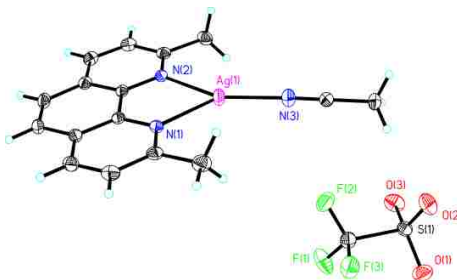


Figure 5.4. Crystal structure of AgOTf-dmp complex

5.3.3.3 Catalyst stability studies of AgOTf-dmp catalyzed reaction

A thorough kinetic study of this reaction system was performed in order to determine the effect that the addition of a nitrogen containing ligand has on the mechanism of decarboxylative fluorination. All kinetic studies were performed under synthetically relevant conditions by ^{19}F NMR, as described in Chapter 4.

When the concentration of only AgOTf was increased, there was no change in rate observed. However, when the concentration of AgOTf-dmp was increased, an increase in rate was observed. This result, coupled with the results found by Wilkins (Section 5.1.1),⁶ suggest that the active catalyst in this reaction is AgOTf-dmp, and that by the time the reaction progress begins to be monitored, the AgOTf-dmp complex has already formed.

Catalyst stability studies were performed for the AgOTf-dmp complex. The reaction was first monitored under the conditions shown in Table 5.4, Run 1. Next, a reaction was performed at the 50% point of that shown in Run 1 (Table 5.4, Run 2). If the concentration of catalyst was constant during the course of the reaction, the rates of both

Run 1 and 2 would be identical. However, when plotted together (Figure 5.5) and then time-adjusted (Figure 5.6), the rate profiles of Runs 1 and 2 do not show graphical overlay, suggesting catalyst deactivation in the system.

Table 5.4. Reaction conditions for catalyst stability studies in fluorination reaction of **9a** with AgOTf and dmp

Run	[9a] (M)	[AgOTf-dmp] (M)	[Selectfluor] (M)
1 - 100	0.1	0.02	0.2
2	0.05	0.02	0.15

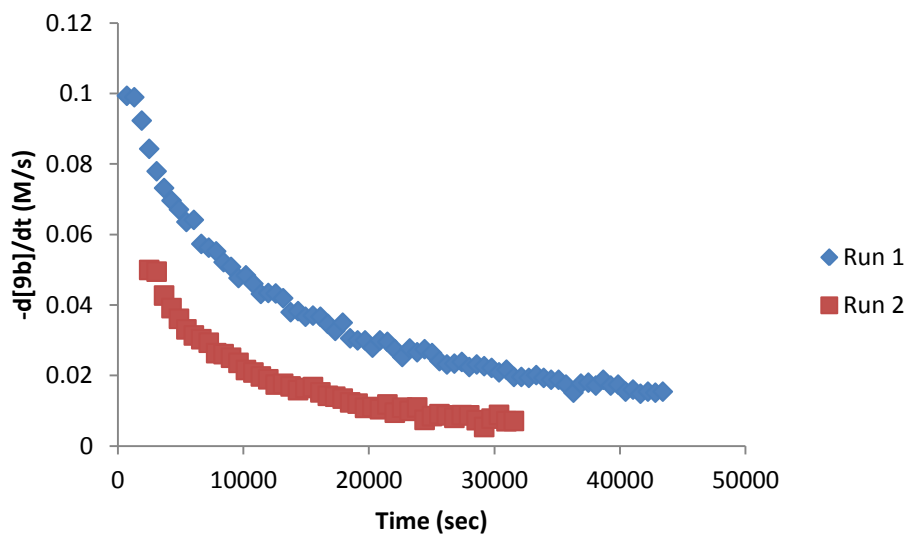


Figure 5.5. Plot of **[9b]** vs. time for Runs 1 and 2 for catalyst stability studies in AgOTf-dmp catalyzed decarboxylative fluorination

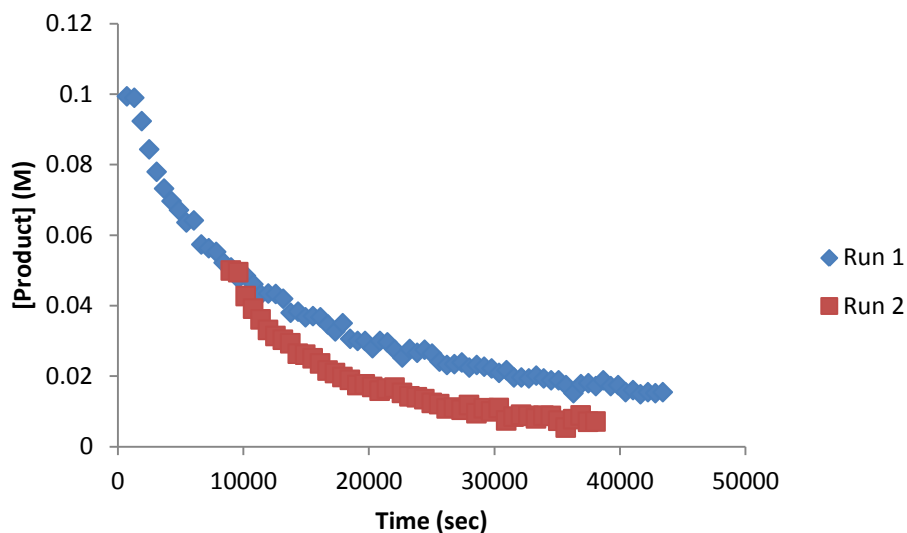


Figure 5.6. Time-adjusted profiles showing catalyst deactivation of Run 1 and 2 in AgOTf-dmp catalyzed decarboxylative fluorination

Catalyst stability studies suggest that AgOTf-dmp catalyst is deactivating in this non-aqueous system, unlike in the acetone-water system described in Chapter 4. It is hypothesized that the deactivation is occurring due to (1) the low solubility of Ag-dmp complexes in almost all solvents, and (2) the formation of silver-carboxylate during the course of the reaction. The limited solubility of these complexes in organic media causes precipitation during the course of the reaction, which is observed in these studies. In addition, higher loadings of silver led to more precipitate in the reactions.

5.3.3.4 Kinetic order studies of AgOTf-dmp catalyzed reaction

The kinetic order of each reaction component was found. To do so, the concentration of only one component was changed at a time to determine the effect of that component on the reaction. These studies were performed under the conditions listed in Table 5.5.

Table 5.5. Reaction conditions for kinetic order studies for fluorination of **9a** with AgOTf and dmp

Run	[9a] (M)	[AgOTf-dmp] (M)	[Selectfluor] (M)
1 - 100	0.1	0.02	0.2
3	0.1	0.04	0.2
4	0.1	0.02	0.15
5	0.07	0.02	0.2

To determine the kinetic order of AgOTf-dmp catalyst, the concentration was increased from 0.02 M (Table 5.5, Run 1) to 0.04 M (Table 5.5, Run 3), which resulted in a significant increase in reaction rate (Figure 5.7). When normalized, the order of AgOTf-dmp was found to be approximately 2 (Figure 5.8). The second order in catalyst is suggestive of a monomer-dimer equilibrium, in which the monomer is the resting state of the catalyst.¹⁷⁻²⁰ The structure of the silver dimer is unclear in this reaction, due to the inability to observe this intermediate by x-ray crystallography or LC-MS. Examples exist in the literature for dimers bonded through the metal center,²¹⁻²³ or connected by bridging ligands.^{9,24,25}

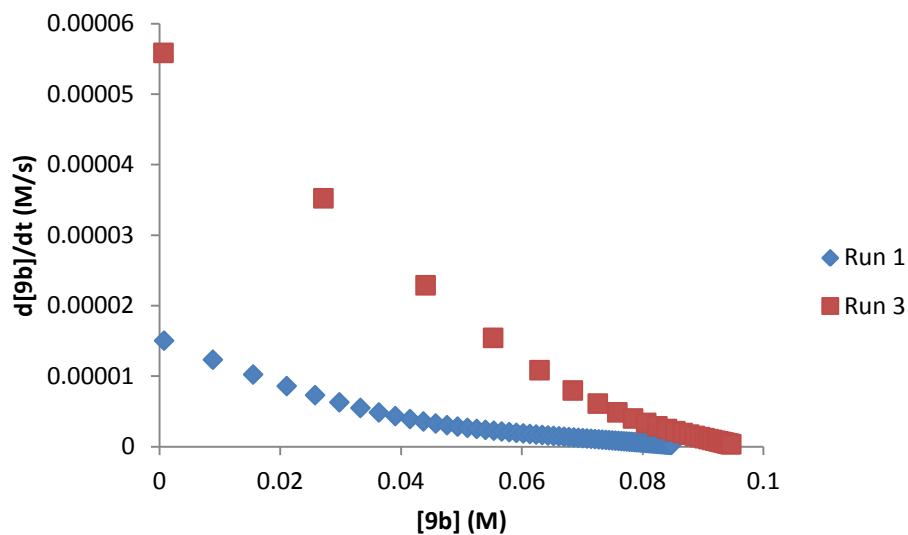


Figure 5.7. $-d[9b]/dt$ vs. $[9b]$ for order of Ag-dmp in AgOTf-dmp catalyzed decarboxylative fluorination

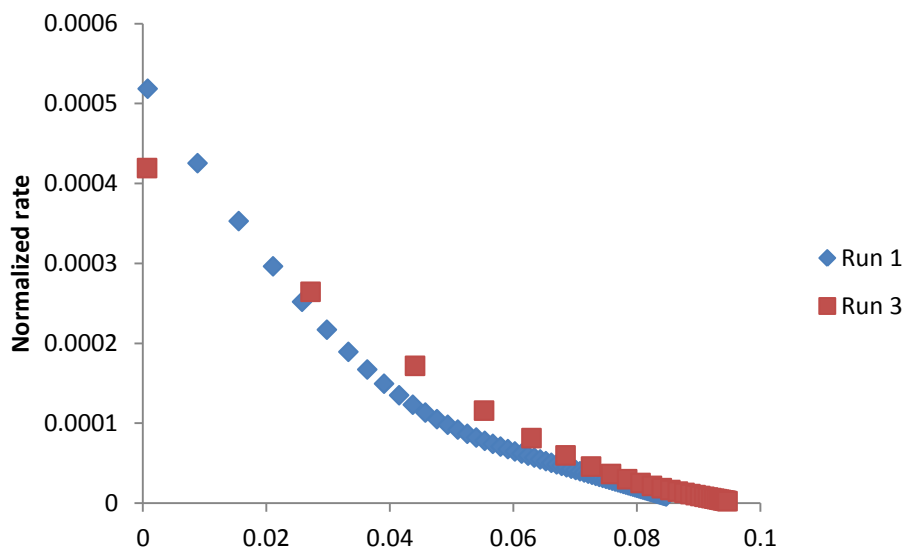


Figure 5.8. Normalized rate vs. $[9b]$ for order of Ag-dmp in AgOTf-dmp catalyzed decarboxylative fluorination

Next, the kinetic order of Selectfluor was determined by lowering the concentration from 0.15 M (Table 5.5, Run 4) to 0.11 M (Table 5.5, Run 5), which

resulted in a decrease in reaction rate (Figure 5.9). When normalized, the order of Selectfluor was determined to be approximately 1 (Figure 5.10). The first order in this component implies that Selectfluor is oxidizing the AgOTf-dmp complex, likely through a single electron transfer, similar to the reaction described in Chapter 4. A single electron transfer mechanism is also proposed for this reaction due to the line-broadening seen in the ^1H NMR spectrum of Selectfluor mixed with an equivalent of AgOTf-dmp in Section 5.3.3.1 (Figure 5.3).

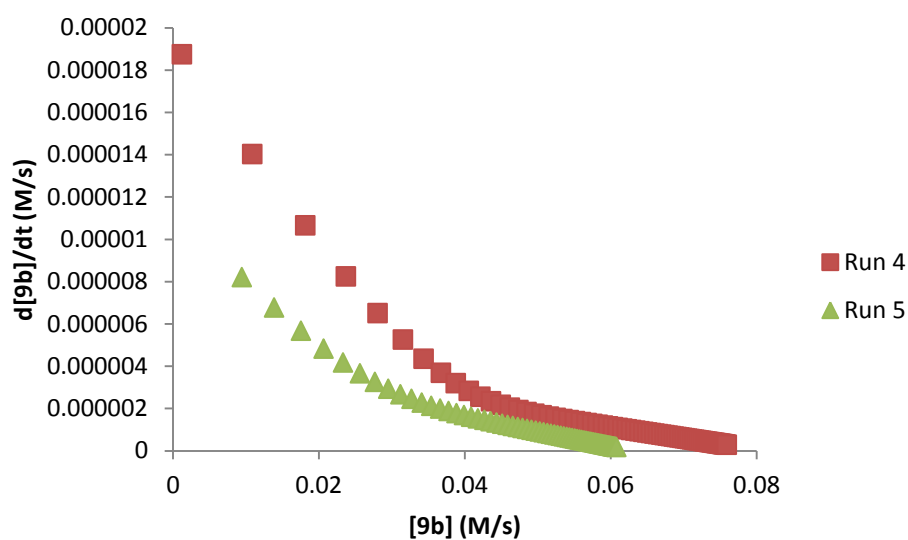


Figure 5.9. $-\text{d}[\mathbf{9b}]/\text{dt}$ vs. $[\mathbf{9b}]$ for order of Selectfluor in AgOTf-dmp catalyzed decarboxylative fluorination

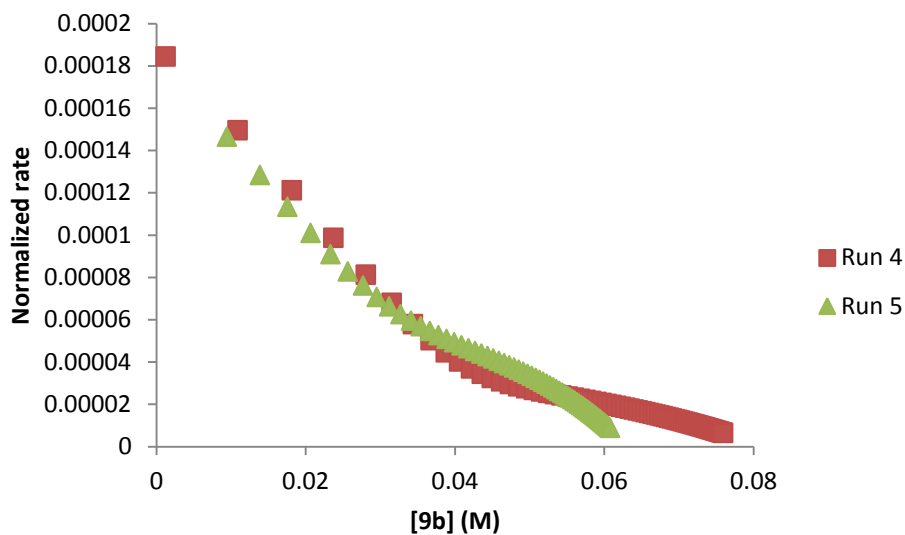


Figure 5.10. Normalized rate vs. [9b] for order of Selectfluor in AgOTf-dmp catalyzed decarboxylative fluorination

Finally, the kinetic order of **9a** was determined by decreasing the concentration from 0.1 M (Table 5.5, Run 1) to 0.07 M (Table 5.5, Run 5), resulting in an increase in reaction rate (Figure 5.11), suggestive of inverse order dependency on **9a**, similar to that found in Chapter 4. To determine the order of **9a**, the linear portion of the rate plots were plotted together and the slopes of each line were found, which are equivalent to rate (Figure 5.12). The order of **9a** was found to be approximately inverse second order.

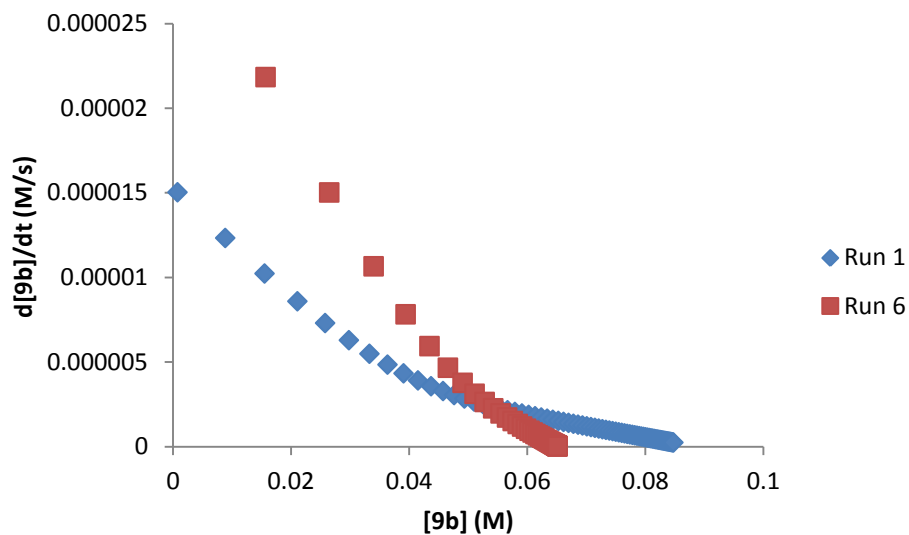


Figure 5.11. $-d[9b]/dt$ vs. $[9b]$ for order of **9b** in AgOTf-dmp catalyzed decarboxylative fluorination

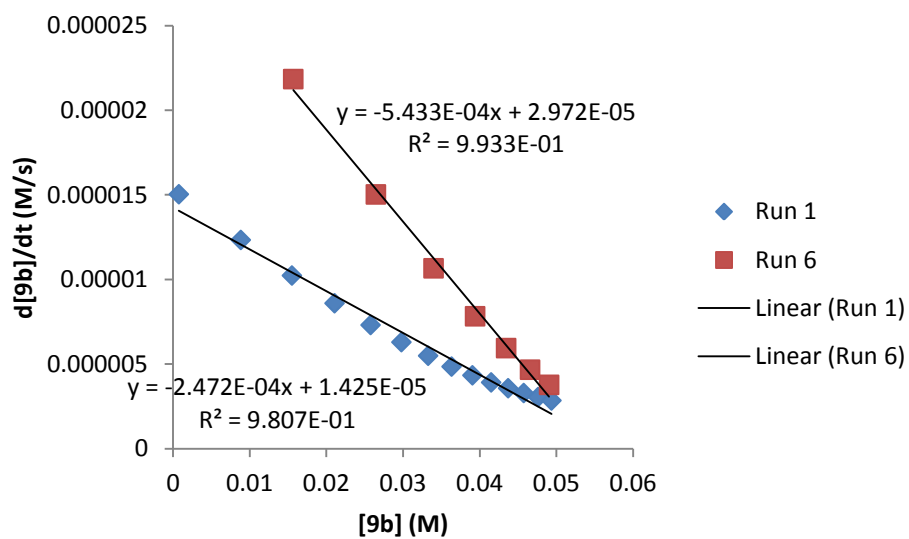


Figure 5.12. Line fits for order of **9b** in AgOTf-dmp catalyzed decarboxylative fluorination

The kinetic orders of each of the substrates were found to differ significantly from those of the aqueous system described in Chapter 4. The orders were determined to be second order in silver-dmp, first order in Selectfluor, and approximately inverse second order in **9a** (Table 5.6). The inverse order found for **9a** suggests that a silver-carboxylate is forming, in which a carboxylate is bound to both metal centers of the silver dimer. The second order found for silver-dmp suggests a monomer-dimer equilibrium, in which the resting state of the catalyst is the monomer. In addition, the first order found in Selectfluor suggests that one equivalent of the fluorinating reagent is needed to oxidize one of the metals of the silver-dimer through a single electron transfer.

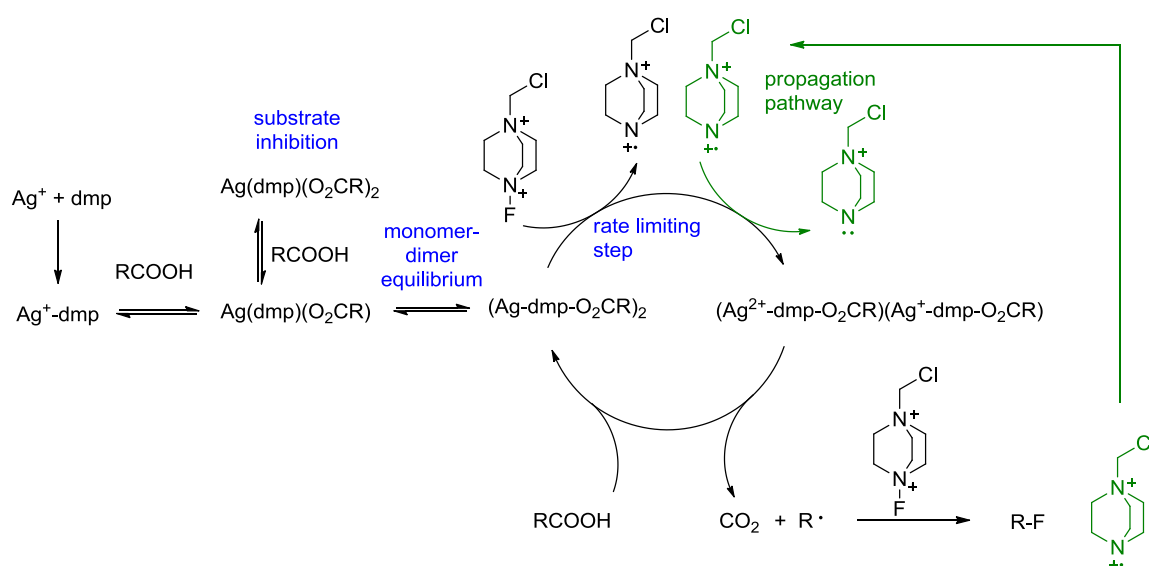
Table 5.6. Rate order for each component in fluorination of **9a** with AgOTf and dmp

9a	AgOTf-dmp	Selectfluor
-2.2	2	1.2

5.3.3.5 Proposed Mechanism of AgOTf-dmp catalyzed reaction

Based on the kinetic studies described above, it is proposed that the addition of a sterically-hindered nitrogen-containing ligand to the reaction in non-aqueous media changes the mechanism of decarboxylative fluorination. Whereas in the aqueous system it is proposed that Ag(I)-carboxylate is oxidized to a Ag(II) intermediate, in the non-aqueous system the mechanism involves the formation of a Ag(I) dimer, which is then oxidized by an equivalent of Selectfluor through single electron transfer to generate a Ag(I)-Ag(II) dimer in the rate limiting step of this reaction (Scheme 5.10). Based on these studies, coupled with those described in Chapter 4, it is proposed that the carboxylic

acid is then oxidized by the mixed-valent dimer to generate an alkyl radical, which can abstract a fluorine atom from another equivalent of Selectfluor. The radical cation produced from the loss of fluorine from Selectfluor then acts as a terminal oxidant to regenerate additional Ag(I)-Ag(II) to continue the catalytic cycle. Similar to the decarboxylative fluorination reaction performed in acetone/water described in Chapter 4, there is substrate inhibition in carboxylic acid, which is proposed to occur due to the formation of a $\text{Ag}(\text{carboxylate})_2$ intermediate.



Scheme 5.10. Proposed catalytic cycle for decarboxylative fluorination reaction of aliphatic acids in non-aqueous media using N-containing ligand

5.3.4 Mechanistic study of AgNO_3 -dmp catalyzed reaction

In addition to AgOTf-dmp , AgNO_3 -dmp is an effective catalyst in the decarboxylative fluorination reaction. Based on this finding, a mechanistic study was performed on the reaction catalyzed by AgNO_3 -dmp (Scheme 5.11).



Scheme 5.11. Decarboxylative fluorination of **9a** using dmp as ligand and AgNO_3 as catalyst

5.3.4.1 Crystallization of AgNO_3 -ligand complex

In addition to silver triflate, a crystal structure of the AgNO_3 -dmp complex was obtained. Crystallization of the intermediate silver-ligand complex was done by stirring silver nitrate and 2,9-dimethyl-1,10-phenanthroline hemihydrate in acetonitrile for 5 minutes and allowing to crystallize by slow evaporation. Unlike the AgOTf -dmp complex, the crystal structure of AgNO_3 -dmp showed the silver-ligand coordinated with the nitrate in two different forms, kappa-1 and kappa-3 (Figure 5.13). In this case, solvent was not bound to the metal center. Based on the difference in catalyst structure between AgOTf and AgNO_3 , an attempt was made to perform kinetic studies on the decarboxylative fluorination through the use of AgNO_3 -dmp catalyst (*vide infra*).

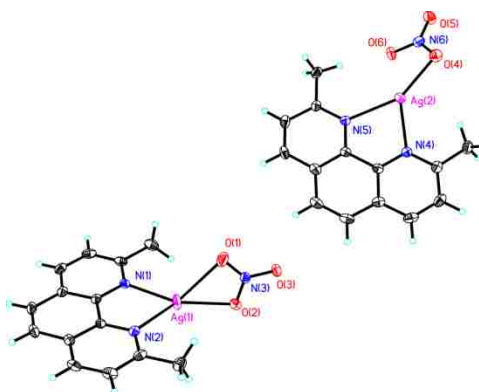


Figure 5.13. Crystal structure of AgNO_3 -dmp complex

5.3.4.2 NMR Studies of AgNO_3 -dmp complex

NMR studies on this interaction were also performed. The ^1H NMR spectrum show slight downfield shifts of the ligand upon addition of silver salt in MeCN-d_3 (Figure 5.14), similar to that seen for AgOTf -dmp in Section 5.3.2.1, suggesting coordination of dmp to the silver metal. The chemical shifts are described in Table 5.7.

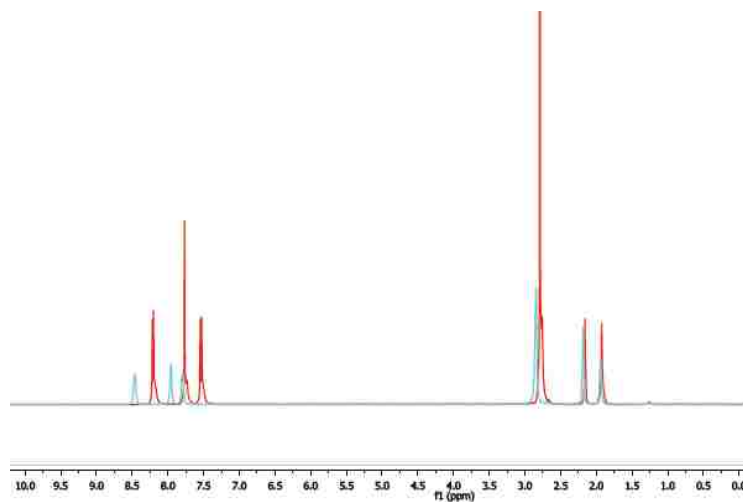


Figure 5.14. ^1H NMR spectra showing shifts in dmp upon addition of AgNO_3

Table 5.7. ^1H NMR shifts of dmp with AgNO_3

	$\Delta 1$ (ppm)	$\Delta 2$ (ppm)	$\Delta 3$ (ppm)	$\Delta 4$ (ppm)	$\Delta 5$ (ppm)
dmp	8.21	7.77	7.54	2.77	2.16
dmp + AgNO_3	8.46	7.96	7.80	2.85	2.18

5.3.4.3 Kinetic order studies of AgNO_3 -dmp catalyzed reaction

When attempting to perform kinetic studies on the AgNO_3 -dmp system, there was difficulty in obtaining reproducible data. This can be attributed to the inefficient nature of the catalyst and reaction, the lack of solubility of AgNO_3 -dmp in the reaction, as well as the significant catalyst deactivation of AgNO_3 -dmp. For these reasons, only the order of AgNO_3 -dmp could be investigated. When the concentration of AgNO_3 -dmp was increased from 0.02 M (Table 5.8, Run 7) to 0.04 M (Table 5.8, Run 8), the rate of the reaction increased (Figure 5.15), suggesting positive order rate dependency on the AgNO_3 -dmp catalyst. Based on this finding, a similar mechanism is proposed for the AgNO_3 -dmp system as for the AgOTf -dmp system.

Table 5.8. Reaction conditions for kinetic order studies for fluorination of **9a** with AgNO_3 -dmp

Run	[9a] (M)	[AgNO_3 -dmp] (M)	[Selectfluor] (M)
7 - 100	0.1	0.02	0.2
8	0.1	0.04	0.2

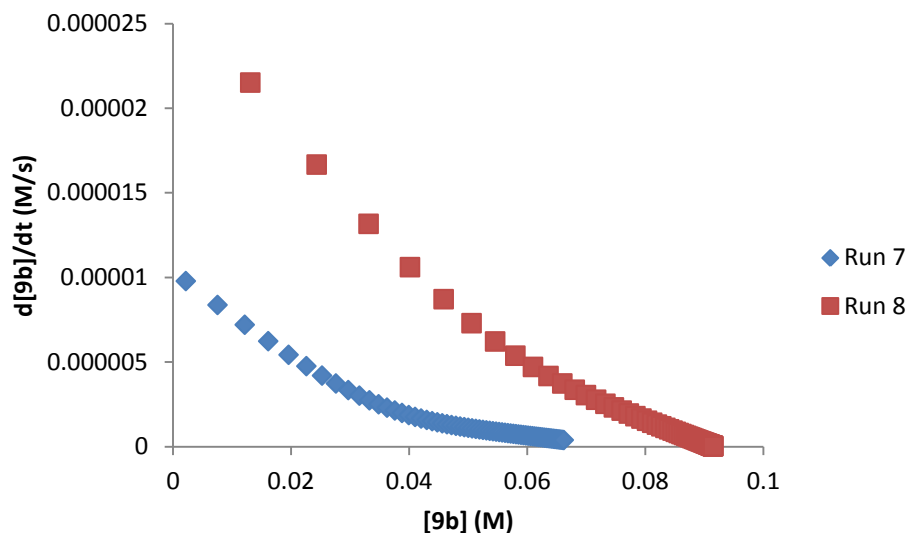
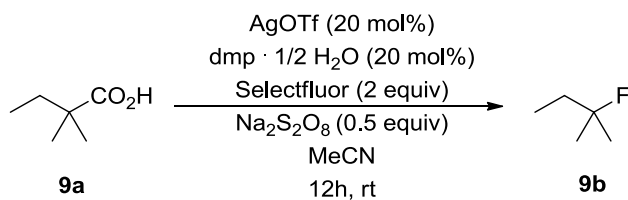


Figure 5.15. $-d[9b]/dt$ vs. $[9b]$ for order of Ag-dmp in AgNO_3 -dmp catalyzed decarboxylative fluorination

5.3.5 Mechanistic study of AgOTf-dmp catalyzed reaction with persulfate

Based on the studies using persulfate described in Chapter 4, an effort was made to investigate the reaction mechanism of the AgOTf-dmp catalyzed reaction in the presence of sodium persulfate as an additive (Scheme 5.12).



Scheme 5.12. Decarboxylative Fluorination Reaction of **9a** with AgOTf-dmp with persulfate

5.3.5.1 Kinetic order studies of AgOTf-dmp catalyzed reaction with persulfate

The kinetic order of each component in the reaction was found by varying the concentration of one component at a time to observe the effect on the reaction rate (Table 5.9).

Table 5.9. Reaction conditions for kinetic order studies for fluorination of **9a** with AgOTf and dmp in the presence of sodium persulfate

Run	[9a] (M)	[AgOTf-dmp] (M)	[Selectfluor] (M)	[Na ₂ S ₂ O ₈] (M)
9 - 100	0.1	0.02	0.2	0.05
10	0.1	0.04	0.2	0.05
11	0.1	0.05	0.2	0.05
12	0.1	0.04	0.13	0.05
13	0.07	0.02	0.2	0.05
14	0.1	0.02	0.2	0.03

When the concentration of AgOTf was increased from 0.4 M (Table 5.9, Run 10) to 0.5 M (Table 5.9, Run 11), the rate of the reaction increased (Figure 5.16). When normalized, the kinetic order of AgOTf-dmp was approximately 2 (Figure 5.17), indicating that even in the presence of persulfate, a monomer-dimer equilibrium of AgOTf-dmp is present in this reaction.

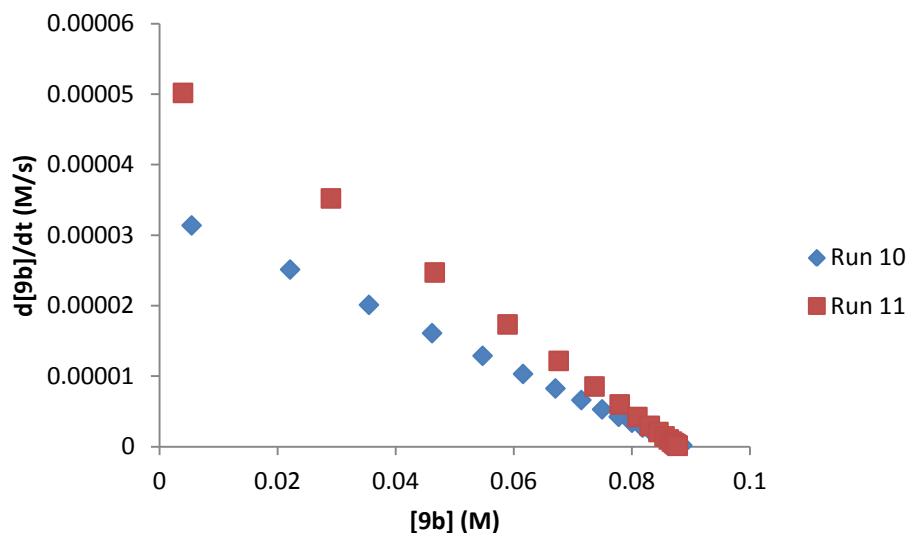


Figure 5.16. $-d[9b]/dt$ vs. $[9b]$ for order of Ag-dmp in AgOTf-dmp catalyzed decarboxylative fluorination with persulfate

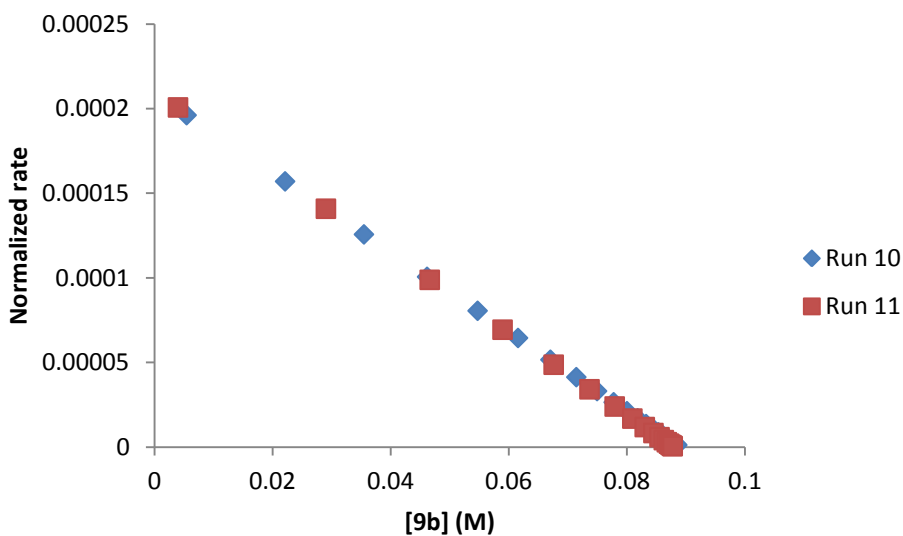


Figure 5.17. Normalized rate vs. $[9b]$ for order of Ag-dmp in AgOTf-dmp catalyzed decarboxylative fluorination with persulfate

Next, the order of Selectfluor was determined by decreasing the concentration from 0.2 M (Table 5.9, Run 10) to 0.13 M (Table 5.9, Run 12). The decrease in concentration did not have an effect on the rate of the reaction (Figure 5.18), indicating a

zero order rate dependence on Selectfluor, which is consistent with the decarboxylative fluorination reaction performed with sodium persulfate additive described in Chapter 4.

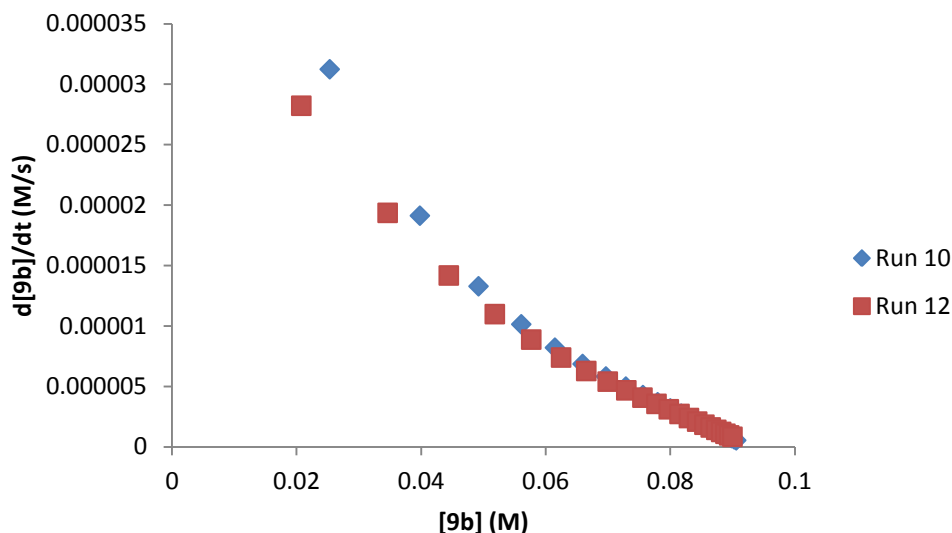


Figure 5.18. $-d[9b]/dt$ vs. $[9b]$ for order of Selectfluor in AgOTf-dmp catalyzed decarboxylative fluorination with persulfate

The order of **9b** was found by decreasing the concentration of carboxylic acid from 0.1 M (Table 5.9, Run 9) to 0.07 M (Table 5.9, Run 13) (Figure 5.19). When the linear portions of the rate plots were plotted together and fitted to straight lines (Figure 5.20), the rates of both Run 9 and 13 were found to be the same, suggesting zero order rate dependence on **9b**. This result suggests that in the presence of persulfate, the rate of oxidation of Ag(I)-Ag(I) is slower than the interaction between carboxylic acid and silver.

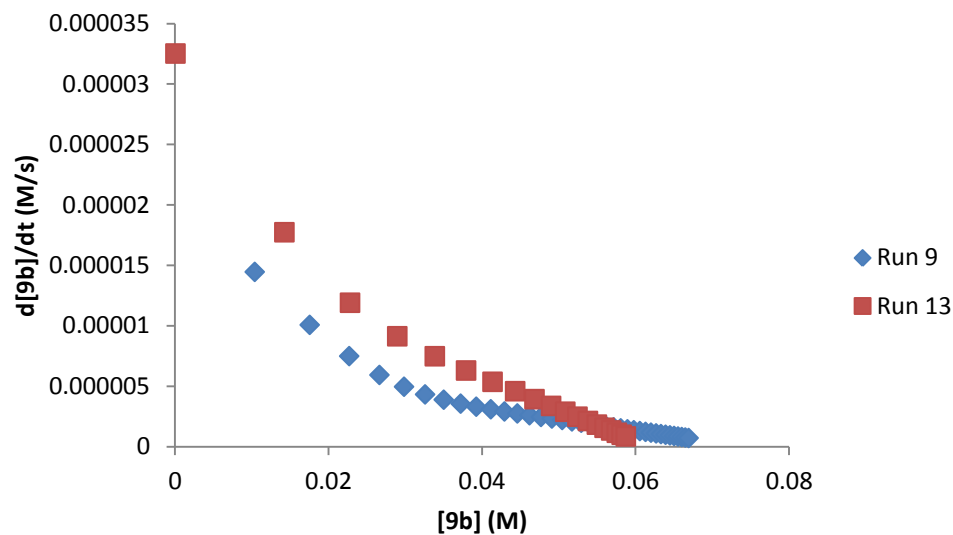


Figure 5.19. $-d[9b]/dt$ vs. $[9b]$ for order of **9b** in AgOTf-dmp catalyzed decarboxylative fluorination with persulfate

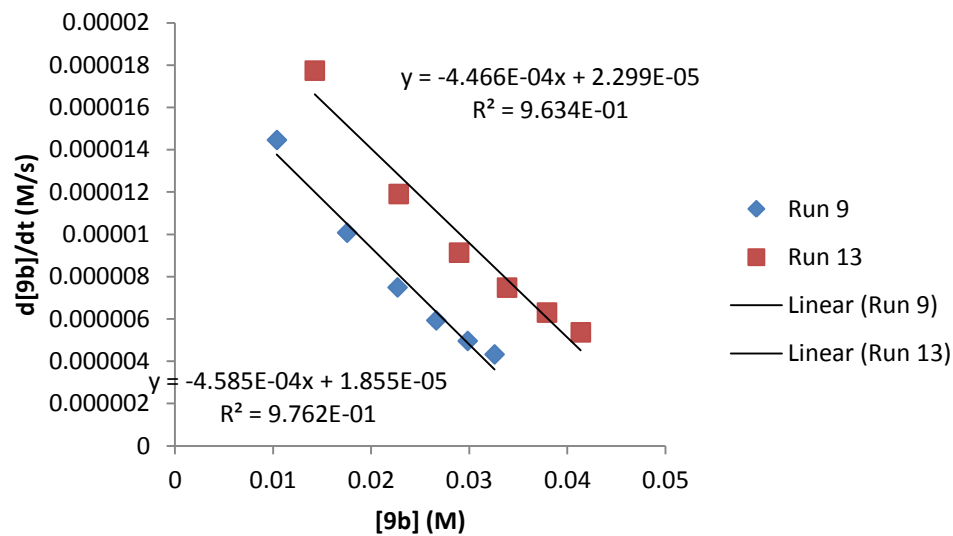


Figure 5.20. Line fits for order of **9b** in AgOTf-dmp catalyzed decarboxylative fluorination with persulfate

The order of persulfate was found by decreasing the concentration from 0.05 M (Table 5.9, Run 9) to 0.03 M (Run 14). This decrease in concentration did not have an

effect on the rate of the reaction (Figure 5.21), suggesting zero order rate dependency on persulfate. This result differs from that found for the reaction described in Chapter 4, in which Ag(I) and persulfate were both first order. In the present reaction, the order of sodium persulfate is likely due to the lack of solubility of the compound in MeCN.

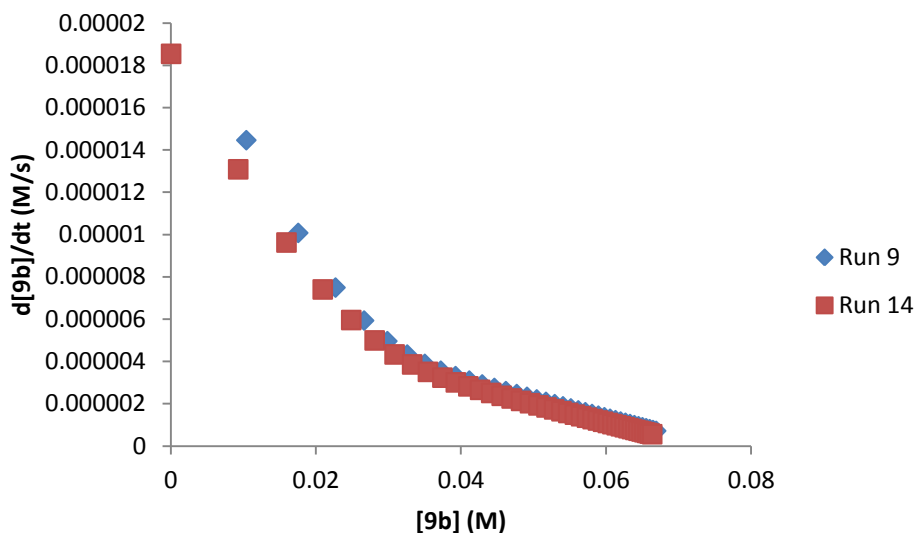


Figure 5.21. $-d[9b]/dt$ vs. $[9b]$ for order of $\text{Na}_2\text{S}_2\text{O}_8$ in AgOTf-dmp catalyzed decarboxylative fluorination

Due to the lack of solubility of sodium persulfate in the reaction medium, an attempt was made to add a slightly more organic soluble persulfate in the form of tetra-n-butyl ammonium persulfate ($(\text{TBA})_2\text{S}_2\text{O}_8$). When decreasing the concentration from 0.03 M (Table 5.10, Run 15) to 0.01 M (Table 5.10, Run 16), the rate of the reaction did not change (Figure 5.22). Even under these conditions, phase transfer of the persulfate affects the ability to observe the kinetic order.

Table 5.10. Reaction conditions for kinetic order studies for fluorination of **9a** with AgOTf and dmp in the presence of tera-n-butyl ammonium persulfate

Run	[9a] (M)	[AgOTf-dmp] (M)	[Selectfluor] (M)	[(TBA) ₂ S ₂ O ₈] (M)
15	0.1	0.02	0.2	0.03
16	0.1	0.02	0.2	0.01

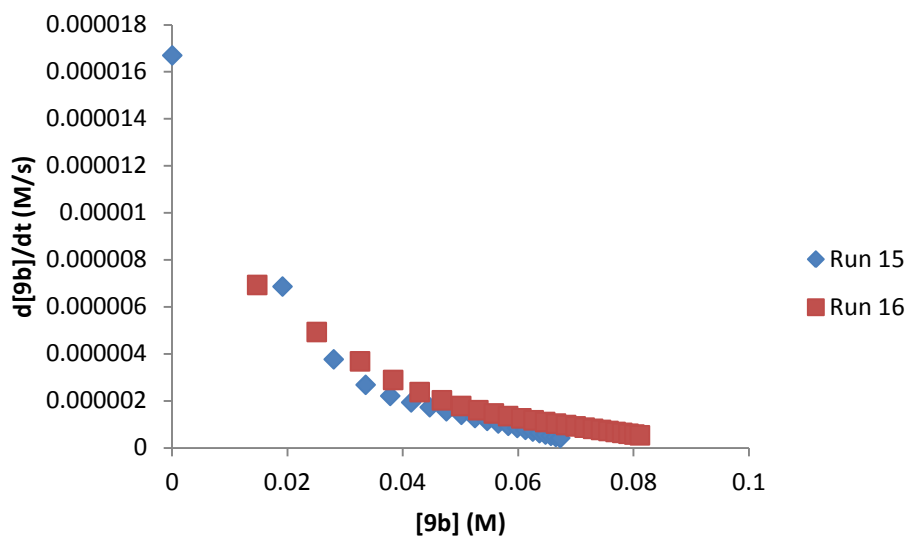


Figure 5.22. $-d[9b]/dt$ vs. $[9b]$ for order of (TBA)₂S₂O₈ in AgOTf-dmp catalyzed decarboxylative fluorination

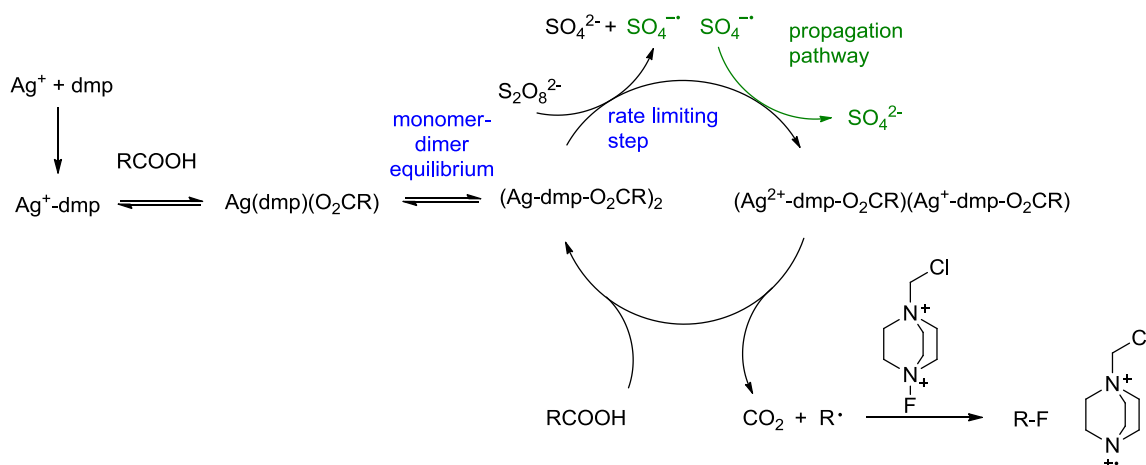
The rate order of each component of the AgOTf-dmp catalyzed reaction in the presence of persulfate are reported in Table 5.11.

Table 5.11. Rate order for each component in fluorination of **9a** using AgNO₃ and dmp in the presence of sodium persulfate

9a	AgOTf-dmp	Selectfluor	Na ₂ S ₂ O ₈
0	2	0	0*

5.3.5.2 Proposed mechanism of AgOTf-dmp catalyzed reaction with persulfate

Based on the kinetic studies described in this section, it is proposed that the addition of persulfate to the AgOTf-dmp catalyzed reaction in non-aqueous media further changes the mechanism of decarboxylative fluorination. A monomer-dimer equilibrium is proposed, in which the dimer is oxidized by an equivalent of persulfate through single electron transfer to generate a Ag(I)-Ag(II) dimer in the rate-limiting step of this reaction (Scheme 5.13). The carboxylic acid is then oxidized by the mixed-valent dimer to generate an alkyl radical, which can abstract a fluorine atom from another equivalent of Selectfluor. Either the radical cation produced from the loss of fluorine from Selectfluor, or sulfate radical anion, can function as a terminal oxidant to regenerate additional Ag(I)-Ag(II) to continue the catalytic cycle.



Scheme 5.13. Proposed catalytic cycle for decarboxylative fluorination reaction of aliphatic acids in non-aqueous media using N-containing ligand and persulfate

5.6 Conclusion

In this chapter, a decarboxylative fluorination reaction was developed in non-aqueous media through the use of a sterically hindered diimine ligand. The sterics of this ligand proved to be essential for reaction success, most likely due to it binding in a 1:1 fashion with the silver salt. A kinetic study of this system showed that the mechanism of this reaction varies significantly from the aqueous system presented in Chapter 4. The coordination of the silver-ligand complex allowed for the formation of a monomer-dimer equilibrium in the reaction, in which the AgOTf-dmp monomer was the resting state of the catalyst. This dimer can be oxidized by Selectfluor through single electron transfer, forming a mixed-valent dimer that can perform a single electron oxidation of the carboxylic acid to produce an alkyl radical.

The role of persulfate in the non-aqueous system was also examined. In the presence of this additive, the AgOTf-dmp complex remained second order, again suggesting a monomer-dimer equilibrium. However, the true order in persulfate was masked by phase transfer due to the lack of solubility of these compounds in organic media.

Based on these studies, a better understanding of the decarboxylative fluorination reaction was obtained. The results found in Chapter 4 allowed for the development of a non-aqueous method, which is presented in this chapter, and the mechanistic studies presented show the mechanistic complexities that arise through the addition of ligands and additives to metal-catalyzed organic reactions.

5.7 References

- (1) Po, H. N. *Coord. Chem. Rev.* **1976**, *20*, 171–195.
- (2) Alexiev, A.; Bonchev, P. R. *Mikrochim. Acta.* **1970**, 13–19.
- (3) Bontschev, P. R.; Alexiev, A.; Dimitrova, B. *Talanta* **1969**, *16*, 597–602.
- (4) Bonchev, P. R.; Aleksiev, A. A. *Theor. Exp. Chem.* **1973**, *9*, 144–147.
- (5) *CRC Handbook of Chemistry and Physics*; 86th ed.; CRC Press: Boca Raton, FL; pp. 8–20.
- (6) Holyer, R. H.; Hubbard, C. D.; Kettle, S. F. A.; Wilkins, R. G. *Inorg. Chem.* **1965**, *4*, 929–935.
- (7) Hall, J. R.; Plowman, R. A.; Preston, H. S. *Aust. J. Chem.* **1965**, *18*, 1345–1349.
- (8) Swarnabala, G.; Rajasekharan, M. V. *Inorg. Chem.* **1989**, *28*, 662–666.
- (9) Swarnabala, G.; Rajasekharan, M. V. *Polyhedron.* **1996**, *15*, 3197–3201.
- (10) Sai, M.; Matsubara, S. *Org. Lett.* **2011**, *13*, 4676–4679.
- (11) Carney, J. M.; Donoghue, P. J.; Wuest, W. M.; Wiest, O.; Helquist, P. *Org. Chem. Front.* **2008**, *10*, 3903–3906.
- (12) Cui, Y.; He, C. *Angew. Chem. Int. Ed.* **2004**, *43*, 4210–4212.
- (13) Wang, Z.; Zhu, L.; Yin, F.; Su, Z.; Li, Z.; Li, C. *J. Am. Chem. Soc.* **2012**, *134*, 4258–4263.
- (14) Rigoli, J. W.; Weatherly, C. D.; Alderson, J. M.; Vo, B. T.; Schomaker, J. M. *J. Am. Chem. Soc.* **2013**, *135*, 17238–17241.
- (15) Alderson, J. M.; Phelps, A. M.; Scamp, R. J.; Dolan, N. S.; Schomaker, J. M. *J. Am. Chem. Soc.* **2014**, *136*, 16720–16723.
- (16) Yin, F.; Wang, Z.; Li, Z.; Li, C. *J. Am. Chem. Soc.* **2012**, *134*, 10401–10404.
- (17) Tokunaga, M.; Larrow, J. F.; Kakiuchi, F.; Jacobsen, E. N. *Science* **1997**, *277*, 936–938.

- (18) Ready, J. M.; Jacobsen, E. N. *J. Am. Chem. Soc.* **2001**, *123*, 2687–2688.
- (19) Hansen, K. B.; Leighton, J. L.; Jacobsen, E. N. *J. Am. Chem. Soc.* **1996**, *118*, 10924–10925.
- (20) Denmark, S. E.; Fu, J. *J. Am. Chem. Soc.* **2000**, *122*, 12021–12022.
- (21) Zhu, H.-L.; Chen, Q.; Peng, W.-L.; Qi, S.-J.; Xu, A.-L.; Chen, X.-M. *Chinese J. Chem.* **2001**, *19*, 263–267.
- (22) Olson, L. P.; Whitcomb, D. R.; Rajeswaran, M.; Blanton, T. N.; Stwertka, B. J.; Company, E. K.; Lake, A. V.; York, N.; Kodak, E.; Way, I.; December, R. V.; Re, V.; Recci, M.; January, V. *Chem. Mater.* **2006**, *18*, 1667–1674.
- (23) Qu, Y.; Su, L.; Wu, J. *J. Chem. Crystallogr* **2007**, *37*.
- (24) Bowmaker, G. A.; Marfua, S.; Skelton, B. W.; White, A. H. *Inorganica Chim. Acta* **2005**, *358*, 4371–4388.
- (25) Di Nicola, C.; Effendy; Marchetti, F.; Nervi, C.; Pettinari, C.; Robinson, W. T.; Sobolev, A. N.; White, A. H. *Dalt. Trans.* **2010**, *39*, 908–922.

Chapter 6. Conclusion

This dissertation focuses on the mechanistic investigations of synthetically relevant reactions of importance that proceed through single electron oxidation via silver catalysis. The motivation for this research lies in the fundamental understanding of electron transfer in metal-mediated organic reactions. A greater understanding of the mechanistic pathways in these reactions can allow for the optimization of existing methods, as well as opening up the possibility for the development of new synthetic reactions.

Chapter 2 explores the mechanism of the silver/persulfate-catalyzed cross-coupling of arylboronic acids with pyridines. Kinetic and spectroscopic studies identify coordination of the silver catalyst to pyridine in a pre-equilibrium step. In addition, an off-cycle step in the catalytic cycle is proposed in which the arylboronic acid undergoes protodeboronation through interaction with the silver-pyridine complex, resulting in catalyst deactivation. Studies using an organotrifluoroborate, as well as a sulfate radical scavenger led to the proposition that Ag(II) was the active single electron oxidant in the reaction as opposed to the sulfate radical anion. The mechanistic studies of this reaction allowed for the optimization of this method through the use of strong mineral acids, allowing for both catalyst and persulfate loadings to be decreased.

In Chapter 3, the mechanism of the silver/persulfate-catalyzed cross-coupling of arylboronic acids with quinones was investigated. Kinetic studies showed that in the absence of a coordinating agent that can bind to the silver catalyst, the mechanism of the

reaction is simplified. Boronic acid shows zero order dependency, as compared to the reaction in the presence of pyridine.

The mechanism of decarboxylative fluorination of aliphatic carboxylic acids in acetone/water media was explored in Chapter 4. Kinetic and spectroscopic studies suggest the oxidation of silver catalyst by Selectfluor in the rate-determining step, while carboxylic acid is involved with the silver catalyst in the induction period as well as substrate inhibition through the formation of silver-carboxylate intermediates. The role of water in this reaction is proposed to be for solubilizing the Selectfluor, which has limited solubility in acetone alone. The addition of persulfate to the reaction resulted in the acceleration of reaction rate, suggesting the action of Ag(II) as the active single electron oxidant in the reaction. In addition, the reaction was modified to replace Selectfluor by NFSI, another electrophilic fluorinating reagent, in the presence of persulfate, suggesting Selectfluor and NFSI are acting as fluorine atom sources in the decarboxylative fluorination, while also showing the adaptability of this reaction. The data provided in this study not only explain the current system, but allow for prediction of reactivity upon further modification.

In chapter 5, the decarboxylative fluorination reaction was adapted and developed in organic media through the addition of a sterically-hindered N-containing ligand. The addition of this ligand resulted in a significant change in reaction mechanism. Kinetic and spectroscopic studies suggest the formation of a silver-ligand dimer, which then undergoes single electron oxidation by the Selectfluor. Addition of persulfate to this reaction again led to the proposal that Ag(II) was the active single electron oxidant in this

reaction. The development of this reaction in organic media was made possible by the fundamental understanding of the reaction described in Chapter 4.

In conclusion, the studies described in this dissertation show the mechanistic complexities that arise in seemingly straightforward metal-catalyzed organic reactions. A greater understanding of the mechanism of these reactions showed that reaction methods could be optimized, or new reactions developed. By gaining a detailed mechanistic understanding of the reaction pathways, these systems can be utilized to their full potential, as well as allowing catalytic silver to be integrated into new areas of synthetic and organometallic chemistry.

Chapter 7. Appendix

7.1 Mechanism of Ag/Persulfate-catalyzed cross-coupling of arylboronic acids to heteroarenes

7.1.1 Spectroscopic data for 3

^1H NMR (500 MHz, CDCl_3) δ (ppm): 8.85 (1H, d), 7.93 (3H), 7.42 (1H, d), 7.32 (2H, d), 2.43 (3H, s); ^{13}C NMR (125 MHz, CDCl_3) δ (ppm): 158.85, 150.54, 140.04, 139.08, 135.32, 129.69, 126.92, 121.95, 117.13, 115.63, 21.31; GC/MS m/z (rel. abundance) 237 (100), 91 (13) (bdiwfb).

7.1.2 Data from kinetic studies

Table 7.1 Conditions for some excess experiments

Run	[1] (M)	[2] (M)	[e] (M)	$\text{K}_2\text{S}_2\text{O}_8$ (M)	[e] (M)	AgNO_3 (M)
100%	0.1	0.15	0.05	0.3	0.2	0.02
50%	0.05	0.1	0.05	0.25	0.2	0.02

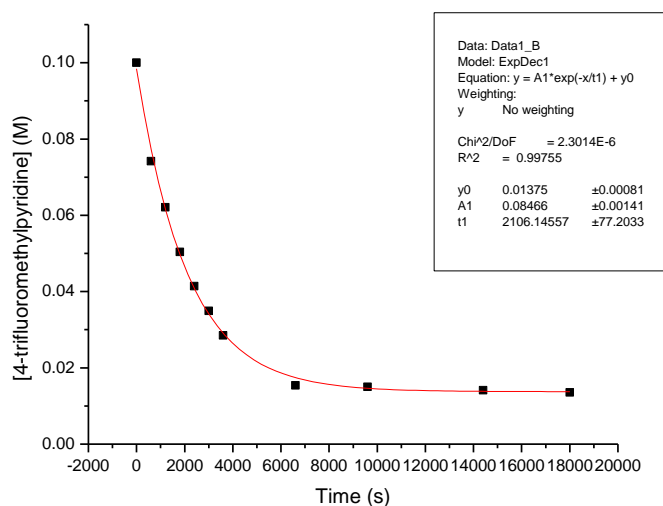


Figure 7.1 Plot of [1] vs. time for 100% run

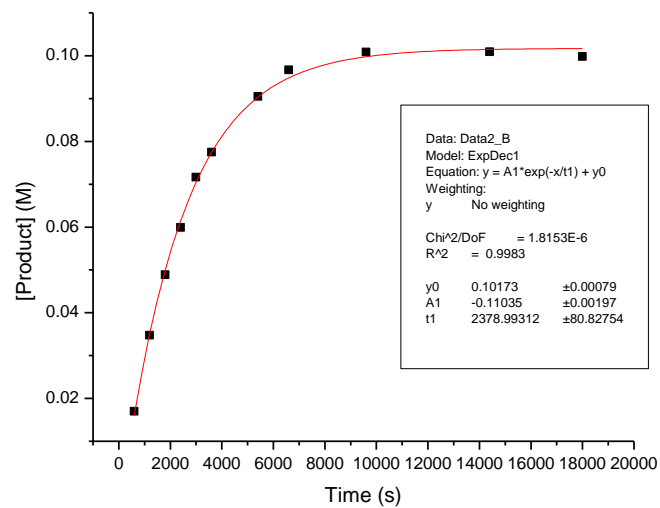


Figure 7.2 Plot of [3] vs. time for 100% run

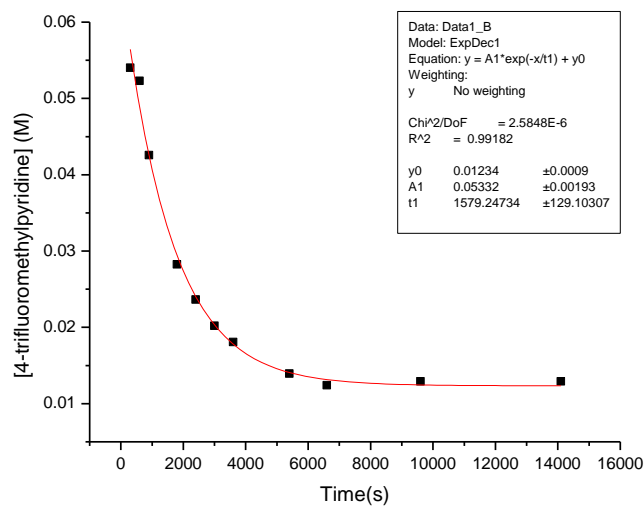


Figure 7.3 Plot of [1] vs. time for 50% run

Table 7.2 Conditions for different excess experiments for rate order for 2

Run	[1] (M)	[2] (M)	[e] (M)	K ₂ S ₂ O ₈ (M)	AgNO ₃ (M)
50%	0.05	0.1	0.05	0.25	0.02
Diff xs	0.05	0.3	0.25	0.25	0.02

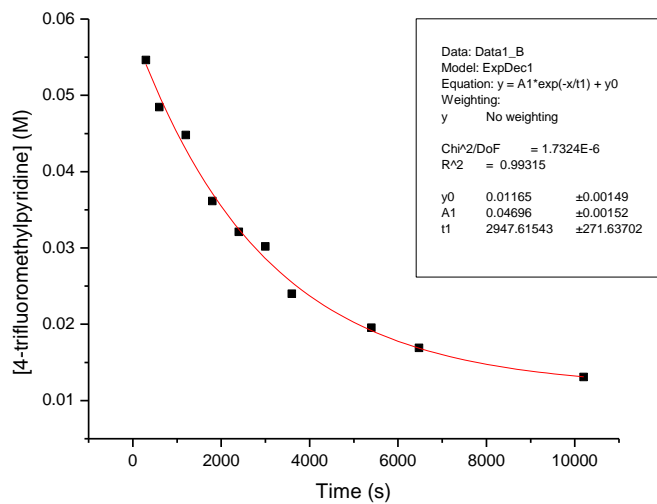


Figure 7.4 Plot of [1] vs. time for order of 2

Table 7.3 Conditions for different excess experiments for rate order for 1

Run	[1] (M)	[2] (M)	K ₂ S ₂ O ₈ (M)	AgNO ₃ (M)
100%	0.1	0.15	0.3	0.02
Diff xs	0.2	0.15	0.3	0.02

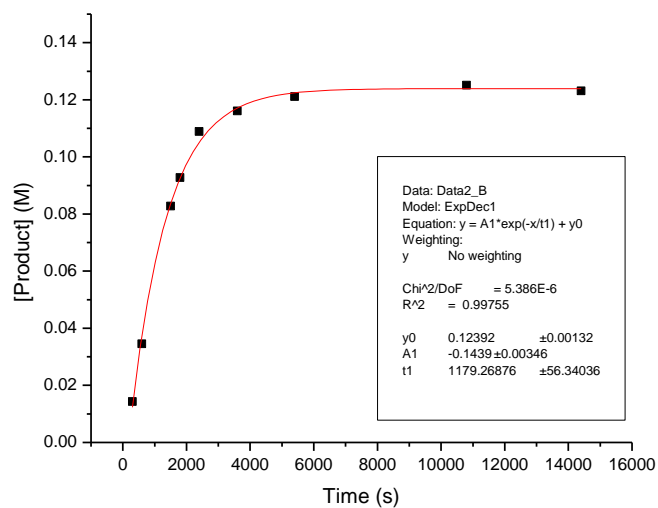


Figure 7.5 Plot of [3] vs. time for order of 1

Table 7.4 Conditions for different excess experiments for rate order for AgNO_3

Run	[1] (M)	[2] (M)	$\text{K}_2\text{S}_2\text{O}_8$ (M)	AgNO_3 (M)	[e] (M)
100%	0.1	0.15	0.3	0.02	0.08
Diff xs	0.1	0.15	0.3	0.04	0.06

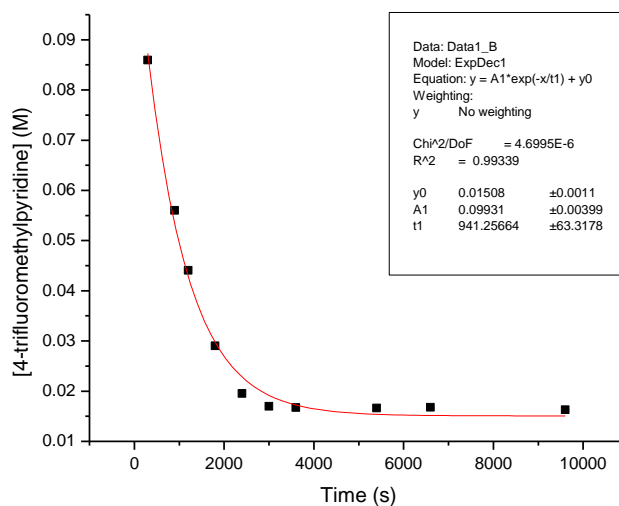


Figure 7.6 Plot of [1] vs. time for order of AgNO_3

Table 7.5 Conditions for different excess experiments for rate order for $K_2S_2O_8$

Run	[1] (M)	[2] (M)	$K_2S_2O_8$ (M)	[e] (M)	$AgNO_3$ (M)
100%	0.1	0.15	0.3	0.2	0.02
Diff xs	0.1	0.15	0.6	0.5	0.02

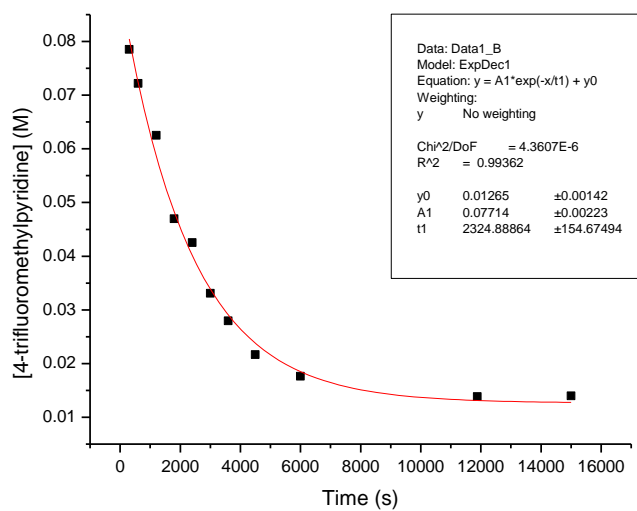


Figure 7.7 Plot of [1] vs. time for order of $K_2S_2O_8$

Table 7.6 Conditions for different excess experiments for rate order for TFA

Run	[1] (M)	[2] (M)	$K_2S_2O_8$ (M)	$AgNO_3$ (M)	TFA (M)
100%	0.1	0.15	0.3	0.02	0.1
Diff xs	0.1	0.15	0.3	0.02	0.2

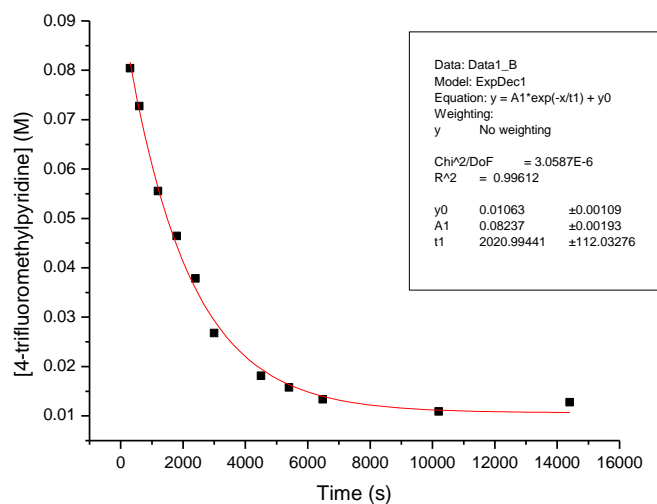


Figure 7.8 Plot of [1] vs. time for order TFA

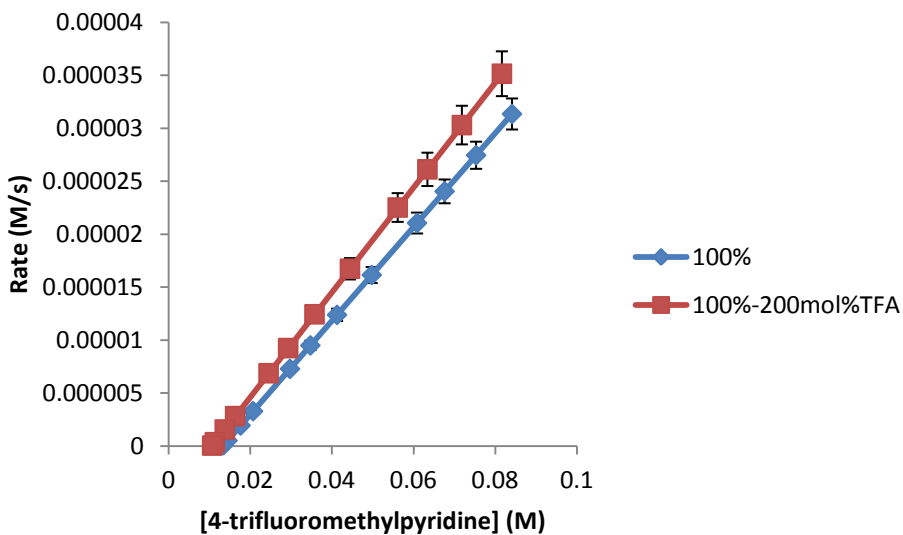


Figure 7.9 Plot of rate vs. [1] for rate order for TFA

Table 7.7 Conditions for different excess experiments for rate order for $\text{Na}_2\text{S}_2\text{O}_8$

Run	[1] (M)	[2] (M)	$\text{Na}_2\text{S}_2\text{O}_8$ (M)	[e] (M)	AgNO_3 (M)
100%	0.1	0.15	0.3	0.2	0.02
Diff xs	0.1	0.15	0.6	0.5	0.02

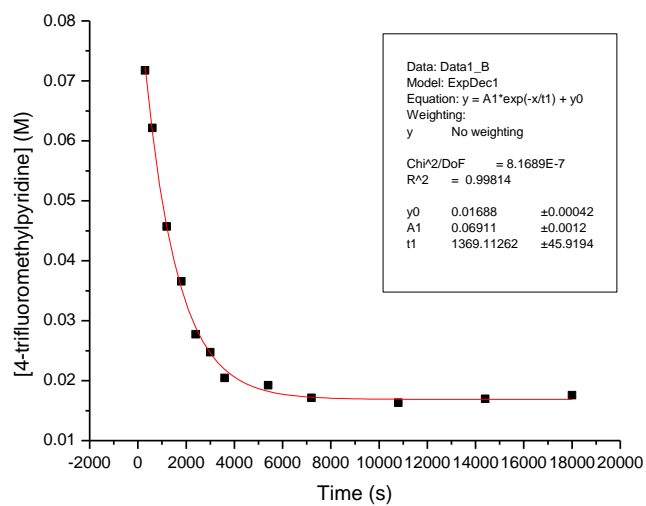


Figure 7.10 Plot of [1] vs. time for 100% Na₂S₂O₈

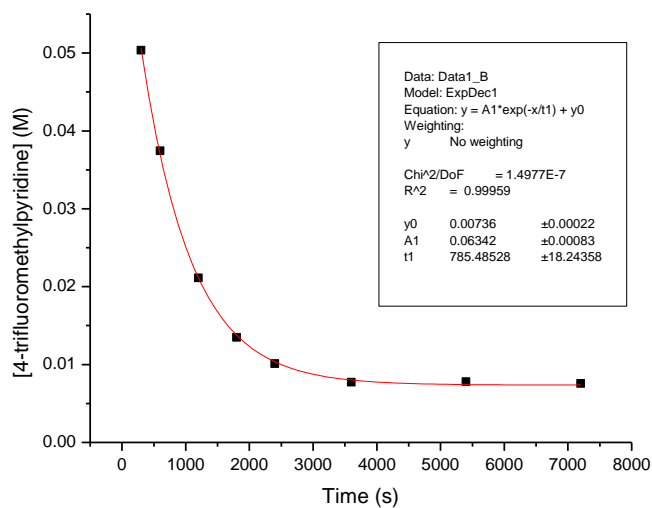


Figure 7.11 Plot of [1] vs. time for order of Na₂S₂O₈

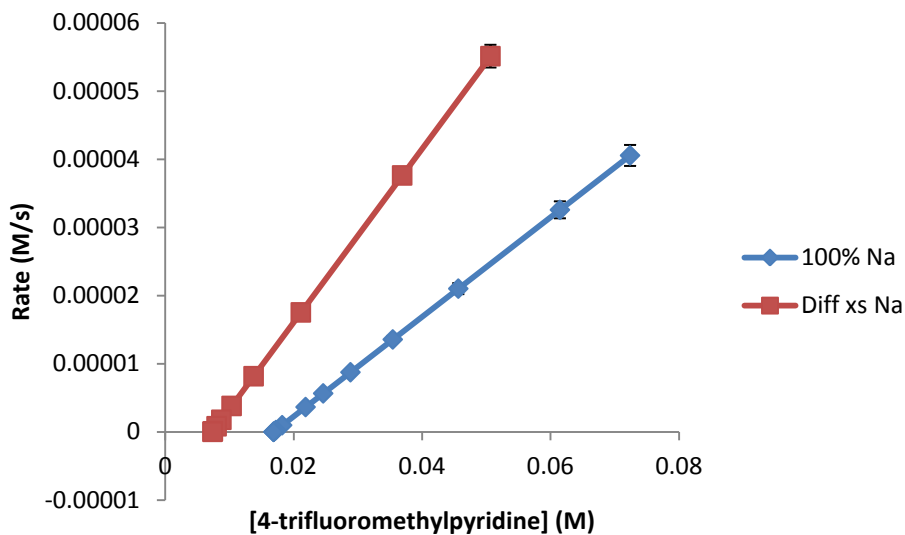


Figure 7.12 Plot of rate vs. [1] for rate order for $\text{Na}_2\text{S}_2\text{O}_8$

Table 7.8 Conditions for experiments using allyl acetate as sulfate radical anion trap

Run	[1] (M)	[2] (M)	$\text{Na}_2\text{S}_2\text{O}_8$ (M)	AgNO_3 (M)	Allyl Acetate (M)
100%	0.1	0.15	0.3	0.02	0.0
AllylAc	0.1	0.15	0.3	0.02	0.6

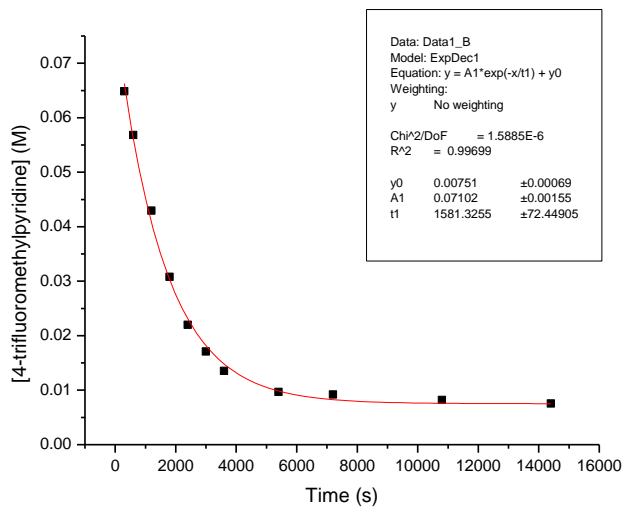


Figure 7.13 Plot of [1] vs. time for addition of allyl acetate

7.1.3 NMR studies

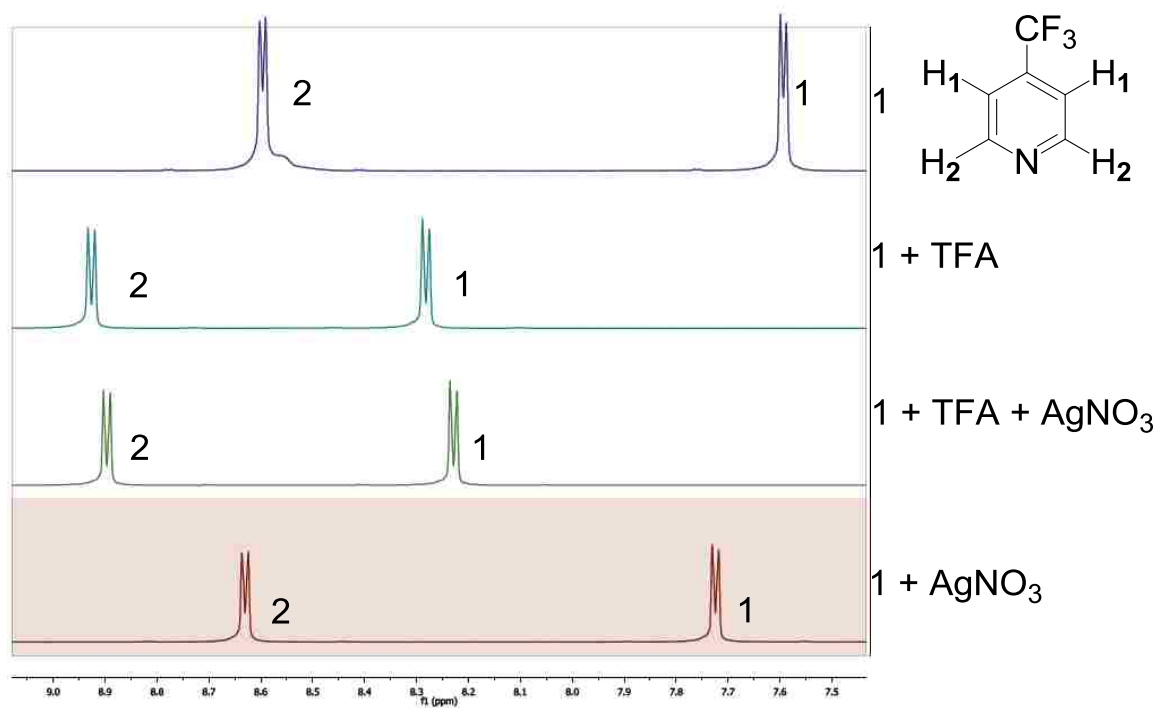


Figure 7.14 Spectral data for pyridine ^1H NMR studies

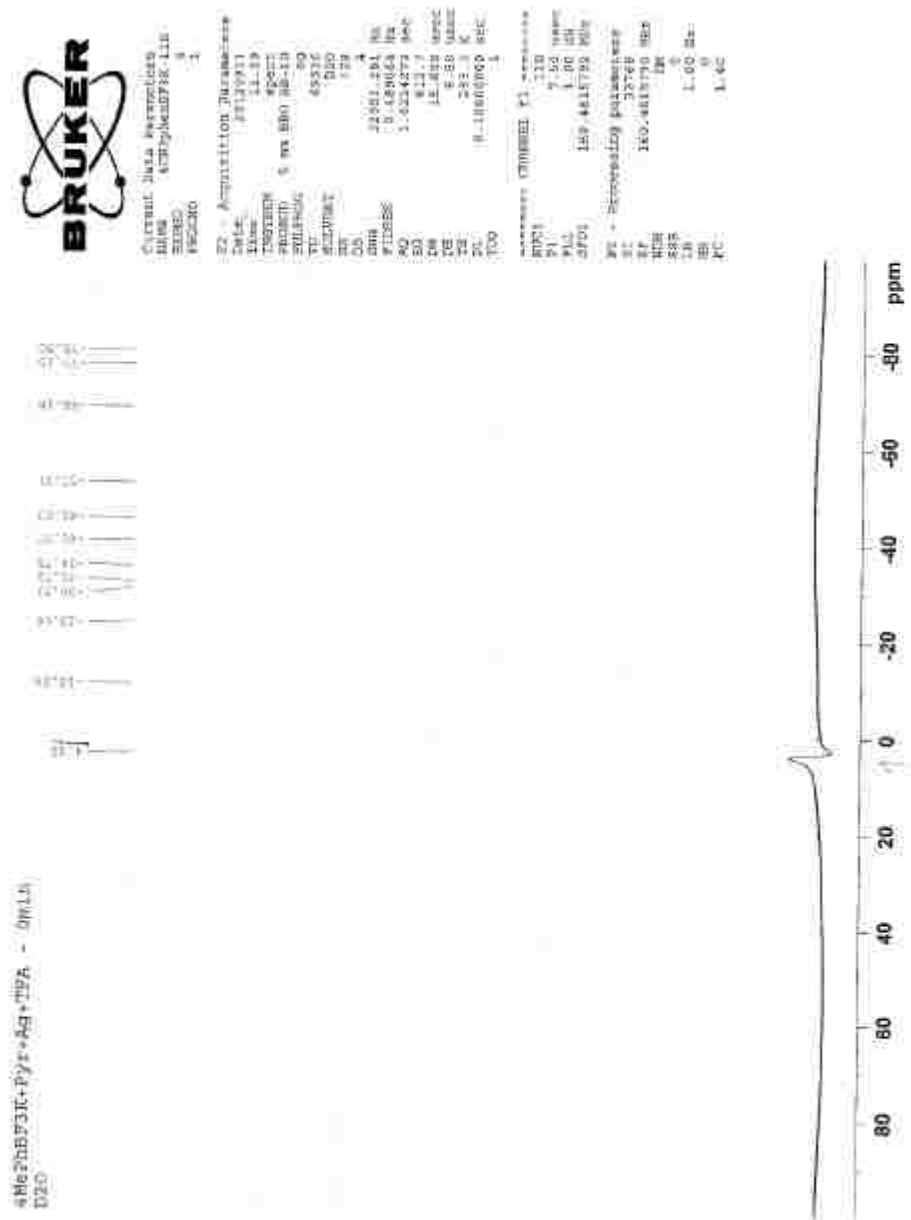


Figure 7.16 ^{11}B NMR spectrum of **4** under reaction conditions at $t = 0$ mins

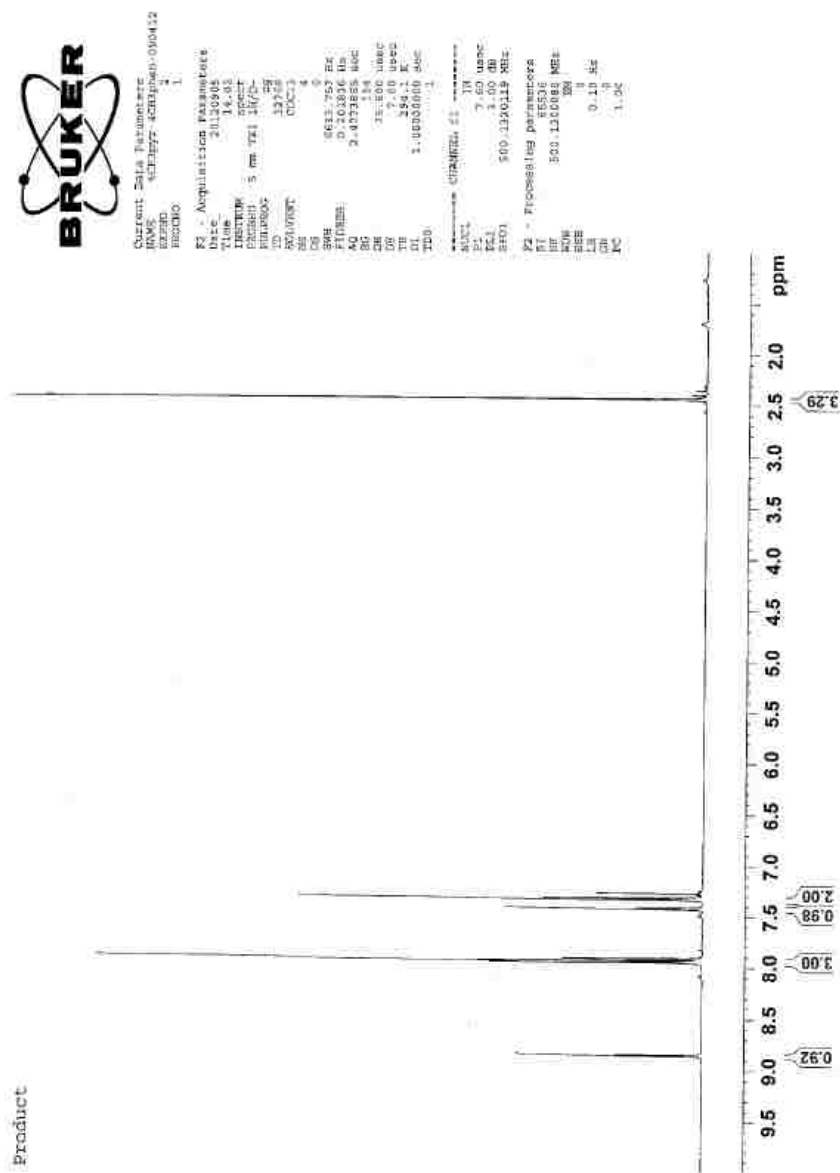


Figure 7.18 ^1H spectrum for cross-coupled product 3

7.2 Mechanism of Ag/Persulfate-catalyzed cross-coupling of arylboronic acids to quinones

7.2.1 Data from kinetic studies

Table 7.9 Conditions for experiment for rate order of 5

Run	[5] (M)	[2] (M)	$K_2S_2O_8$ (M)	$AgNO_3$ (M)
100% (Quinone)	0.1	0.15	0.3	0.02

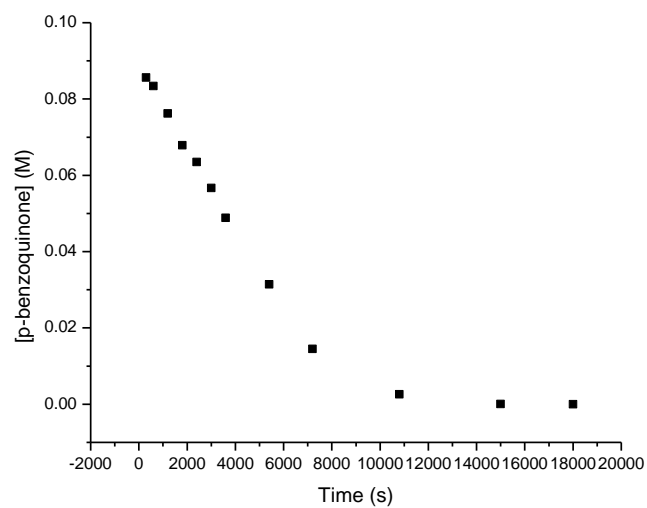


Figure 7.20 Plot of [5] vs. time for 100% run

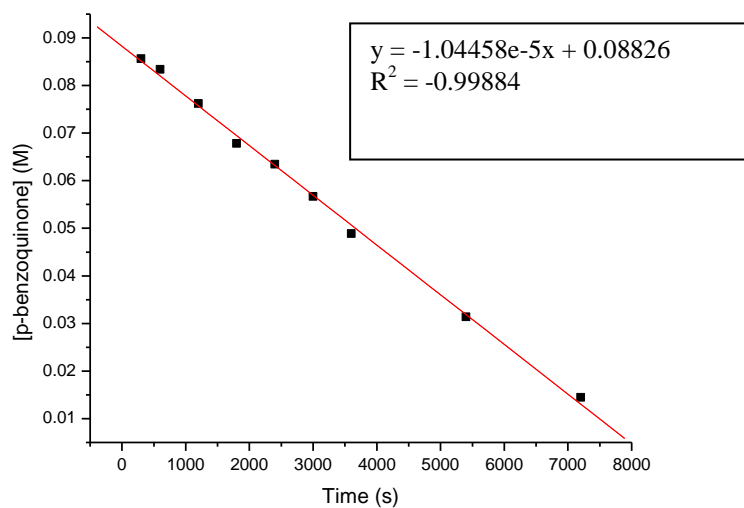


Figure 7.21 Linear fit of 100% run

Table 7.10 Conditions for different excess experiments for rate order of 2

Run	[5] (M)	[2] (M)	$K_2S_2O_8$ (M)	$AgNO_3$ (M)
100% (Quinone)	0.1	0.15	0.3	0.02
Diff xs	0.1	0.3	0.3	0.02

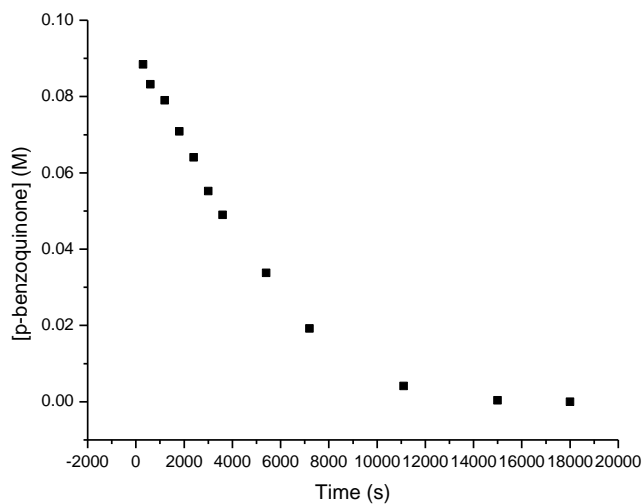


Figure 7.22 Plot of [5] vs. time for order of 2

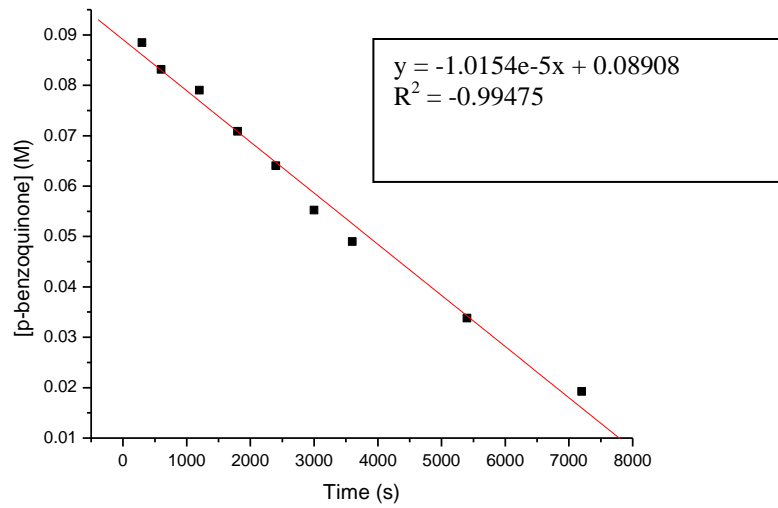


Figure 7.23 Linear fit [5] vs. time for order of 2

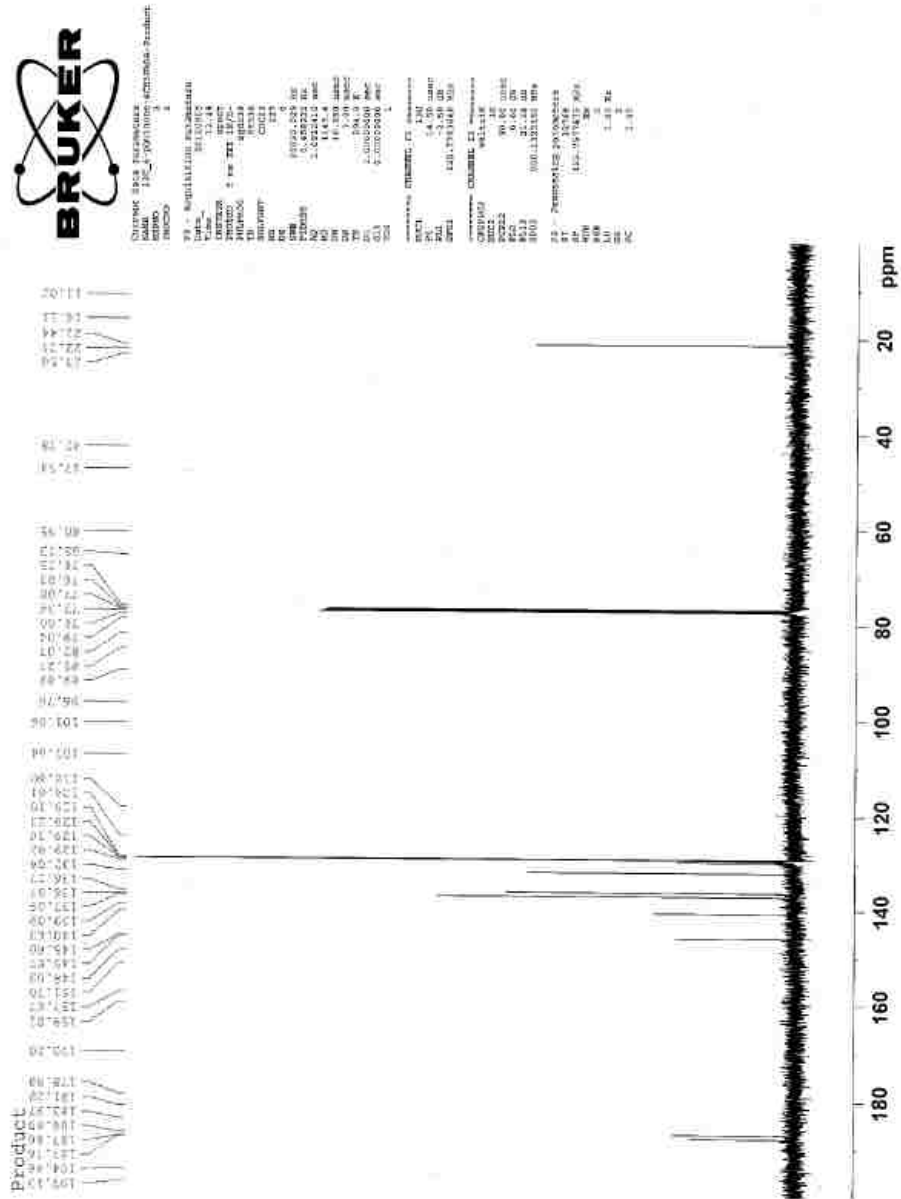


Figure 7.25 ¹³C NMR spectral data for cross-coupled product 6

7.3 Mechanistic study of decarboxylative fluorination in acetone/water

7.3.1 Spectroscopic Data

Spectroscopic data for 2 (4-fluoro-4-methylpentanoic acid): ^1H NMR (500 MHz, $\text{CDCl}_3/\text{acetone-d}_6$) δ (ppm): 2.34 (2H, m), 1.87 (2H, m), 1.26 (6H, d); ^{13}C NMR (125 MHz, $\text{CDCl}_3/\text{acetone-d}_6$) δ (ppm): 174.7, 94.50 (d), 36.00 (d), 28.48, 21.36 (d); ^{19}F NMR (470 MHz, $\text{CDCl}_3/\text{acetone-d}_6$): -135.4 (m).

Spectroscopic data for 3b (2-fluoro-2-methylbutane): ^1H NMR (500 MHz, $\text{CDCl}_3/\text{acetone-d}_6$) δ (ppm): 1.55 (2H, m), 1.23 (6H, dd), 0.86 (3H, t); ^{13}C NMR (125 MHz, $\text{CDCl}_3/\text{acetone-d}_6$) δ (ppm): 34.01, 25.97, 8.06; ^{19}F NMR (470 MHz, $\text{CDCl}_3/\text{acetone-d}_6$): -134.3 (m).

Spectroscopic data for 4a (2,2-dimethyl-3-phenylpropanoic acid)

^1H NMR (500 MHz, $\text{CDCl}_3/\text{acetone-d}_6$) δ (ppm): 7.29 (5H, m), 2.92 (2H, s), 1.22 (6H, s); ^{13}C NMR (125 MHz, $\text{CDCl}_3/\text{acetone-d}_6$) δ (ppm): 179.40, 132.47, 125.19, 122.99, 121.50, 40.80, 38.39, 19.60.

Spectroscopic data for 4b (2-fluoro-2-methylpropyl)-benzene: ^1H NMR (500 MHz, $\text{CDCl}_3/\text{acetone-d}_6$) δ (ppm): 7.19 (5H, m), 2.82 (2H, d); 1.23 (6H, d); ^{13}C NMR (125 MHz, $\text{CDCl}_3/\text{acetone-d}_6$) δ (ppm): 137.07, 130.42, 128.06, 126.49, 95.64, 94.29, 47.53, 47.35, 26.56, 26.37; ^{19}F NMR (470 MHz, $\text{CDCl}_3/\text{acetone-d}_6$): -138.1 (m).

Spectroscopic data for 5b (2-fluoropropane): ^1H NMR (500 MHz, $\text{CDCl}_3/\text{acetone-d}_6$) δ (ppm): 4.73 (1H, ds), 1.24 (6H, dd); ^{13}C NMR (125 MHz, $\text{CDCl}_3/\text{acetone-d}_6$) δ (ppm): 88.03, 22.68; ^{19}F NMR (470 MHz, $\text{CDCl}_3/\text{acetone-d}_6$): -162.9 (m).

7.3.2 Data from kinetic studies

Table 7.11 Reaction conditions for kinetic order studies of each component

[carboxylic acid] (M)	[AgNO_3] (M)	[F-TEDA- BF_4] (M)	Excess F-TEDA- BF_4 (M)
0.1	0.02	0.2	0.1
0.1	0.04	0.2	0.1
0.1	0.02	0.15	0.05
0.075	0.02	0.2	0.125

7.3.2.1 Reaction of 2,2-dimethylglutaric acid

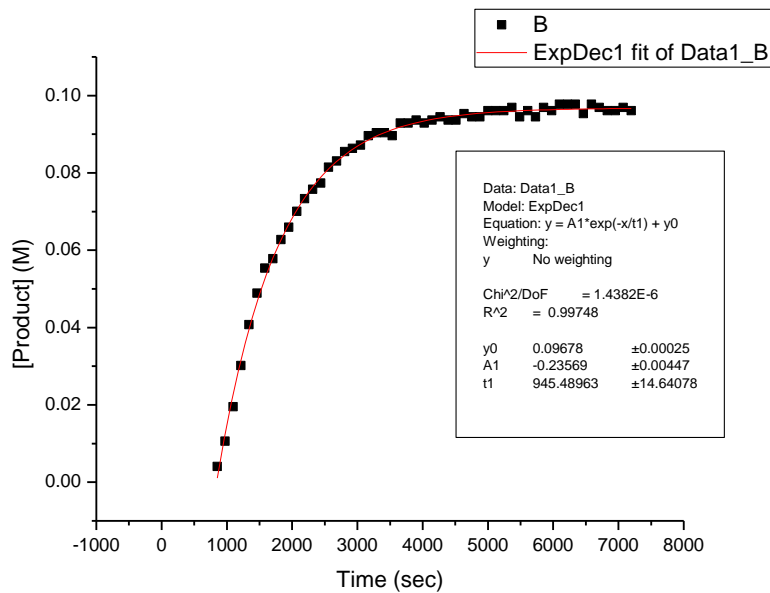


Figure 7.26 Plot of [8] vs. time for 100% run

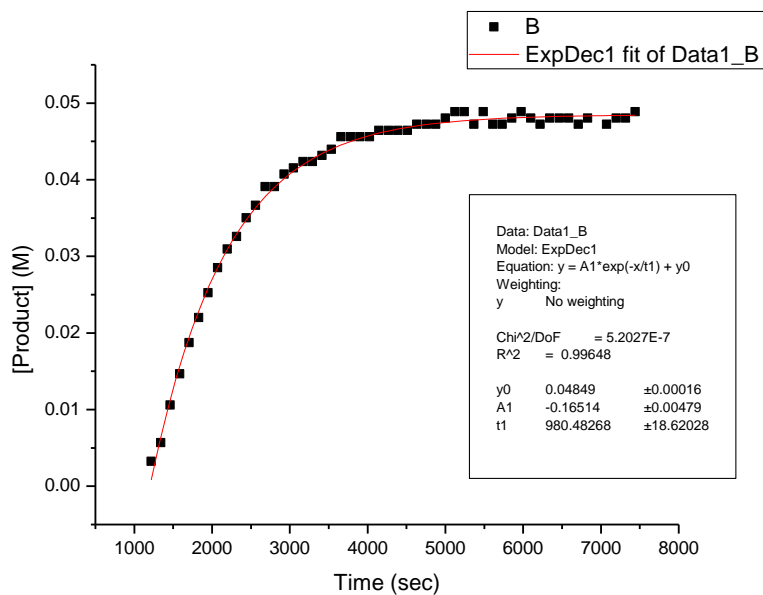


Figure 7.27 Plot of [8] vs. time for 50% run

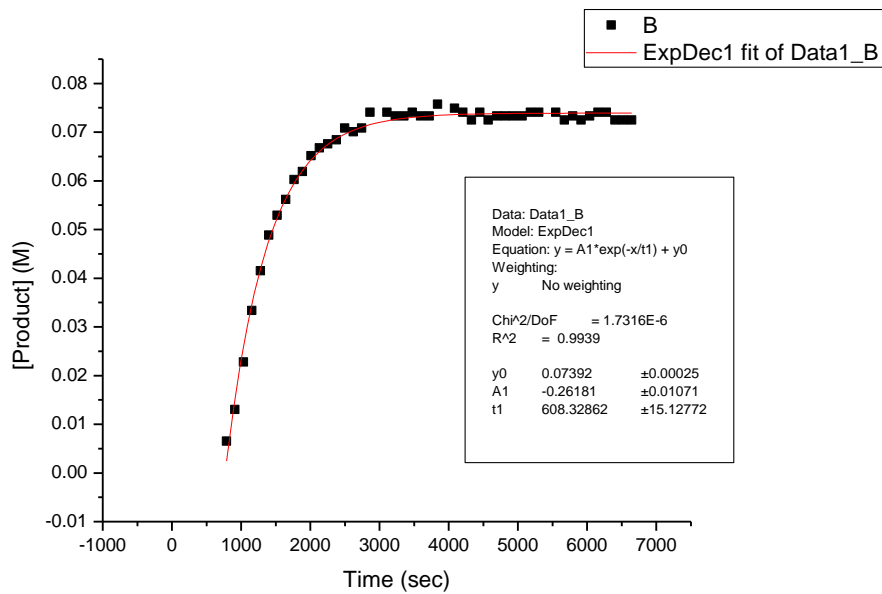


Figure 7.28 Plot of [8] vs. time for order of 7

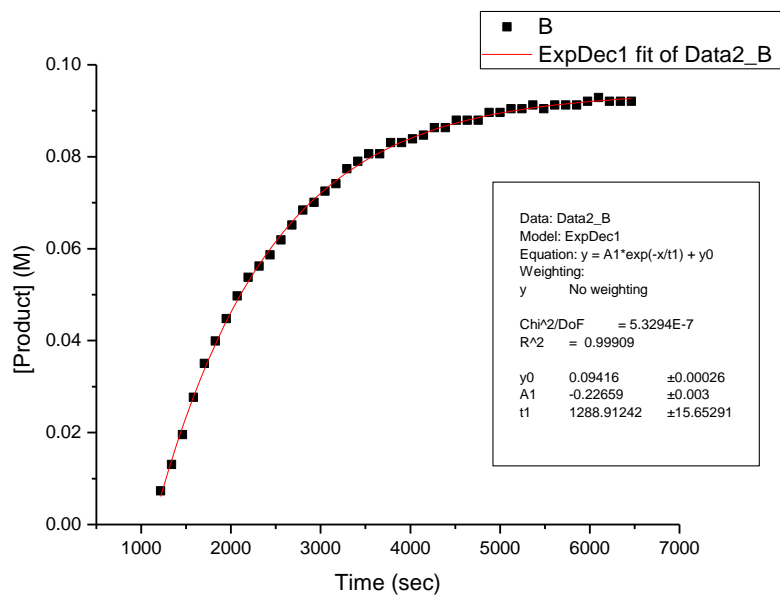


Figure 7.29 Plot of [8] vs. time for order of Selectfluor

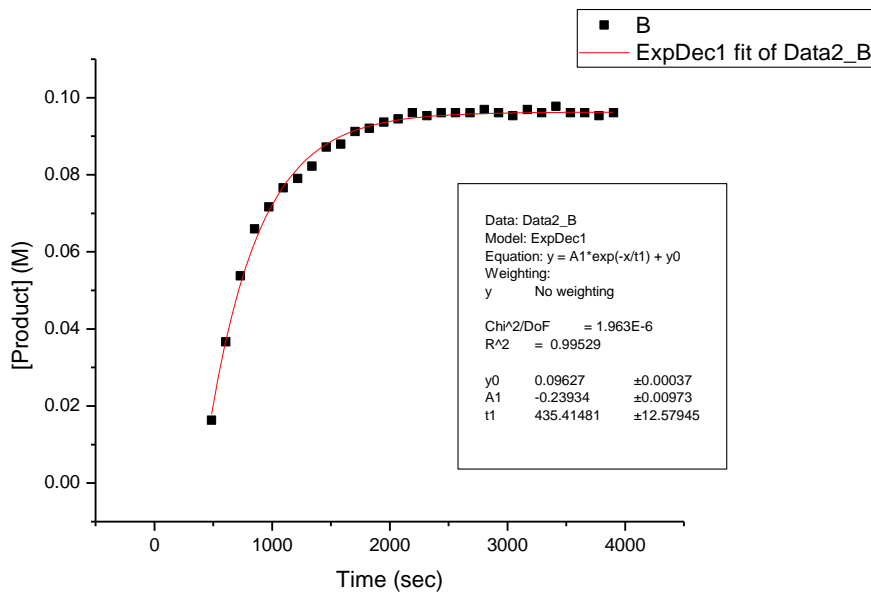


Figure 7.30 Plot of [8] vs. time for order of AgNO_3

Polynomial fit for reaction of 7

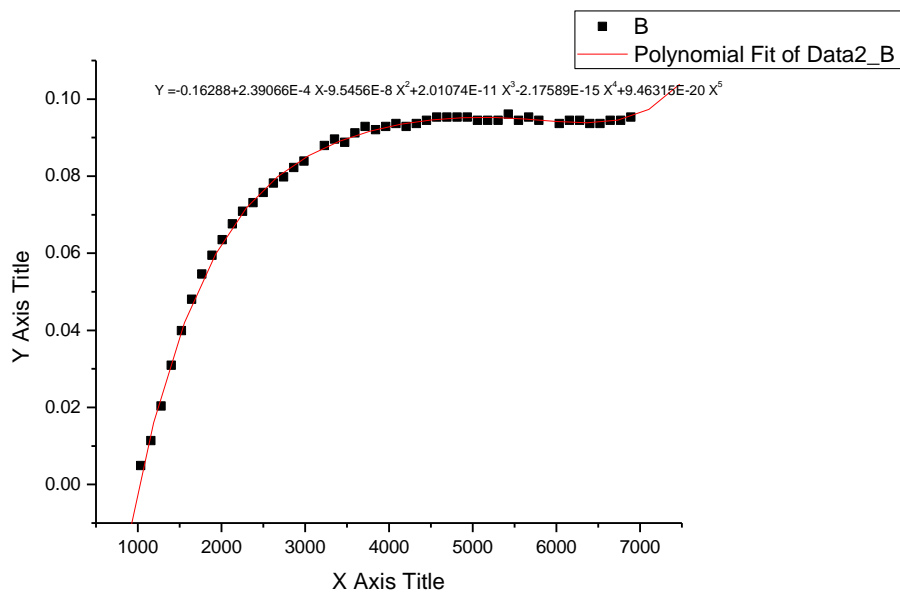


Figure 7.31 Polynomial fit of [8] vs. time for 100% run

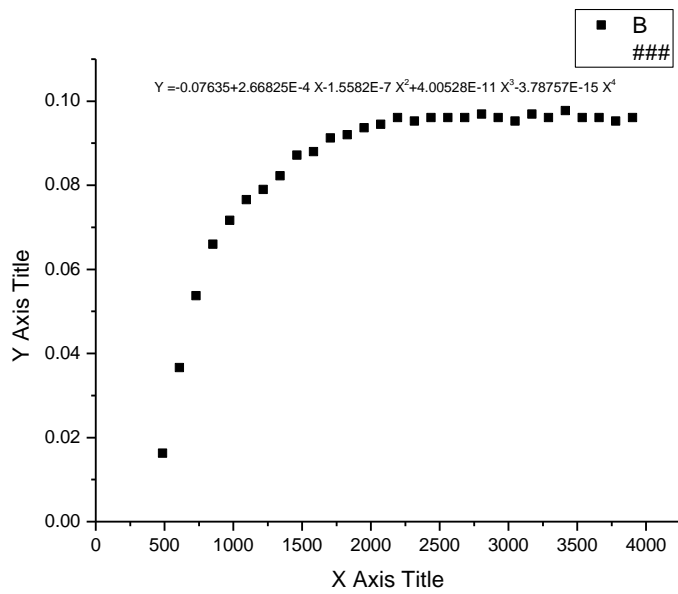


Figure 7.32 Polynomial fit of [8] vs. time for order of AgNO₃

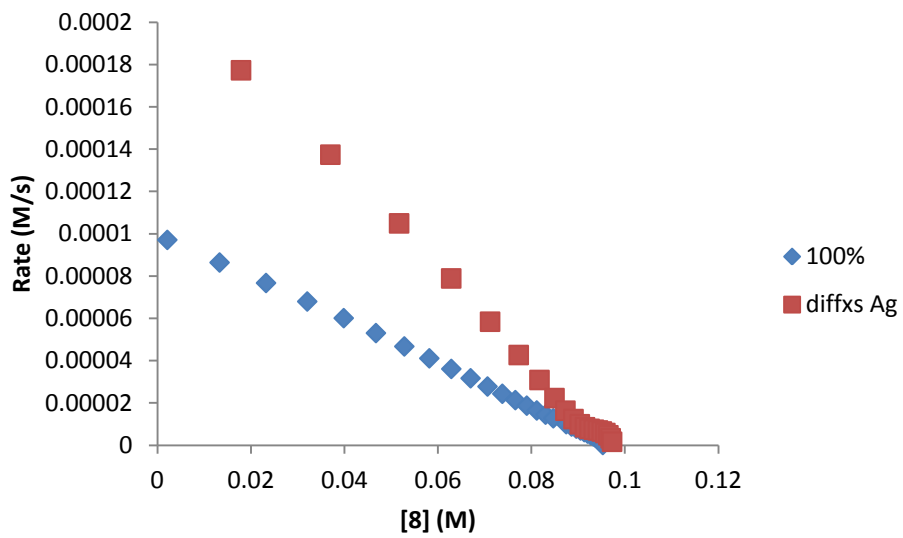


Figure 7.33 Plot of Rate vs. [8] for order of AgNO₃

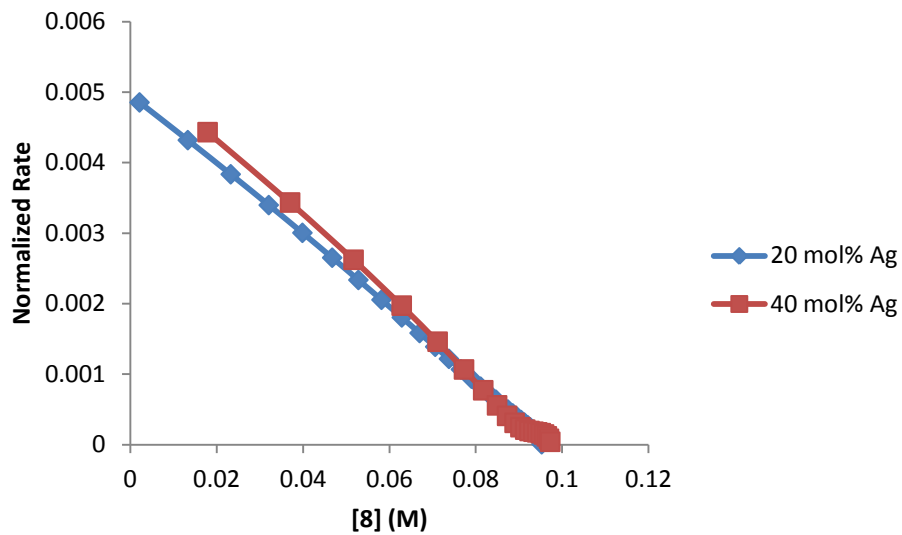


Figure 7.34 Normalized plot of Rate vs. [8] for order of AgNO_3

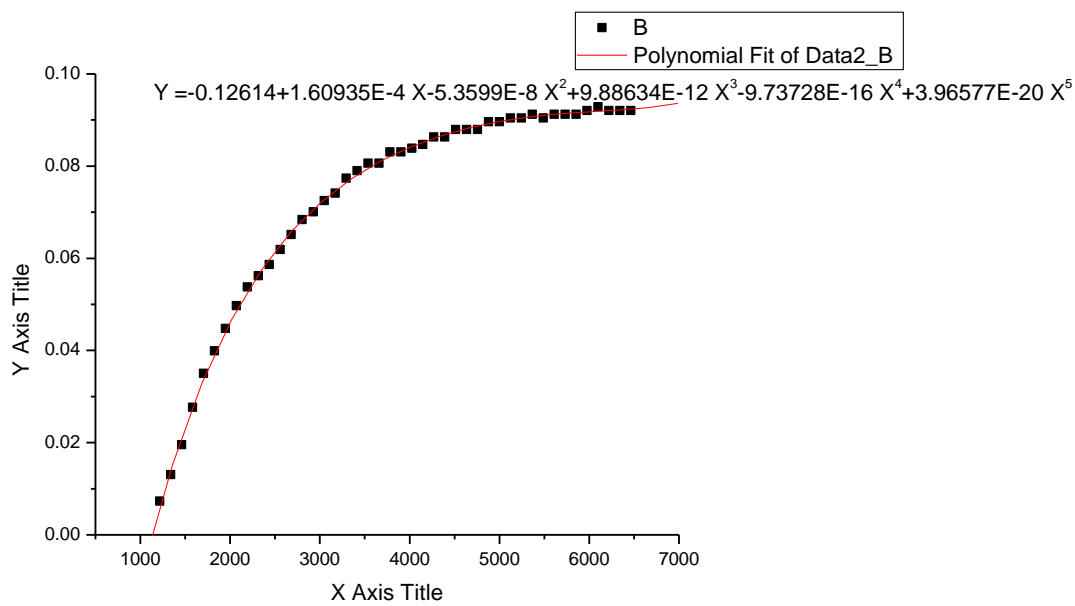


Figure 7.35 Polynomial fit of [8] vs. time for order of Selectfluor

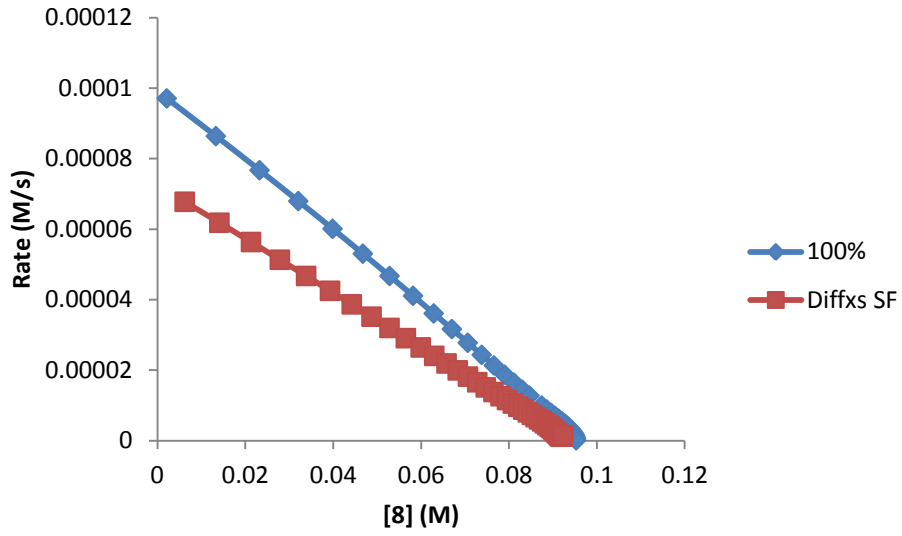


Figure 7.36 Plot of Rate vs. [8] for order of Selectfluor

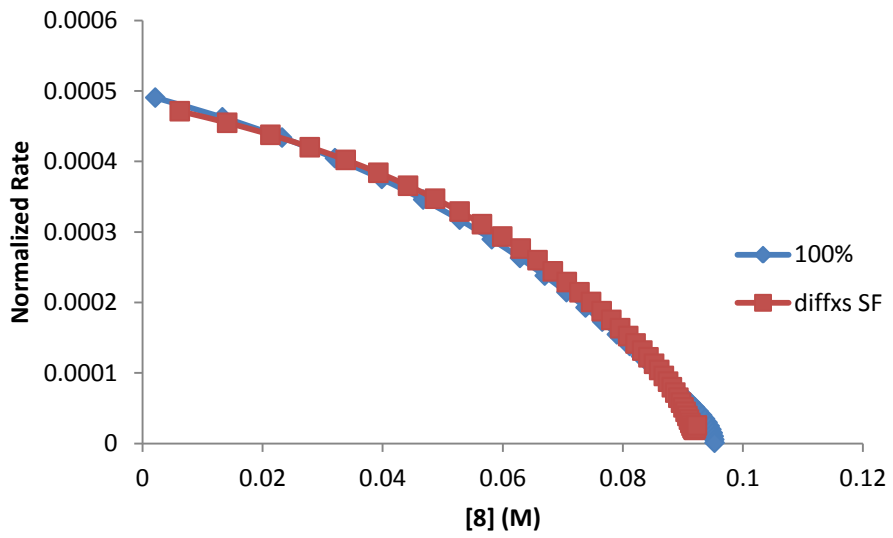


Figure 7.37 Normalized plot of Rate vs. [8] for order of Selectfluor

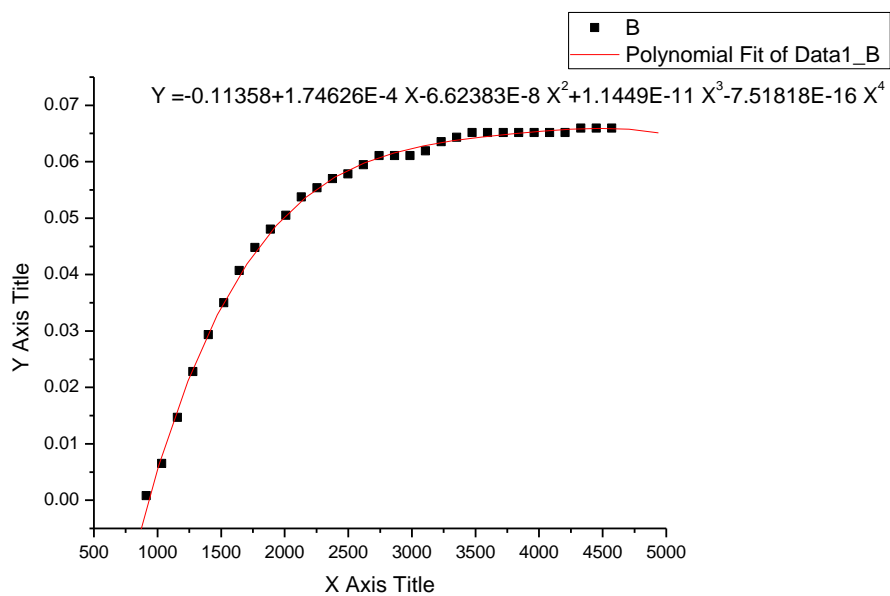


Figure 7.38 Polynomial fit of [8] vs. time for order of 7

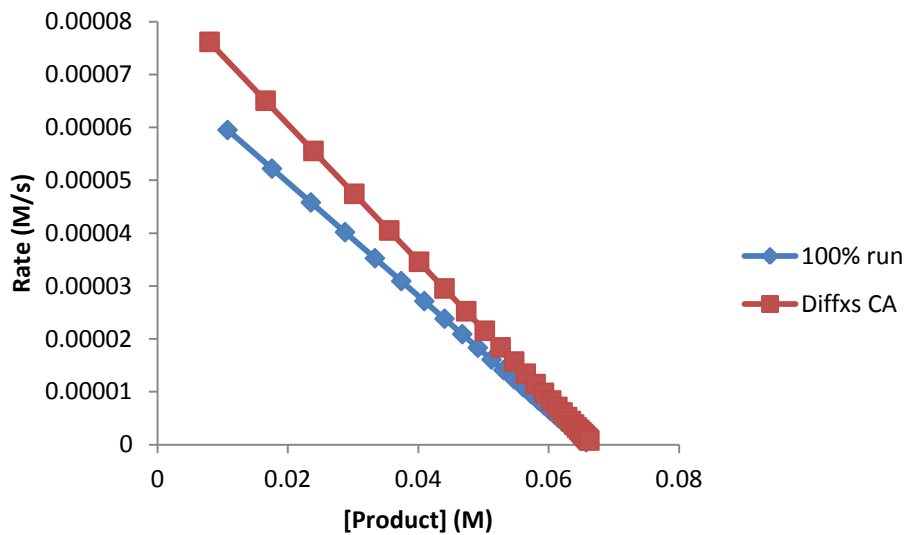


Figure 7.39 Plot of Rate vs. [8] for order of carboxylic acid

7.3.2.2 Reaction of 2,2-dimethylbutyric acid

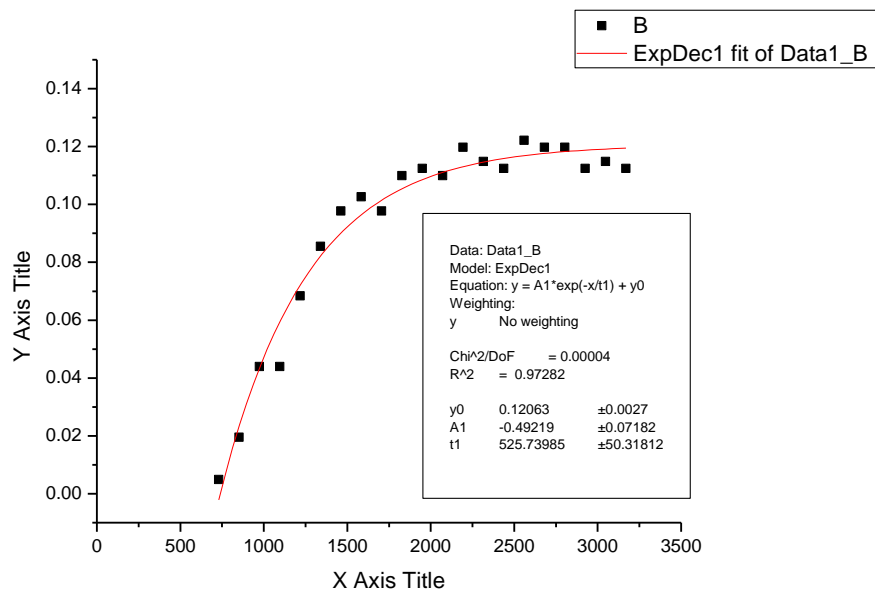


Figure 7.40 Plot of [9b] vs. time for 100% run

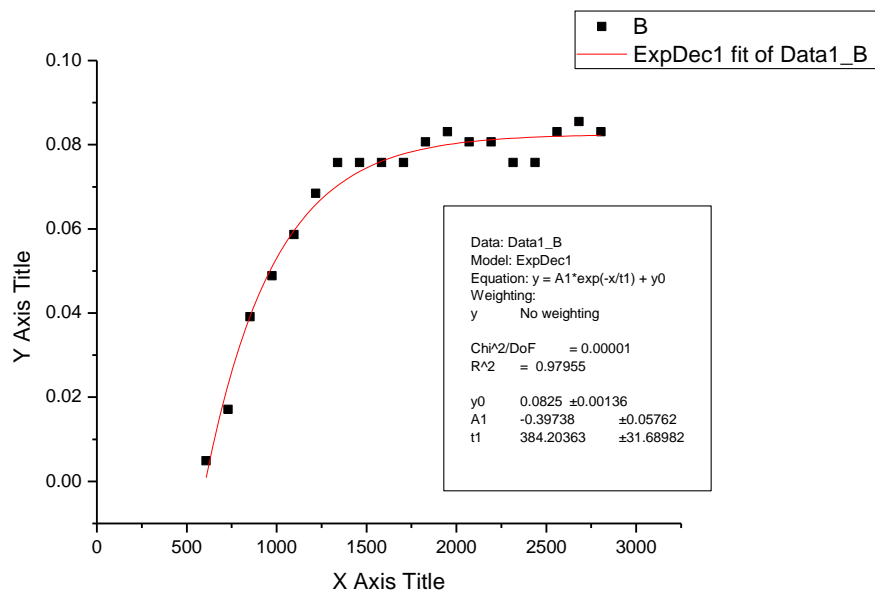


Figure 7.41 Plot of [9b] vs. time for order of 9

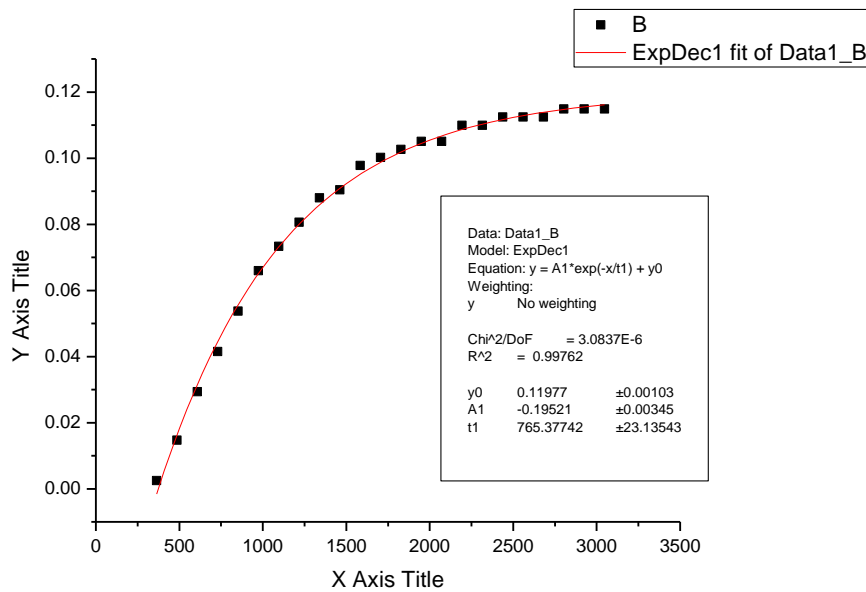


Figure 7.42 Plot of [9b] vs. time for order of Selectfluor

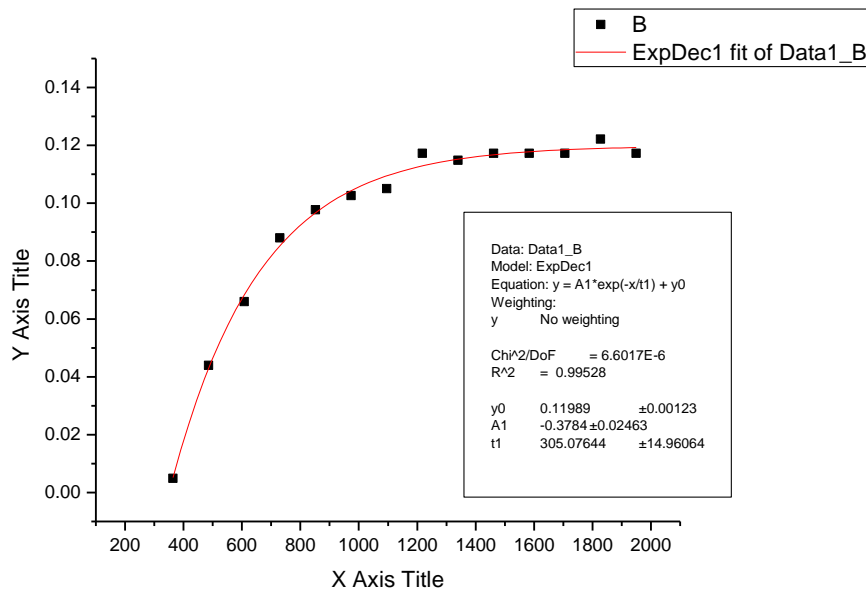


Figure 7.43 Plot of [9b] vs. time for order of AgNO₃

7.3.2.3 Reaction of 2,2-dimethylphenylpropanoic acid

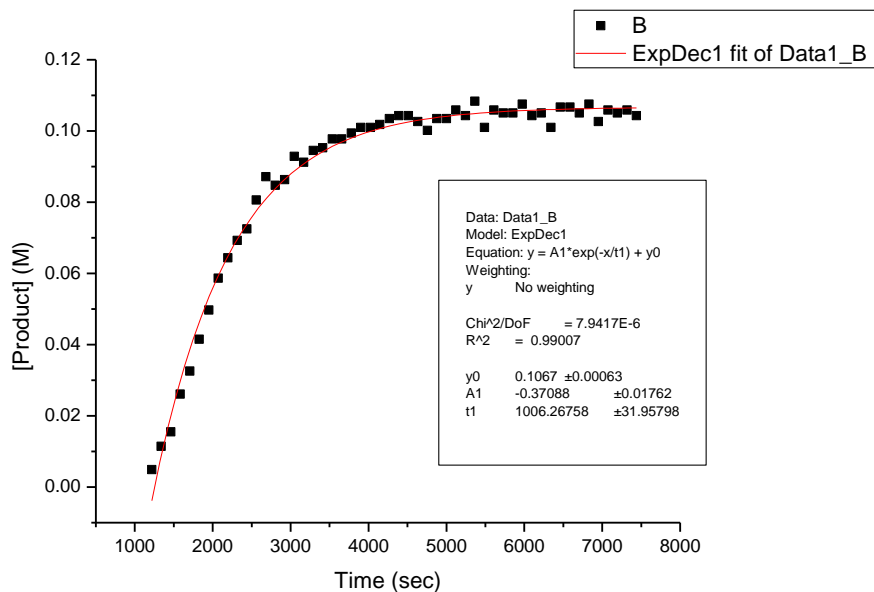


Figure 7.44 Plot of [10b] vs. time for 100% run

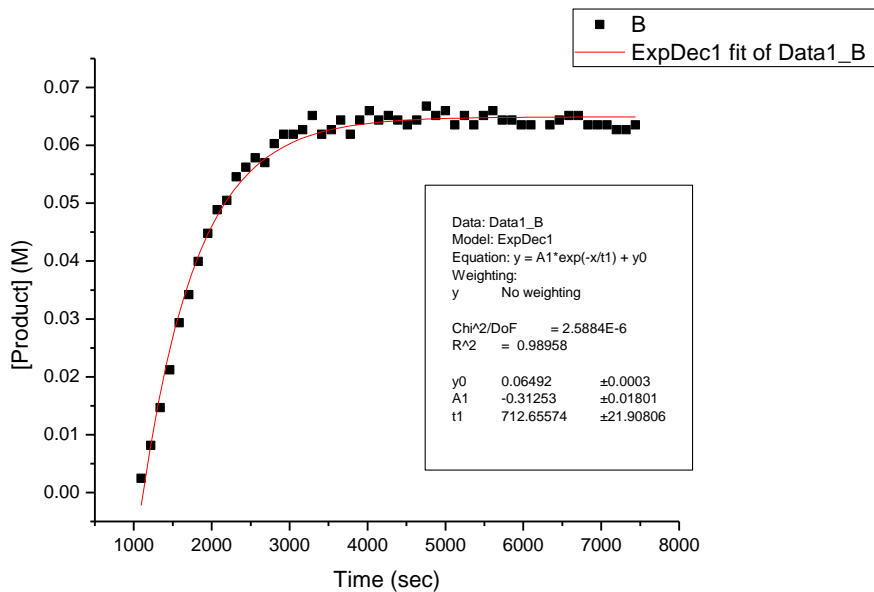


Figure 7.45 Plot of [10b] vs. time for order of 10

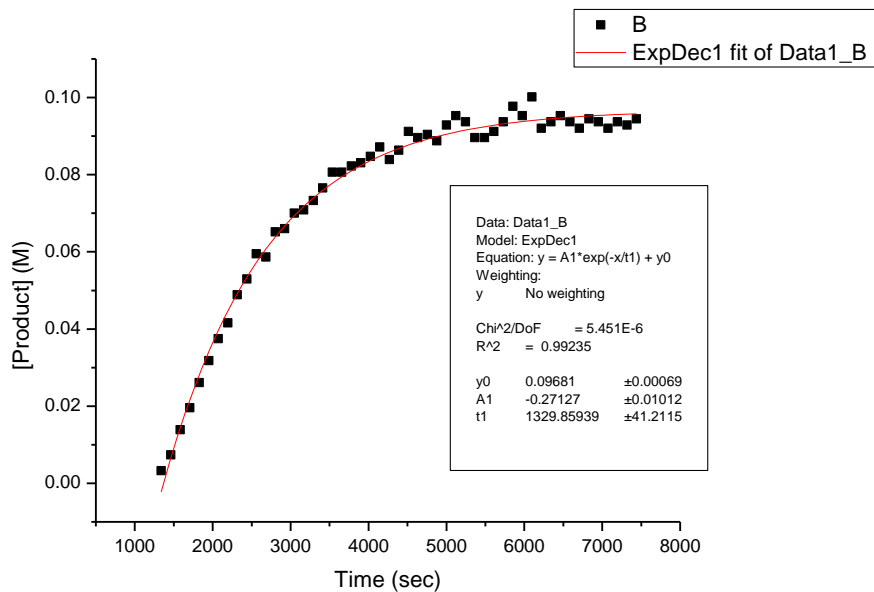


Figure 7.46 Plot of [10b] vs. time for order of Selectfluor

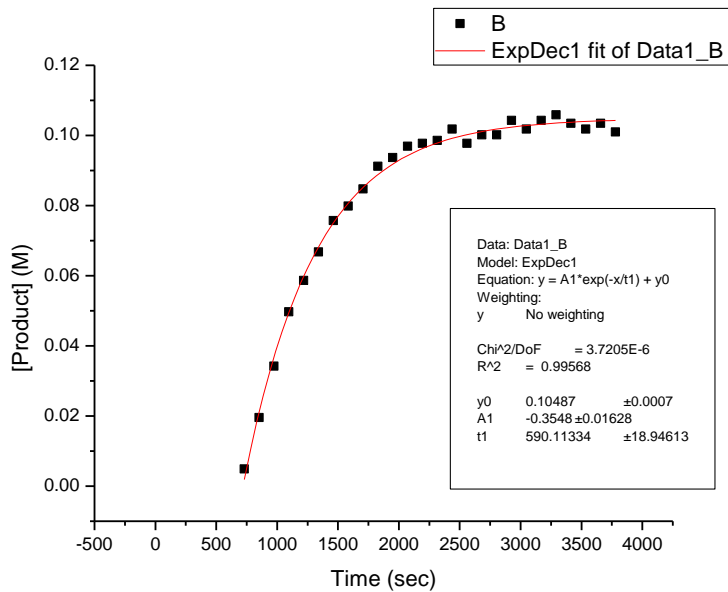


Figure 7.47 Plot of [10b] vs. time for order of AgNO₃

7.3.2.4 Reaction of isobutyric acid

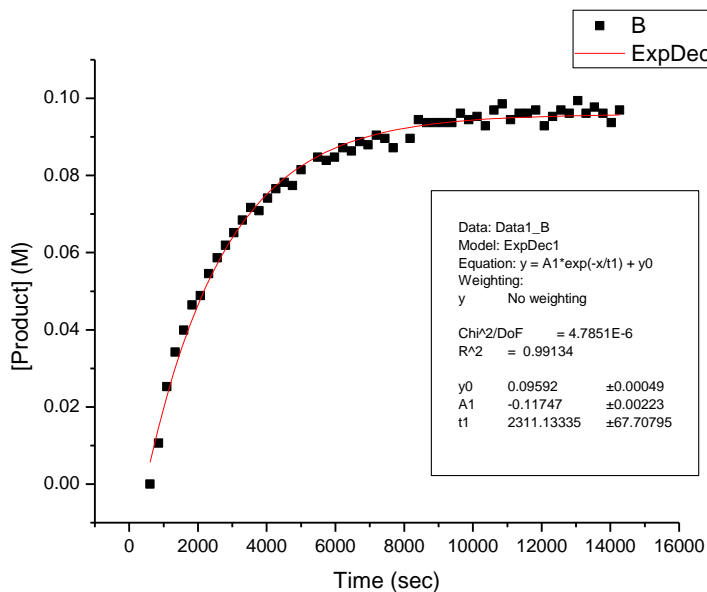


Figure 7.48 Plot of [11b] vs. time for 100% run

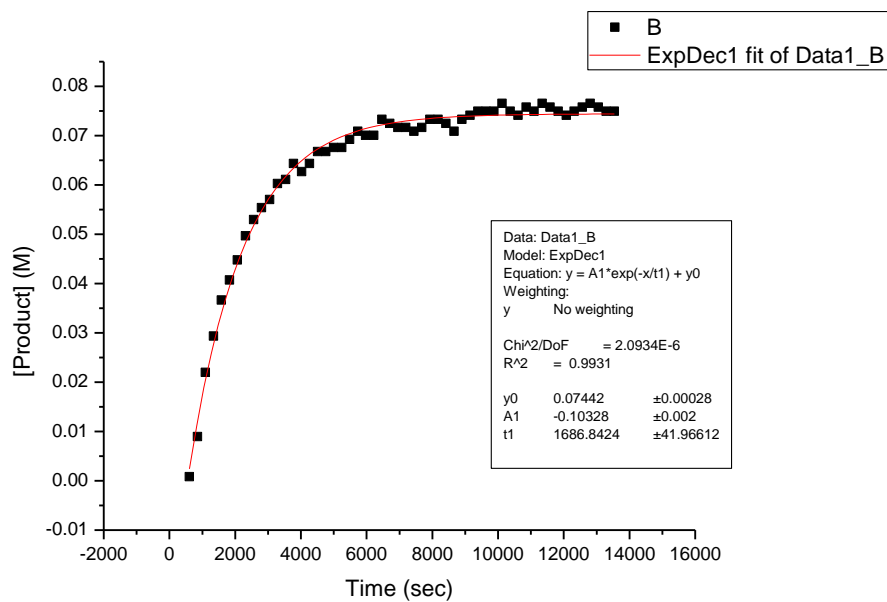


Figure 7.49 Plot of [11b] vs. time for order of 11

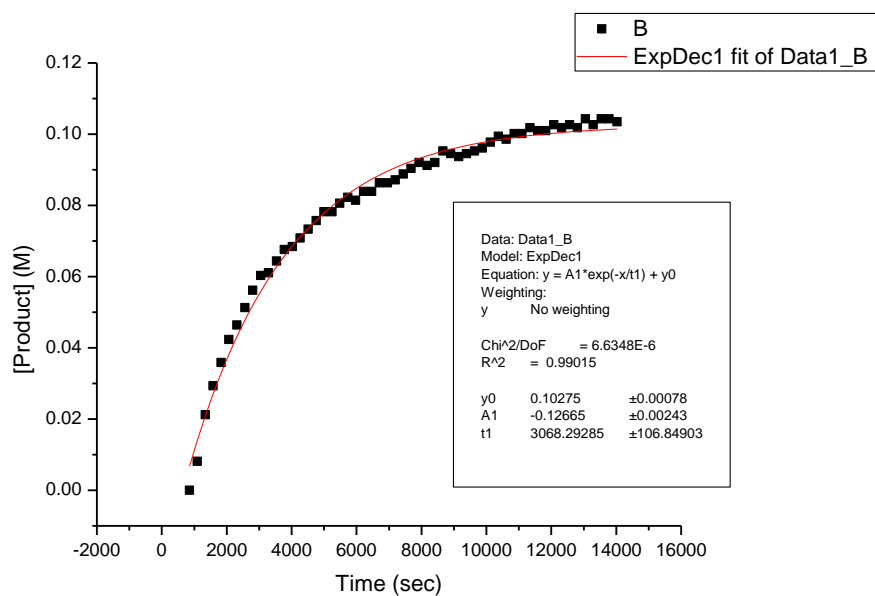


Figure 7.50 Plot of [11b] vs. time for order of Selectfluor

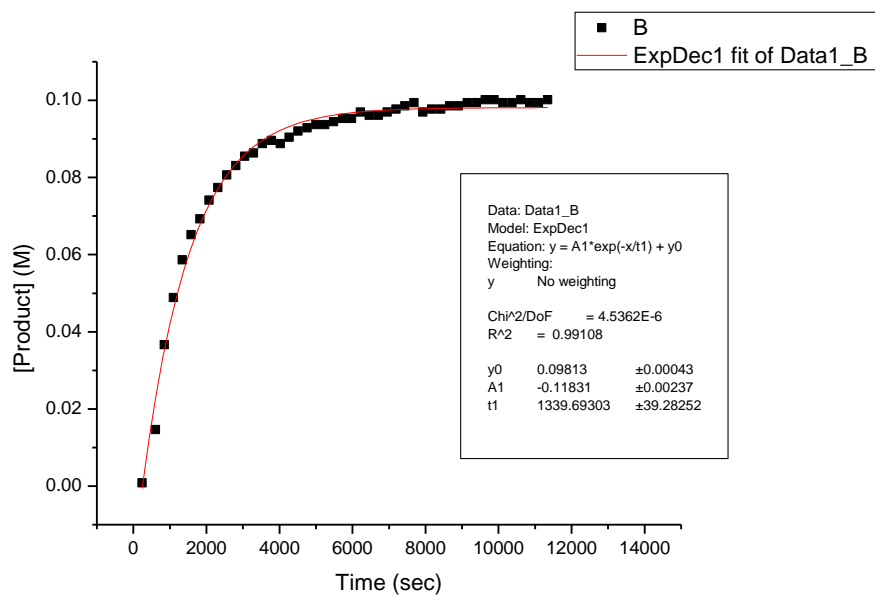


Figure 7.51 Plot of [11b] vs. time for order of AgNO_3

7.3.2.5 Activation Parameters for reaction of 7

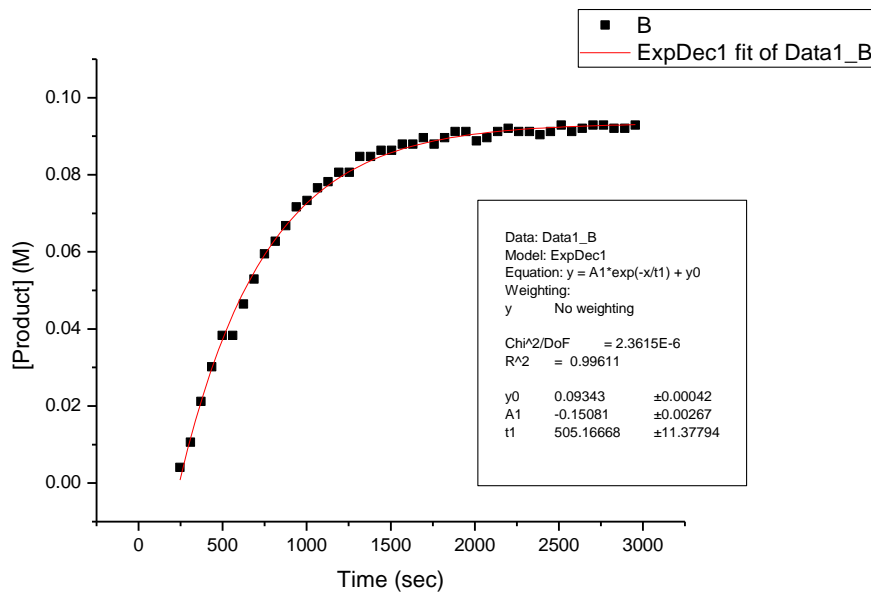


Figure 7.52 Plot of [8] vs. time for activation parameters at 30 °C

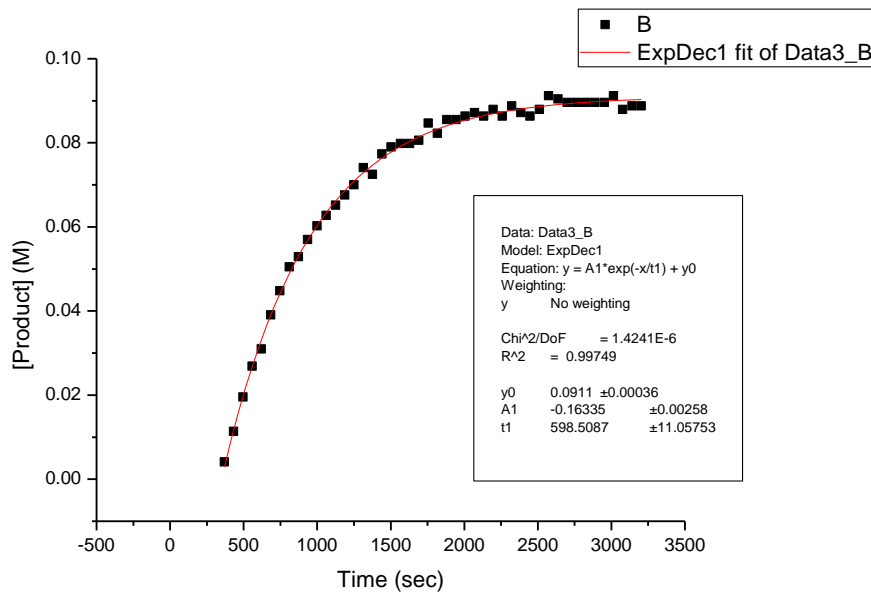


Figure 7.53 Plot of [8] vs. time for activation parameters at 35 °C

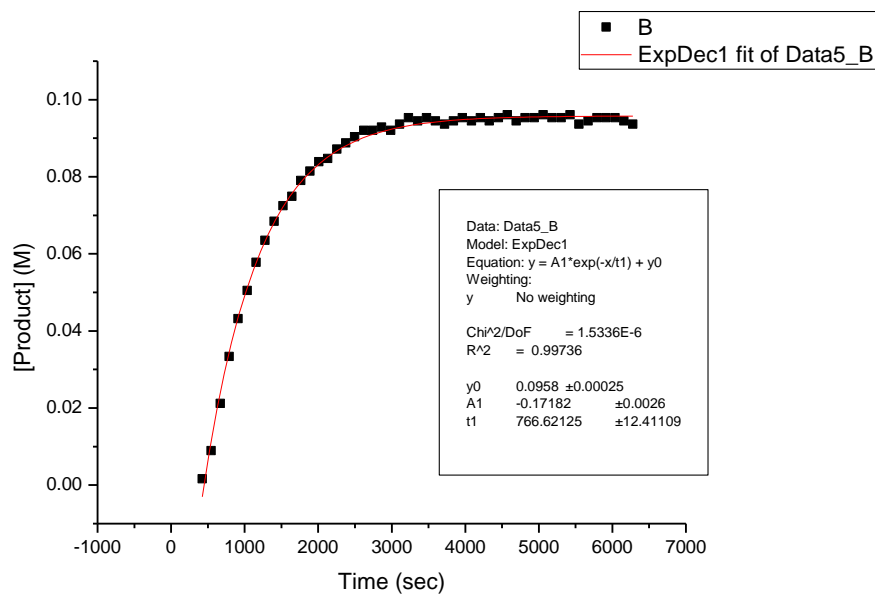


Figure 7.54 Plot of [8] vs. time for activation parameters at 40 °C

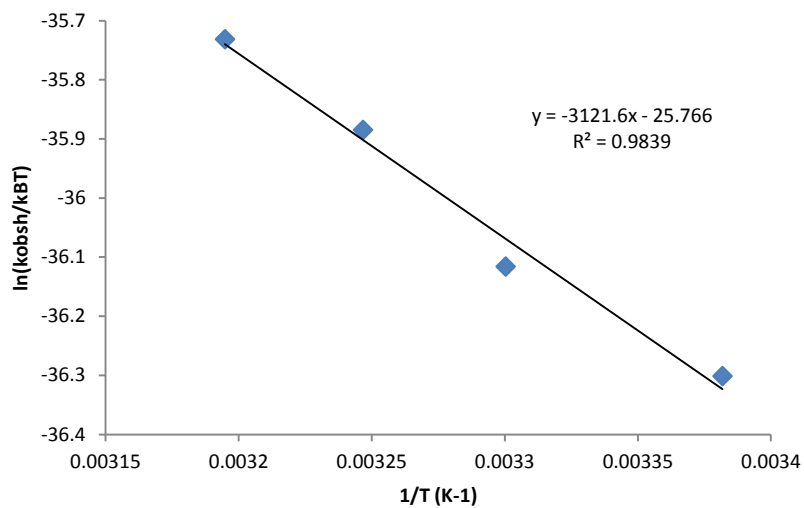


Figure 7.55 Activation Parameters for reaction of 7

Table 7.12 Activation Parameters for reaction of 7

ΔH^\ddagger (kcal/mol)	ΔS^\ddagger (cal/K·mol)	ΔG^\ddagger (kcal/mol) [at 23°C]	E_a (kcal/mol) [at 23°C]
6.2	-51.2	21.4	6.8

7.3.2.6 Reaction of 2,2-dimethylglutaric acid with sodium persulfate**Table 7.13 Persulfate Kinetic Studies Data Reaction Conditions**

run	[1] (M)	[AgNO ₃] (M)	[Na ₂ S ₂ O ₈] (M)	[F-TEDA-BF ₄] (M)	Excess F- TEDA-BF ₄ (M)
100%	0.1	0.02	0.05	0.2	0.1
Diffxs CA	0.07	0.02	0.05	0.2	0.1
Diffxs SF	0.1	0.02	0.05	0.15	0.05
Diffxs Ag	0.1	0.01	0.05	0.2	0.1
Diffxs Per	0.1	0.02	0.3	0.2	0.1

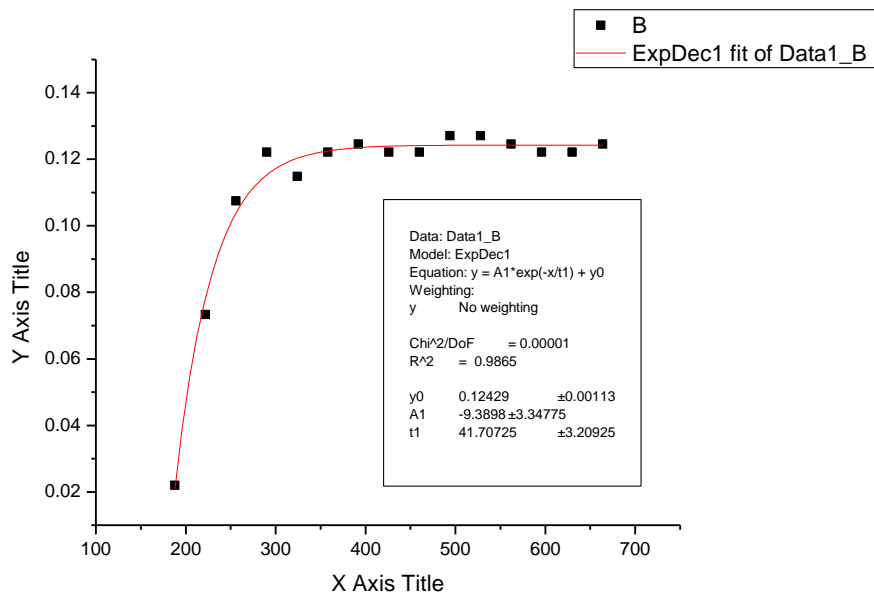


Figure 7.56 Plot of [9b] vs. time for 100% run

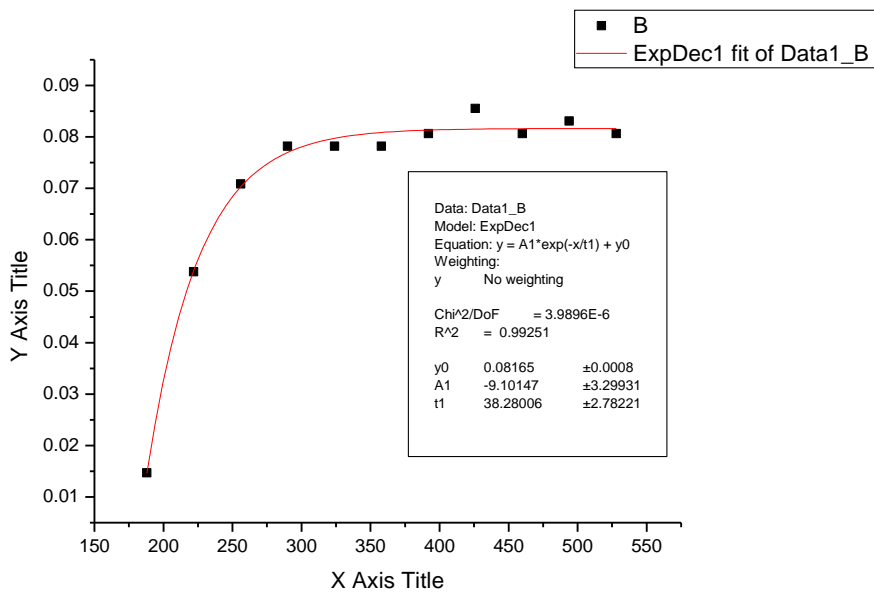


Figure 7.57 Plot of [9b] vs. time for order of 9

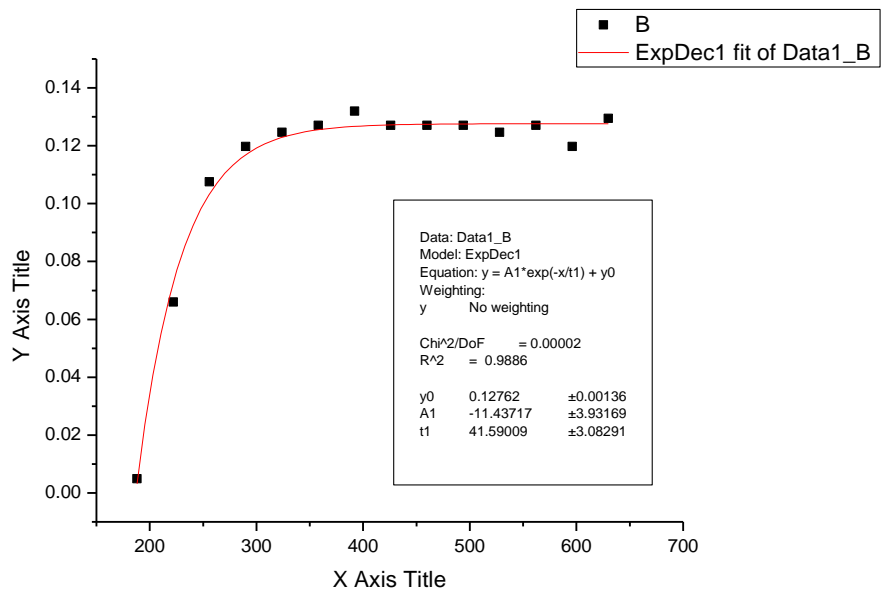


Figure 7.58 Plot of [9b] vs. time for order of Selectfluor

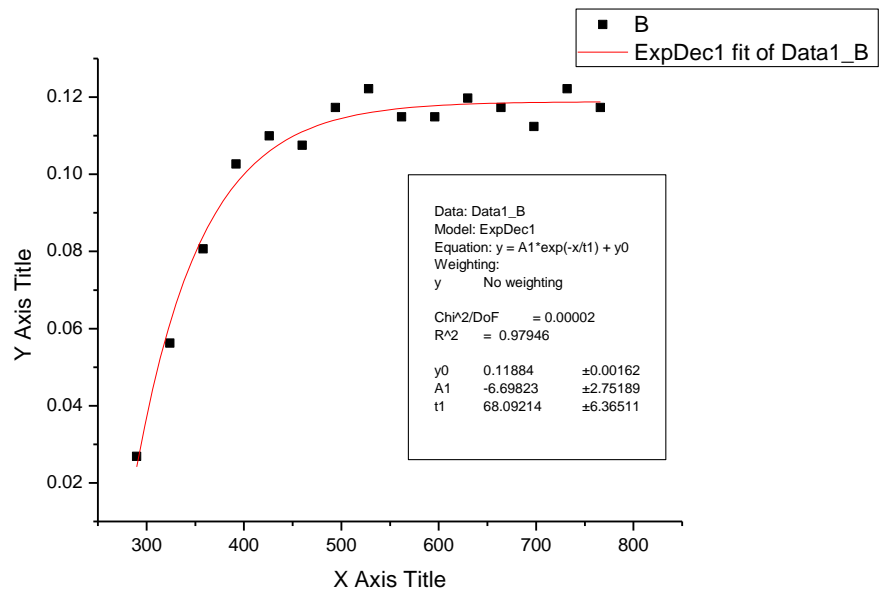


Figure 7.59 Plot of [9b] vs. time for order of AgNO₃

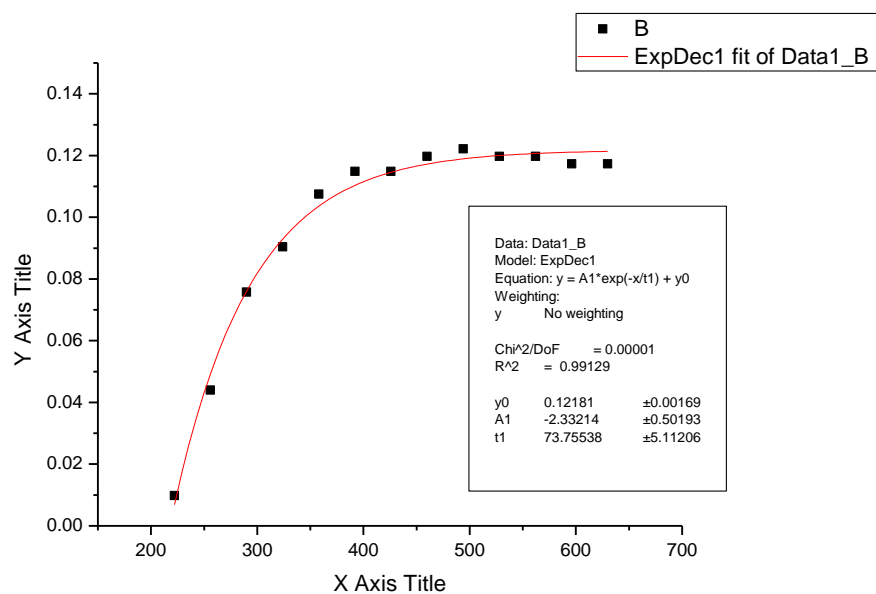


Figure 7.60 Plot of [9b] vs. time for order of sodium persulfate

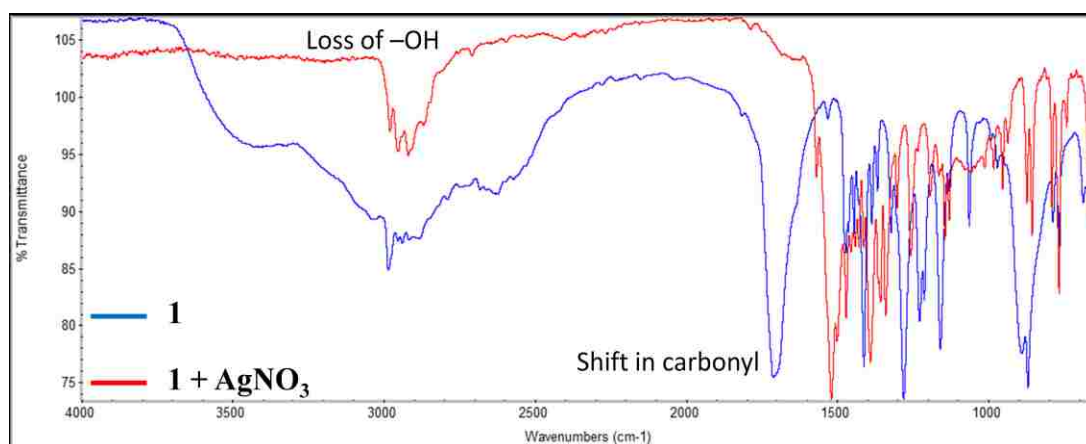


Figure 7.61 Ag-carboxylic acid interaction IR data

7.3.3 Data from NMR studies

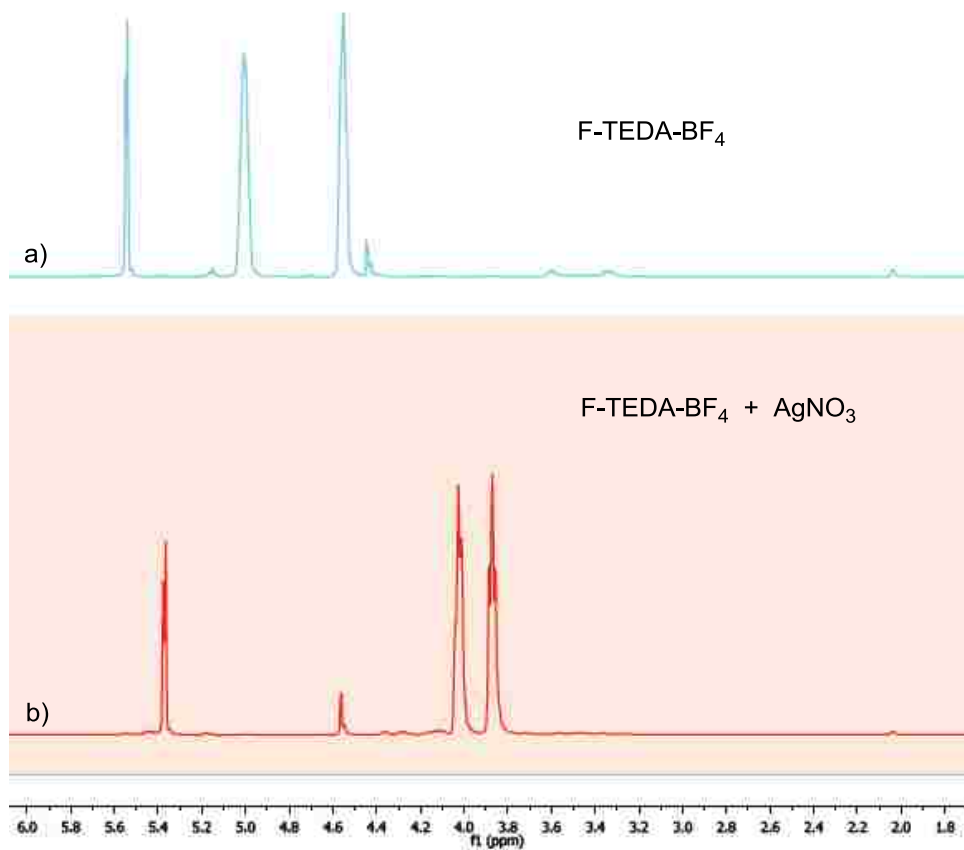


Figure 7.62 Proton NMR for Ag-Selectfluor interaction

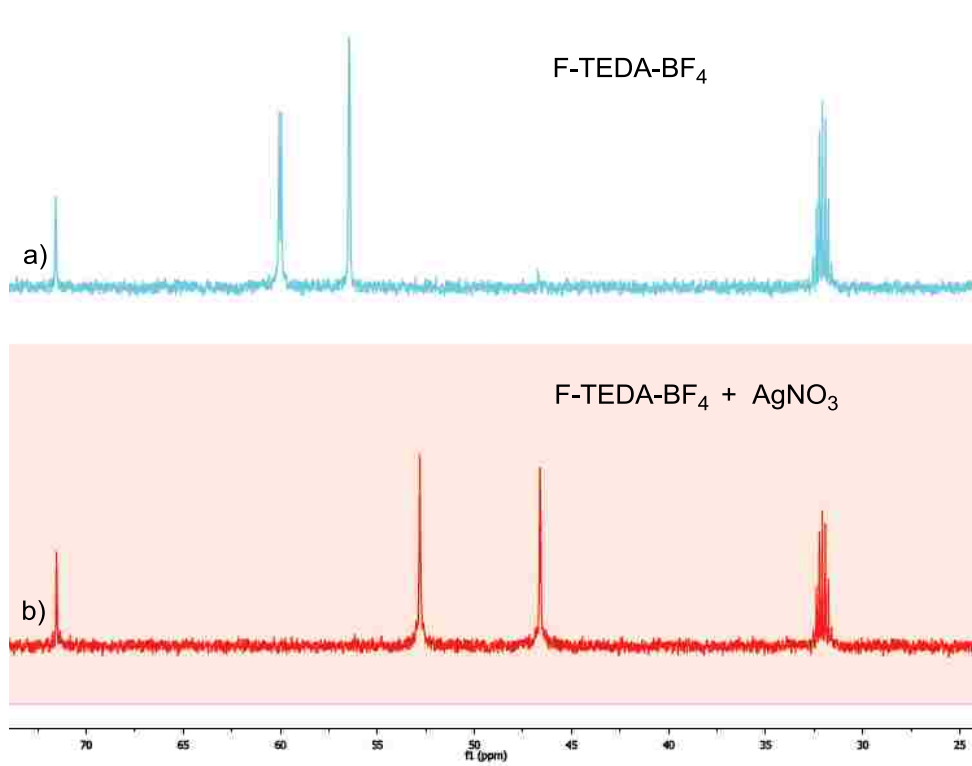


Figure 7.63 Carbon-13 NMR for Ag-Selectfluor interaction

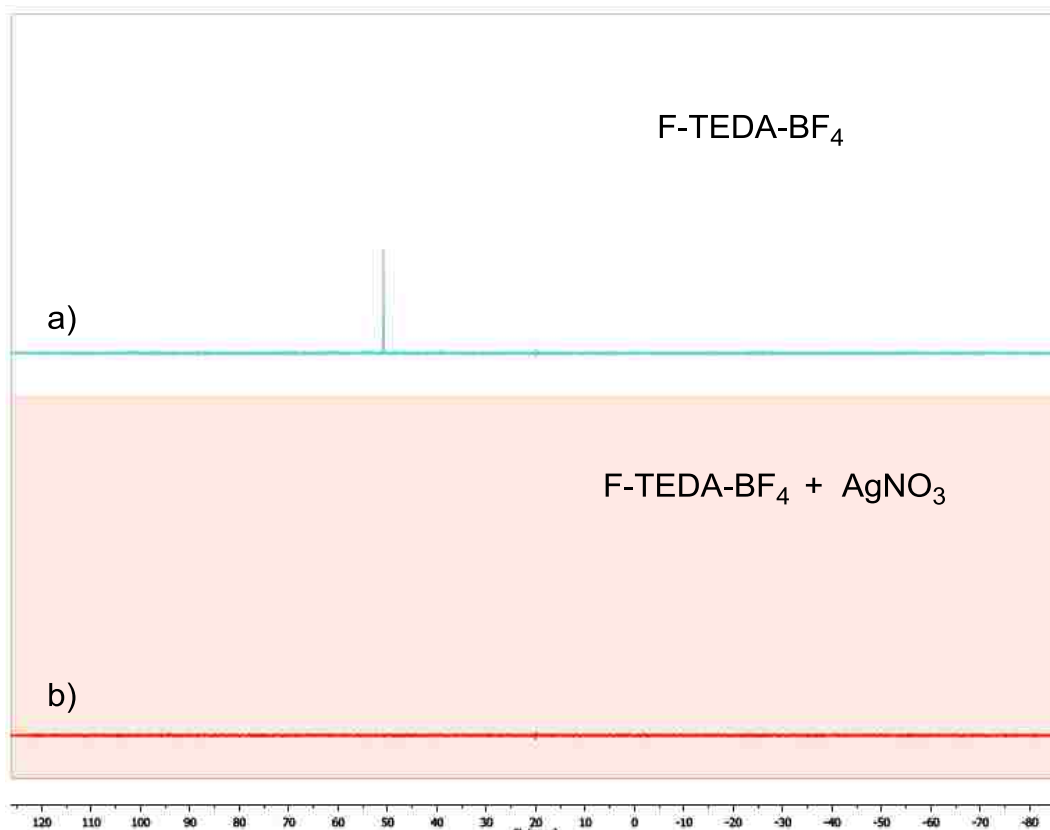


Figure 7.64 Fluorine-19 NMR for Ag-Selectfluor interaction

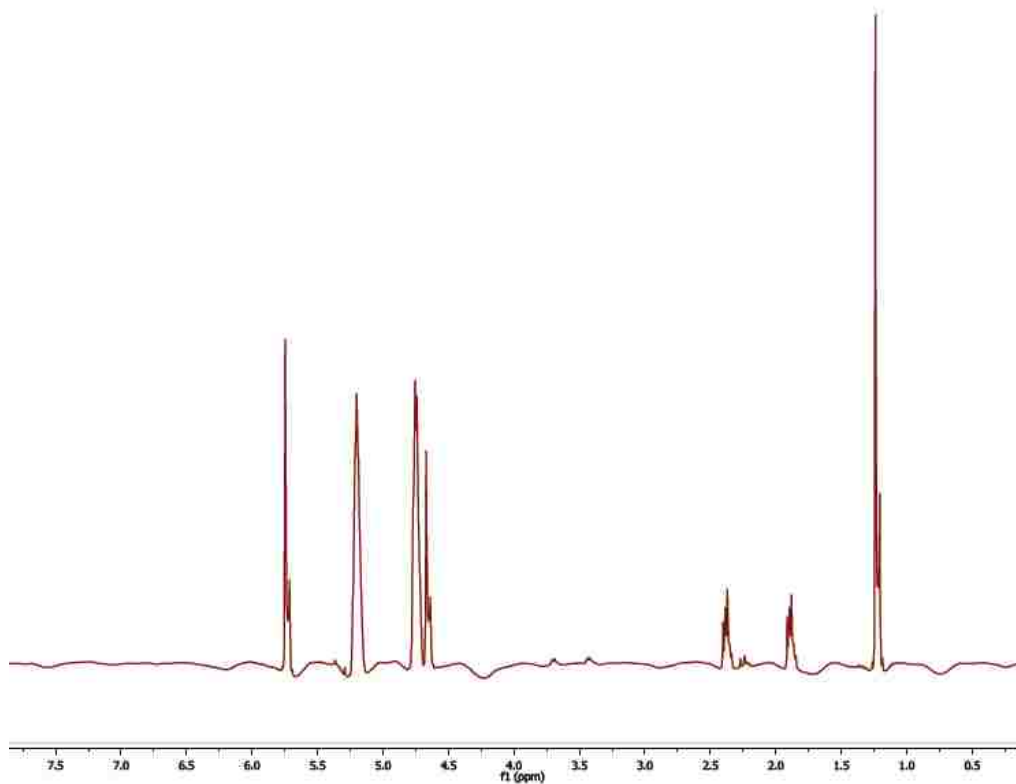


Figure 7.65 Monitoring the reaction of **7** by proton NMR @ time = 30 sec

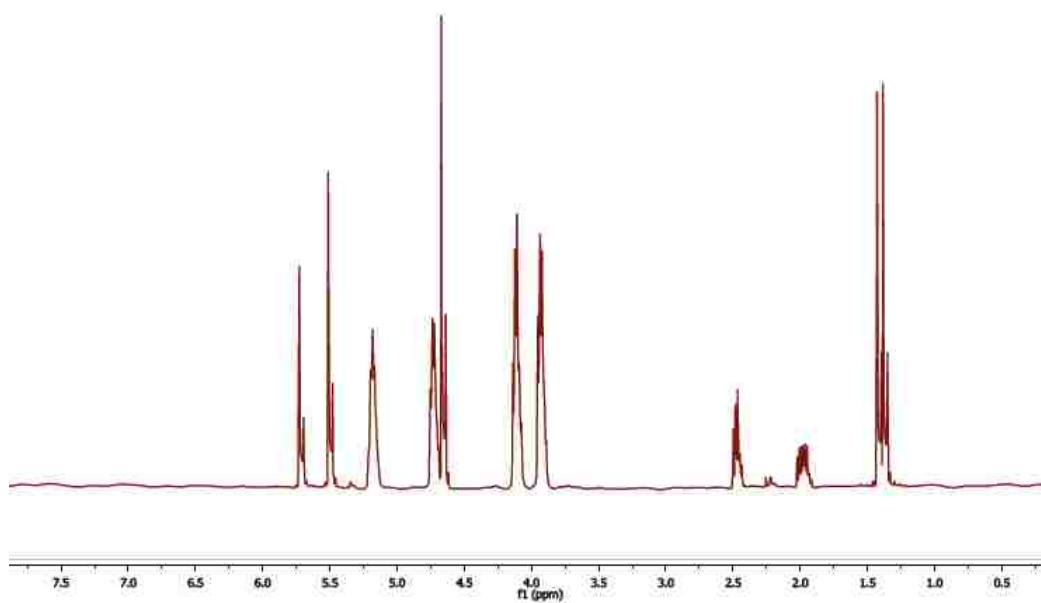


Figure 7.66 Monitoring the reaction of **7** by proton NMR @ time = 110 min

Ag-ligand NMRs with addition of F-TEDA-BF₄

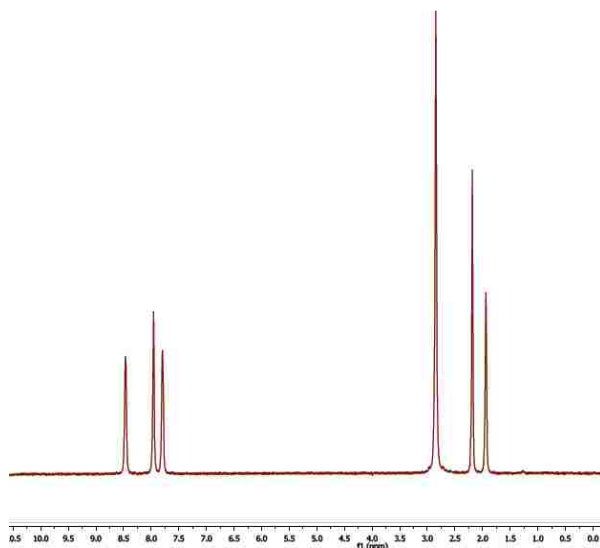


Figure 7.67 ¹H NMR spectrum of dmp with 1 equiv AgNO₃ in MeCN-d₃.

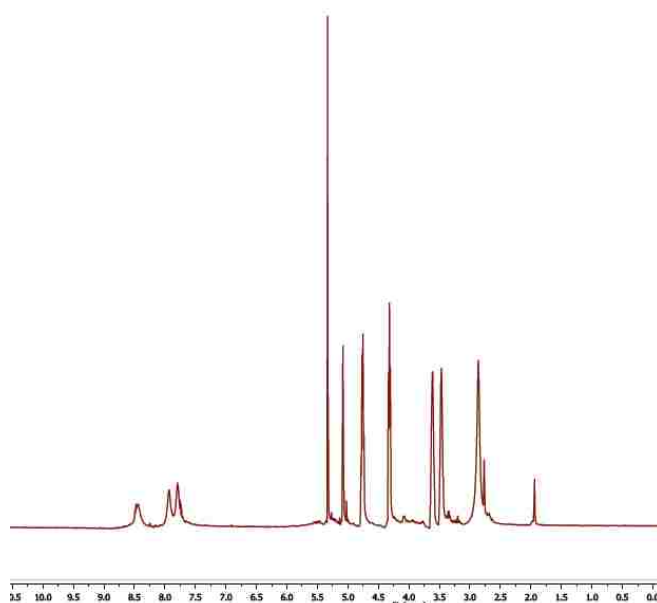


Figure 7.68 ¹H NMR spectrum of dmp with 1 equiv AgNO₃ and Selectfluor in MeCN-d₃.

Terpyridine:

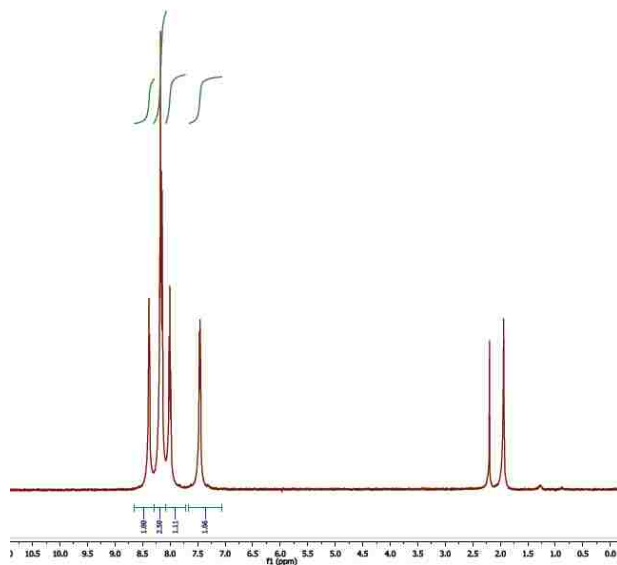


Figure 7.69 ¹H NMR spectrum of terpy with 1 equiv AgNO₃ in MeCN-d₃.

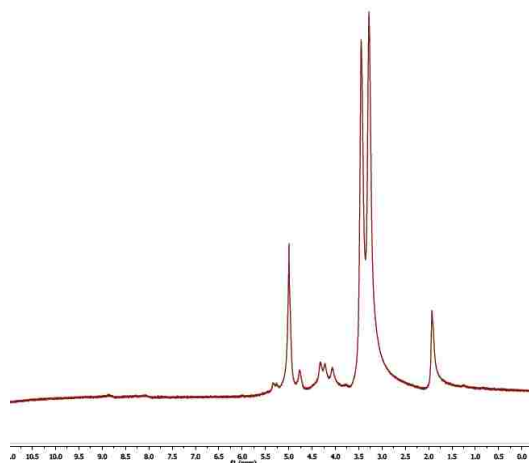


Figure 7.70 ¹H NMR spectrum of terpy with 1 equiv AgNO₃ and Selectfluor in MeCN-d₃.

BEt₃ reaction with Selectfluor

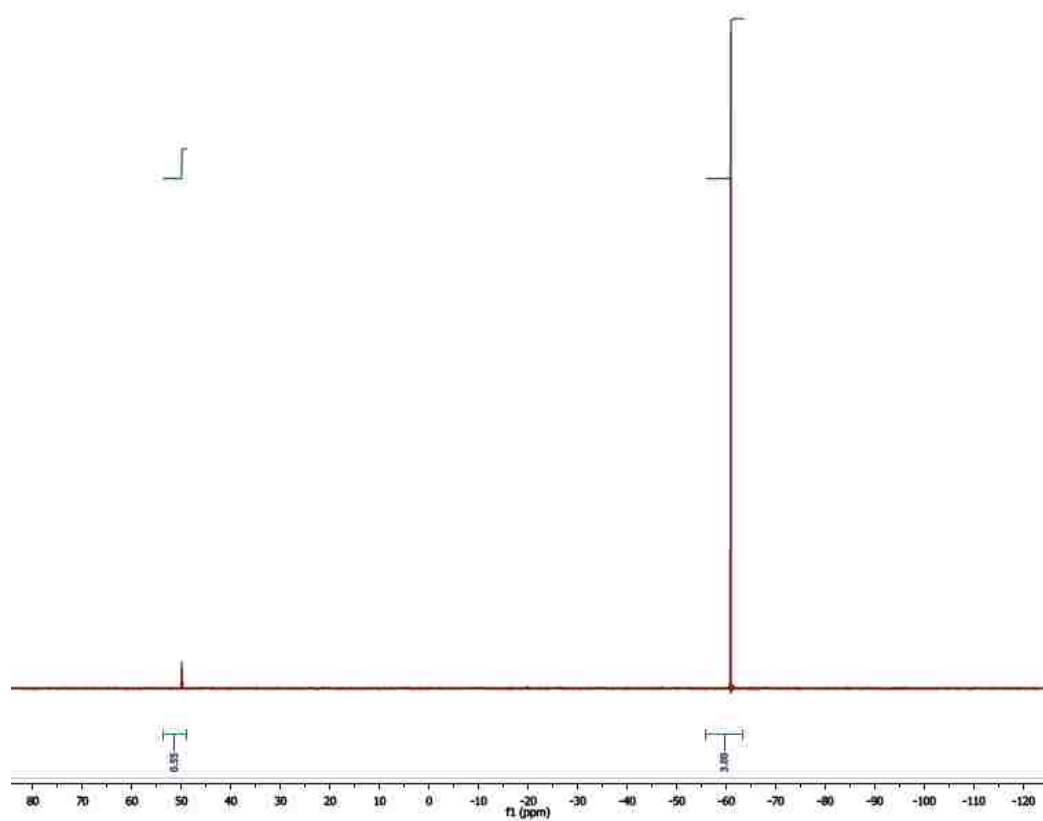


Figure 7.71 Proton NMR of BEt₃ reaction with Selectfluor at t = 0 h (Integration 0.55 = 0.043 M)

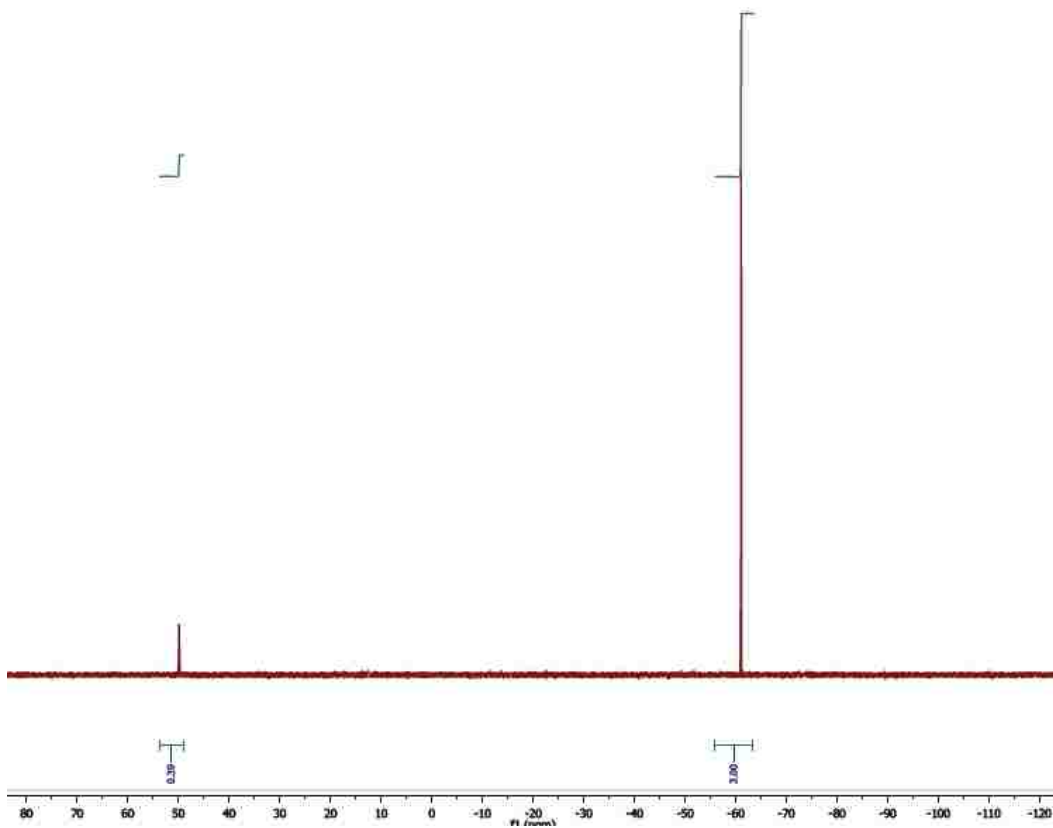


Figure 7.72 Proton NMR of BEt_3 reaction with Selectfluor at $t = 5$ h (Integration 0.39 = 0.031 M)

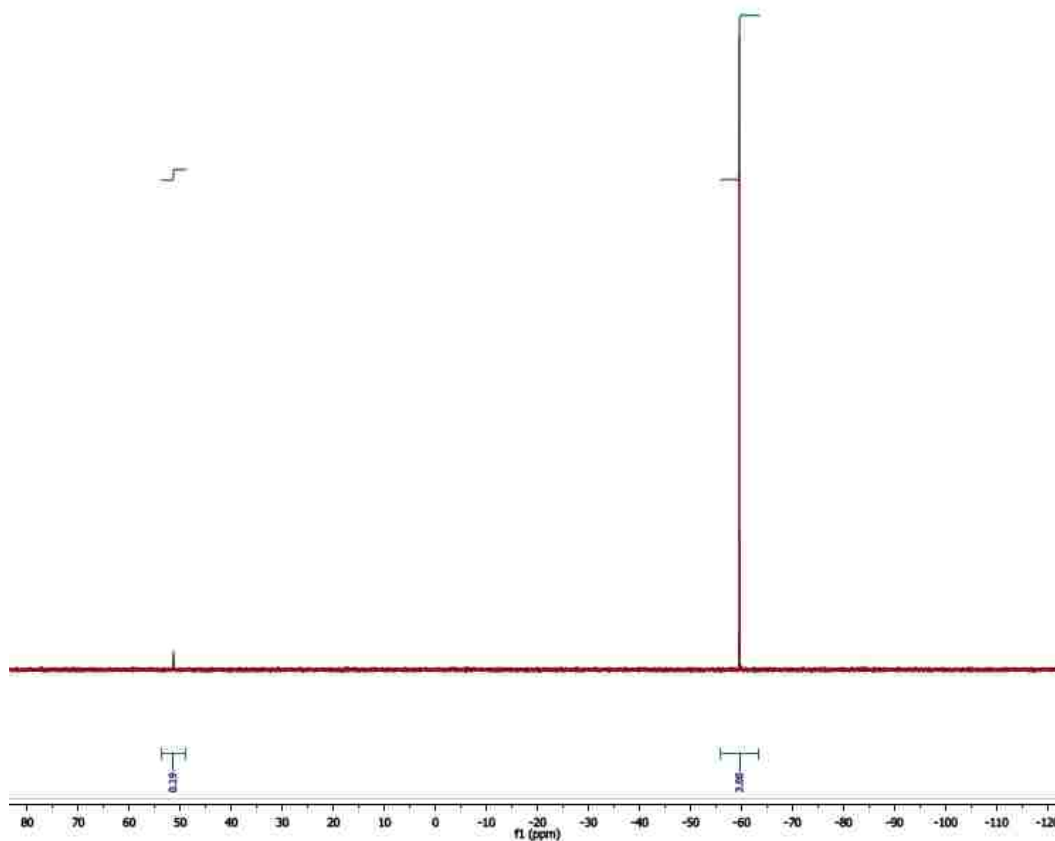


Figure 7.73 Proton NMR of BEt₃ reaction with Selectfluor at t = 23 h (Integration 0.19 = 0.015 M)

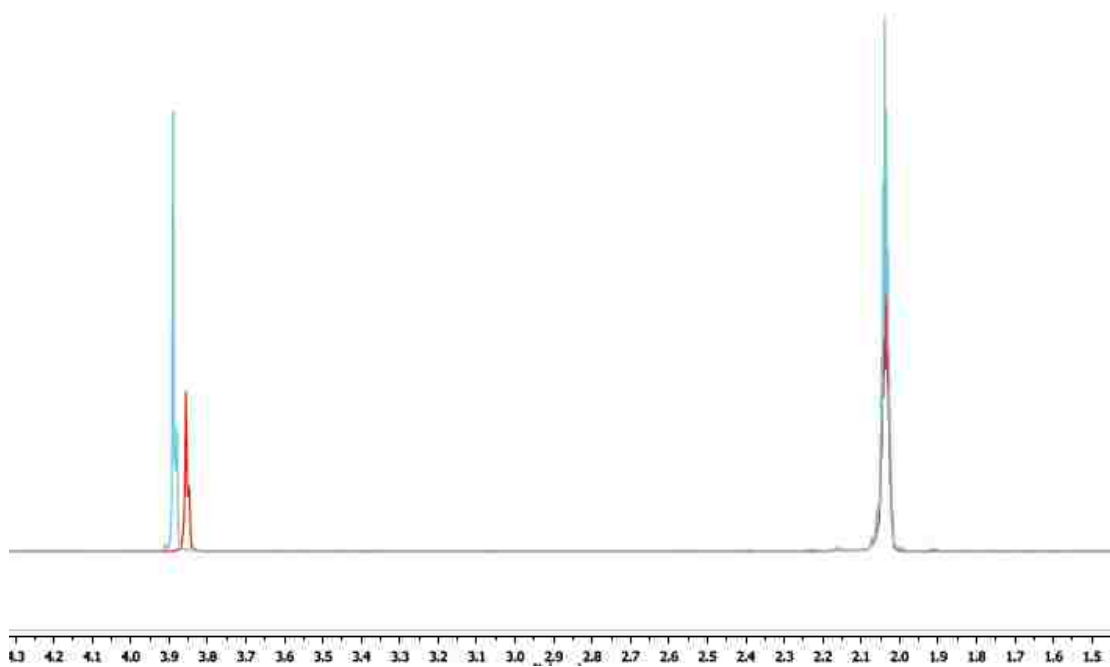


Figure 7.74 Proton NMR spectra of water interaction with AgNO_3 in 9:1 acetone:water

NMR Spectra for 8 (4-fluoro-4-methylpentanoic acid)

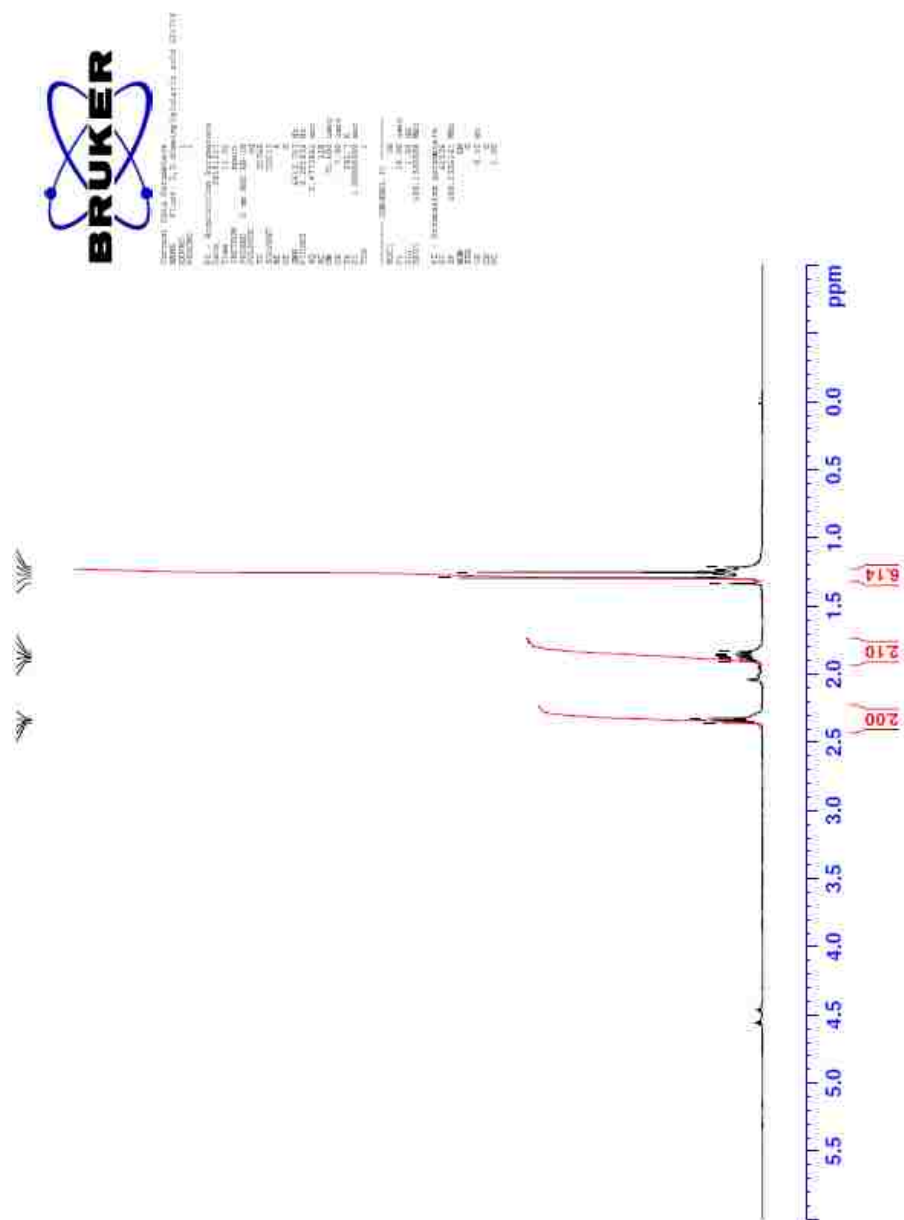


Figure 7.75 ¹H NMR Spectrum of 8 (4-fluoro-4-methylpentanoic acid)

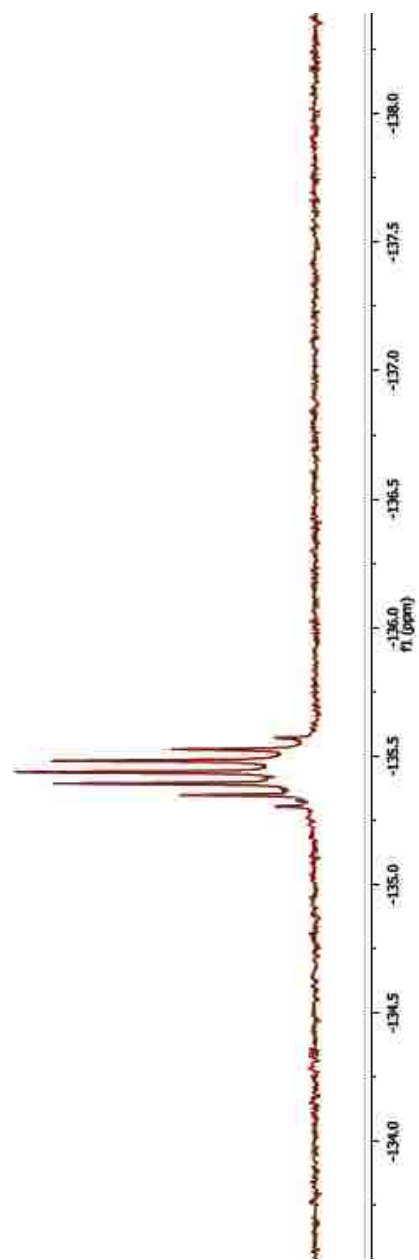


Figure 7.77 ^{19}F NMR Spectrum of **8** (4-fluoro-4-methylpentanoic acid)

NMR Spectra for 9b (2-fluoro-2-methylbutane)

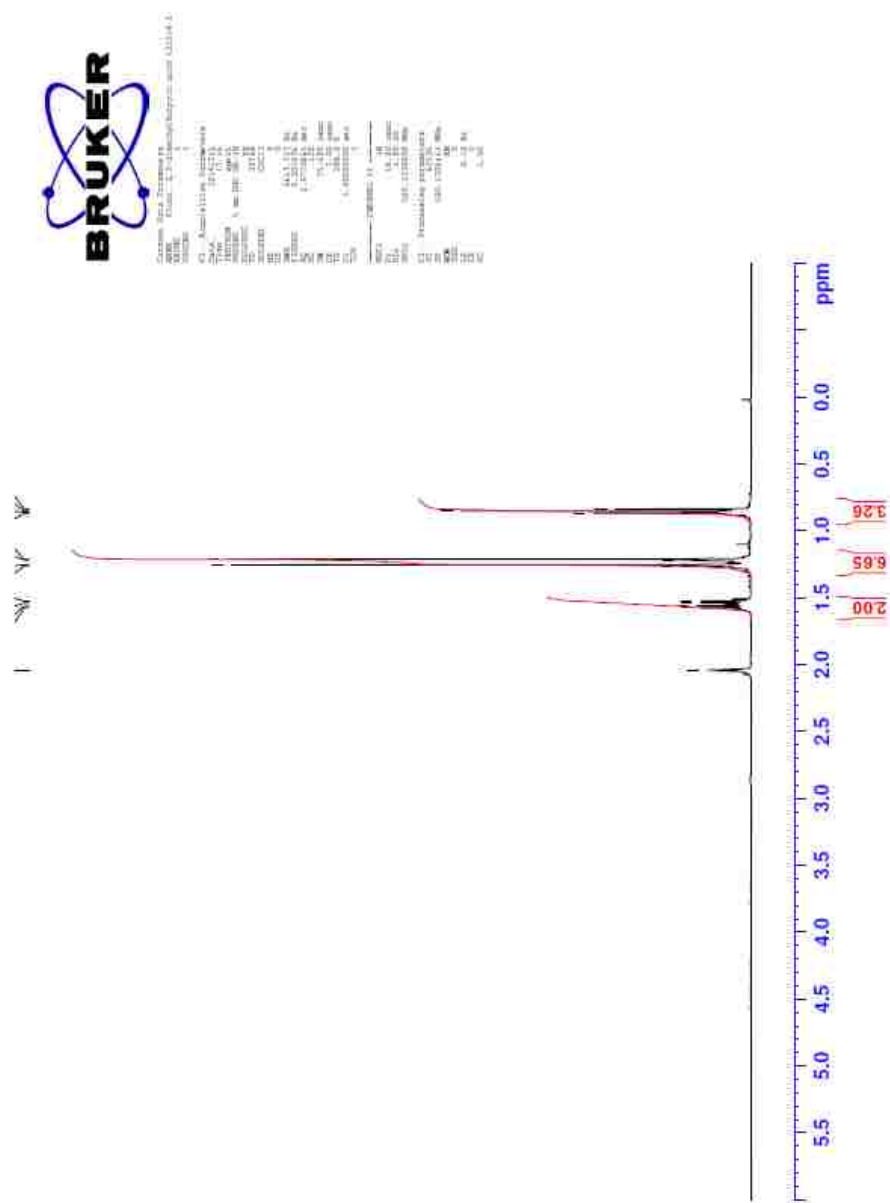


Figure 7.78 ¹H NMR Spectrum of 9b (2-fluoro-2-methylbutane)

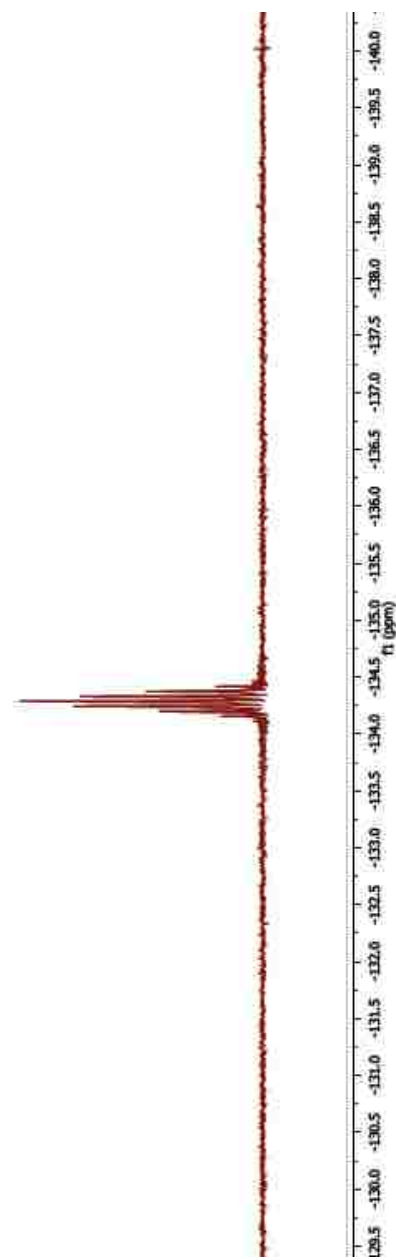


Figure 7.80 ^{19}F NMR Spectrum of **9b** (2-fluoro-2-methylbutane)

NMR Spectra for 10a (2,2-dimethyl-3-phenylpropanoic acid)

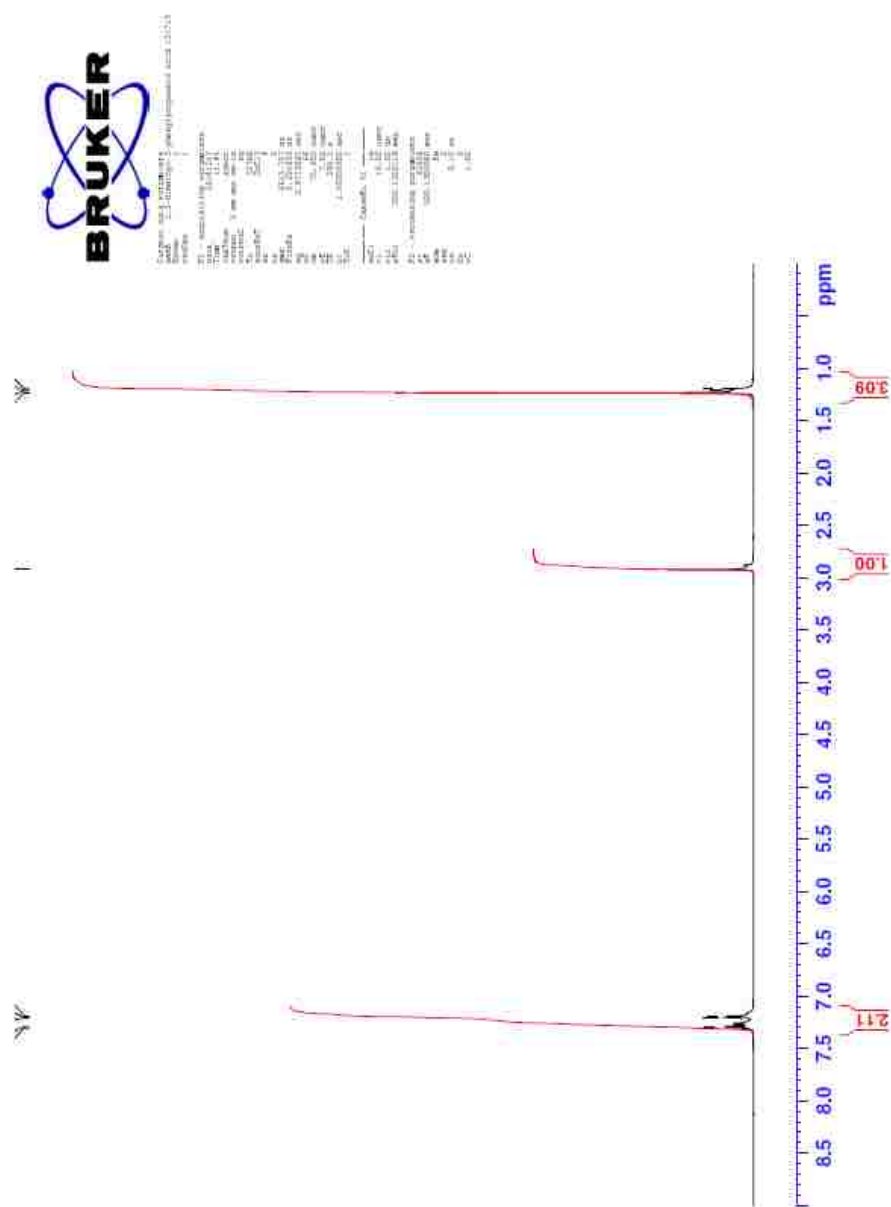


Figure 7.81 ¹H NMR Spectrum of 10a (2,2-dimethyl-3-phenylpropanoic acid)

NMR Spectra for 10b ((2-fluoro-2-methylpropyl)-benzene)

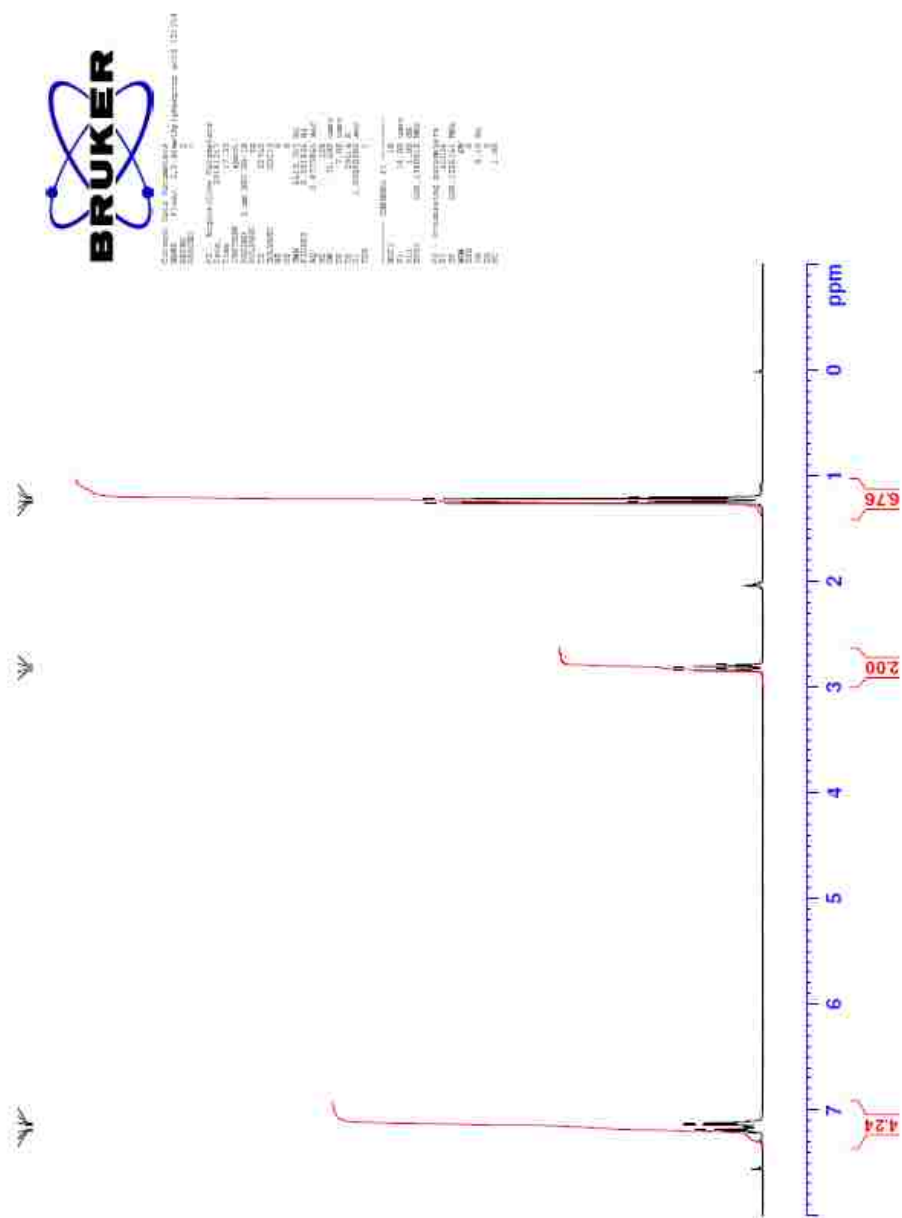


Figure 7.83 ¹H NMR Spectrum of 10b ((2-fluoro-2-methylpropyl)-benzene)

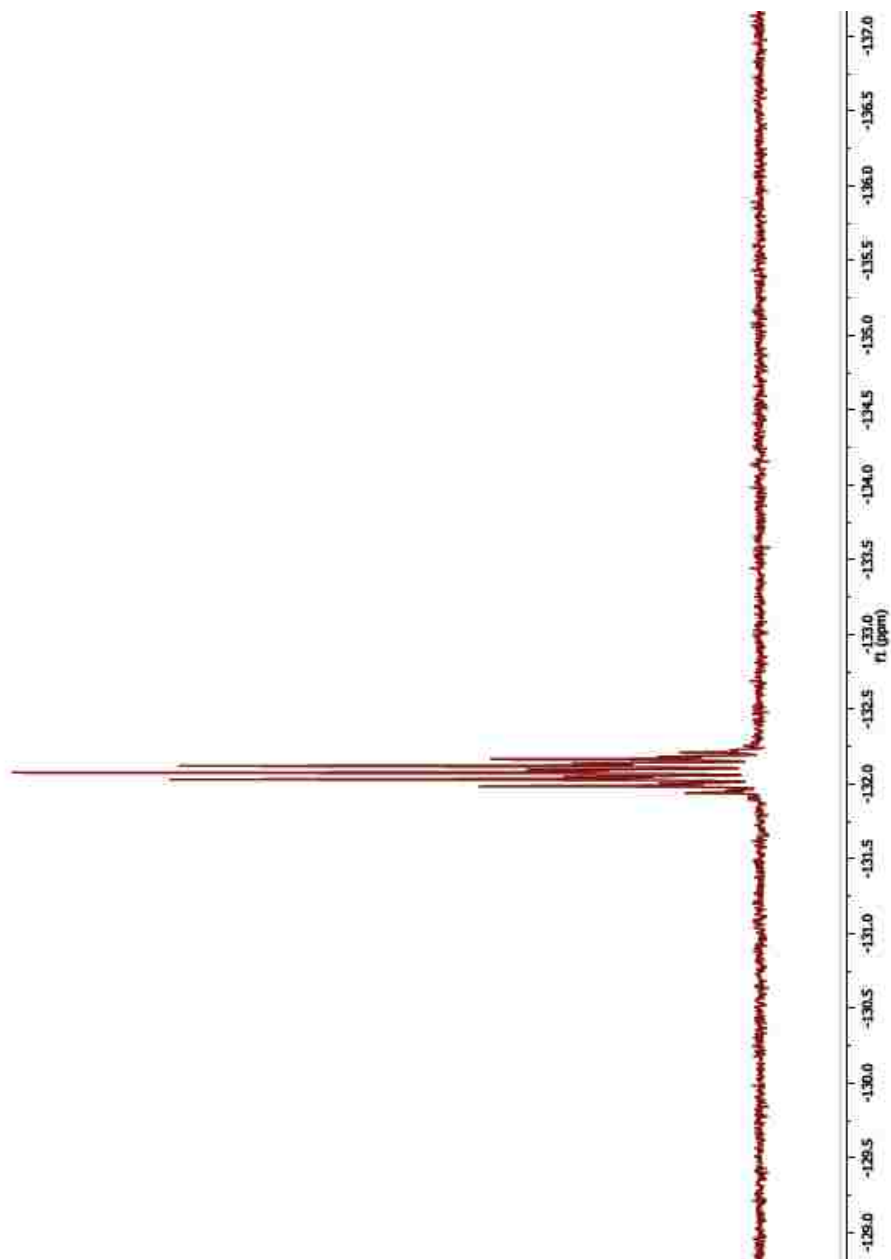


Figure 7.85 ^{19}F NMR Spectrum of **10b** ((2-fluoro-2-methylpropyl)-benzene)

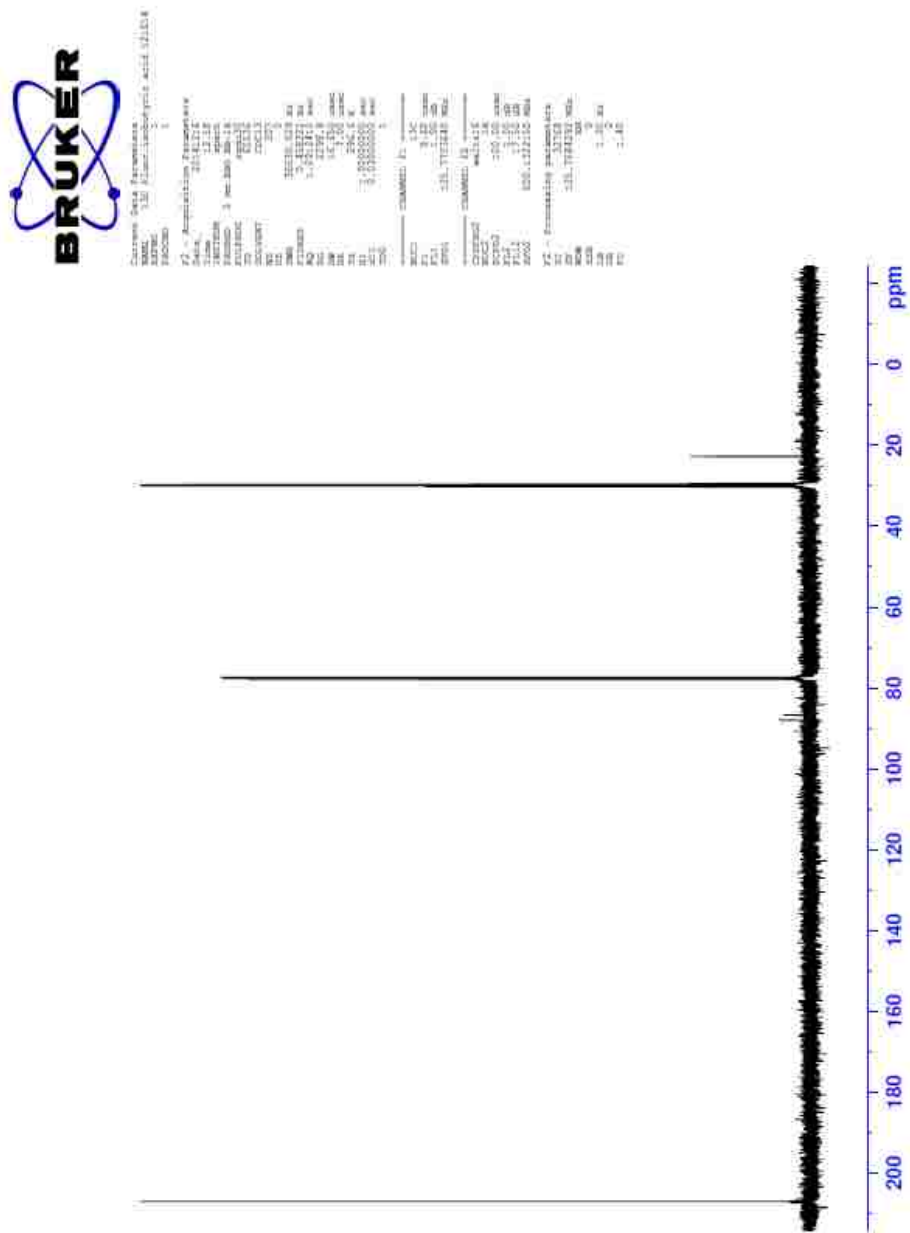


Figure 7.87 ^{13}C NMR Spectrum of **11b** (2-fluoropropane)

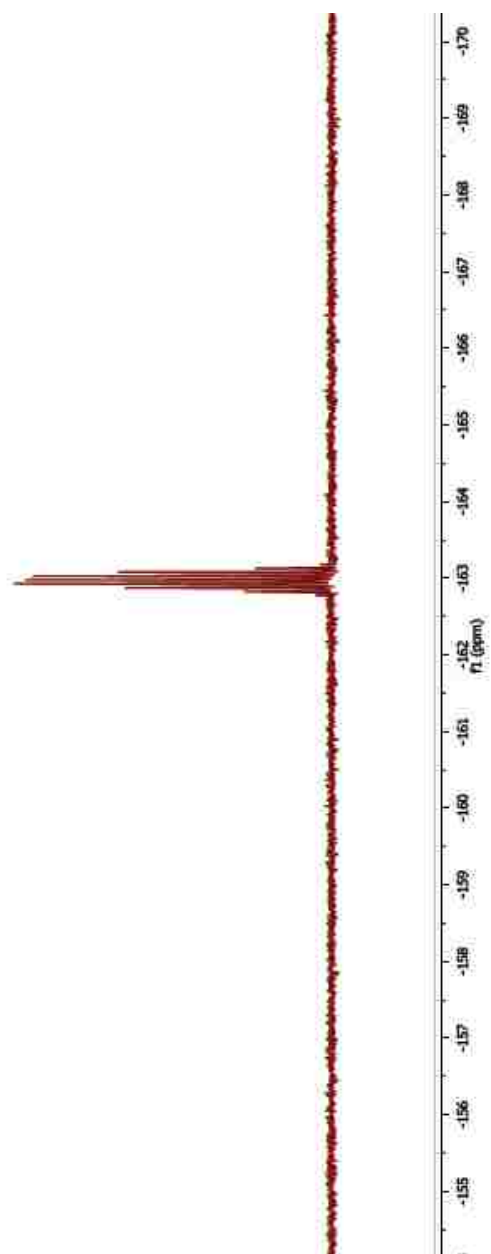


Figure 7.88 ^{19}F NMR Spectrum of **11b** (2-fluoropropane)

7.4 Mechanistic study of decarboxylative fluorination with N-containing ligand in non-aqueous media

7.4.1 Data from kinetic studies

7.4.1.1 AgOTf-ligand reaction

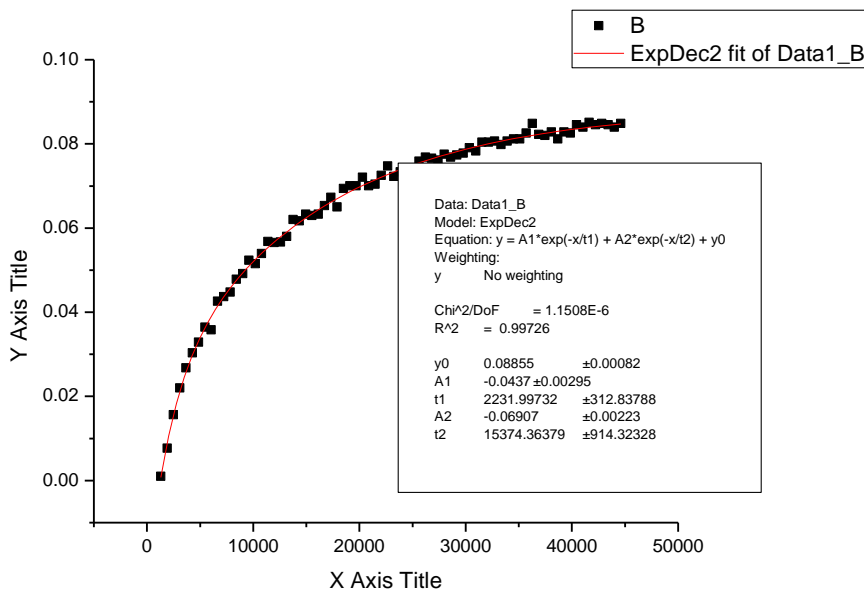


Figure 7.89 Plot of [9b] vs. time for 100% run

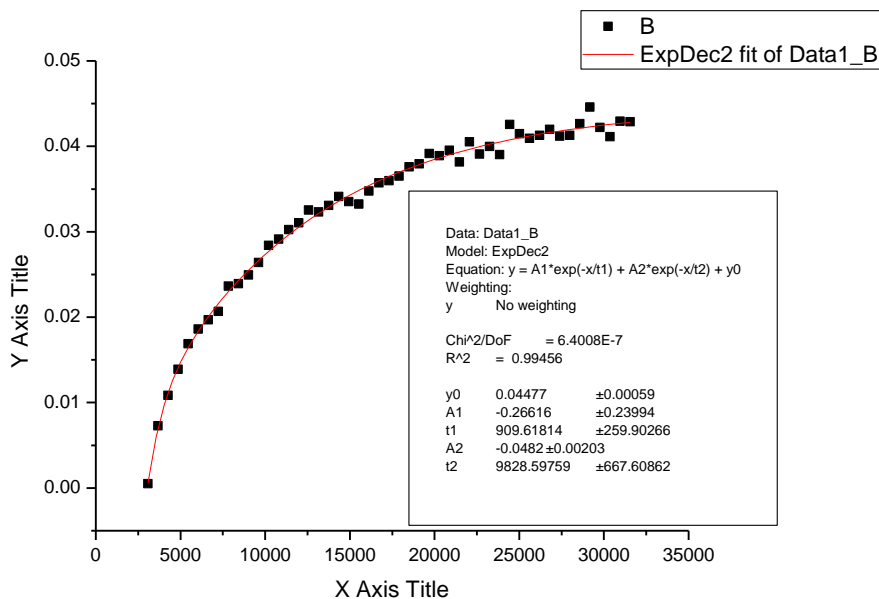


Figure 7.90 Plot of [9b] vs. time for 50% run

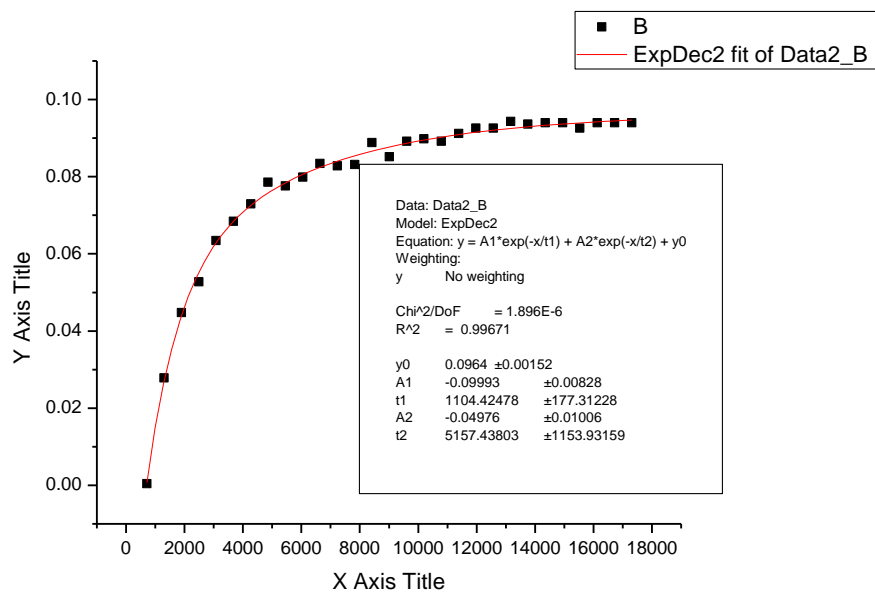


Figure 7.91 Plot of [9b] vs. time for order of AgOTf

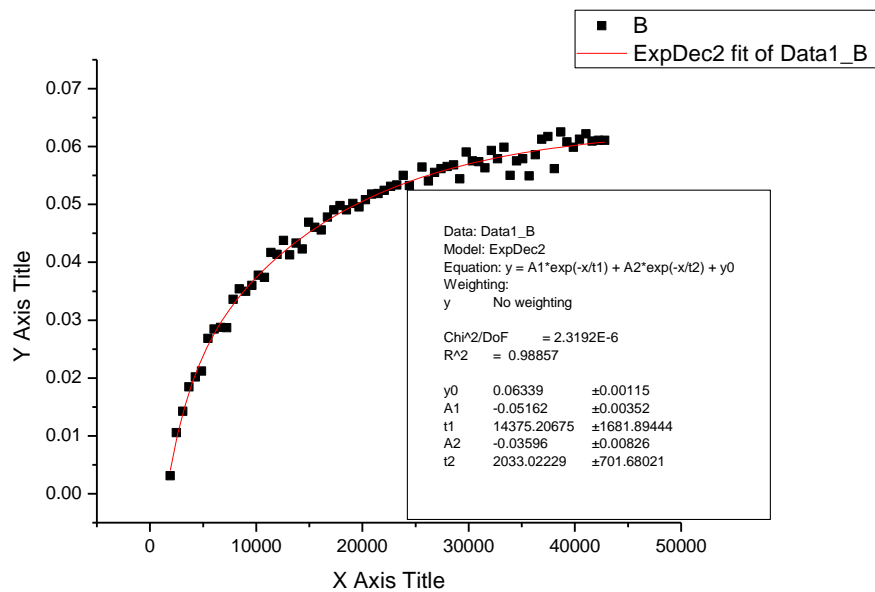


Figure 7.92 Plot of [9b] vs. time for order of Selectfluor

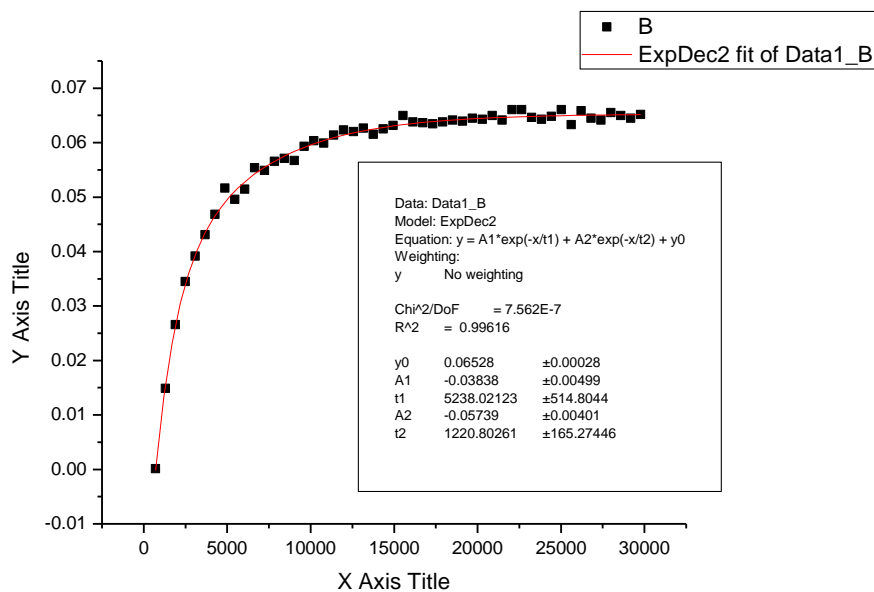


Figure 7.93 Plot of [9b] vs. time for order of 9

7.4.1.2 AgNO₃-ligand

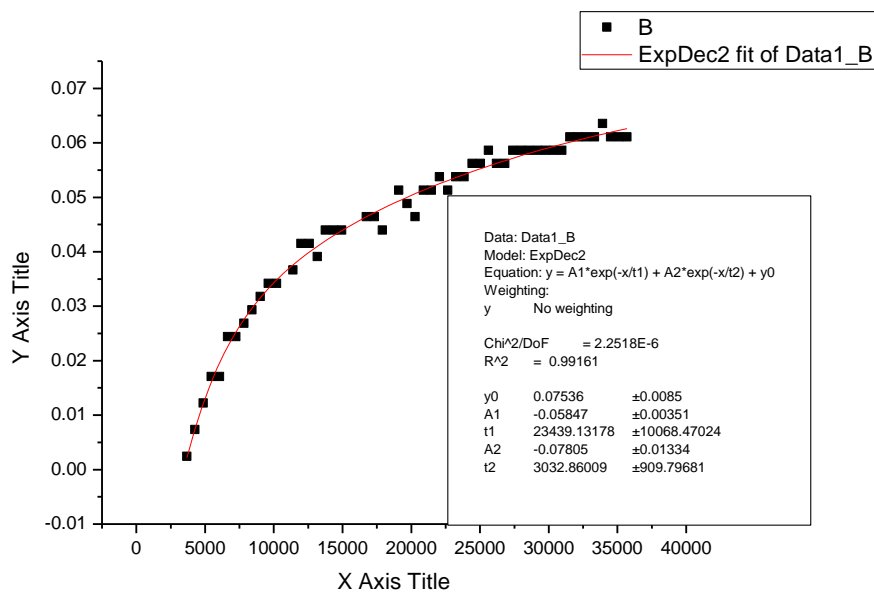


Figure 7.94 Plot of [9b] vs. time for 100% run

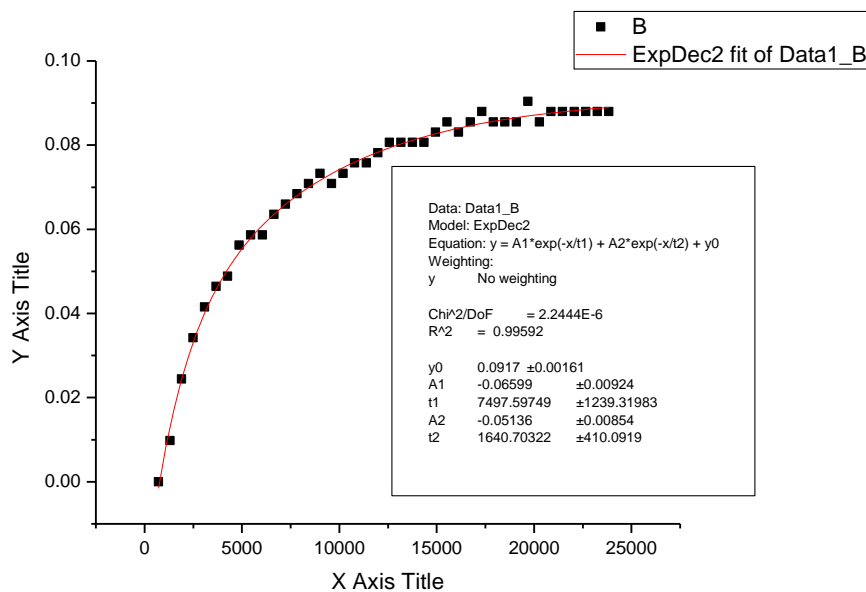


Figure 7.95 Plot of [9b] vs. time for order of AgNO_3

7.4.1.3 AgOTf-Ligand-Persulfate

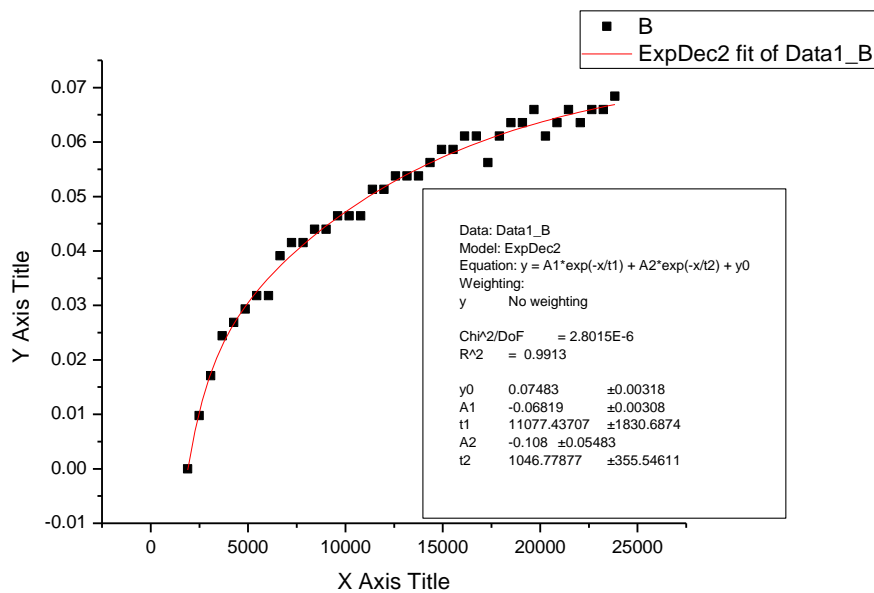


Figure 7.96 Plot of [9b] vs. time for 100% run in Persulfate reaction

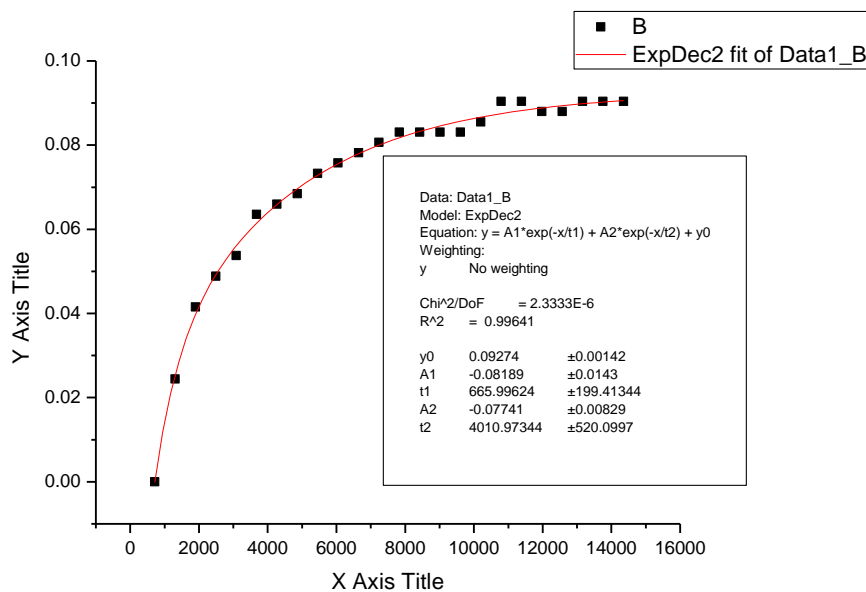


Figure 7.97 Plot of [9b] vs. time for order of AgOTf in Persulfate reaction

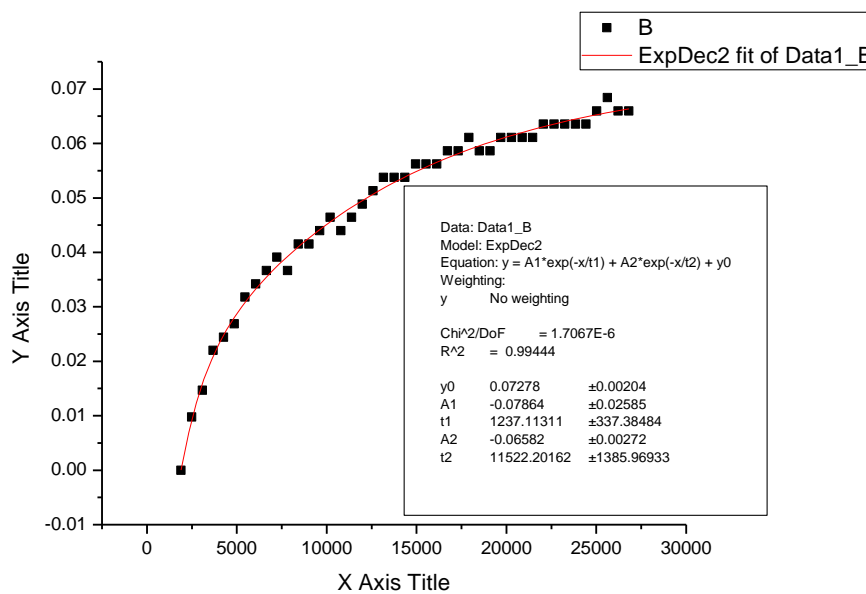


Figure 7.98 Plot of [9b] vs. time for order of sodium persulfate in Persulfate reaction

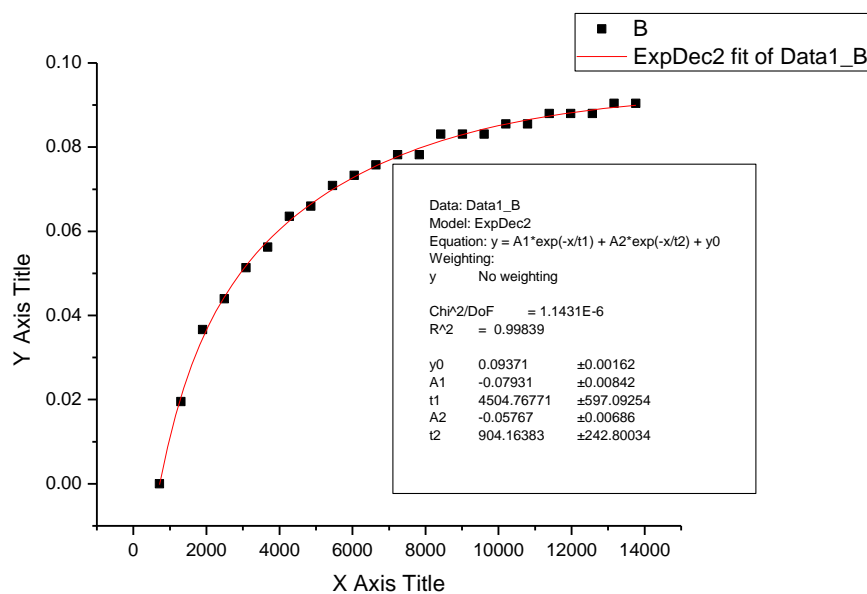


Figure 7.99 Plot of [9b] vs. time for order of Selectfluor in Persulfate reaction

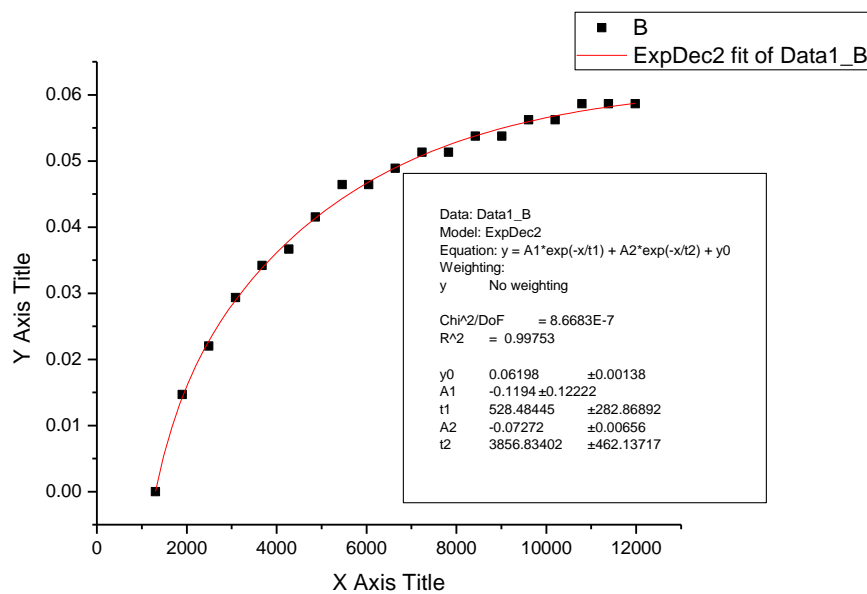


Figure 7.100 Plot of [9b] vs. time for order of 9 in Persulfate reaction

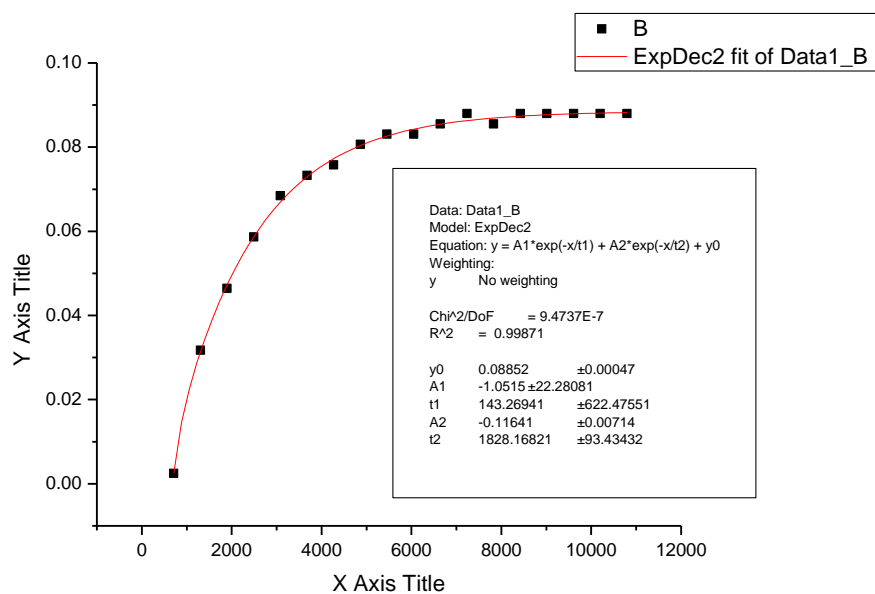


Figure 7.101 Plot of [9b] vs. time using 50 mol% catalysts for order of AgOTf in Persulfate reaction

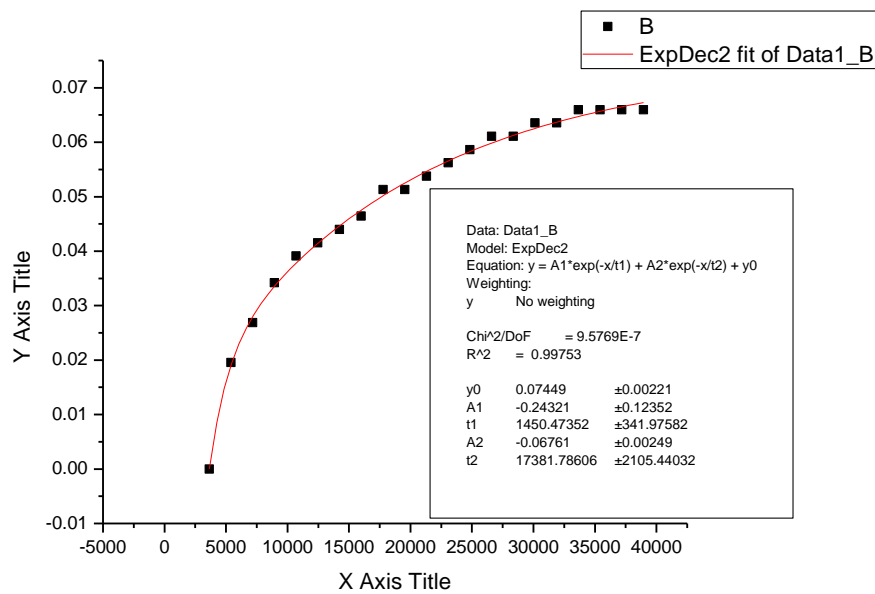


Figure 7.102 Plot of [9b] vs. time for order of TBApersulfate using 0.3 equiv

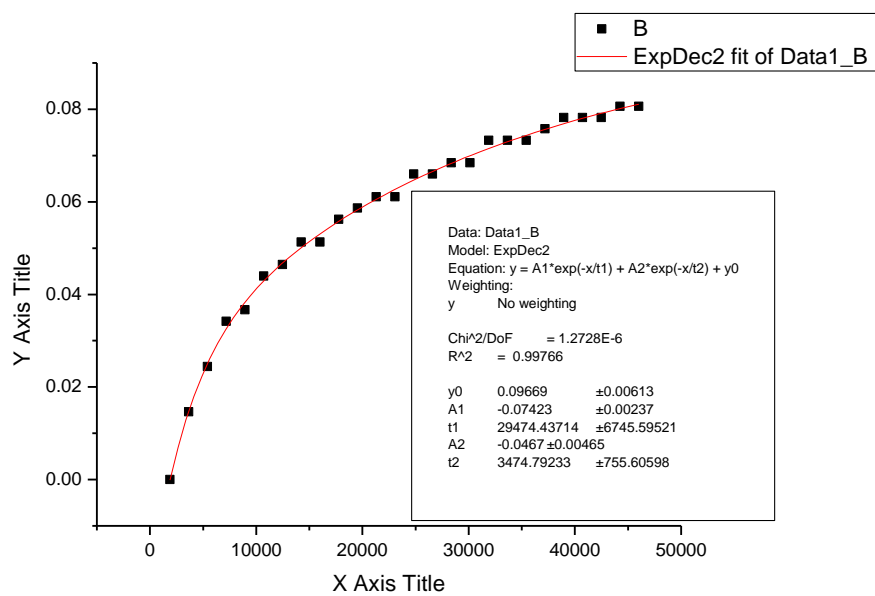


Figure 7.103 Plot of [9b] vs. time for order of TBAPersulfate using 0.1 equiv

Niki Patel
1910 Reilly Road
Philadelphia, PA 19115
nrp210@lehigh.edu / 267-303-4976

Education

Lehigh University
Bethlehem, PA
Ph.D., Organic Chemistry 2010 – present

Lehigh University
Philadelphia, PA
M.S., Chemistry 2010 – 2012

Temple University
Philadelphia, PA
B.S., Chemistry 2006 – 2010

Publications

Patel, N. R., Flowers, R. A., II. On the Mechanism of Silver-Catalyzed Decarboxylative Fluorination. *In preparation*. **2015**.

Patel, N. R., Flowers, R. A., II. Uncovering the Mechanism of the Ag(I)/Persulfate-Catalyzed Cross-Coupling Reaction of Arylboronic Acids and Heteroarenes. *J. Am. Chem. Soc.* **2013**, *135* (12), 4672–4675.

Conference Presentations

American Chemical Society National Meeting, Denver, CO

- *On the Mechanism of Silver-Catalyzed Decarboxylative Fluorination*
- Oral Presentation
- March 23, 2014

ACS Division of Organic Chemistry Graduate Research Symposium, Irvine, CA

- *On the Mechanism of Silver-Catalyzed Decarboxylative Fluorination*
- Oral Presentation (Selected Speaker)
- July 25, 2014

National Organic Symposium, Seattle, WA

- *On the Mechanism of Ag(I)-Catalyzed Decarboxylative Fluorination*
- Poster Presentation
- June 26, 2013

Lehigh University, College of Arts and Science Research Symposium

- *Uncovering the Mechanism of the Silver(I)/Persulfate-Catalyzed Cross-Coupling of Arylboronic Acids with Heteroarenes*
- Poster Presentation
- March 25, 2013

American Chemical Society National Meeting, Philadelphia, PA

- *Uncovering the Mechanism of the Silver(I)/Persulfate-Catalyzed Cross-Coupling of Arylboronic Acids with Heteroarenes*
- Oral Presentation
- August 20, 2012

Research Experience

Lehigh University, Research Assistant (December 2010-present)

Bethlehem, PA

- Adviser: Professor Robert A. Flowers
- Mechanistic studies of Ag(I)-catalyzed reactions
- Mechanistic studies of Yb(III)-mediated reactions
- Experienced in methods of kinetic analysis of complex reactions
- Applied understanding from kinetic studies to method development
- Mentored undergraduate students
- Instrumentation: GC, GC-MS, LC-MS, UV-Vis, FTIR, NMR (^1H , ^{13}C , ^{11}B , and ^{19}F), Glovebox, Stopped-Flow Spectrophotometry, React-IR
- Laboratory Skills: chemical kinetics measurements, crystallization, column chromatography, organic synthesis, purification techniques, spectral analysis, advanced wet chemistry
- Technical Skills: MS Excel, Word, Powerpoint, Origin, SciFinder Scholar, Chembiodraw

Temple University, Undergraduate Researcher (January 2009-May 2010)

Philadelphia, PA

- Adviser: Professor Scott McN. Sieburth
- Synthesis of ribozyme inhibitor derivatives

Temple University, Undergraduate Researcher (Summer 2009)

Philadelphia, PA

- Adviser: Professor Rominder Suri
- Mass transfer studies of ozone for use in the removal of emerging contaminants from water

Teaching Experience

Lehigh University, Teaching Assistant (Fall 2011, Spring 2012, Spring 2013)

Bethlehem, PA

- Organic Chemistry I and II Laboratories
- Supervised and assisted students with multi-step syntheses of compounds designed to teach general laboratory techniques; graded all work, including lab reports, midterm exams and final exams; met with students upon request

Awards & Fellowships

Newton and Constance Buch Research Fellowship, Lehigh University (2014-2015)

College of Arts & Sciences Fellowship, Lehigh University (2010-2011)

References

Robert A. Flowers, II (Graduate Advisor, Ph.D. Committee Chair)

Danser Distinguished Faculty Chair in Chemistry

Department of Chemistry

Lehigh University

(610) 758-4048

rof2@lehigh.edu

David Vicic (Ph.D. Committee)

Professor

Department of Chemistry

Lehigh University

(610) 758-3466

vicic@lehigh.edu

Marcos Pires (Ph.D. Committee)

Assistant Professor

Department of Chemistry

Lehigh University

(610) 758-2887

map311@lehigh.edu